

17219

cl

THE GEOLOGY OF THE PINCHI LAKE AREA,
CENTRAL BRITISH COLUMBIA

by

IAN ARTHUR PATERSON

B.Sc.(Hons.), Aberdeen University, 1967

A THESIS SUBMITTED IN PARTIAL FULFILMENT OF
THE REQUIREMENTS FOR THE DEGREE OF
DOCTOR OF PHILOSOPHY

in the Department
of
Geological Sciences

We accept this thesis as conforming to the
required standard

THE UNIVERSITY OF BRITISH COLUMBIA

June 1973

In presenting this thesis in partial fulfilment of the requirements for an advanced degree at the University of British Columbia, I agree that the Library shall make it freely available for reference and study. I further agree that permission for extensive copying of this thesis for scholarly purposes may be granted by the Head of my Department or by his representatives. It is understood that copying or publication of this thesis for financial gain shall not be allowed without my written permission.

Department of **GEOLOGICAL SCIENCES**

The University of British Columbia
Vancouver 8, Canada

Date 12th June, 1973

ABSTRACT

THE GEOLOGY OF THE PINCHI LAKE AREA

The area mapped, 75 square miles, lies astride the Pinchi Fault near Fort St. James in central British Columbia. Northeast of the fault system is the lower Mesozoic Takla Group composed of greywackes, conglomerates and minor limestones. Southwest of the fault system is the Pennsylvanian-Permian Cache Creek Group, made up of limestones, cherts, argillites and greenstones. Between these regions, a complex northwesterly-trending fault system involves a series of elongate fault-bounded blocks of contrasting lithology and/or metamorphic grade. Rock types making up individual blocks include:

- (a) lawsonite-glaucophane metasediments and meta-volcanics,
- (b) pumpellyite-aragonite greenstones,
- (c) serpentized harzburgites and dunites and
- (d) a sequence of amphibolitized gabbro-diabase basalt.

Boulders of lawsonite-glaucophane eclogite are also found in the area.

Within the glaucophanitic rocks a metamorphic foliation (S_1) parallels the bedding and contains a mineral lineation

(L_1). This foliation is deformed by F_2 folds and mullions which are accompanied by a prominent L_2 crenulate lineation. These structures are deformed by F_3 kink folds.

Significant mineral assemblages within the glaucophanitic rocks include:

- (i) quartz + lawsonite + sphene + phengite + glaucophane
± carbonaceous material (metacherts)
- (ii) aragonite + dolomite (limestones)
- (iii) jadeitic pyroxene + lawsonite + quartz + white mica + chlorite (metagreywacke)
- (iv) quartz + white mica + lawsonite ± glaucophane
+ pyrite + carbonaceous material (carbonaceous schists)
- (v) acmitic pyroxene + lawsonite + sphene + chlorite
(metavolcanics)
- (vi) glaucophane + lawsonite + sphene + chlorite
(metavolcanics).

Comparison of these assemblages with experimentally determined phase equilibria favours the hypothesis that the glaucophanitic rocks formed at high lithostatic pressures and relatively low temperatures. Because there is no evidence for a metamorphic zonation with respect to the Pinchi Fault, and because metagreywackes and metavolcanics are commonly unsheared, tectonic overpressures are not considered to have contributed

appreciably to the total pressure. In the late stages of metamorphism the fluid phase in carbonaceous schists became progressively more reducing and may have contained appreciable methane. This fluid reacted with acmitic metavolcanics (v) to give glaucophane bearing assemblages (vi). Thus high pressure mineral assemblages with high Fe^{3+}/Fe^{2+} (i.e. v) existed within the metavolcanics prior to reaction with the reducing fluid.

A three stage tectonic model is proposed. Firstly, during the Late Permian, a narrow wedge of Upper Paleozoic sediment was metamorphosed in the blueschist facies along an easterly dipping subduction zone approximately on the site of the Pinchi Fault. This event is considered to be contemporaneous with the formation of F_1 structures. At a higher crustal level, an ophiolite sequence of which unit (d) is a remnant was obducted over the Cache Creek Group sediments which had accumulated above the subduction zone. During the second stage, a change in the stress system converted the subduction zone into a right-lateral strike-slip or oblique-slip fault. This event marked the beginning of the F_2 deformation. Strike-slip movement resulted in formation of zones of low pressure where there were deflections or offsets in the original fault. At Pinchi, such zones were at once filled from below by diapirs of low average density consisting of subducted blueschist, serpentinitized ultramafites and minor eclogite which rose

in the crust to a level governed by isostasy. It is considered that the Middle or Upper Triassic K-Ar dates obtained from phengitic micas (211, 214, 216 and 218 ± 7 m yrs) record either the time of cooling of the uplifted blueschists or the end of the F_2 deformation. The third stage, during the Upper Triassic, involved erosion of the ophiolites exposed on a topographic high to the west of the Pinchi Fault and flysch deposition in the adjacent trough to the east.

The F_3 deformation was contemporaneous with carbonatization of fault zones and possibly occurred during the Eocene.

TABLE OF CONTENTS

	Page
ABSTRACT	ii
LIST OF TABLES	xiv
LIST OF FIGURES	xvi
LIST OF PLATES	xiv
LIST OF MAPS	xx
ACKNOWLEDGEMENTS	xxi
I. INTRODUCTION	1
General Introduction	1
Location and Accessibility	1
Physiography and Glaciation	3
Previous Work	4
Work Done in this Study	6
II. GENERAL GEOLOGY	7
Regional Setting	7
Cache Creek Group	11
Introduction	11
Greenstones of Pinchi Mountain	13
Lithology and petrology	14
Internal structure and contacts	14
Age	15
Origin	16

	Page
Glaucophane-lawsonite bearing rocks around Pinchi Lake	16
Distribution	16
Rock types and proportions	17
Petrology	18
Internal structure	21
External contacts	22
Age	22
Origin	23
Basic rocks south of Pinchi Lake	24
Distribution and petrology	24
Internal structure and contacts	25
Age and origin	26
Massive limestones and cherts of the Mount Pope belt	27
Distribution	27
Lithology and petrology	27
Fauna and age	29
Internal structure and contacts	29
Origin	30
Takla Group	32
Introduction	32
Lithology	34
Conglomerate	36
Internal structure and contacts	39

	Page
Fauna	40
Origin	41
Diorite	43
Cretaceous (?) Conglomerate.	44
III. ULTRAMAFITES AND SILICA-CARBONATE ROCKS	46
Ultramafites	46
Introduction	46
Rock types	46
Internal structure	48
Contact relationships	51
Petrology	51
Discussion on the origin of ultramafites	53
Origin of Pinchi ultramafites	57
Silica-carbonate Rocks	62
Distribution	62
Rock types, internal and external structure	62
Petrology	64
Age and origin	65
IV. METAMORPHISM	68
PART I - METAMORPHISM IN GREENSTONE AND BLUESCHIST FAULT BLOCKS	68
Introduction	68
Paragenetic Sequence of Minerals	71

	Page
Mineral Assemblages	74
Metamorphic Reactions	78
Metabasic rocks	78
Metasediments	83
Relevant Phase Equilibria	84
Aragonite stability	84
Jadeite and acmite-jadeite stability	87
Phengite stability	90
Stability of sodic amphiboles	91
Lawsonite stability	91
Pumpellyite and prehnite stability	92
Eclogite stability	93
Oxygen isotopes	94
Pressure-temperature Conditions of Metamorphism	96
Fluid Phase Composition	96
Fluid Phase Composition at 10 kb and 327°C	104
Evolution of Fluid Phase	108
Pressure-Temperature Trajectories of Pinchi Rocks	110
PART II - METAMORPHISM IN THE REMAINING FAULT BLOCKS	
Metabasic Rocks South of Pinchi Lake	112
Mount Pope Belt	114
Takla Group	114

	Page
Ultramafites	116
V. STRUCTURAL GEOLOGY	118
Introduction	118
Structural Elements in the Lawsonite- Glaucophane Bearing Rocks	123
<i>F</i> ₁ Deformation	125
<i>F</i> ₂ Deformation	127
<i>F</i> ₃ Deformation	128
Microscopic Analyses	130
Timing of Metamorphism and Deformation	134
Structural Geology of Remaining Fault Blocks	139
Greenstones of Pinchi Mountain	139
Mount Pope belt	139
Ultramafites	140
Basic rocks south of Pinchi Lake	141
Takla Group	142
Important Faults in the Pinchi Area	142
Pinchi Fault (No.1)	143
Fault system no. 2	145
Fault system no. 3	147
Fault system no. 4	148
Fault system no. 5	148
Faults in the vicinity of Pinchi Mine	149

	Page
VI. TECTONIC IMPLICATIONS	150
Introduction	150
Constraints to Tectonic Model (Factual and Inferred)	152
Conclusions of this study	152
Inferred crustal structure in central British Columbia	153
The Pinchi Fault as a "Suture Zone"	157
Evidence for strike-slip movement on the Pinchi Fault	160
Possibility that the Pinchi Geanticline was overlain by oceanic crust	161
Absence of metamorphic zonation within the Cache Creek Group	161
Tectonic Models	162
Subduction model	162
Subduction/obduction model	168
Mesozoic and Tertiary events	172
REFERENCES CITED	174
APPENDIX I - FOSSIL LOCALITIES IN THE PINCHI AREA	188
APPENDIX II - MINERALOGY	191
Analytical Methods	191
Minerals	193
Sodic amphiboles	193
Brown and green amphiboles	198
Pyroxenes	200

	Page
Chlorite	207
Aragonite	209
White mica	212
Celadonite	215
Albitic plagioclase	215
Pumpellyite	216
Stilpnomelane	216
Lawsonite	216
Prehnite	217
Garnet	217
Deerite	217
Opaques	218
Carbonaceous material	220
APPENDIX III - BULK CHEMICAL ANALYSES	221
Metabasic rocks	221
Metagreywackes	228
APPENDIX IV - PETROLOGY	231
Greenstones of Pinchi Mountain	231
Lawsonite-Glaucophane Bearing Rocks	237
Metabasic rocks	237
Dolomitic carbonates	241
Metagreywackes	245
Metacherts	247
Quartz-carbonate rocks and schists	249

	Page
APPENDIX V - ECLOGITE BOULDERS	250
APPENDIX VI - POTASSIUM-ARGON RADIOMETRIC DATES	253
APPENDIX VII - CALCULATION OF EQUILIBRIUM CONSTANT FOR REACTION: PLAGIOCLASE = JADEITIC PYROXENE + QUARTZ	256
APPENDIX VIII - SPECIMEN NUMBERING SYSTEM	258
PLATES	(following page 261)
MAPS	(at end of thesis) <i>in envelope filed beside thesis</i>

LIST OF TABLES

Table	Page
1.	TABLE OF FORMATIONS IN PINCHI AREA 9
2.	MODAL ANALYSES OF GREYWACKES FROM THE TAKLA GROUP 33
3.	PEBBLE CONTENT OF CONGLOMERATES WITHIN TAKLA GROUP 38
4.	GENERALIZED PARAGENETIC SEQUENCE OF METABASALTS 75
5a.	POSSIBLE REACTIONS IN METABASIC ROCKS 76
5b.	MINERAL COMPOSITIONS USED IN REACTIONS 77
6.	OPTICAL PROPERTIES OF PYROXENES AND AMPHIBOLES 194
7.	CELL DIMENSIONS FOR GLAUCOPHANE AND JADEITIC PYROXENE 195
8.	ELECTRON MICROPROBE ANALYSES OF GLAUCOPHANES 196
9.	ELECTRON MICROPROBE ANALYSES OF RELICT AUGITE 199
10.	ELECTRON MICROPROBE ANALYSES OF METAMORPHIC PYROXENES 201-202
11.	ELECTRON MICROPROBE ANALYSES OF CHLORITES 208
12.	CARBONATE MINERALOGY AND SAMPLE DISTRIBUTION 211
13.	PARTIAL ELECTRON MICROPROBE ANALYSES OF PHENGITES AND CELADONITE 213
14.	STANDARD DEVIATIONS FOR SELECTED MINERAL ANALYSES 214
15.	ACCURACY OF BULK CHEMICAL ANALYSES 222
16a.	CHEMICAL ANALYSES OF METABASALTS FROM THE PINCHI AREA 223

Table	Page
16b. ADJUSTED CHEMICAL ANALYSES OF METABASALTS	224
17. C.I.P.W. NORMS FOR ANALYZED META- BASALTIC ROCKS	224
18. SUMMARY OF SIGNIFICANT CHEMICAL CHARACTER- ISTICS OF METABASALTS	227
19. CHEMICAL ANALYSES OF METAGREYWACKES	229
20. EQUILIBRIUM MINERAL ASSEMBLAGES IN THE GREENSTONES OF PINCHI MOUNTAIN	232
21. TEXTURAL DOMAINS WITHIN THE PINCHI MOUNTAIN GREENSTONES	233
22. EQUILIBRIUM MINERAL ASSEMBLAGES IN THE LAWSONITE-GLAUCOPHANE BEARING METAVOLCANICS	238
23. TEXTURAL DOMAINS IN LAWSONITE-GLAUCOPHANE BEARING METABASIC ROCKS	239
24. EQUILIBRIUM MINERAL ASSEMBLAGES IN METAGREYWACKES	244
25. EQUILIBRIUM MINERAL ASSEMBLAGES IN CHERTS AND CHERTY GRAPHITE SCHISTS	244
26. SAMPLE LOCATIONS AND ANALYTICAL DATA FOR POTASSIUM-ARGON ANALYSES	254

LIST OF FIGURES

Figure	Page
1. Location and regional geology map	2
2. Major tectonic elements of British Columbia	8
3. Geological subdivisions at Pinchi Lake	12
4. Takla Group: sections, fossil and specimen localities	12
5. Structural features in Harzburgites	47
6. Paragenetic sequence of metamorphic minerals in metabasalts and eclogites	72
7. Paragenetic sequence of metamorphic minerals in metasediments	73
8. Phase equilibria relevant to formation of mineral assemblages	85-86
9. Pressure-temperature conditions of metamorphism of greenstones, blueschists and eclogites	95
10. Phase equilibria relevant to fluid phase chemistry	97-99
11. Schematic illustration of fluid phase chemistry	105-106
12. T- f_{O_2} diagram illustrating evolution of fluid phase composition	106
13. Pressure-temperature trajectories for greenstone, blueschist and eclogite	111
14. Phase equilibria in the system MgO- SiO ₂ -H ₂ O	111
15. Stereographic projections illustrating S_1 , L_2 and F_3 orientations	119

Figure	Page
16. Structural elements in schists	120
17. F_2 folds	121
18. Recumbent isoclinal F_2 folds (22a, 22b) and F_2 folded by F_3 (22c)	122
19. Relation of metamorphic recrystallization to deformation	131
20. Depth-time trajectory for Pinchi rocks . . .	135
21. Crustal model for central British Columbia	154
22. Generalized diagram illustrating location of major geologic units in central British Columbia in relation to the problematical belt of Paleozoic rocks between the Takla Group and the Omineca Geanticline	158
23. Subduction model	163
24. Subduction - obduction model	166-167
25. Possible mechanism for intrusion of blue- schists and serpentized ultramafites along strike-slip faults	169
26. Element variation in zoned glaucophane . . .	197
27. Compositional variation of pyroxenes from Pinchi and California	203-205
28. Map of aragonite occurrences in Pinchi area	210
29. Map of prehnite, pumpellyite and selected glaucophane-lawsonite occurrences	210
30. Textures in opaque minerals	219
31. A-F-M diagram illustrating basalt compositions	225
32. Alkali-silica variation diagram for metabasalts	225

Figure		Page
33.	Textures in Pinchi Mountain greenstones. .	236
34.	Textures in lawsonite-glaucophane bearing metabasic rocks	240
35.	Textures in carbonates	242
36.	Textures in metasediments	246
37.	Eclogite localities and source areas as inferred from glacial transport directions	251

LIST OF PLATES
(following p. 261)

Plate

1. View of the Pinchi Lake area looking northwest from the summit of Mount Pope
2. Laminated siltstones and sandstones in the Takla Group
3. Northwesterly plunging mullions in quartz-mica carbonate schists
4. Angular limestone cobble conglomerates in Takla Group
5. Northerly dipping compositional layering in silica-carbonate rocks
6. Primary (?) two phase fluid inclusion in metacherts
7. Late pyroxenite layers parallel to dunite rich layers in harzburgite
8. Late discordant pyroxenite layer cross-cutting irregular dunite
9. Smooth weathering dunite layer parallel to foliation in harzburgite outlined by varying olivine: pyroxene ratio
10. Folded early pyroxenite layers
11. Folded dunite layers in foliated harzburgite

LIST OF MAPS

(Following p.263 at end of thesis)

in envelope filed beside thesis

Map

- I. Geology of Pinchi Lake area
- II. Cross sections of Pinchi Lake area
- III. Aeromagnetic map of Pinchi area
- IV. Geology in the vicinity of Pinchi Mine
- V. Geology of an area on the northwest shore of Pinchi Lake
- VI. Important faults in the Pinchi area
- VII. Specimen location map

ACKNOWLEDGEMENTS

Cominco Ltd. permitted access to their claims which lie within the area mapped. The kindness, cooperation and advice of employees in the course of this study is gratefully acknowledged, especially G. Warning, geologist at Pinchi Lake Mercury Mine.

The author is deeply indebted to Drs. H.J. Greenwood and K.C. McTaggart of the University of British Columbia who introduced the writer to the project, provided early supervision and made constructive criticisms of the manuscript. Helpful suggestions for improvements to various parts of the manuscript were also made by Drs. W.C. Barnes, W.R. Danner and P.B. Read² (all at U.B.C.). Fossil identifications were made by Drs. W.R. Danner (U.B.C.), B.E.B. Cameron and H. Frebold (G.S.C.). K-Ar radiometric dates were obtained by J.E. Harakal and V. Bobik in the laboratories of the departments of Geological Sciences and Geophysics at the University of British Columbia. Assistance and training in the use of the electron microprobe at the University of Washington were provided by Dr. B.W. Evans and L. Leitz. The author also wishes to thank members of the Vancouver branch of the Geological Survey of Canada who gave generously of their time in helpful discussions and were

instrumental in obtaining fifteen chemical analyses from the G.S.C. laboratory in Ottawa.

Costs of field work were defrayed by a grant from the Geological Survey of Canada and logistical support was provided by Cominco Ltd. From 1968-71, the author was supported by a scholarship from the National Research Council of Canada.

Finally, the author's sincere thanks are extended to the faculty, technical staff and graduate students at the University of British Columbia for their interest and constructive suggestions in the course of this study. Special thanks are due to my wife Barbara for assistance in the field and in editing the manuscript.

ADDENDA

p. 65, Line 23. Recent (1972) radiometric dates from the Sustut Group show it to be of Upper Cretaceous to Eocene age (G.H. Eisbacher, oral commun.)

p. 180 The following reference was omitted:
Fyfe, W.S., Turner, F.J., and Verhoogen, J., 1958, Metamorphic reactions and metamorphic facies, Geol. Soc. Am., Mem 73.

INTRODUCTION

General Introduction

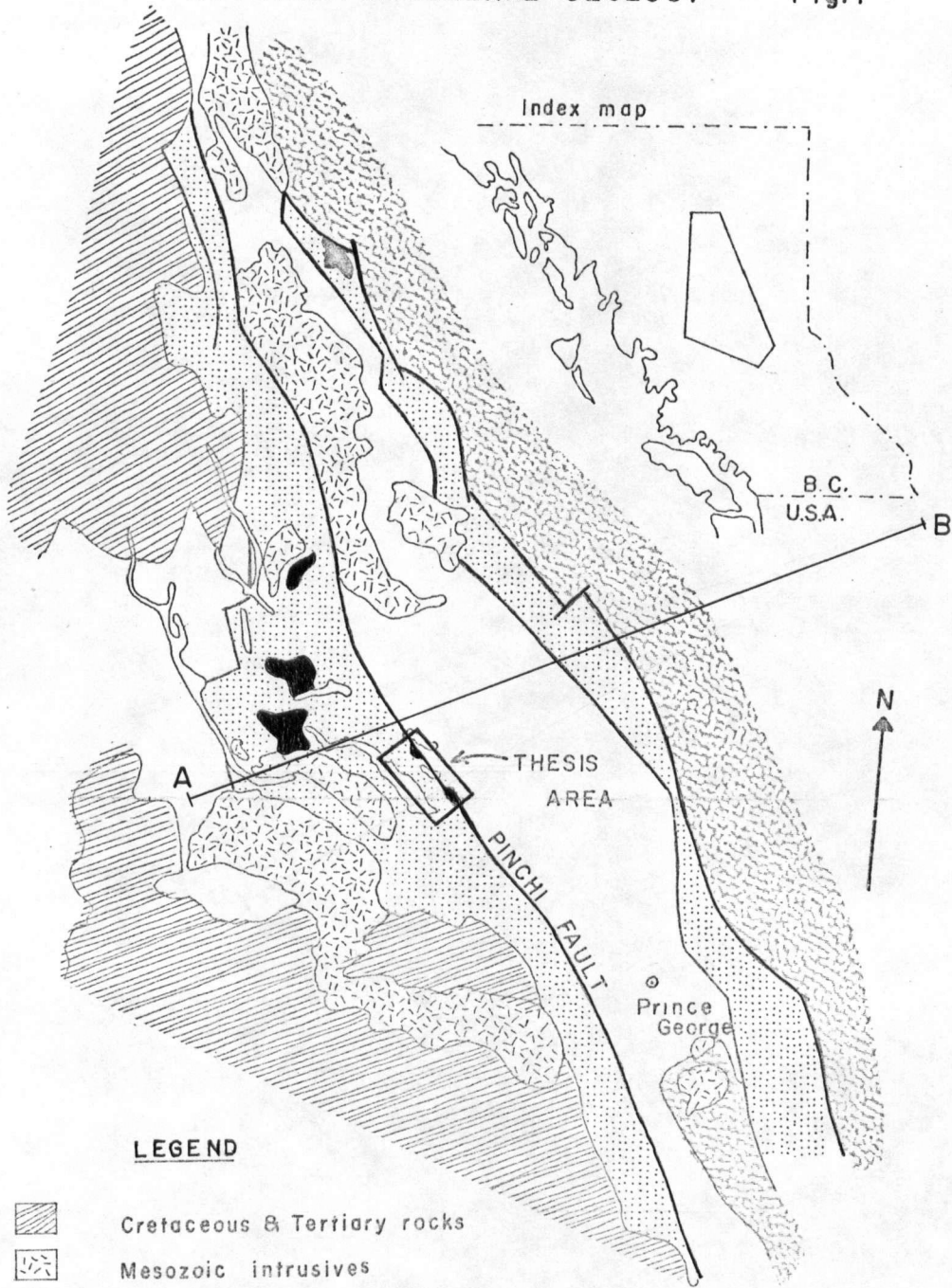
The purpose of this thesis is to describe the general geology in the vicinity of Pinchi Lake, central British Columbia. This area is 325 square km in extent and lies astride the Pinchi Fault zone, one of the major tectonic lineaments in the Canadian Cordillera. Particular attention is paid to the structure, metamorphism and petrogenesis of rocks of the lawsonite-glaucophane facies.

Location and Accessibility

The map area is situated in central British Columbia, 600 km north of Vancouver, and can be reached via Prince George and Fort St. James (Fig. 1). A road 49 km long connects Fort St. James with Pinchi Lake Mercury Mine on the northern shores of Pinchi Lake. The region between Pinchi and Stuart Lakes is served by the British Columbia Railway and a gravel road leading to Tachie Indian Reserve (Map I).

LOCATION & GENERAL GEOLOGY

Fig.1



LEGEND

-  Cretaceous & Tertiary rocks
-  Mesozoic intrusives
-  Lower Mesozoic (Takla & Hazelton Groups)
-  Ultramafites (Trembleur Intrusives)
-  Carboniferous & Permian
-  Proterozoic & Cambrian

40 miles
64.5 km

Compiled by W.H.White (1966)

Physiography and Glaciation

There is a close relationship between the geology and the topography within the Pinchi Lake area. Mount Pope (1472 m) is the highest point on a long limestone ridge between Pinchi and Stuart Lakes, forming a prominent feature in the landscape (Plate 1). Other landmarks to the northeast of this ridge are Pinchi Mountain (1270 m) and Murray Ridge (1400 m) both of which are composed of ultra-mafic rocks. Between these landmarks and the limestone ridge the area is of subdued relief, broken only occasionally by bluffs of limestone or carbonatized serpentinite.

The area is forested with spruce, silver birch and lodgepole pine. Alpine fir and juniper are found above 1000 m.

Armstrong (1949) and Tipper (1971) give accounts of the Pleistocene glacial history of the area. In brief, the following events took place which strongly influenced the development of the landforms:

- (a) the development of the Cordilleran icecap led to the deposition of an extensive cover of glacial till;
- (b) after the ice retreated, it advanced again and formed a drumlinised till plain. The direction of ice flow was towards the east-northeast;

(c) during recession of the ice, drainage channels were blocked and glacial lakes formed.

One such lake, of which Pinchi Lake is a remnant, covered much of the ground below 840 m. Silt, sand and clay deposited in the lake and the earlier drift deposits cover most of the area and are responsible for the scarcity of outcrops.

Previous Work

On the grounds of lithologic similarity, A.R.C. Selwyn (1877) correlated rocks in the Fort St. James area with those in the Lower Cache Creek Group which he had previously defined (1872) in the Cache Creek area. In this area he had found brachiopods indicative of a Late Paleozoic age. In the course of a journey across central British Columbia in 1876, G.M. Dawson collected fusulinid bearing limestones from the Mount Pope area and verified Selwyn's correlation. J.G. Gray (1938) mapped the area for the Geological Survey of Canada and worked out the general stratigraphy in the area. He also discovered cinnabar in 1937 on a limestone bluff on the north shore of Pinchi Lake.

During the Second World War, a mercury shortage stimulated prospecting and a development in the region. Pinchi Mine, on the site of Gray's discovery, came into

production in 1940. Stevenson (1940) published a report which included a section on the geology of the mine and vicinity. He recognized that the Cache Creek Group sediments had been dynamically metamorphosed and recorded the presence of glaucophane. The cinnabar mineralization took place after the glaucophanitic metamorphism and was associated with considerable metasomatic replacement and complex faulting.

In 1942, A.C. Freeze completed a Ph.D. thesis on the geology of the Pinchi Lake area. He divided the stratified rocks into lithologically and structurally distinct series separated by unconformities: a pre-Upper Triassic series (the Cache Creek Group), an Upper Triassic series (the Takla Group) and a Cretaceous-Tertiary (?) series. He also suggested that the formation of glaucophane was due to soda metasomatism at relatively shallow depths and moderate temperatures.

J.E. Armstrong of the Geological Survey of Canada published a number of reports on the Pinchi Lake mercury belt (1942, 1944) and produced a memoir on the Fort St. James map-area (1949). A major contribution was the recognition of the Pinchi Fault which juxtaposed late Paleozoic Cache Creek Group rocks to the west with Mesozoic Takla Group rocks to the east. An important observation, also made by Freeze (1942) was that the diagnostic Upper Triassic pelecypod *Monotis subcircularis* occurred in close

association with a conglomerate containing detrital chromite. Armstrong also noted the association between the fault and mercury deposits.

A review of the literature pertaining to the genesis of glaucophane schists will be given in Chapter IV.

Work Done in This Study

Geological mapping of a 40 km by 8 km area astride the Pinchi Fault was carried out during 1968 (1 month), 1969 (3 months), and 1971 (3 weeks). Two localities in the Cache Creek Group were mapped in detail in an attempt to interpret stratigraphic and structural relations adjacent to the fault zone. Drilled cross sections were logged and sampled. Reconnaissance trips were made to the north-west arm of Stuart Lake, Tsayta Lake and the Vital Mountains in order to compare Cache Creek Group rocks exposed elsewhere with those at Pinchi Lake.

Laboratory work has involved the examination of 230 thin sections and supplemental examinations of X-ray diffraction traces where necessary. Bulk chemical analyses of 15 rocks were carried out by the Geological Survey of Canada and mineral analyses were obtained with an A.R.L. microprobe belonging to the University of Washington. Details of analytical techniques are given in the appendices.

II

GENERAL GEOLOGY

Regional Setting

In central British Columbia, the 450 km-long Pinchi Fault demarcates the Pinchi Geanticline, largely consisting of the Late Paleozoic Cache Creek Group, from the Quesnel Trough, composed of the Lower Mesozoic Takla Group. To the east of the Quesnel Trough is the Omineca Geanticline, a mountainous region carved from rocks of Proterozoic and Cambrian age (Figs. 1 & 2).

The Late Paleozoic Cache Creek Group to the west of the Pinchi Fault consists of interbedded chert, cherty phyllite, argillite, greenstone, minor greywacke and massive limestone, the last mentioned forming a conspicuous unit striking parallel to the Pinchi Fault. During Permian-Triassic times, these rocks were: (a) deformed about northerly or northeasterly trending fold axes; (b) intruded by alpine type peridotites and (c) metamorphosed under lower greenschist or locally lawsonite-glaucophane facies conditions. These rocks were then intruded by diorites, granodiorites and granites during the Jurassic Period.

FIG. 2

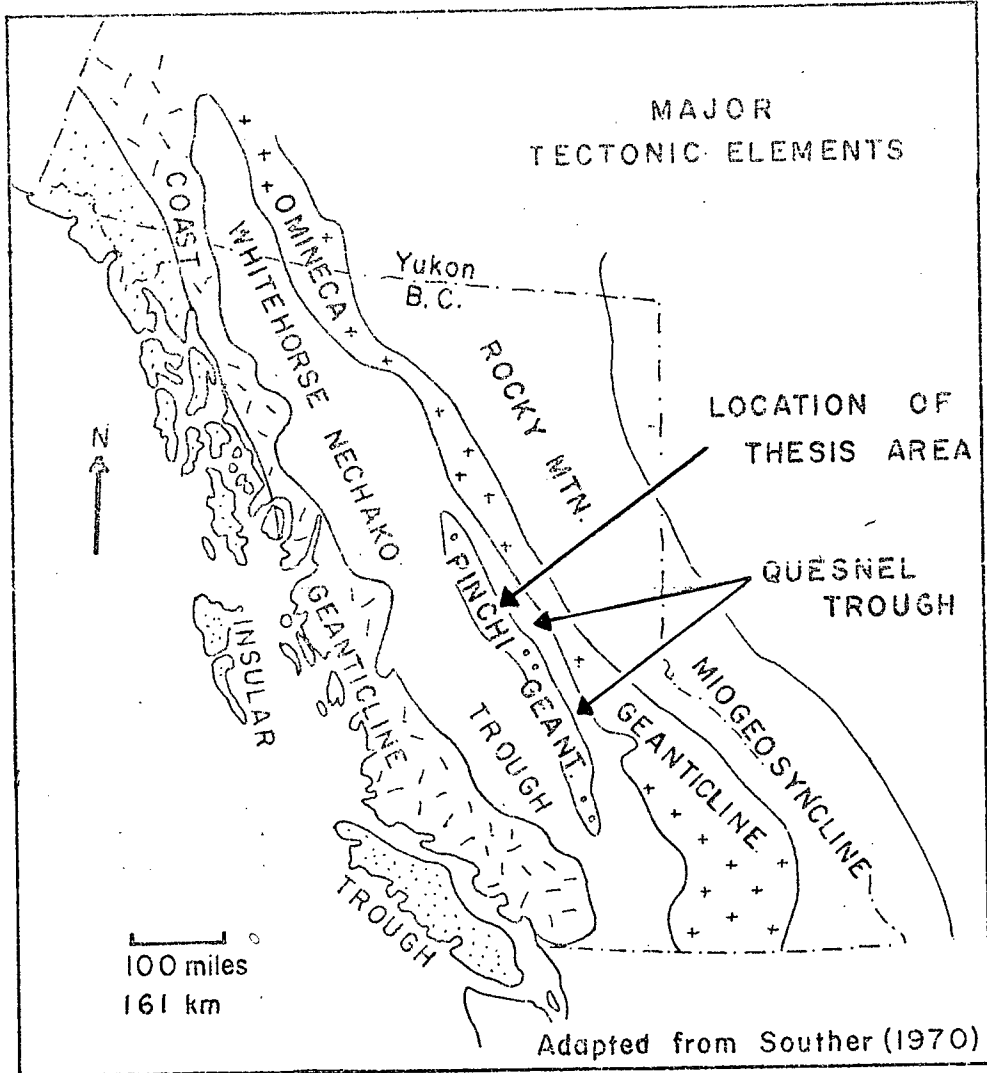


TABLE 1 FORMATIONS PRESENT IN THE PINCHI AREA

ERA	PERIOD OR EPOCH	GROUP OR FORMATION	LITHOLOGY
MESOZOIC	CRETACEOUS (?)	USLIKA FORMATION	chert conglomerate
		UNCONFORMITY	
MESOZOIC	JURASSIC UPPER TRIASSIC	OMINECA INTRUSIONS	hornblende diorite
		TAKLA GROUP	plagioclase arkose, siltstones limestones, conglomerates and minor tuff.
		FAULT CONTACT	
PALEOZOIC OR MESOZOIC	PRE-UPPER TRIASSIC POST-LOWER PERMIAN	TREMBLEUR INTRUSIONS	serpentinite, harzburgite, dunite and pyroxenite.
PALEOZOIC	LOWER PERMIAN PENNSYLVANIAN	FAULT CONTACT	
		CACHE CREEK GROUP MOUNT POPE BELT	limestone, chert, minor volcanic breccia
	MISSISSIPPIAN (?) TO PERMIAN	CACHE CREEK GROUP (?) GREENSTONES OF PINCHI MOUNTAIN	pumpellyite bearing basalts, minor aragonitic limestone and graphite schist
		BASIC ROCKS SOUTH OF PINCHI LAKE	basalt, diabase, gabbro
		GLAUCOPHANITIC ROCKS OF PINCHI LAKE	metabasalts, metacherts, schists, greywacke, dolomitic limestone.

The Takla Group lies to the east of the fault and everywhere appears to be in fault contact with the Cache Creek Group. A dominantly sedimentary Upper Triassic sequence of greywackes, siltstones, limestones and occasional conglomerates is overlain by Jurassic andesites, breccias, tuffs and intercalated sediments. In contrast to the Cache Creek Group, Takla Group rocks are unfoliated and have undergone a low grade burial rather than dynamic metamorphism. Also, faulting rather than folding is the characteristic type of deformation in these younger rocks. Extensive emplacement of diorites and granodiorites occurred during the Mesozoic.

Cretaceous or Paleocene continental sediments were deposited unconformably on Takla Group rocks, and outliers are preserved at various localities along the Pinchi Fault zone. Such rocks, described by Roots (1954) in the Aiken Lake area to the north, have been involved in post-Paleocene fault movements.

These disturbances were followed by eruption of Oligocene and Miocene flood basalts, remnants of which are preserved mainly in the southern part of the Fort St. James area.

The foregoing sequence of events is summarized in the table of formations (Table 1).

The area mapped (Map I) includes most of the above mentioned rock units and lies astride the Pinchi Fault

system. For descriptive purposes, rock units are considered under five headings: Cache Creek Group, Ultramafites, Takla Group, Diorite and Cretaceous (?) conglomerate.

Cache Creek Group

Introduction

In 1875, A.R.C. Selwyn noted the lithological similarity of limestones in the vicinity of Mount Pope with those of Late Paleozoic age which he had found previously on the banks of the Thompson River in the Cache Creek area. The following year, G.M. Dawson (1876) visited Mount Pope and collected fusulinids which confirmed the correlation.

Armstrong (1949) concluded that

The Cache Creek Group may be defined as a very thick assemblage 20,000 ft or more of interbedded sedimentary and volcanic rocks, mainly of Permian age, but also probably in part of Pennsylvanian age. The whole of the Permian may be represented. Foraminiferal limestones and ribbon cherts are characteristic of the group.

He recognized four main lithological divisions in the Cache Creek Group, namely slate, ribbon chert, limestone and greenstone divisions. On account of structural complexity, stratigraphic relations are in doubt but he suggested that the greenstone division predominates in the upper part of the group.

Fig. 3. GEOLOGICAL SUBDIVISIONS AT PINCHI LAKE.

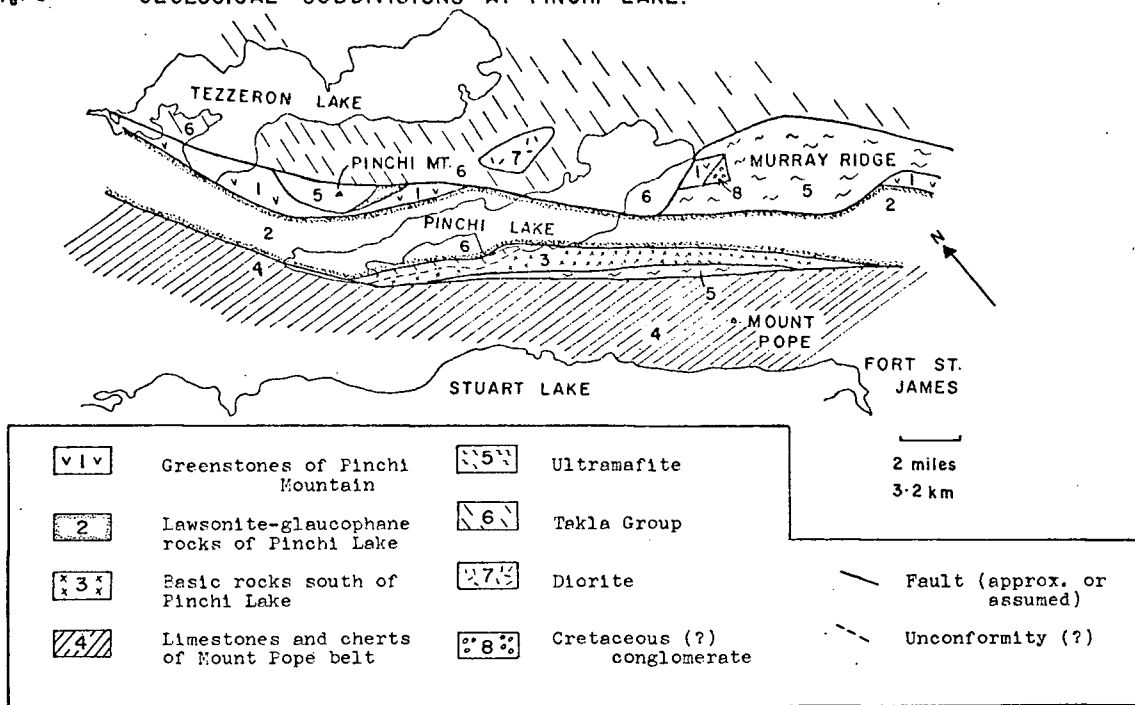
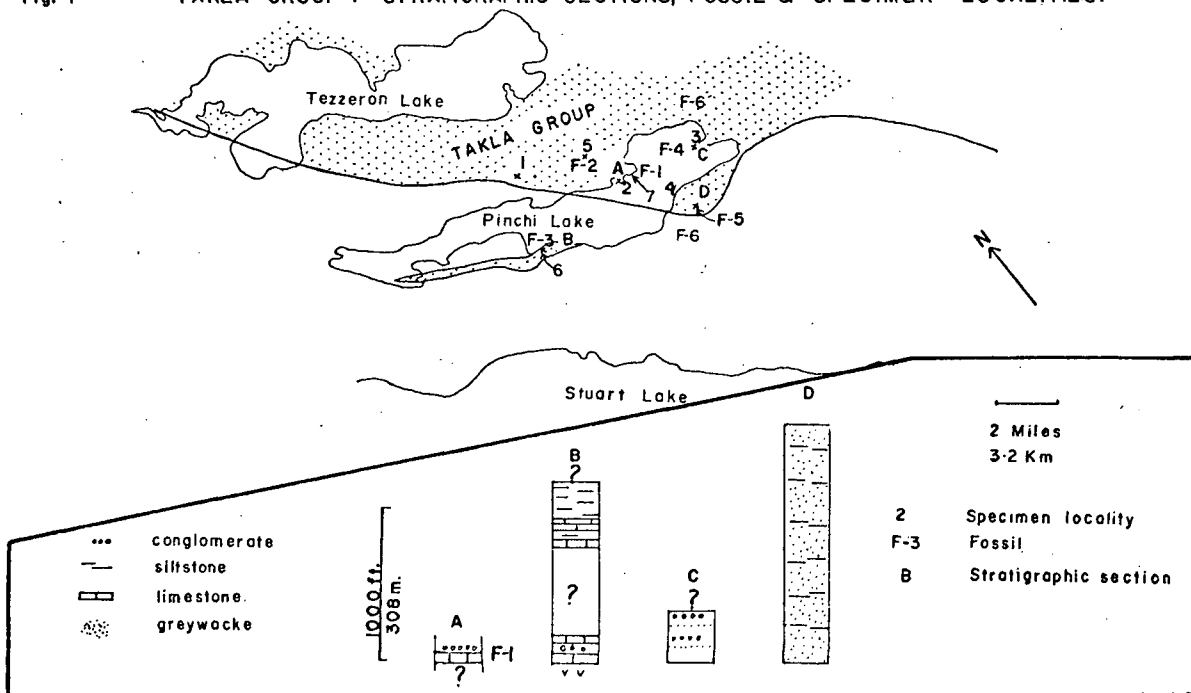


Fig. 4. TAKLA GROUP: STRATIGRAPHIC SECTIONS, FOSSIL & SPECIMEN LOCALITIES.



Within the area covered by this thesis, four subdivisions (Fig. 3) have been made in rocks thought to belong to the Cache Creek Group, namely:

- (a) greenstones of Pinchi Mountain,
- (b) glaucophane bearing rocks around Pinchi Lake,
- (c) basic rocks south of Pinchi Lake and
- (d) massive limestones and cherts of the Mount Pope belt.

Each of these units is bounded by faults which juxtapose blocks of contrasting metamorphic grade. In this chapter only the lithological and microscopic features related to the primary rock type will be discussed. Description of metamorphism and structure is reserved for Chapters IV and V respectively.

Greenstones of Pinchi Mountain

The main occurrence of greenstone is on the southern slopes of Pinchi Mountain between the lawsonite-glaucophane bearing rocks and the Pinchi Mountain ultramafite to the north. Exposure is poor and much information has been obtained from trenches and drill holes. Rocks correlated with these are found at the west end of Murray Ridge and 11 km northeast of Fort St. James (Map I).

1. Lithology and petrology

This unit consists dominantly of brown weathering, highly fractured basalts or, locally, fine grained diabasic intrusives. Some members are porphyritic, containing euhedral plagioclase laths (1 cm) or augite phenocrysts (8 mm) set in a green aphanitic matrix; elongate 4 mm chlorite blebs are also common.

Within this dominantly volcanic unit, occasional outcrops and drill hole data show the presence of two sedimentary units separated by 28 m of greenstone. The upper unit consists of 15 m of graphitic chert in 1 cm beds, grading into a grey limestone containing stylolites. The lower unit contains green laminated tuff, limestone and graphitic schist.

In thin section, the greenstones consist of relict augite or albitised plagioclase phenocrysts set in a fine grained matrix of metamorphic minerals (see Appendix IV). Chlorite-filled blebs are common and may originally have been amygdules, or olivine or hornblende phenocrysts. Relict ilmenite is occasionally present in diabasic rocks.

2. Internal structure and contacts

The metabasalts on the northern slopes of Pinchi Mountain strike at 100° and dip to the north at 45° , approximately parallel to the fault which separates the unit from

silica-carbonate rocks and ultramafites to the north. To the south, the unit is juxtaposed against rocks of the lawsonite-glaucophane facies by a nearly vertical fault which is locally carbonatized. A similar situation exists on the Darbar claim group, where a northeasterly dipping fault separates porphyritic augite basalts from lawsonite-glaucophane bearing rocks. The existence and attitude of all the faults mentioned above have been confirmed by diamond drill holes.

Thicknesses are in doubt owing to poor exposure and pervasive shearing. It is suggested that the unit is not less than 450 m thick, of which approximately 30 m is composed of intercalated sediments.

3. Age

Freeze (1942) and Armstrong (1949) included these rocks in the Takla Group. This possibility cannot definitely be excluded but evidence that the unit may belong to the Cache Creek Group includes the following:

- (a) the presence of aragonite, acmitic pyroxene and possible lawsonite (Chapter IV) suggests that metamorphism was contemporaneous with the Triassic glaucophanitic metamorphism of the Cache Creek Group, and therefore that the unit is of pre-Takla Group age;

- (b) graphitic cherts interbedded with the basalts suggest an affinity with the Cache Creek Group.

It is concluded that this unit may be representative of the "upper greenstone division" of the Cache Creek Group (Armstrong, 1949) and presumably of late Permian age.

4. Origin

These rocks have been called basalts or diabases because of their basic composition and relict mineralogy. Chemical evidence (Appendix III) indicates that the basalts are of the alkali-olivine type. The presence of intercalated limestones, graphitic cherts and laminated tuffs suggests that the basalts may have been extruded in a submarine environment.

Glauco-phane-lawsonite bearing rocks around Pinchi Lake

1. Distribution

Glauco-phane-lawsonite-bearing rocks form a narrow fault-bounded belt, 2.5 km wide, extending the length of the map area. The best exposures are in the immediate vicinity of Pinchi Lake Mercury Mine and along the northwest shore of Pinchi Lake; both of these areas were mapped in detail (Maps IV and V). Glauco-phane rocks are also found on the Darbar claim group, (Map I), 11 km northeast

of Fort St. James, and it is presumed that such rocks underlie much of the low unexposed ground between Murray Ridge and Mount Pope. An exposure, of importance because of its proximity to the southwest margin of the fault block, lies 3.6 km south of Pinchi Mine on a small island near the southwest shore of Pinchi Lake. The most northwesterly outcrops are 1.6 km south of the west end of Tezzeron Lake. Beyond this, little is known about the geology because of poor exposure and difficult access.

2. Rock types and proportions

The glaucophane-lawsonite bearing belt consists of metabasic rocks, dolomitic limestones, cherts, graphitic cherts, greywackes and schists. Estimates of lithological proportions are difficult because of poor exposure, but it is fairly certain that much of the low ground is underlain by graphitic cherts which grade into greywacke and schists. Because of resistance to erosion, limestones, basic rocks and cherts tend to form ridges with outcrops giving a false impression of their abundance. Lithological proportions are estimated as follows: limestone, 10%; metabasic rocks, 5%; metagreywackes, 15%; metacherts, 25%; graphitic cherts and schists, 45%.

3. Petrology

(a) Metabasic rocks

Metabasic rocks are associated with the limestone lenses along the northern shores of Pinchi Lake. Metabasic rocks were also intersected in diamond drill holes 2.4 km northwest of Pinchi Mine. For descriptive purposes, these rocks are subdivided into foliated and massive rocks but rock types with intermediate characteristics are very common.

Foliated rocks are blue, fine to medium grained and have a well defined foliation outlined by parallel acicular crystals of glaucophane. They may also show a compositional layering consisting of 1 cm alternating blue and green layers parallel to the foliation. Commonly crenulations can be seen on foliated surfaces which cross-cut the glaucophane mineral lineation.

Massive metabasic rocks are recognized in outcrop by brownish weathering, complex fracturing and lack of measurable structures. Fractures are commonly filled with quartz, carbonate or glaucophane, the latter growing perpendicular to the walls. Fresh rock between veins is green, fine grained, and occasionally microporphyritic or amygdaloidal. One distinctive layer contains 1 cm blastoporphyritic augites set in a light green aphanitic matrix.

In thin section, foliated rocks are thoroughly metamorphically reconstituted. Massive rocks, however, display a variety of relict textures similar to those observed in the metabasic rocks on Pinchi Mountain. Relict amygdules contain aragonite or chlorite and relict plagioclase laths contain lawsonite, chlorite and white mica. Blastoporphyritic augites are common and trachytic or pyroclastic textures occur occasionally.

Two large metabasic boulders, containing a different mineralogy from anything previously mentioned were found in the area. A glaucophane-eclogite boulder is located 9 km east of Pinchi Mercury Mine on the Tezzeron Lake logging road (locality E on Map I). It measures 12 by 4 by 3 m, is rounded and is embedded in glacial till. It appears to have been transported eastwards from the vicinity of Pinchi Mine during glaciation. The boulder contains foliated and lineated blocks up to 30 cm in diameter consisting of green pyroxene, and garnet altering to stilpnomelane. Glaucophane and lawsonite occupy the interstices between the blocks and also permeate them. Late cross-cutting fractures are filled with chlorite and a brown amphibole. A second boulder is located 3.2 km northwest of the mine (location Br on Map I). It lies in a belt of low ground between two silica-carbonate bluffs astride a major fault zone and is thought to be little transported float. This boulder contains green brecciated

fragments up to 2 cm in diameter set in a dark blue glaucophanitic matrix.

(b) Metasedimentary rocks

Dolomitic limestones grading into calcitic dolomites form a discontinuous series of steep bluffs (180 m high) along the shore of Pinchi Lake northwest of the mine. They are grey weathering massive recrystallized rocks consisting of varying proportions of dolomite, metamorphic aragonite, calcite and carbonaceous material. The dolomite content varies from 20% to 90% and occurs as evenly distributed rhombs or mottled anastomosing patches. Locally the limestones possess a well developed foliation, characterized by alternating streaky laminations of grey aragonite, carbonaceous material and white aragonite with occasional dolomitic laminae (Fig. 35). Petrographic data on the limestones is given in Appendix IV.

Massive metagreywackes are of limited extent and form a unit 30 m in thickness 1.6 km northwest of Pinchi Mine. Fresh surfaces are grey or bluish green and 1 mm white clasts or 2 mm carbonaceous fragments can usually be seen in hand specimen. Thin sections show that metagreywackes possess a recrystallized fabric, but relict angular poorly sorted quartz grains and pseudomorphs after plagioclase can still be detected. A steep dipping fracture cleavage

is sporadically developed and late quartz or carbonate veins (less than 1 mm in width) are common.

Metacherts are fairly resistant to erosion and are best exposed immediately north of the large limestone bluff west of the mine. They weather grey and the fresh surface has a pale bluish sheen due to the presence of acicular nematoblastic glaucophane. Thin schistose laminae containing white mica and glaucophane occur between cherty layers (2 to 5 cm thick) and show a well developed lineation defined by crenulations.

Poorly exposed pyritic carbonaceous schists and quartz + white mica + lawsonite ± glaucophane schists are interbedded with the cherts and limestones. Being incompetent rocks, they tend to be contorted and on exposure to weathering decompose to a micaceous or black carbonaceous mud. A typical specimen of carbonaceous schist contains white beds of cherty quartzite generally less than 3 cm in thickness with interlayers of micaceous carbonaceous schist. Quartz + mica + lawsonite ± glaucophane schists are green with white 2 mm lawsonite and 6 mm blue acicular glaucophane porphyroblasts.

4. Internal structure

Limestones form isolated lenses, striking north-westerly and dipping at approximately 60° northeast. Generally the lenses show no trace of bedding, but a

foliation may be present locally. The rapid variation in thickness and the lensing out of the limestone may either be the result of folding (Chapter V) or a primary depositional phenomenon. Some contacts may be faulted but at Pinchi Mine massive limestone grades into well bedded (15 cm max) cherty quartzite, mica schist and limestone with no suggestion of a fault contact.

Metavolcanic rocks have sharp contacts and appear in many cases to have an inter-tonguing relationship with limestones. This relationship could also be attributed to folding.

Drill holes 1.6 km northwest of Pinchi Mine indicate that carbonaceous cherts and schists have gradational contacts with greywackes.

5. External contacts

All glaucophane-lawsonite bearing rocks are faulted against adjacent rocks. In some places contacts have been drilled, giving intersections of fault breccias and carbonatized rocks.

6. Age

The association of rock types is similar to that found in the Cache Creek Group. However, no fossils have been found in this subdivision and the possibility remains

that these rocks are older than the Pennsylvanian-Permian Cache Creek Group. Since it is to be inferred (Chapter IV) that these rocks have been buried to far greater depths than the Cache Creek rocks to the southwest, they may be of Mississippian age or older. Lithologically, these rocks are also similar to those of the Mississippian Slide Mountain Group (Sutherland-Brown 1963).

7. Origin

Prior to metamorphism and deformation, the sediments consisted of black shale, chert, carbonaceous dolomitic limestone and greywacke in order of decreasing abundance. Porphyritic basalt flows and tuffs were closely associated with the dolomitic limestones.

On account of the complexity of the structure, the largely unknown stratigraphic relations and conflicting opinions on the origin of dolomitic carbonates, cherts and pyritic black shales, the nature of the depositional environment is highly speculative. According to Pettijohn (1957, p. 421) early formation of dolomite suggests a near shore facies, a situation which receives some confirmation with the presence of greywackes at Pinchi. Bedded cherts have been assigned a deep water origin by Rich (1951), and Trumphy (1960). However, Danner (1967) suggests a shallow water origin for at least some cherts and their depth significance is therefore still uncertain. The presence

of pyritic black shales suggests accumulation under stagnant reducing conditions but it is also possible that the reducing environment formed in the sediment during diagenesis. It appears, therefore, that all that can be said about the depositional environment is that it may have been adjacent to a land mass.

Basic rocks south of Pinchi Lake

1. Distribution and petrology

A belt of basic rocks lies to the southwest of Pinchi Lake, between a sliver of Takla Group sediments and an elongate serpentinite body (Map I). It is at least 16 km long and 1500 m in maximum width.

The basic rocks are crudely layered parallel to the elongation of the body. The southern half of the belt consists of brown weathering massive gabbro, with equigranular texture, containing 60% mafic constituents and 40% feldspar. Quartz veins and epidotization along fractures occur locally. Towards the northeast, finer grained rocks with diabasic texture predominate and contain sporadic anastomosing patches of medium grained gabbro. These rocks are highly sheared and chloritized along fractures. Finally, the most northerly rocks in the belt are basalts (?) containing 2 mm calcite blebs.

The gabbro consists primarily of equigranular sub-hedral plagioclase (2 mm average) and interstitial augite; ilmenomagnetite and orthopyroxene are also present. Plagioclase is albitic and is mottled with sericite or granular epidote making identification difficult. Interstitial pyroxenes commonly are replaced by a green pleochroic amphibole ($Z^c = 22^\circ$ max) and all that remains of anhedral ilmenomagnetite grains is a reticulate sphene skeleton.

Diabasic rocks are altered in a similar fashion, the assemblage commonly consisting of saussuritized plagioclase + actinolite + chlorite + sphene. Average grain size is approximately 0.4 mm.

Basalts are inequigranular, containing augite phenocrysts and albitic sericitised plagioclase (1 mm max) in a sub-ophitic fine-grained matrix of augite, albite, chlorite, and sphene.

2. Internal structure and contacts

Takla Group sediments appear to be conformable with the northern contact of the basic rocks. They also young northwards and are overturned. As pebbly limestones near the base of the sequence contain skeletal ilmenomagnetite and chloritised amphibolitic pebbles lithologically similar to the basic rocks (Table 3), it may be that the northern contact is an unconformity which has been overturned and dips to the southwest at 60° .

3. Age and origin

The age and origin of these basic rocks is problematical. A summary of facts and reasonable inferences is as follows:

- (a) gabbro occurs lowest in the sequence followed by diabase and basic volcanics (?) at the top. Relationships between the rock types are apparently gradational;
- (b) the gabbro and diabase belong to the lower greenschist facies;
- (c) a serpentinite belt bounds the gabbro to the south;
- (d) there may be an unconformity between Upper Triassic sediments and the underlying basic sequence, as the latter appears to provide detritus to the Takla Group (Table 3); and
- (e) if an unconformity is present, the sequence has been overturned.

The basic rocks apparently lie below Upper Triassic (?) sediments and are presumably of Cache Creek Group or Triassic age. It is suggested that the greenschist facies metamorphism was contemporaneous with the lower greenschist facies metamorphism in the Cache Creek Group (*see* Chapter IV, Part 2).

The apparent succession serpentinite-gabbro-diabase-basalt is of great interest. Such basic or ophiolitic

complexes are being increasingly recognized elsewhere as oceanic crust (Bailey *et al.*, 1970 and Page, 1972). This possibility will be further discussed in Chapter VI.

Massive limestones and cherts of the Mount Pope belt

1. Distribution

Between Pinchi and Stuart Lakes the topography is controlled by a continuous ridge of limestone which stretches the length of the map-area. This ridge is almost entirely composed of massive crystalline limestone with two minor intercalations of volcanic breccia. Flanking this limestone to the northeast and southwest are belts of chert, locally containing interbeds of tuff and siltstone.

2. Lithology and petrology

The limestone ranges from light grey to dark grey in colour and weathers light grey. In contrast to the limestones north of Pinchi Lake, it is only locally carbonaceous, and dolomite is a minor constituent which occurs in late veins. Brecciated iron stained zones occur adjacent to fractures.

Crinoidal discs and columnals are the most abundant faunal elements, occurring as fragments up to 1 cm in length. Fusulinids, corals and algal structures are also occasionally

seen in hand specimen. The proportion of bioclastic allochemical constituents ranges between 40% and 70% in the four specimens studied in thin section. The framework grains are poorly sorted and set in a micritic matrix. Most limestones could be classified as fine, medium or coarse biomicritic calcarenites (Folk, 1968) locally grading into fine or medium calcirudites.

Flanking the limestone belt are grey to black bedded cherts with thin argillaceous partings. Individual beds are generally from 2 to 5 cm thick but occasionally may reach 12 cm. Siliceous siltstones are commonly interbedded with cherts. In thin section, cherts are cryptocrystalline with microcrystalline quartz replacing radiolaria tests. The grey to black colour is caused by diffuse opaque stringers which have a black amorphous appearance in reflected light and are probably carbonaceous. Cross cutting dilatational quartz veins occasionally give the chert a brecciated appearance.

Volcanic breccias occur at two localities on the southwestern flanks of the limestone. Fragments include green and purple flow rocks and minor siltstone set in a sparry calcite cement. In thin section, plagioclase laths in volcanic fragments are highly sericitised and set in a green or dark brown chloritic matrix.

A schistose tuff, intercalated with chert on the north side of the limestone, contains blastoporphyritic augite and quartz in a chloritic matrix.

3. Fauna and age

Faunas from the Mount Pope belt have been collected by several workers. All previous localities, together with several found in the course of this work, are tabulated in Appendix I. G.M. Dawson collected fusulinids from the Mount Pope area, which were later dated as Early Permian (Freeze, 1942). Thompson (1953) collected from a number of localities and concluded that in the vicinity of Fort St. James the limestone belt ranged in age from Pennsylvanian to Early Permian. Forty miles north, between Trembleur and Kloch Lakes, Armstrong (1949) collected fusulinids of Leonardian and Guadalupian age. No such fusulinids were found in the Mount Pope area.

Algal structures, bryozoa, echinoderm fragments, crinoidal debris and occasional corals have also been found in the area but few are diagnostic of age. Radiolaria tests were found by the author in cherts north of Mount Pope.

4. Internal structure and contacts

Most bedded cherts flanking the limestone belt dip southwest. The oldest fusulinids of Desmoinesian age (Thompson, 1965) are found adjacent to cherts at two localities: on the northwest shore of Pinchi Lake and

two miles northwest of Fort St. James at the base of Mount Pope (Map I). Thompson also states that fusulinids become progressively younger stratigraphically towards the summit of Mount Pope and northwestwards along the shore of Stuart Lake. From these observations the following could be inferred: (a) limestones overlie the cherts; (b) the part of the limestone belt south of Mount Pope has been locally overturned and (c) the limestone belt contains a syncline with axial plane dipping southwest. Undoubtedly, the structure is not as simple as this, but further unravelling must await detailed faunal studies.

The northern boundary of the belt appears to be the site of a major fault closely associated with slivers of ultramafic rock for much of its length.

5. Origin

The limestone belt is remarkably continuous. In central British Columbia, limestones of similar age and lithology form a persistent belt, 200 km in length, striking sub-parallel to the Pinchi Fault. Similar limestones occur on the Atlin Horst (Aiken, 1959 and Monger, 1969) and in the Cache Creek area (Selwyn, 1872 and Danner, 1964, p. 109). The continuity of the belt suggests that it may have formed a barrier reef during the Late Paleozoic. Whether it formed adjacent to a land mass is not known.

The origin and depositional environment of bedded cherts are controversial. In the past, many geologists felt that they originated from inorganic precipitates resulting from submarine volcanism and silica saturation of sea water (e.g. Bailey, Irwin and Jones, 1964). However, this is not considered a valid argument where there is no evidence for volcanic activity (Krauskopf, 1967, p. 169). It is now commonly accepted that most bedded cherts formed as a result of accumulation of siliceous organic skeletons (Bramlette, 1946) either at great depths (Trumpy, 1960 and Dietz, 1966) or in shallow water (Danner, 1967). In the latter case, Danner noted the close association of organically derived bedded cherts and fusulinid or algal limestones in the Cache Creek area, and was led to postulate a shallow water origin for the cherts. The cherts occur preferentially in the lower part of the Cache Creek succession and grade upwards into limestones (Danner, 1964, p. 109).

With respect to the origin of cherts in the Mount Pope belt three factors are of significance:

- (a) the cherts contain radiolaria and are not associated with significant amounts of volcanic material;
- (b) they appear to underlie shallow water limestones;
- (c) the chert-limestone contact is sharp.

There are three possible explanations for these relationships. Firstly, the cherts could have been deposited in

deep water and subsequently raised to a near surface environment where limestones were deposited. Secondly, cherts and limestones may have originated in a shallow basin with rate of subsidence roughly equal to rate of deposition. Lastly, shallow water limestones may have been thrust over deep water cherts.

Takla Group

Introduction

The term Takla Group was first used by Armstrong (1949) to describe rocks of sedimentary and volcanic origin deposited during the Upper Triassic and Jurassic. Armstrong recognized two subdivisions:

- (a) Upper Triassic *Monotis* --bearing sedimentary rocks,
- (b) Undivided Takla Group consisting of basic volcanics, pyroclastics and interbedded sediments.

The rocks exposed at Pinchi belong to the first subdivision and occur mainly on the northeast side of the Pinchi Fault zone. A belt of sediments allocated to the Takla Group is also found on the southwest side of the fault, striking subparallel to the southern shore of Pinchi Lake (Fig. 3).

TABLE 2
 MODAL ANALYSES OF GREYWACKES FROM THE TAKLA GROUP

Specimen Number	4	7	1
Feldspar	43.0*	26.7	44.9
Matrix	40.6	50.5	30.1
Hornblende	-	-	12.2
Clinopyroxene	-	3.9	-
Rock fragments	10.0	14.4	10.1
Quartz	6.4	3.6	2.6

Notes:

1. 1000 point counts made on each thin section.
2. Rock fragments include hornblende plagioclase porphyry, and trachytic basic volcanics.
3. Sample locations are given in Fig. 4.
- * 4. Minor K-Feldspar.

Lithology

The rock types present within the area are, in decreasing order of abundance, arkosic greywacke, laminated siltstone, limestone, conglomerate, basic intrusives and basic volcanics.

Arkosic greywackes are dark grey weathering rocks, generally thick to massive bedded (1-3 m) and possessing shale or laminated siltstone interbeds (8-30 cm). On fresh surfaces, they are dark grey or green, and clasts of feldspar, biotite and hornblende can be seen. Most beds are graded, with particle size averaging 1 mm at the base grading into silt size at the top. Black lithic clasts of siltstone occur sporadically. Thin sections (Table 2) show that the dominant constituent is plagioclase, but augite, brown hornblende, volcanic lithic fragments, and calcite can attain appreciable amounts. Accessory constituents include quartz, K-feldspar, pyrite and hematite. Grains are poorly sorted, angular and embedded in an incipiently metamorphosed microcrystalline matrix consisting of chloritic or limonitic material, plagioclase and calcite. Porphyritic volcanic fragments, with phenocrysts of plagioclase and/or hornblende in a microgranular trachytic or felted matrix, rarely constitute more than 2% of the rock. Micaceous quartzite clasts and tremolite-epidote aggregates were also identified. Interbedded siltstones

possess similar mineralogy and textures.

Siltstones, calcareous siltstones and silty shales are dark grey weathering, thin-bedded (2-10 cm) rocks with occasional buff weathering fine grained sandstone interbeds (Plate 2). Beds may show fine silty intralaminar and graded bedding, fine crossbedding, convolutions or intraformational siltstone clasts. Plagioclase is again the dominant constituent, with quartz also abundant in a few samples. Clinopyroxene and hornblende have decomposed to chlorite which constitutes the matrix along with carbonate.

Limestones lie in the belt of sediments southwest of Pinchi Lake, between Murray Ridge and Pinchi Lake and intermittently along the north shore of the lake. At the first locality the limestones are grey weathering, dark grey to black rocks which emit a bituminous odour on fracturing. Well bedded biomicritic calcarenites grade into, or are interbedded with, dark grey calcilutites, calcareous siltstones and pebbly calcarenites. Limestones at the second locality are massive, bituminous and contain colonial corals and crinoidal debris. At the third locality, on the north shore of Pinchi Lake, the limestones are indistinctly bedded, weather grey and are buff coloured on a fresh surface. They are dominantly poorly sorted biomicritic calcarenites containing abundant crinoidal discs,

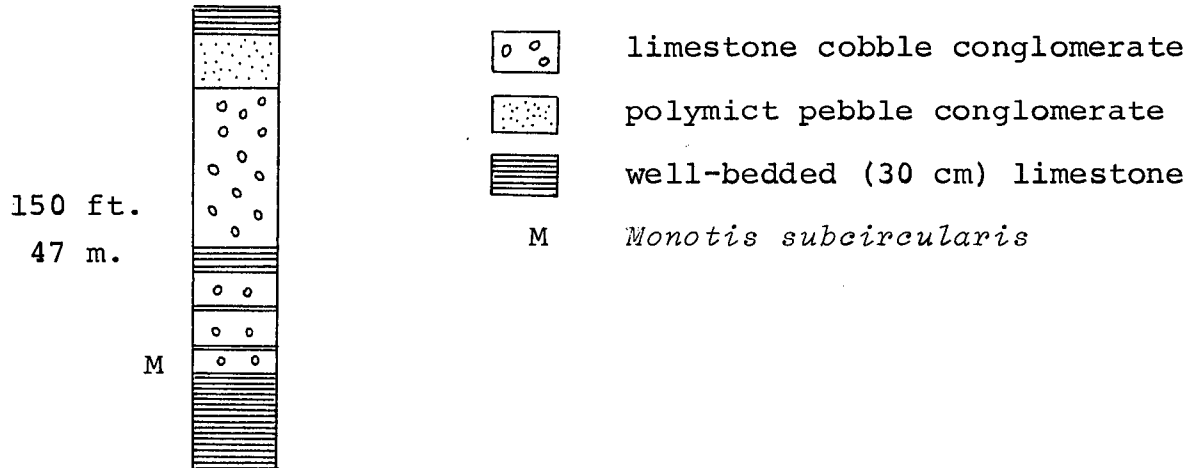
coral and shell fragments. Pebbles (1 cm max) are commonly found in thin layers or are distributed sporadically through the limestones. Limestones associated with conglomerates at this locality are discussed later.

Basic rocks were found at only two localities (Map I). A basaltic lapilli tuff is found 200 m east of the conglomerate on the north shore of Pinchi Lake and an unusual biotite-quartz gabbro is located on the south shore of Pinchi Lake 1.6 km west of the east end of the lake.

Conglomerate

Conglomerate has been treated separately because of its importance regarding the depositional environment and provenance of the Takla Group sediments.

The most interesting locality (Fig. 4, No. 2) lies on a promontary on the north shore of the lake 6.4 km from the east end. The limestone beds associated with the conglomerate are near vertical and the way-up could not be determined. A stratigraphic section is as follows.



Fine grained, well bedded limestones containing *Monotis* grade into intraformational conglomerates consisting of angular poorly sorted limestone cobbles (Plate 4). The cobbles also contain *Monotis* and are up to 18 cm in diameter. Adjacent to this cobble conglomerate is a very interesting 5 m thick bed of polymict pebble conglomerate. The pebbles (4 cm max) are grey to black, sub-rounded, poorly sorted and are embedded in a biomicritic calcarenite matrix. The composition of the pebbles is given in Table 3 (loc. 2). Sub-angular intraformational limestone cobbles (10 cm max) are also present in this layer.

The presence of detrital chromite at this locality was first noted by Freeze (1942). In the course of this

TABLE 3 PEBBLE CONTENT OF CONGLOMERATES WITHIN TAKLA GROUP

LOCATION (See FIG. 4)	PETROLOGY OF PEBBLES	ABUNDANCE (% of total pebbles in specimen)	SOURCE ROCK
N. shore of Pinchi Lake. Loc. 2.	Type A : medium grained; ab-actin- -sph-ep-qtz-relict opx.	40%	amphibolitised gabbro.
	Type B : fine grained; ab-actin- chl ; relict diabasic texture.	50%	metadiabase, metabasalt.
	Type C : ab laths in micro- granular matrix; trachytic texture	2%	basalt.
	Type D : cryptocrystalline chert	5%	bedded chert.
	Type E : chromite grains	1%	harzburgite, dunite.
East of Pinchi Mine, Loc. 5	Type A : cryptocrystalline chert	75%	bedded chert.
	Type B : trachytic basalt.	5%	basalt.
	coarse grained plagioclase and quartz grains are also present.	20%	intrusives ?
S. shore of Pinchi Lake, Loc. 6	Type A : ab-sph-chl ; porphyritic or equigranular texture.	50%	metabasalt.
	Type B : cryptocrystalline chert	45%	bedded chert.
	Type C : assorted grains : skeletal ilmenomagnetite, clinopyroxene, serpentine.	5%	gabbro, serpentinite ? .
ab=albite; actin=actinolite; sph=sphene; qtz=quartz; opx=orthopyroxene; chl=chlorite.			

study the identification of chromite was verified by partial electron probe analyses and reflecting microscopy. Two types of chromite were noted, opaque chromite and dark brown translucent picotite. Both varieties were observed in nearby ultramafites. The chromite grains are monomineralic and are embedded in the limestone matrix. Within the basic amphibolitic pebbles, the opaque grains were found to consist of skeletal ilmenomagnetite altered to sphene and hematite, suggesting that these basic pebbles could not have been the source for the chromite.

Conglomerates are also found elsewhere in the Takla Group (Table 3). Two beds of medium pebble conglomerate (8-18 m thick) are interbedded with siltstones at the east end of Pinchi Lake. They contain rounded, moderately sorted grey and black chert pebbles (1-2 cm max) in a siliceous matrix. Pebbley (5 mm) sandstones were found 4.8 km east of Pinchi Mine (Fig. 4, loc. 5) and in the belt of Takla Group sediments south of Pinchi Lake (loc. 6).

Internal structure and contacts

The lack of distinctive marker horizons, poor exposure and paucity of fossils have obscured stratigraphic relations of the Takla Group within the area. The stratigraphy observed in areas of favourable exposure is given in Fig. 4 together with approximate thicknesses. Correlation between sections is problematical but it appears that there is at

least 900 m of Takla Group sediments in the area.

Northeast of the Pinchi Fault zone, the rocks of the Takla Group seem to be highly faulted rather than folded. A marked change in strike in the northeastern part of the map area suggests that a major fault passes from Murray Ridge to Tezzeron Lake. South of Pinchi Lake, the northern margin of the Takla Group is faulted against glaucophane bearing metacherts. Because sediments at the base of this belt contain gabbro and basalt detritus, it may be that the southern contact is an unconformity rather than a fault (*see* also p. 25).

Fauna

Armstrong (1949) made fossil collections at two localities in the Takla Group. In addition to these, three new localities (Fig. 4) were discovered in the course of this study. Descriptions of the fauna are as follows:

1. Limestones on the north shore of Pinchi Lake 6.5 km from the east end contain *Monotis sub-circularis* of Upper Triassic age (Armstrong, 1949).
2. Sandstones 6.4 km east of Pinchi Mine, 60 m south of the road contain *Nerinea*, *Astarte* and *Trigonia* indicating a Jurassic age (Armstrong, 1949).

3. A bioclastic limestone in Takla Group sediments south of Pinchi Lake contains crinoid columnals, bivalve fragments, oolites or pseudoolites, echinoid spines and echinoid shells (Cameron, G.S.C., written commun.). Cameron also suggested that the limestone formed in a high energy environment and was of late Paleozoic or early Mesozoic age.
4. An ammonite fragment was found in a shale bed at the west end of the island at the east end of Pinchi Lake. H. Frebold considered it to be Jurassic (oral commun.).
5. An outcrop of limestone 30 m north of a carbonatized ultramafite between Murray Ridge and Pinchi Lake contains colonial corals thought to be of Upper Triassic age (Danner, oral commun.).
6. Carbonaceous wood fragments were found in sandstone at two localities.

Origin

The oldest rocks appear to be *Monotis* bearing limestones and associated conglomerates, siltstones and greywackes. The shelly fauna, the presence of intraformational limestone breccias and pebble conglomerates suggest shallow water deposition. According to Souther and Armstrong (1966), conglomerates occur at intervals along the eastern margin

of the Pinchi Fault zone and mark the time of emergence of the Pinchi Geanticline at the beginning of the Upper Triassic.

The stratigraphic relationship of the thick arkosic greywacke sequence to the above mentioned limestones is unknown, but it is suggested that the former was deposited on the latter during rapid subsidence of a basin lying northeast of the fault zone. Graded bedding and the poorly sorted angular nature of the clasts imply deposition by turbidity currents.

The composition of the arkosic greywacke and of the pebbles in the conglomerates (Table 3) indicate that the source for the Takla Group sediments included the following rocks:

- (a) amphibolitised gabbro, diabase, amphibolite, and chlorite schist;
- (b) porphyritic basic volcanics with phenocrysts of plagioclase, hornblende and occasionally clinopyroxene or biotite;
- (c) chert;
- (d) limestone;
- (e) K-feldspar bearing intrusives or volcanics;
- (f) chromite bearing ultramafites.

Porphyritic basic volcanics and hornblendized basic intrusives seem to have provided the bulk of the detritus. Because

basic intrusive pebbles contain albite, amphibole and epidote (a lower greenschist facies mineralogy) it seems that metamorphic rocks must have been exposed at the surface prior to deposition of the Upper Triassic. The presence of ultramafites at the surface is implied by the presence of detrital chromite within Takla Group sediments. It could be argued that the chromite originated in a layered basic intrusion. However, chromite bearing gabbroic rocks have not yet been found in the Cache Creek Group.

The most reasonable hypothesis for the provenance of the Takla Group sediments is that the detritus originated from the limestones, cherts, gabbros and greenstones belonging to the Cache Creek Group, southwest of the fault zone. It is significant that many of the basic pebbles are very similar to the gabbros and basalts exposed south of Pinchi Lake.

The presence of carbonaceous fragments suggests that the area being eroded was nearby and covered with vegetation.

Diorite

A body of hornblende diorite apparently intrudes Takla Group greywackes east of Pinchi Lake Mercury Mine, just north of the road. It is grey-green or brownish weathering and is well foliated; locally it is porphyritic or contains greenstone xenoliths. Hand specimens show

aligned phenocrysts of plagioclase (5 mm) and acicular hornblende (5 mm) set in a grey aphanitic matrix.

In thin section, 75% of the rock consists of euhedral plagioclase laths, well zoned with cores in the range An_{80-70} and extremely altered to sericite, epidote (?) and carbonate. Patchy low relief suggests partial albitization. Subhedral brown pleochroic hornblende, and minor clinopyroxene and biotite phenocrysts are also present, the first being highly altered to calcite, chlorite and sphene. The matrix consists of a microgranular mixture of plagioclase, quartz, chlorite and sphene.

Contacts, where observed, are faulted and argillites showing no signs of thermal metamorphism can be seen within a few metres of the diorite. The northeast contact has not been examined.

The age of the intrusive is uncertain. The incipient metamorphism or alteration suggests an Early Mesozoic age.

Cretaceous (?) Conglomerate

Cretaceous (?) conglomerate is exposed only at the western end of Murray Ridge where it forms two elongate knolls 1.6 km southwest of the east end of Pinchi Lake. The pebbles and cobbles are poorly sorted, sub-rounded and up to 12 cm in diameter. They consist of green chert (85%), black chert (2%), red chert (2%) and grey limestone

(3%) in a red weathering sandstone matrix (8%).

The unit dips to the south at 50° and appears to be faulted against greenstones to the north.

The age is uncertain, but because of its poorly indurated nature and lithological resemblance to conglomerates described by Armstrong (1949), it is thought to be of Cretaceous or Paleocene age.

A reddish limonitic matrix suggests subaerial deposition in a continental environment. Presumably the chert and limestone pebbles were derived from the Cache Creek Group.

III

ULTRAMAFITES AND SILICA-CARBONATE ROCKS

Ultramafites

Introduction

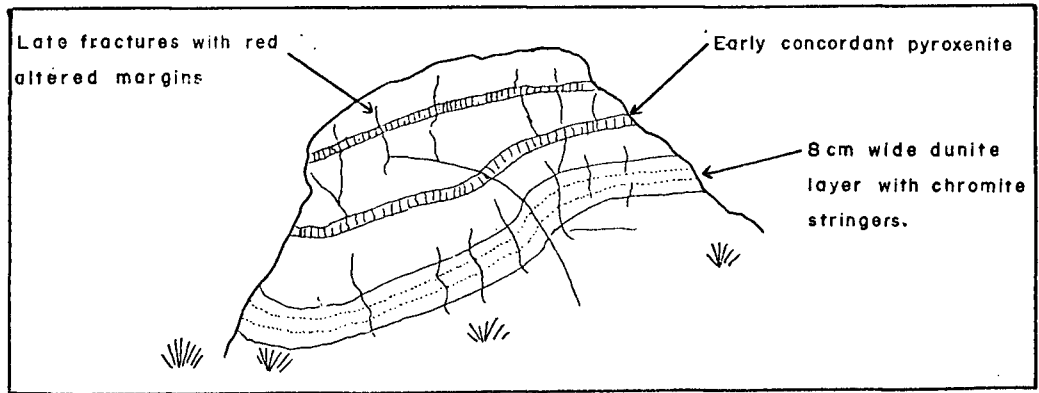
Three ultramafic bodies, on Murray Ridge, Pinchi Mountain and the northern slopes of Mount Pope, form conspicuous northwest striking ridges (Map I). Each of these ultramafites is lenticular in outline and appears to be bounded by faults.

Swampy areas, which are belts of magnetic highs, lie along the sides of the ultramafites and also along some fault zones. Diamond drilling of a magnetic high east of Pinchi Mercury Mine and near the Pinchi Fault zone intersected serpentinite. This suggests that such anomalies elsewhere in the map area are also the location of buried serpentinites. Aeromagnetic data (Map III) has been used in extrapolating serpentinite contacts beneath drift cover.

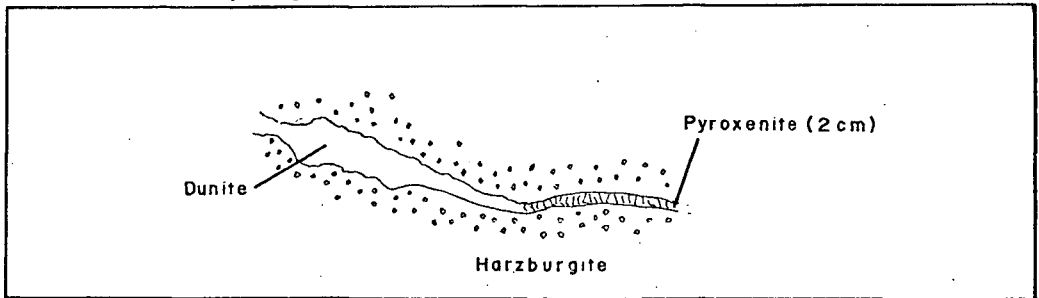
Rock Types

The dominant rock type, constituting 95% of the exposures, is harzburgite. In outcrop, it is generally

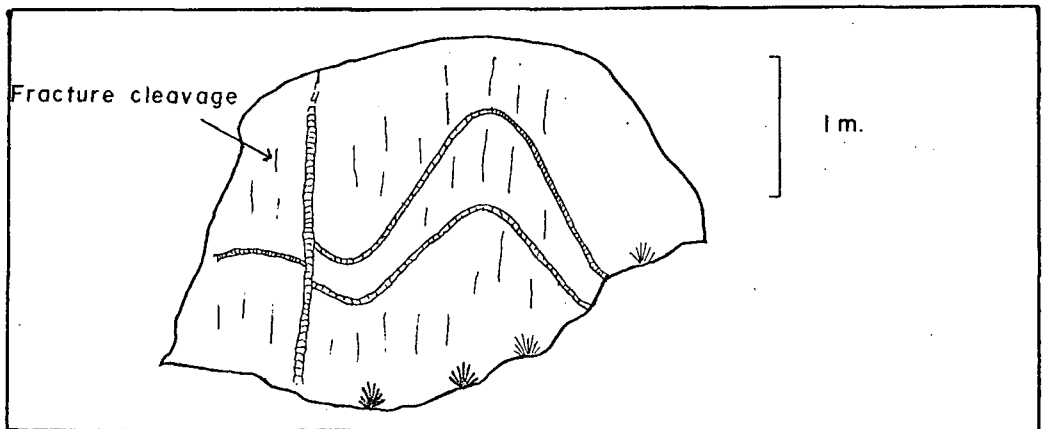
Fig. 5 STRUCTURAL FEATURES IN HARZBURGITES



(a) Concordant dunite and pyroxenite layers in harzburgite at western edge of Murray Ridge.



(b) Dunite-pyroxenite vein in harzburgite Murray Ridge



(c) Folded pyroxenite layer cut by late pyroxenite.

massive or blocky, weathers reddish brown to buff and possesses a rough mottled surface. Locally it may be intensely serpentized or fractured and difficult to recognize. However, the platy bastite serpentine which replaces 1 cm orthopyroxene grains generally persists. Dunites, comprising over 4% of the ultramafites, have a characteristic buff weathered surface which is smooth in comparison to that of the harzburgite, and are highly fractured. Pyroxenite layers are minor but are conspicuous by their differential weathering characteristics (Plates 7 & 8).

Internal structure

Much of the harzburgite is massive with no obvious foliation. However, in the vicinity of dunite or pyroxenite layers, a foliation outlined by differing olivine-orthopyroxene ratios can occasionally be discerned (Plate 9). Contacts of the dunite and pyroxenite layers with the harzburgite are gradational over 1 cm.

Dunite bodies are of two varieties: sill or vein-like dunites up to 1.5 m in thickness, and irregular dunite bodies up to 100 m in diameter. The former are commonly concordant with the layering in the harzburgite and generally contain chromite stringers (Fig. 5a, Plate 9). Occasionally, rootless folds with limbs of variable thickness are outlined by the sill-like dunites (Plate 11). Dunite veins, up to

5 cms in width, were occasionally observed giving way to pyroxenite layers (Fig. 5b). The transition from dunite to pyroxenite is sharp and occurs where the dunite vein narrows down to 2 cm in thickness. Irregular dunite bodies are relatively rare, the only well defined example being on the southern slopes of Pinchi Mountain. Contacts with harzburgite are sharp and very irregular.

Two distinct types of pyroxenite layer were observed: early concordant layers and late discordant layers. However, many layers could not be categorized.

Early concordant pyroxenite layers occur in swarms parallel to the harzburgite foliation (Plate 10). Individual layers range from 2 to 6 cm in thickness. They do not have great lateral continuity, and commonly wedge out, disappear into shear zones or are cut off by shears. Occasionally, the pyroxenite layers are folded (Plate 10) and in one case (Fig. 5c) a cross-cutting pyroxenite layer has an axial planar orientation with respect to earlier layers. The orientation of these layers is fairly regular in some regions and erratic in others. Strikes are generally westerly to northwesterly with steep northerly dips.

Late discordant pyroxenite layers are commonly up to 10 cm in width. Within harzburgite, they occasionally occur in groups (Plate 7) parallel to dunite rich layers, but usually they occur as single pyroxenite layers which

cross-cut earlier layers and irregular dunite bodies (Plate 8). A distinctive feature at a few localities is a black-weathering, serpentine-rich zone, 5 cm wide, in the harzburgite or dunite adjacent to the contacts of the pyroxenite layers. Folding of late pyroxenite layers is related to movement along late fractures.

Joints are well developed and are highly variable in frequency and orientation. One sub-horizontal and two vertical joint sets can be detected in most outcrops. Commonly one particular joint set becomes dominant and closely spaced (1 cm), in which case the term cleavage might be more appropriate, especially where there are indications of movement along the planes of discontinuity. It appears that the spacing of the joint or cleavage planes depends on the lithology and the amount of local deformation. Generally, dunites are friable because of the presence of a pervasive fracture system which subdivides the rock into a series of rhombs. Weathered pyroxenites possess a conspicuous columnar structure (Plates 7 and 8) caused by differential weathering along the serpentinized cleavage planes which transect the pyroxenite layers and offset the contacts.

In summary, field observations indicate the following sequence of events:

- (a) formation of early pyroxenite layers and dunite bodies,
- (b) folding,
- (c) formation of late pyroxenite layers,
- (d) pervasive serpentinization, and
- (e) formation of joints and cleavages and minor serpentinization.

Contact relationships

As is the case with most alpine ultramafites, contacts are poorly exposed. Where contacts are visible, in outcrop or in drill holes, highly sheared serpentinite is juxtaposed against siliceous sediments or volcanics showing no signs of thermal metamorphism. In general, contacts are thought to be the sites of major fault zones (Chapter V) which have been locally carbonatized.

Petrology

Harzburgites have an average olivine: pyroxene ratio of 7:3 and occasionally contain up to 3% clinopyroxene. Picotite constitutes 2% of the rock, and serpentine a minimum of 20%. Olivine grains (4 mm) are anhedral and veined by serpentine, giving rise to a mesh texture in highly serpentinized rocks. Disseminated grains or stringers of magnetite are commonly associated with the serpentine. Kink

bands or deformation lamellae (Loney *et al.*, 1971) are present in olivine in most thin sections.

Enstatite (En_{90} - En_{94}) partly replaced by platy bastite (lizardite according to Page, 1967) forms 1 cm grains which occasionally appear to have an intergranular relationship to olivine or to have olivine inclusions. Such textures suggest magmatic crystallization of olivine followed by orthopyroxene. Most enstatite grains contain faint exsolution lamellae parallel to (010) and blebs of augite aligned along cleavage planes. Locally, the lamellae are deformed by fractures. There is a marked tendency for both augite blebs and exsolution lamellae to survive replacement by bastite. Contrary to the observations of Raleigh (1963), there is no indication of offsetting of exsolution lamellae because of expansion during replacement by bastite. Clinopyroxene has an intergranular relationship to both orthopyroxene and olivine. Picotite grains are usually intergranular and equant but may be irregular. Commonly they are cross-cut by stringers of serpentine.

Dunites contain, on average, 70% serpentine and brucite, 30% olivine and 1% picotite or chromite. Textural features of olivine and spinel are similar to those in the harzburgites. Three types of serpentine were noted: (a) grey banded mesh serpentine, (b) cross-cutting colourless ribbon serpentine and (c) brownish serpentine grading into iddingsite. The brownish serpentine appears to be related to the pervasive

fracture cleavage and the ribbon serpentine is often found near fractures associated with chromite grains. The presence of brucite in three dunite samples was confirmed by X-ray diffraction.

The early pyroxenite layers contain on average 88% enstatite, 10% olivine and 2% picotite. Enstatite contains the characteristic (010) exsolution lamellae, occasionally contains olivine inclusions and may possess kink bands. Coarse blebs of clinopyroxene are aligned along the cleavage planes. Olivine occurs as irregular intergranular grains which have rounded boundaries with the enstatite. Picotite is intergranular and associated with olivine. The minerals in the pyroxenite layers are remarkably unaltered, with serpentine limited to the margins of the layers and to cataclastic zones formed by cross-cutting cleavages.

Only one specimen was obtained from the late discordant pyroxenite layers. It consists of 90% orthopyroxene, 8% clinopyroxene and 2% picotite.

Discussion on the origin of ultramafites

The problem of the origin of alpine ultramafites, that is harzburgite-dunite bodies possessing no apparent association with stratiform cumulate type ultramafites, is longstanding and no attempt will be made to review the various hypotheses. This has been adequately done by

Turner and Verhoogen (1960, p. 307).

Recent sampling of ultramafites in oceanic areas (Bonatti, 1971; Aumento, 1971) and a renewed interest in terrestrial ultramafites has shed much light on their origin and on crustal structure in oceanic areas. Geologists working in Cyprus (Moores and Vine, 1971) and California (Bailey *et al.*, 1970) think that ultramafites are derived from the upper mantle and that relatively undisturbed sections of oceanic crust can be found on the continents. The suggestion has been made (Monger, Souther and Gabrielse, 1972; Danner, oral communication) that much of central British Columbia is underlain by oceanic crust. This is because the Cache Creek Group possesses no apparent continental basement and contains an ophiolitic association of rock types. Ten years ago, similar ideas were tentatively suggested for the Franciscan Group, and now many geologists (Ernst, 1965; Page, 1972) accept the view that the Franciscan Group and part of the Great Valley sequence were deposited on oceanic crust. This hypothesis must be tested seriously for British Columbia.

Concerning the origin of the ultramafites in the area, two theories will be discussed as representative of current hypotheses. McTaggart (1971) suggested that "Ultramafic bodies originated as cumulates in basic magma chambers high in the crust. . . . These were subsequently folded, or dismembered by faulting, and because of their

high density, subsided during tectonism, to form cold fault enclosed intrusions." The main advantage of this hypothesis is that it explains why bodies of high density should be found at high levels in the earth's crust amidst sediments of relatively low density. It does, however, possess serious deficiencies. First, in the cases where data on fabric and mineral compositions are available, (Loney *et al.*, 1971) it has been demonstrated that the alpine ultramafites are metamorphic tectonites which have recrystallized at approximately 1200°C after primary magmatic crystallization. High temperature recrystallization could not have taken place during tectonism of an ultramafite situated within the low greenschist facies Cache Creek Group rocks. Secondly, McTaggart suggests that ultramafites of British Columbia are complementary to Late Paleozoic or Triassic volcanics. However, according to Stueber and Murthy (1966), typical alpine ultramafites possess unique Rb/Sr and Sr^{87/86} values which are not related genetically to spatially associated gabbros and volcanics. Because data on fabric and Rb/Sr values are not available for ultramafites in British Columbia, McTaggart's hypothesis cannot yet be disproved.

A second, more attractive theory is that proposed by the Californian school (Coleman and Keith, 1971; Coleman, 1971). Their model involves crystallization of a primary ultramafic magma followed by plastic deformation and recrystallization during which a mineralogical foliation,

olivine microfabric and characteristic interlocking textures were formed. Fracturing and serpentinization of the cooled peridotite occurred on tectonic emplacement in the Franciscan melange. This model is, of course, influenced by current ideas on plate tectonics. It is envisaged that the primary peridotite forms at an active oceanic ridge, acquires a tectonic fabric in the upper mantle and undergoes cooling, fracturing, emplacement and serpentinization at a subduction or obduction zone at the plate margin. The main weakness of this theory is the problem, effectively dealt with by McTaggart, of emplacement of dense peridotites high in the crust. Presumably this is overcome by density lowering during partial serpentinization, tectonic emplacement and/or "rafting up" of ultramafites by relatively light sediments on isostatic uplift (Burch, 1968).

Recent intensive work on the Burro Mountain peridotite in California (Burch, 1968; Page, 1967; Loney *et al.*, 1971; Coleman and Keith, 1971) has contributed to the formation of the above mentioned model. This ultramafite closely resembles those in the Pinchi area, both petrologically and structurally. Fabric data and detailed structural information are not available for the Pinchi ultramafites, but it is felt that the similarity to Burro Mountain is sufficiently great to warrant some extrapolation of conclusions.

Origin of Pinchi ultramafites

The origin of the primary mineralogy and textures in ultramafites is conjectural. Loney *et al.* (1971) suggest that harzburgite and dunite crystallized penecontemporaneously from genetically related ultramafic magmas rather than having differentiated from a basic magma or having formed as a residual product of partial melting of the primitive mantle. They substantiate this by pointing out the lack of cryptic or rhythmic layering in alpine ultramafites and the dearth of cumulate textures compared with stratiform layered complexes such as the Bushveld and Stillwater. As positive evidence for a magmatic origin, they state that the differences in the chemistry of olivine and chromite in different dunite bodies suggest that the harzburgite has been intruded by dunite magmas of contrasting composition. Ringwood (1962) suggested that alpine ultramafites are the residual products of partial melting of the primitive mantle. This possibility is given some support by the Rb/Sr work of Stueber and Murthy (1966) who suggested that alpine ultramafites are residual and were probably depleted of lithophile elements at some early stage in their history.

On the basis of the work done at Pinchi so far, the above mentioned hypotheses cannot be substantiated or refuted. However, textures which are suggestive of magmatic

crystallization (p. 52) do exist and may be a relict feature of a primary magmatic origin.

The origin of the concordant harzburgite-dunite-pyroxenite layering is also problematical. Four hypotheses have been suggested:

- (a) crystal settling from a magma (Raleigh, 1965),
- (b) magmatic intrusion of dunite and pyroxenite dykes and sills (Loney *et al.*, 1971),
- (c) metasomatic replacement along fractures (Bowen, 1949) and
- (d) metamorphic differentiation caused by shearing stress and differing physical properties of olivine and pyroxene (Burch, 1968).

The first hypothesis receives support from a study by Raleigh (1965) carried out on the Cypress Island peridotite, considered to be a typical alpine type ultramafite. It contains a dunite-chromitite-harzburgite layering and accumulative textures which Raleigh considered to have formed by crystal settling from a magma. Later recrystallization and penetrative deformation produced a preferred orientation of olivine. However, Burch (1968) decided against such an origin for the pyroxenite-dunite-harzburgite layering in the Burro Mountain peridotite because of the sharpness of contacts between layers and absence of cryptic layering, rhythmic layering, graded bedding and well defined cumulate

textures. This also appears to be the case at Pinchi but, because little is known about the primary magmatic conditions and the extent of modification by recrystallization and deformation, crystal settling must be considered a possible mechanism for layer formation.

Magmatic intrusion (b) is a plausible hypothesis for the origin of the irregular dunites. However, it does not explain the common parallelism of dunite and pyroxenite layers, the similarity in thickness of pyroxenite layers and the absence of cross-cutting relationships between dunite layers and early pyroxenites. Bowen (1949) suggested that SiO_2 -deficient fluids moving along fractures (c) could result in replacement of orthopyroxene by olivine, forming dunite layers. Presumably, it would also be possible for SiO_2 -rich fluids to cause replacement of olivine by orthopyroxene. This hypothesis possesses similar deficiencies to that of magmatic intrusion. In addition, it is difficult to explain why metasomatic fluids should be of different compositions in adjacent layers.

Burch (1968) suggested that pyroxenite and dunite layers are formed by metamorphic differentiation along shears because of the differing physical properties of olivine and orthopyroxene. He argued that dunite would tend to concentrate in areas of shear, as olivine yields readily by plastic flow, and pyroxene would concentrate in areas of least stress or potential tension fractures.

As dunite and pyroxenite layers are concordant, olivine segregation in a shear plane may have left a pyroxene-rich residue, thus giving rise to the observed parallelism of dunite and pyroxenite layers. This hypothesis is also considered acceptable because it explains the absence of early pyroxenite layers in dunites.

The pyroxenite and dunite layers within the Pinchi ultramafites have been folded. Similar structures have been observed at Burro Mountain (Loney *et al.*, 1971) where olivine fabric data indicated the presence of a pervasive planar fabric which cross-cuts harzburgite-dunite contacts and is axial planar to minor folds. Analyses of co-existing olivine and chrome spinel suggest that this fabric recrystallized at an approximate temperature of 1200°C. This conclusion is supported by experimental work on olivine deformation at 1200°C which produced a fabric similar to that present in dunites from Burro Mountain (Ave L'Allement and Carter, 1969). On the basis of similarities in internal structure between the Burro Mountain and Pinchi ultramafites it is suggested that the latter has also undergone a deep-seated plastic deformation at 1200°C.

The origin of the late discordant pyroxenite layers can possibly be explained by folding of pre-existing layers and formation of a new generation of shear planes cross-cutting the early layers. However, this hypothesis cannot explain the occurrence of late pyroxenite veins

cutting irregular dunite bodies. It is therefore concluded that the origin of the late discordant pyroxenites has to be accounted for by magmatic intrusion of an "orthopyroxenite magma," or, more likely, by metasomatic activity.

The formation of kink bands in olivine is related to the glide system {Ok1} [100]. Experimental evidence (Ave L'Allemand, 1968) indicates that this glide system operates predominantly in the temperature range 900° to 1200°C and suggests that kink band formation took place after recrystallization at 1200°C and prior to serpentinization.

The main period of serpentinization is believed to have been contemporaneous with fracturing and emplacement during the F_1 and F_2 deformations (Chapter V). The pressure-temperature conditions of serpentinization are discussed in Chapter IV (p.116).

Two hypotheses are considered for the emplacement of ultramafites. The first involves overthrusting of oceanic crust during Permo-Triassic tectonism, in which case, the Pinchi ultramafites may be downfaulted remnants of an ophiolitic cover to the Cache Creek Group. The second hypothesis suggests solid emplacement of a fault-bounded block of low average density (2.7-2.8 gms/cc) containing cherts, limestones, schist and serpentinized peridotite, along zones of low pressure in the Pinchi Fault system. These hypotheses are further discussed in Chapter VI.

The latest deformational event within the ultramafites was the formation of a complex fracture cleavage associated with minor serpentinization. This may have occurred during the latter stages of the F_2 deformation or during the F_3 deformation (Chapter V).

Silica-carbonate Rocks

Distribution

Because of their resistance to erosion, carbonatized serpentinites are conspicuous in the field. Generally they form a colinear series of rusty weathering south facing bluffs up to 120 m wide occurring sporadically along fault zones at the margins of ultramafites. The best examples are on the southern slopes of Pinchi Mountain and at the southeast end of Pinchi Lake. Carbonatized ultramafites are also found in the vicinity of Pinchi Mercury Mine and the Darbar claim group, 7 miles northeast of Fort St. James.

Rock types, internal and external structure

Ferroan magnesite, the predominant constituent in the silica-carbonate rocks, is orange-brown and has a rough weathered surface because of the presence of anastomosing quartz veinlets. Relict chromite grains or pale green mariposite (fuchsite) are commonly seen in hand specimen.

Layers of sugary white magnesite, up to 1 m in thickness are occasionally found. These layers contain inclusions of ferroan magnesite.

Compositional layering within the ferroan magnesite zones is parallel to the contacts and is defined by silicified breccia zones and white magnesite layers (Plate 5). The contacts of relict lenses of serpentized harzburgite are concordant with the layering and are highly sheared and veined by magnesite. Dips are to the north or northeast at approximately 60° . A magnesite zone on the south side of Pinchi Mountain lies structurally beneath ultramafic and glaucophanitic rocks and overlies the Pinchi Mountain greenstones. However, on the assumed path of the Pinchi Fault, at the southeast end of Pinchi Lake, silica-carbonate rocks appear to pass under Upper Triassic rocks. On the Darbar claim group the foliation in carbonatized serpentinites parallels a fault zone which dips under greenstones at 60° to the northeast. All the evidence is compatible with the hypothesis that the layering originated during contemporaneous carbonatization and movement along major faults.

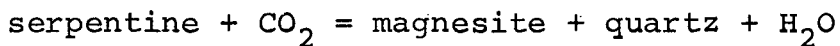
Late brecciation affected all the above mentioned rocks. Dilatational fractures or voids were filled in turn by dolomite, chalcedonic quartz or agate and crystalline quartz. Dolomite veins cut by quartz veins are common, the former possessing striated crystals with long axes

perpendicular to the sides of fractures. These late veins are cross-cut by a near vertical set of north-south striking fractures.

Petrology

The silica-carbonate rocks consist of ferroan magnesite ± quartz ± serpentine. Magnesite and quartz are usually microcrystalline but may be locally coarse grained. Relict subhedral chromite possessing reddish translucent margins is common in all specimens. Annabergite ("nickel bloom") is found on fracture surfaces near Pinchi Mine.

The presence of relict chromite and lenses of serpentinized harzburgite within the silica-carbonate rocks demonstrates that they were ultramafites prior to alteration by CO₂ along fault zones. The most common equilibrium mineral assemblage is magnesite + quartz, but antigorite + magnesite is also present in one specimen. Talc is not present. Considering these assemblages, the reaction:



is applicable. This has been studied experimentally and theoretically by Greenwood (1967) and Johannes (1969).

Their data indicate:

- (a) the assemblage antigorite + magnesite must have formed at low partial pressure of CO₂ (X_{CO_2} less than 0.03 at 1 kb);

- (b) the predominant assemblage magnesite + quartz is stable at X_{CO_2} greater than 0.03 at 1 kb and 300°C and
- (c) the temperature of the reaction was less than 350°C at 4 kb and less than 310°C at 1 kb.

Antigorite is considered a "high temperature" serpentine mineral (Wenner, 1971; Coleman, 1971). Therefore, the occurrence of antigorite and the quartz-magnesite assemblage suggest that the temperature of formation of the silica-carbonate rocks was in the 200° to 300°C range.

Age and origin

Carbonatization is restricted to the major faults in the area. Because of the presence of silicified magnesite breccias it is considered likely that the layering within the silica-carbonate rocks was controlled by movement along faults during alteration. Therefore, the problem of the timing of the alteration is associated with the timing of active faulting.

A number of authors consider that active faulting associated with the Laramide orogeny took place before the Late Eocene. In the McConnell Creek map area and on the Spatsizi Plateau, Sustut Group rocks of Upper Cretaceous to Paleocene age have been actively involved in northeasterly directed thrust faulting (Lord, 1949; Eisbacher, 1969). North of Fort St. James, conglomerate beds of Cretaceous

or Paleocene age are found intermittently along the Pinchi Fault zone (Armstrong, 1949) and such a conglomerate is found at the west end of Murray Ridge apparently in fault contact with older rocks. Roots (1953) stated that rocks of the Takla Group are carbonatized adjacent to a mercury mineralized fault zone the continuation of which is believed to displace rocks of Cretaceous or Paleocene age in the Aiken Lake map area. For these reasons, evidence favours a period of active faulting associated with carbonatization in the Fort St. James area during the Eocene.

The formation of silica-carbonate rocks is commonly considered as an early stage of the hydrothermal activity which later results in the deposition of cinnabar (Bailey, 1963; Henderson, 1968). Cinnabar mineralization is generally considered epithermal, and cinnabar is at present being deposited by hot springs at various locations in the western United States (White, 1968, p. 1675). Henderson (1968) states that cinnabar deposits in the silica-carbonate rocks of California occur at depths of less than 800 m and commonly the sequence of events is:

- (a) silica-carbonate alteration of serpentinite,
- (b) fracturing of silica-carbonate rock, and
- (c) cinnabar vein mineralization of the fractures.

In the Pinchi area, cinnabar mineralization occurs as fracture fillings in silica-carbonate rocks at two localities

and it is suggested that the history of mineralization is similar to that of the Californian occurrences and that the mineralization took place in a near surface environment after the formation of the silica-carbonate rocks. J.E. Armstrong (1966) and H.W. Tipper (oral communication) also consider the mercury mineralization in British Columbia to be of Tertiary age.

In summary, evidence favours the following sequence of events:

- (a) The silica-carbonate rocks were formed during a reactivation of the Pinchi Fault in the Eocene. Carbon dioxide--rich fluids, possibly acting as lubricants in the fault plane, reacted with adjacent ultramafites giving rise to the magnesite + quartz assemblage. The type of faulting and sense of movement is unknown, but northeasterly directed thrusting was widespread 240 km to the north during the Eocene (Eisbacher, 1970). The common occurrence of northeasterly dipping fault planes suggests that similarly oriented stresses may have given rise to underthrusting in the Pinchi area, but this is speculative.
- (b) Fracturing of the silica-carbonate rocks occurred during the Eocene, Oligocene or Miocene contemporaneous with hot spring activity and mercury mineralization.

IV

METAMORPHISM

I. METAMORPHISM IN GREENSTONE AND BLUESCHIST FAULT BLOCKS

Introduction

Four possible hypotheses currently exist which attempt to explain the occurrence of the "high pressure" blueschist facies mineralogy. The hypotheses are listed below together with their principal exponents.

- (a) The necessary pressures are attained by tectonic overpressures in addition to lithostatic pressures (Blake, Irwin and Coleman, 1967, 1969).
- (b) High pressures are attained by an "internally created gas overpressure" (Brothers, 1970).
- (c) Blueschist facies minerals are formed metastably at lower pressures than those indicated in experimental studies because of reducing conditions in the pore fluid accompanying metamorphism (Gresens, 1969).
- (d) Blueschist facies mineral assemblages are formed at high lithostatic pressures and relatively low temperatures (Fyfe, Turner and Verhoogen, 1958, p. 226; Ernst, 1965, 1971b).

A brief summary of each of these hypotheses follows with emphasis on aspects of the metamorphism at Pinchi which bear directly on the problem of discriminating between the suggested hypotheses.

The hypothesis of Blake, Irwin and Coleman (1967, 1969) that tectonic overpressures in a fault zone can explain blueschist mineralogy has been shown to be unlikely by Brace *et al.*, (1970) who showed experimentally that Franciscan greywacke cannot support even one kilobar of tectonic overpressure and by Ernst (1971b) who concludes that none of the geologic, structural, petrographic or experimental work is consistent with the existence of sufficient tectonic overpressure.

At Pinchi, the hypothesis of tectonic overpressures finds no support in structure or tectonic fabric. No gradation exists in metamorphic reconstitution towards the Pinchi Fault and metabasalts and jadeitized metagreywackes commonly contain relict igneous or clastic textures (Appendix IV). Their unsheared nature excludes the possibility of a significant contribution from tectonic overpressure. There may well be a tectonic-genetic relationship between the glaucophanitic rocks and the Pinchi Fault but there is no evidence that movement on the fault produced tectonic overpressure in the adjacent rocks.

Brothers (1970) proposed an hypothesis involving the crystallization of lawsonite-aragonite rocks in an

environment with an "internally created gas overpressure." This overpressure was thought to be contained by an impermeable tectonic seal in the form of an overlying ultramafite. Under such conditions, $P_{\text{fluid}} = P_{\text{solids}}$ (Greenwood, 1961) but locally, $P_{\text{fluid}} = P_{\text{solids}} > P_{\text{lithostatic}}$. This hypothesis is unsupported by the Pinchi rocks because it seems unlikely that P_{fluid} could exceed $P_{\text{lithostatic}}$ throughout a regionally metamorphosed terrain and because there is no evidence for an "impermeable tectonic seal" which could have encapsulated the blueschists.

Gresens (1968) emphasized the global association of ultramafites with blueschists and suggested that the presence of ultramafites undergoing serpentinization and oxidation of iron resulted in the formation of a reducing pore fluid in the adjacent sediments. This pore fluid induced the metastable growth of the characteristic blueschist facies minerals at lower pressures than those indicated by experimentally produced P/T stability diagrams.

In addition to the arguments advanced by Ernst (1971b) against this hypothesis, field evidence at Pinchi demonstrates that ultramafites are commonly associated with greenstones belonging to the prehnite-pumpellyite facies rather than the lawsonite-glaucophane bearing rocks. Gresens' hypothesis is therefore not directly applicable

to the Pinchi blueschists. However, there is evidence at Pinchi that indicates some of the blueschist facies minerals crystallized under reducing conditions and certain aspects of the hypothesis are therefore worthy of consideration. These are discussed later (p. 96).

The fourth hypothesis for blueschist formation involves high lithostatic pressures and relatively low temperatures (Fyfe, Turner and Verhoogan, 1958; Ernst, 1965, 1970, etc.). The hypothesis is based largely on the favourable comparison of the observed mineral paragenesis with experimentally determined phase equilibria.

In the succeeding sections, it is demonstrated

- (a) that the Pinchi blueschists formed at high pressures, and
- (b) that methane may have been an important constituent of the fluid phase in metamorphic assemblages which contain carbonaceous material.

Paragenetic Sequence of Minerals

Possible mineral paragenetic sequences for metabasic rocks and metacherts based on textural and field evidence are given in Figs. 6 & 7. As extensive work has been done recently on progressive metamorphism of Franciscan greywackes, a paragenetic sequence is taken from Ernst (1971) and the stage of evolution of the Pinchi greywackes is indicated for comparison.

FIG. 6

MINERAL PARAGENESES

NETABASALTS

Minerals	Greenstones	Blueschists	Late minerals
albite	—————		-----
sodic pyroxene	-----		
aegirite-jadeite		—————	
chlorite	—————		
quartz	—————		
calcite	-----		-----
aragonite	-----		-----
pumpellyite	—————		
white mica	—————		-----
celadonite	—————		
sphene	—————		
glaucophane		—————	-----
lawsonite		—————	
stilpnomelane			-----
prehnite	-----		-----
brown amphibole			-----
deerite			-----
pyrite	-----	?	
magnetite		-----?	
hematite			-----
	Increase in P →		← Decrease in P

ECLOGITE

	Early minerals	Late minerals
omphacite	—————	
garnet	—————	
rutile	-----?	
glaucophane		—————
lawsonite		—————
sphene		—————
brown amphibole + chlorite		-----
		Decrease in P (?) →

————— : major constituent
 ----- : minor constituent
 ----- : accessory constituent

FIG. 7

MINERAL PARAGENESES

METACHERTS

Minerals	Early minerals	Blueschist facies	Late minerals
glaucophane			
lawsonite			
quartz			
white mica	-----?		-----
pyrite	-----?		
hematite			-----
albite	-----?		-----
carbonaceous material			
sphene			
acmitic pyroxene			-----

METAGREYWACKES

Minerals	Diablo Range (Ernst, 1971) increasing grade	Finchi area
clastic biotite	-----	
pumpellyite	-----	
lawsonite	-----	
albite	-----	
jadeitic pyroxene	-----	
glaucophane	-----	
white mica		
chlorite	-----	
stilpnomelane	-----	
calcite	-----	
aragonite	-----	
quartz	-----	
rock fragments	-----	
sphene	-----	

— : major constituent
 — : minor constituent
 ----- : accessory constituent

Mineral Assemblages

Details of the petrography, mineral assemblages and specimen locations of the fault bounded blocks containing the greenstones of Pinchi Mountain and the glaucophanitic rocks are given in Appendix IV.

Equilibrium phase assemblages can be summarized as follows:¹

(a) Greenstones of Pinchi Mountain

(i) ab + NaPx + chl + sph ± wh m ± arag ± pump ± celad

(ii) qtz + NaPx + chl + sph ± wh m ± arag

(iii) arag + dol (only in intercalated limestones)

(iv) ab + chl + pump + sph ± prehn ± cc ± celad ± wh m

(only found at west end of Murray Ridge)

(b) Glaucophane-lawsonite bearing assemblages

Metabasic rocks

(v) acm-jd + lws + sph + chl ± wh m ± arag ± glph (massive)

(vi) glph + lws + sph ± chl ± wh m (foliated)

Limestone

(vii) arag + carbonaceous material ± dol ± qtz

Metasediments

(viii) arag + qtz ± wh m

(ix) qtz + lws + glph + wh m + chl

(x) qtz + wh m ± lws ± glph ± carb mat ± sph ± py

¹Abbreviations

glph = glaucophane; NaPx = sodic pyroxene; acm-jd = acmite-jadeite; lws = lawsonite; qtz = quartz; ab = albite; chl = chlorite; sph = sphene; wh m = white mica (phengite); arag = aragonite; pump = pumpellyite; celad = celadonite; prehn = prehnite; cc = calcite; dol = dolomite; stilp = stilpnomelane; py = pyrite; carb mat = carbonaceous material.

TABLE 4

GENERALIZED PARAGENETIC SEQUENCE OF METABASALTS

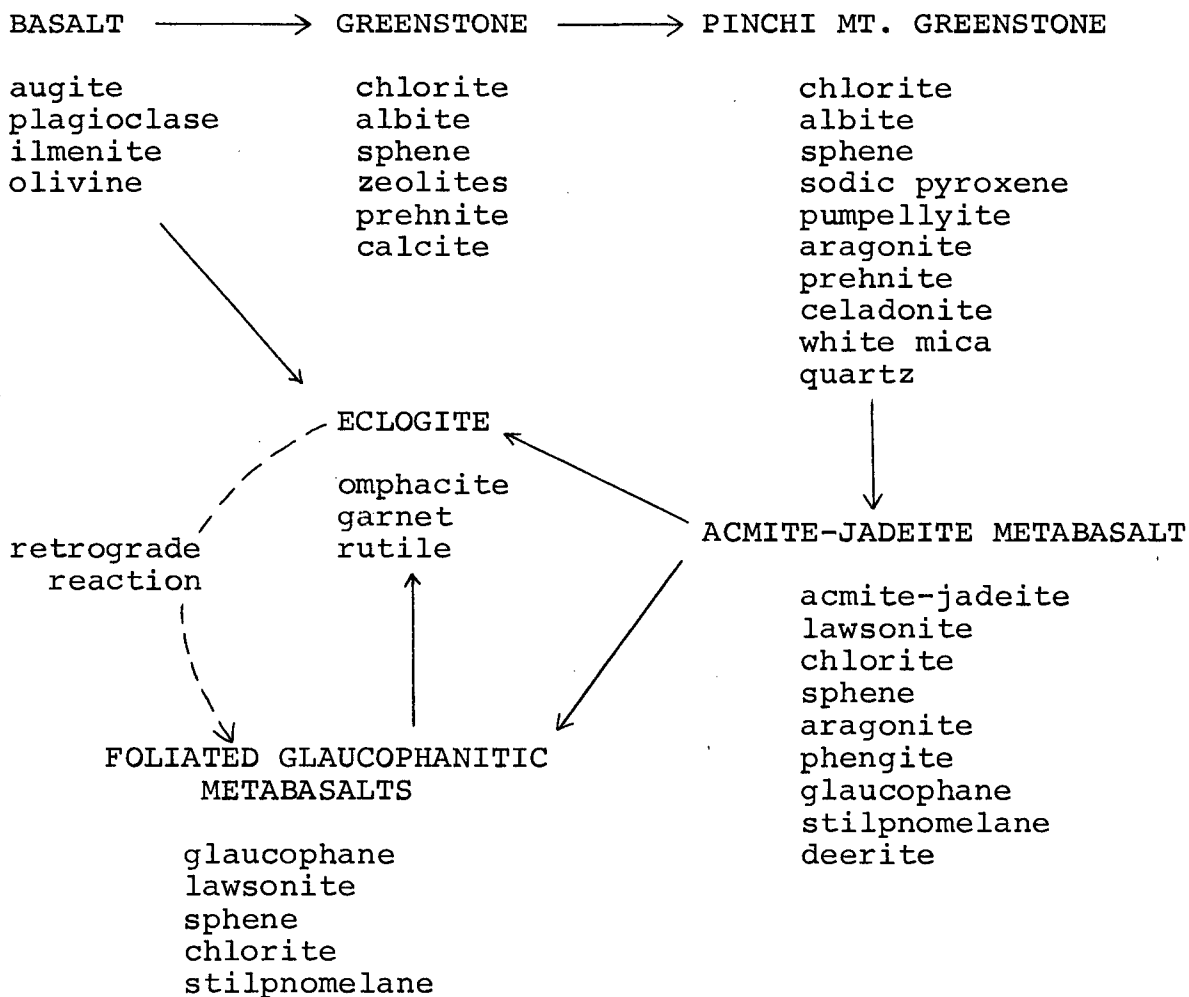


TABLE 5a POSSIBLE REACTIONS IN METABASIC ROCKS

(A) Metastable reactions

- (1) plagioclase = x albite + (1-x) anorthite
 (2) 2 ilmenite + $\frac{1}{2}$ O₂ = hematite + 2 rutile
 (3) anorthite + rutile = sphene + Al₂SiO₅
 (Al-Si component in phengite or chlorite)
 (4) 7 anorthite + 5 diopside + 10H₂O = 6 prehnite + chlinochlore + 3 quartz
 (5) 6Ca(Mg,Fe)Si₂O₆ + 4H₂O + 6CO₂ = (Mg,Fe)₆Si₄O₁₀(OH)₈ + 6CaCO₃ + 8SiO₂
 augite chlorite calcite

(B) Significant prograde reactions (i.e. greenstones — lawsonite-glaucophane metabasites)

- * (6) calcite = aragonite
 ** (7) laumontite + prehnite + chlorite = pumpellyite + quartz + H₂O
 (8) amesite(chlorite) + 8 prehnite + 2H₂O = 4 pumpellyite + 2 quartz
 * (9) laumontite = lawsonite + 2 quartz + 2H₂O
 * (10) heulandite = lawsonite + 5 quartz + 4H₂O
 ** (11) Ca(Mg,Fe)Si₂O₆ + Na⁺ + (Al,Fe)³⁺ = Na(Al,Fe)Si₂O₆ + Ca²⁺ + (Mg,Fe)²⁺
 augite soln. jadeite-acmite soln.
 (12) NaAlSi₃O₈ + 0.33Fe₃O₄ + 0.17O₂ = NaFeSi₂O₆ + 0.5 Al₂O₃ + SiO₂
 albite hematite acmite comp. Al-Si component in phengite or
 in pyroxene chlorite
 (13) NaAlSi₃O₈ + (Mg,Fe)₆Si₄O₁₀ + 0.12O₂ = NaAl_{.5}Fe_{.5}Si₂O₆ + (Mg,Fe)_{5.5}Al_{.5}Si_{3.88}O₁₀(OH)₈
 albite chlorite-1 acmite-jadeite chlorite-2
 + 1.12 SiO₂
 * (14) albite = jadeite + quartz
 ** (15) 2 albite + Ca²⁺ + 2H₂O = lawsonite + 2 Na⁺ + 4 SiO₂
 H₂ $\frac{1}{2}$ O₂
 (16a) 2 acmite + 3 hematite + 4 quartz + CH₄ = riebeckite + magnetite + C + H₂O
 * H₂O O₂
 H₂ .25O₂
 (16b) 2 acmite + 1.5 hematite + 4 quartz + CH₄ + .25O₂ = riebeckite + C + H₂O
 H₂O .75O₂
 fluid fluid
 (17) 2 albite + 0.5 chlorite(serpentine) = glaucophane + water

(C) Possible reactions relating Pinchi assemblages, with higher temperature

(i.e. greenschist facies) assemblages.

- * (18) lawsonite = anorthite + 2H₂O
 * (19) 4 lawsonite = 2 zoisite + kyanite + quartz + 7H₂O
 sillimanite
 * (20) 12 prehnite + 6 clinochlore + 2 quartz = 12 clinzoisite + 5 serpentine + 10H₂O
 * (21) 20 pumpellyite = 16 clinzoisite + 5 amesite + 16 grossular + 14 quartz + 2H₂O
 (22) 24CaAl₂Si₂O₇(OH)₂·H₂O + 5Mg₆(Si₄O₁₀)(OH)₈ = 12Ca₂Al₃Si₃O₁₂(OH) + 6Mg₃Al₂Si₃O₁₀(OH)₈
 lawsonite chlorite clinzoisite chlorite
 + 14SiO₂ + 38H₂O (Turner, 1968. p.155)
 * (23) ferroglaucophane + $\frac{1}{2}$ O₂ = 2 albite + 2 quartz + magnetite + H₂O

* experimental determination - see Fig. 8 for position of equilibrium curve and author
 ** unbalanced or ionic reaction
 mineral compositions are given in Table 5b

TABLE 5b

MINERAL COMPOSITIONS

pumpellyite: $\text{Ca}_4\text{MgAl}_5\text{O}(\text{OH})_3(\text{Si}_2\text{O}_7)_2(\text{SiO}_4)_2 \cdot 2\text{H}_2\text{O}$;

prehnite: $\text{Ca}_2\text{Al}_2\text{Si}_3\text{O}_{10}(\text{OH})_2$;

grossular: $\text{Ca}_3\text{Al}_2(\text{Si}_3\text{O}_{12})$;

clinozoisite: $\text{Ca}_2\text{Al}_3\text{Si}_3\text{O}_{12}(\text{OH})$;

amesite: $\text{Mg}_4\text{Al}_4\text{Si}_2\text{O}_{10}(\text{OH})_8$;

clinochlore: $\text{Mg}_5\text{Al}_2\text{Si}_3\text{O}_{10}(\text{OH})_8$;

serpentine: $\text{Mg}_6\text{Si}_4\text{O}_{10}(\text{OH})_8$;

laumontite: $\text{CaAl}_2\text{Si}_4\text{O}_{12} \cdot 4\text{H}_2\text{O}$;

heulandite: $\text{CaAl}_2\text{Si}_7\text{O}_{18} \cdot 6\text{H}_2\text{O}$;

glaucophane: $\text{Na}_2\text{Mg}_3\text{Al}_2\text{Si}_8\text{O}_{22}(\text{OH})_2$;

riebeckite: $\text{Na}_2\text{Fe}_3^{+2}\text{Fe}_2^{+3}\text{Si}_8\text{O}_{22}(\text{OH})_2$;

ferroglaucophane: $\text{NaFe}_3^{+2}\text{Al}_2\text{Si}_8\text{O}_{22}(\text{OH})_2$;

(c) Eclogite

(xi) garnet + omphacite

(xii) glph + lws + sph + stilp (retrograde).

Metamorphic Reactions

Mineral chemistry is given in Appendix II and bulk rock chemistry in Appendix III.

Metabasic rocks

Prior to metamorphism, the mineralogy of the metabasic rocks was augite + plagioclase + ilmenite ± olivine. These minerals are metastable under low grade metamorphic conditions in the presence of water. Introduction of H₂O may have had a catalytic effect on their breakdown. Reactions illustrating breakdown of primary minerals are illustrated in Table 5. Chlorite, albite, calcite and sphene were probably the most important breakdown products, with prehnite and the zeolites heulandite and laumontite as possible additional phases. Progressive depth zonation involving such minerals has been demonstrated by Coombs (1961) and Jolly and Smith (1972). It is suggested that the Pinchi greenstones may also have passed through this stage during burial.

The greenstones of Pinchi Mountain are characterized by the absence of calcite, zeolites and prehnite and the presence of aragonite, pumpellyite and sodic pyroxene. Glaucofane and lawsonite are present as minor constituents

in two samples. Aragonite presumably recrystallized from calcite present in amygdules, veins or interbedded limestones. Pumpellyite formation is problematical. Coombs (1961) considers that reaction 7 (Table 5) is applicable and Hinrichsen and Schurmann (1972) experimentally investigated breakdown of pumpellyite in reaction 8. The absence of the zeolites laumontite and heulandite can be explained by reactions 9 and 10.

Sodic pyroxene may have formed as the result of two processes. Firstly, relict augite may have taken part in a cation exchange reaction with the fluid phase (reaction 11). Epitaxial sodic pyroxenes are common and analyses (p. 206) show them to be poorer in Ca and Mg and richer in Na, Al and Fe with respect to relict augites. Secondly, Kerrick (1971) proposed reaction 12 as being of importance in the formation of the acmitic component in jadeitic pyroxene in metagreywackes. In the Pinchi rocks, iron oxides would have been available on the breakdown of ilmenite at low temperatures. On depletion of iron oxides, albite may coexist with sodic pyroxene, a compatibility often observed. Hematite and albite were not found together in any specimen. The residual Al_2O_3 and SiO_2 most likely take part in reactions forming chlorite or pumpellyite. The assemblage sodic pyroxene + chlorite + sphene + quartz \pm aragonite, present in a few rocks,

presumably reflects reaction 12 having gone to completion because of suitable compositional requirements, f_{O_2} or kinetics. There is no evidence to suggest that the absence of albite is because of higher pressure conditions.

The lawsonite-glaucophane bearing rocks probably developed by reconstitution of the assemblages present in the Pinchi Mountain Greenstones. These blueschists are distinguished by the absence of pumpellyite, prehnite, albite and celadonite and the presence of widespread glaucophane, lawsonite and jadeite-acmite. Stilpnomelane, phengite and deerite may also be present. Pyroxene, glaucophane and chlorite compositions are given in Appendix II. Two main assemblages are commonly recognized within the metabasic rocks and are characterized by the presence of acmite-jadeite or glaucophane. Textural relationships indicate that the glaucophanitic assemblages formed later. Therefore, it appears that greenstones reacted to form acmite-jadeite assemblages which in turn reacted to give glaucophanitic assemblages (Table 4).

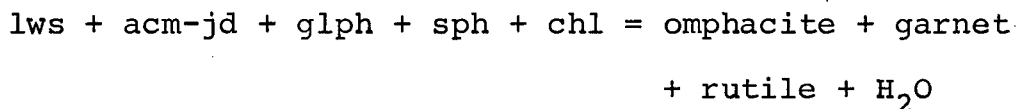
The main minerals within acmite-jadeite metabasalts are lawsonite, chlorite, acmite-jadeite and sphene. Lawsonite formation (Table 5, reaction 15) commonly occurs within albite pseudomorphs. It appears that on the breakdown of albite, Ca entered the pseudomorphs and lawsonite nucleated. The calcium originated from the breakdown of relict augite (Reaction 11), pumpellyite or prehnite.

The presence of white mica and chlorite in pseudomorphs associated with lawsonite, suggests inward diffusion of potassium, magnesium and iron in addition to calcium. The jadeite-acmite component in the pyroxene progressively increased as a result of reactions 11 and 12 (described previously). Reaction 13 may have been of importance but there is little evidence to support it from the available chlorite analyses. The absence of celadonite as a separate phase can be accounted for by increase in extent of solid solution in phengite (see p. 90).

Glaucophanitic rocks appear to have formed from acmite-jadeite assemblages. Evidence for this is seen in the common occurrence of glaucophane veins which cross-cut acmite-jadeite bearing assemblages. Many rocks show transitional characteristics and contain glaucophane and acmite-jadeite. In such rocks, glaucophane commonly rims or cross-cuts acmite-jadeite porphyroblasts. Inspection of bulk compositions (Table 16a) reveals only minor differences between acmite-jadeite and glaucophane rocks and it is suggested that glaucophanitic assemblages were formed from acmite-jadeite assemblages as a result of a reaction similar to no. 16 (Table 5). Glaucophane may also have been produced by reaction of albite and chlorite. This reaction (17) can be combined with no. 16 to give crossite.

It is generally considered that the prehnite-pumpellyite and blueschist facies pass into the greenschist facies with increase in temperature. Associated with this transition is the breakdown of such minerals as prehnite, pumpellyite and lawsonite and the growth of epidote and tremolite-actinolite (Table 5). The absence of these last mentioned minerals at Pinchi puts a somewhat ill-defined upper limit on the temperature of metamorphic recrystallization.

The occurrence of eclogite boulders in the Pinchi area might suggest, as illustrated in Table 4, that they are the product of the next stage in the metamorphism of the metabasic rocks. Presumably, the critical reaction must be of the type:



Being a dehydration reaction, it would be favoured by increase in temperature as univariant curves for such reactions have steep slopes on the petrogenetic grid. However, according to Morgan (1970) eclogites may form directly from dry basalts without the involvement of H_2O . Within the eclogite, garnet and omphacite are replaced by glaucophane, lawsonite, sphene and stilpnomelane. It is suggested that this occurred during retrogressive metamorphism associated with decrease in temperature and pressure, reversal of the above

reaction and re-entry into the glaucophane-lawsonite facies.

Metasediments

Assemblages in metasedimentary rocks are given in Tables 24 and 25. Little can be said about prograde metamorphic reactions as the mineralogy of lower grade rocks is not known with certainty.

Within metacherts, glaucophane crystals may be zoned with Fe-rich cores (crossite) and margins (Fig. 26). Mg and Al show an antipathetic variation. In the sample studied (No. 151) glaucophane co-exists with quartz, lawsonite, phengite, carbonaceous material and magnetite. Partial microprobe analyses of phengites (Table 13) indicate that they are compositionally homogeneous and presumably have equilibrated with the Fe-rich rims of glaucophane crystals. This zoning could be a result of the changing composition of the fluid phase during metamorphism but the presence of carbonaceous material, lawsonite and magnetite defines a narrow range of fluid composition (*see* p. 104). A second alternative is that the zoning in the glaucophane reflects the changing composition of the co-existing phengite with increase and decrease in pressure. According to Velde (1965) there is evidence that increase in pressure favours solid solution between muscovite and various celadonite end-members. The effect of pressure on the

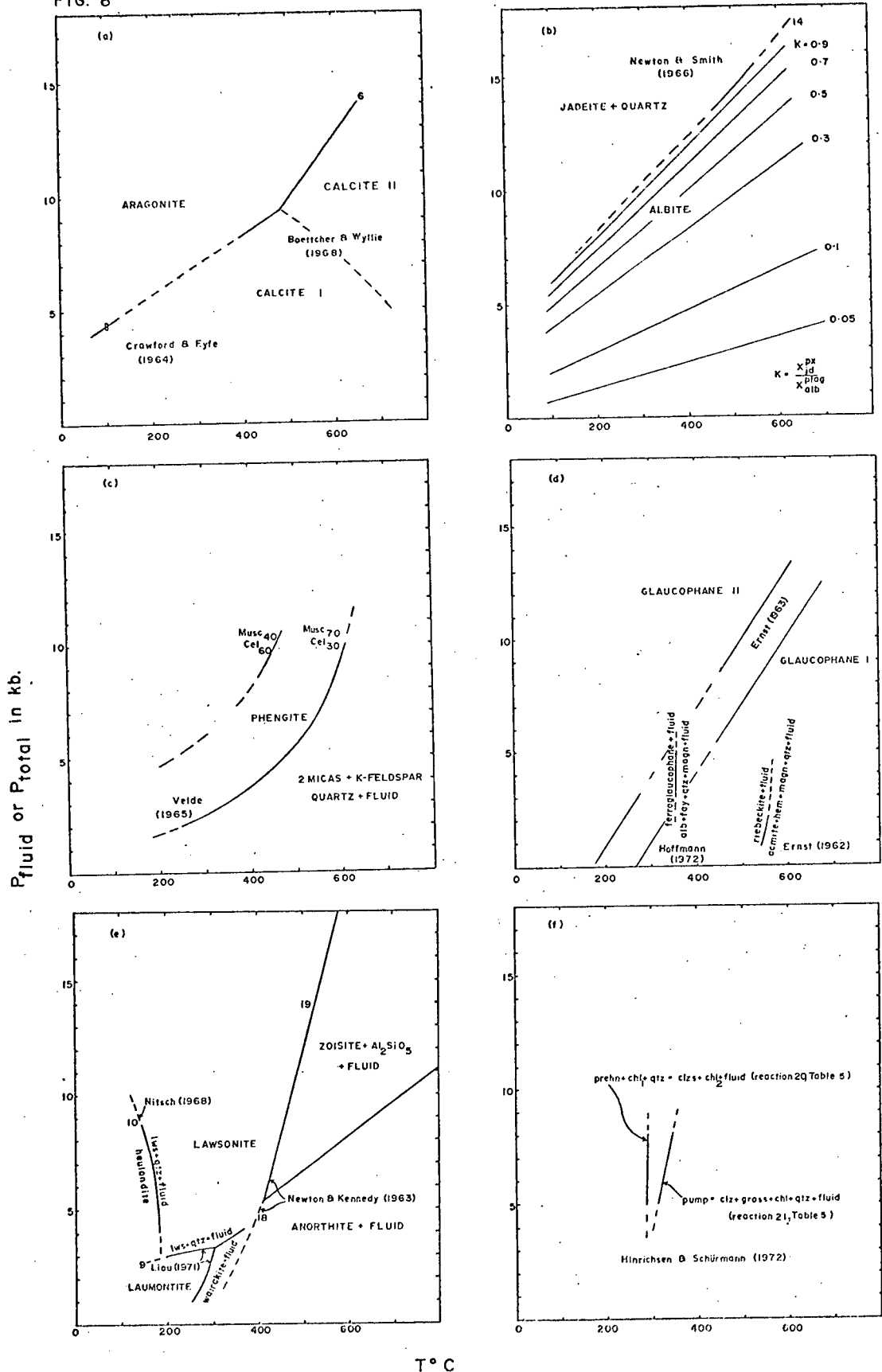
extent of phengite solid solution with Mg-Al celadonite (Fig. 8c) is particularly notable but is also appreciable with Mg-Fe⁺³ celadonites. It is suggested that an Fe-rich phengite may coexist with glaucophane at high pressures. Decrease in pressure would result in instability of the Fe-phengite and reaction with glaucophane to give phengite + crossite. This suggests that the crossite cores, zoned to glaucophane, crystallized during an episode of increasing pressure and that the narrow crossite rims formed during a retrogressive phase of metamorphism associated with decrease in pressure. An alternative explanation of the zoning could be sought in Raleigh fractionation during growth at constant P and T (Hollister, 1966). However, this does not explain the Fe-rich rims in the glaucophane crystals.

Relevant Phase Equilibria

Aragonite stability

For the calcite-aragonite transition, the experimental results of Boettcher and Wyllie (1968) and Crawford and Fyfe (1964) are shown in Figure 8a. Reversals were obtained by Crawford and Fyfe between 4.2 and 4.5 kb at 100°C and by Boettcher and Wyllie between 7.8 and 8.6 kb at 400°C. The common occurrence in nature of aragonite co-existing

FIG. 8



FIGS. 8a to 8f : Experimentally determined phase equilibria relevant to the formation of minerals in Pinchi rocks. Where H_2O is involved in the reaction $P_{fluid} = P_{total}$.

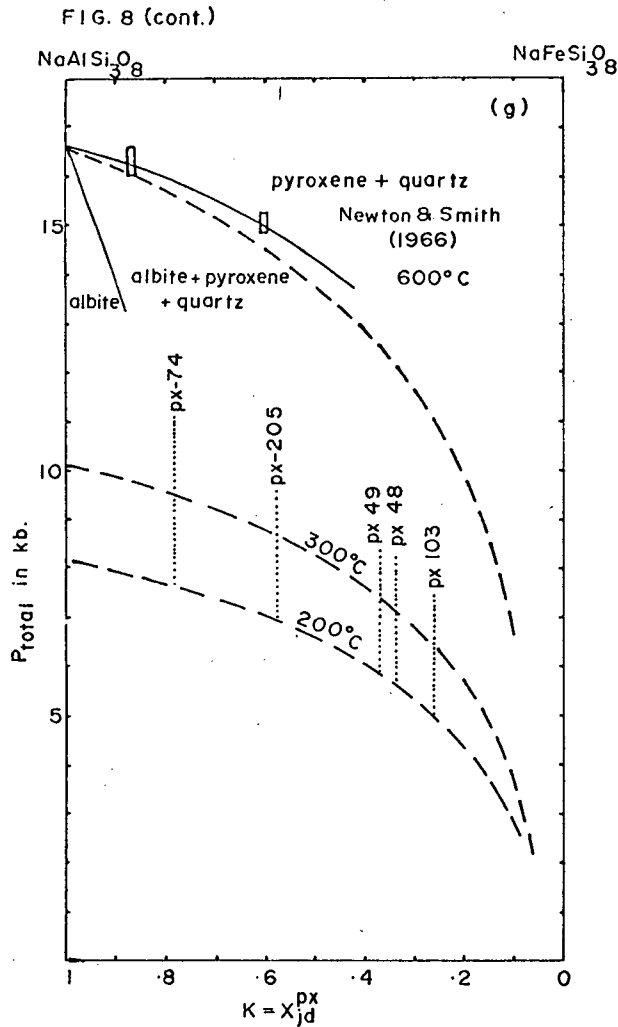


Fig. 8g P-X diagram illustrating effect of solid solution in lowering the pressure of formation of jadeitic pyroxene from albite. The experimental results of Newton and Smith in the system NaAlSi₃O₈-NaFeSi₃O₈ at 600°C are indicated by a solid line. Calculated equilibrium curves for different temperatures and values of $K = X_{jd}^{px}$ are indicated by dashed lines (see also Appendix VII). Values of X_{jd}^{px} for each of the analysed pyroxenes (Fig. 27b) are also shown.

with definitive high pressure minerals such as jadeitic pyroxene substantiates the experimental results.

However, a number of authors have given evidence for, or implied the "metastable" crystallization of aragonite at pressures significantly lower than that given by accepted transitions. Newton *et al.*, (1969) demonstrated the growth of aragonite from strained calcite several kilobars below the stability field given by previous authors. Bischoff and Fyfe (1968) showed that a high Mg^{2+}/H^+ ratio in aqueous solutions inhibited the growth of calcite nuclei within the calcite stability field. This could result in metastable precipitation of aragonite if the formation of aragonite nuclei was not inhibited. Vance (1968) noted the occurrence of aragonite in prehnite-pumpellyite bearing metabasic rocks and suggested on geologic grounds that the pressure during metamorphism did not exceed 3 kb. This is 1.3 kb less than the accepted transition pressure at temperatures of 100°C.

At Pinchi, aragonite occurs in several different associations. Firstly, it is the common $CaCO_3$ polymorph within dolomitic limestones, lawsonite-glaucophane bearing metabasic rocks and jadeitic metagreywackes. Secondly, aragonite co-exists with the greenstone assemblage albite + sodic pyroxene + sphene + chlorite ± pumpellyite. The presence of sodic pyroxene and the absence of prehnite differentiates the Pinchi assemblages from those described

by Vance (1968) in the San Juan Islands. Thirdly, an occurrence of aragonite was noted within Upper Triassic (?) limestones south of Pinchi Lake (*see* Fig. 28 for location). This was the only occurrence discovered outside of units 1 and 2 (Fig. 3).

Greenstones at the west end of Murray Ridge contain calcite coexisting with prehnite and pumpellyite. There are no indications that the calcite has formed by inversion from aragonite and it is inferred that calcite was the stable polymorph during metamorphism. It is perhaps significant that this is the only region where prehnite occurs in greenstones.

Despite the possibility of metastable crystallization, it is concluded from this evidence at Pinchi Lake that the aragonite-calcite transition is a valid geobarometer. This means that the dolomitic limestones, metagreywackes, lawsonite-glaucophane metavolcanics and most of the greenstones crystallized at pressures above the transition. The prehnite-calcite bearing greenstones formed at lower pressures. The presence of aragonite in the Upper Triassic (?) limestones is problematical. There is no evidence for deep burial and the preservation of detrital aragonite seems unlikely.

Jadeite and acmite-jadeite stability

The equilibrium curve for the reaction albite = jadeite + quartz according to Newton and Smith (1967) is given in Fig. 8b. This curve was used rather than that of Birch and LeComte (1960) as it takes into account the entropy change of disordering of albite. Also shown on Fig. 8b are values of the equilibrium constant for the reaction plagioclase = jadeitic pyroxene + quartz. In this case, $K = X_{jd}^{px} / X_{alb}^{plag}$ assuming unit activities for pure phases and mole fraction (X) = activity. If the plagioclase is pure albite, the values of K correspond to mole fraction of jadeite in clinopyroxene. For details of calculation see Appendix VII. Newton and Smith also investigated the effect of Fe in the system using synthetic glasses with or without mineral seeds. They concluded that the presence of 10 mole per cent acmite has at the most a few hundred bars effect on the stability of jadeite with quartz (Fig. 8g). Using 40 mole per cent acmite, the pressure of the albite breakdown curve is lowered by 1.6 kb at 600°C. The calculated pressures for the transition for different values of X_{jd}^{px} are compatible with Newton and Smith's experimental results at 600°C.

Microprobe analyses of pyroxenes from the Pinchi area are given in Table 10 and illustrated in Fig. 27. Two groups of pyroxenes were noted; acmite-jadeites from

metavolcanics and jadeitic pyroxenes from metagreywackes. Both are considered to have formed under similar P-T conditions and the compositional difference is assigned to the contrast in bulk composition. The minimum pressure of crystallization of the jadeitic pyroxene (coexisting with quartz) can be obtained from the calculated stability curves for different values of the equilibrium constant (Fig. 8g). For the pyroxene $Jd_{78}Ac_{11}Di_{11}$ (No. 74), $K = 0.78$ and the minimum pressure of crystallization is 9.5 kb at 300°C and 7.6 kb at 200°C. These values lie approximately 800 and 600 bars below the stability of pure jadeite with quartz. The minimum pressures for formation of the acmite-jadeite pyroxenes are below those for jadeitic pyroxenes and can be obtained from Fig. 8g.

Phengite stability

Velde (1965) carried out a study of the stability of phengitic micas. His results show that the extent of solid solution is dependent on pressure, temperature and composition of the celadonite end-member. Increase in solid solution is favoured by high pressures, low temperatures and involvement of the Mg-Al celadonite end-member. Other end-members show a less pronounced increase in solid solution with high pressures. Figure 8c indicates the equilibrium boundary for the reaction $Musc_{70}Cel_{30}$ going to muscovite, biotite,

K-feldspar, quartz and fluid as given by Velde. The equilibrium refers to the $\text{KAlMgSi}_4\text{O}_{10}(\text{OH})_2$ celadonite end-member. The approximate position of the $\text{Musc}_{40}\text{Cel}_{60}$ boundary shown on the figure was obtained from graphical extrapolation of Velde's results.

Stability of sodic amphiboles

Experimental work on the stability of glaucophane and riebeckite (Ernst, 1961, 1962) demonstrates that these sodic amphiboles have broad stability fields and that they do not impose restrictions on the P-T conditions of crystallization of blueschist facies minerals. More recently, Hoffman (1972) has determined the stability of natural and synthetic ferroglaucophane (Fig. 8d). The breakdown curve has a steep slope and is little affected by change of oxygen buffer. Thus ferroglaucophane, when identified, could restrict metamorphic temperatures to less than 360°C. The T-log f_{O_2} stability fields of sodic amphiboles will be discussed in the section on fluid phase chemistry.

Lawsonite stability

The breakdown curve for lawsonite was investigated by Newton and Kennedy (1963) and is shown in Fig. 8e. This gives a maximum temperature for the stability of lawsonite at a given pressure. In nature, coupled reactions with

minerals such as chlorite will doubtless shift the curve to lower temperatures. Phase relations for the reaction: laumontite = lawsonite + quartz + H₂O have been determined separately by Liou (1971), Thompson (1970) and Nitsch (1968). The univariant curves for the reaction are fairly compatible and suggest that lawsonite is unstable at pressures less than 2.5 kb at 200°C and 3 kb at 300°C in the presence of quartz and water. The equilibrium curve for the reaction: heulandite = lawsonite + quartz + fluid according to Nitsch (1968) is also given on Fig. 8e.

Pumpellyite and prehnite stability

Hinrichsen and Schürmann (1972) defined the curve for the breakdown of Fe-free pumpellyite shown in Figure 8f. During their experiments, they noticed that, with the inclusion of iron in the system, reaction rates were increased and equilibrium curves shifted towards lower temperatures. The pleochroism scheme and extinction angle of Pinchi pumpellyites shows them to be iron bearing, and therefore at 5 kb temperatures in the greenstones must have been less than 315°C. Reaction 20 (Fig. 8f) defines the breakdown of prehnite in the presence of chloritoid and quartz to give clinozoisite, serpentine and water. This experimental determination was not well defined in that there was some doubt about the compositions of the

chlorites involved, but it does yield a maximum temperature of 285°C at 5 kb for the metamorphism of the prehnite bearing greenstones at the west end of Murray Ridge.

Eclogite stability

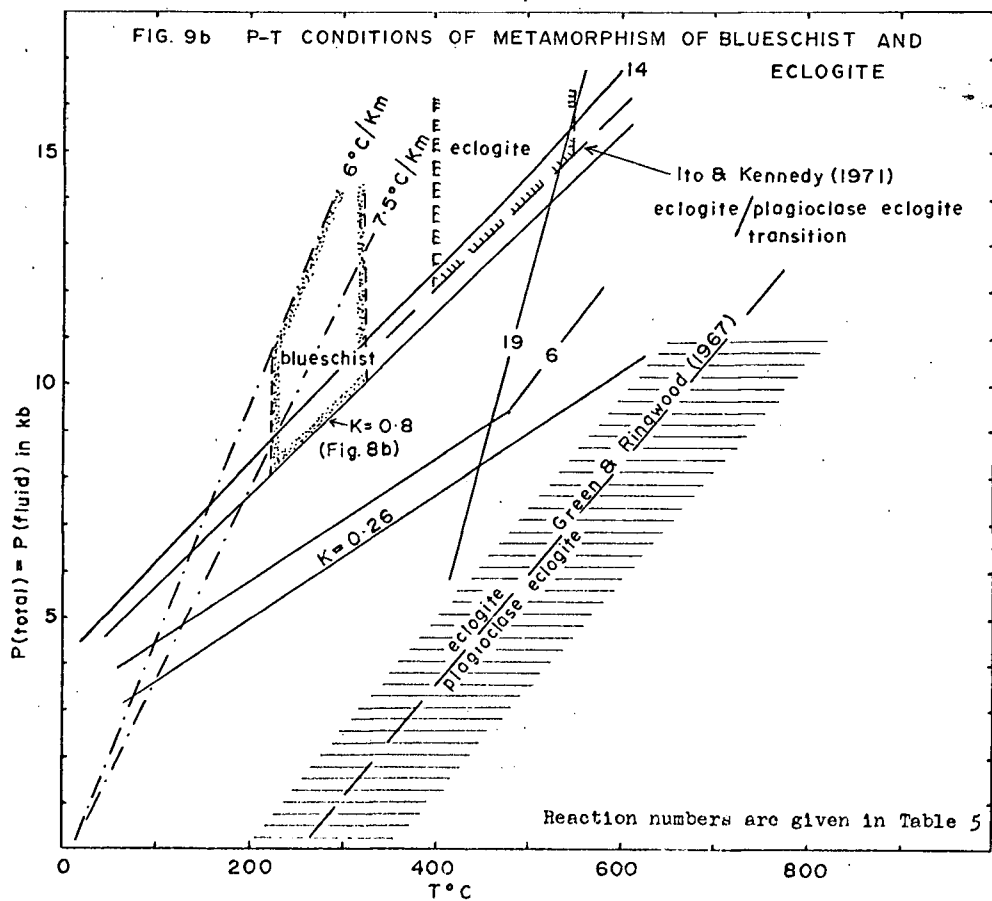
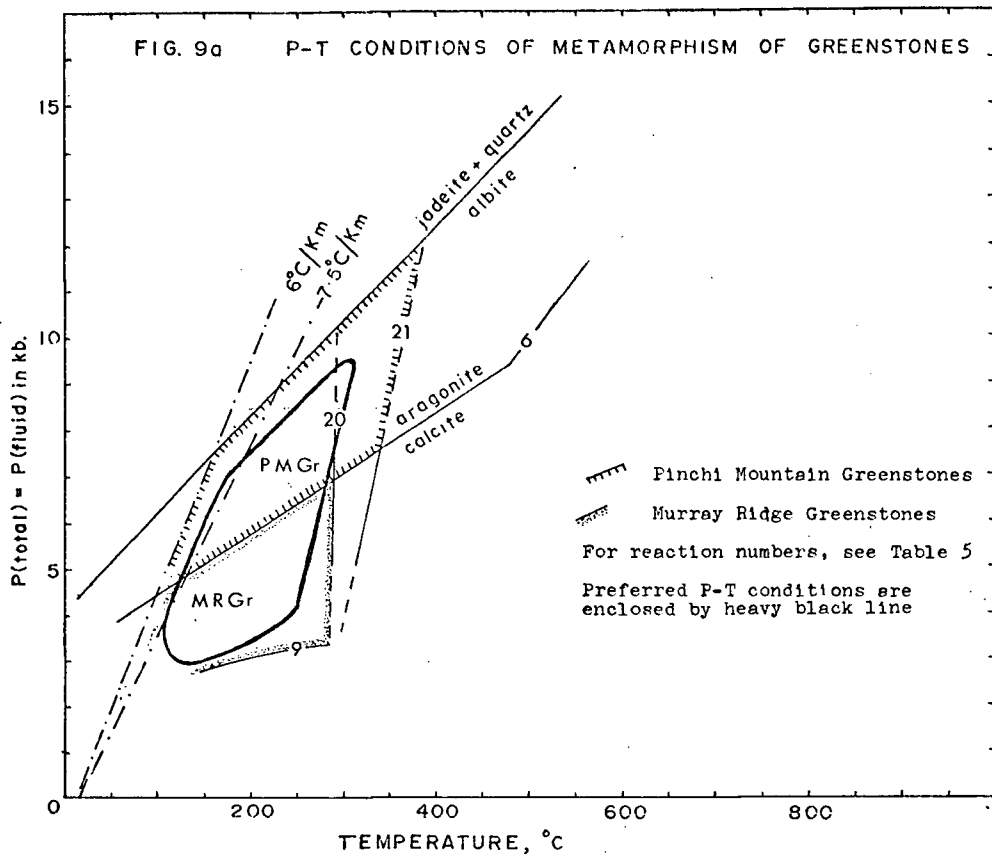
Extrapolations of the garnet granulite-eclogite transition to temperatures below 800°C have been made by Green and Ringwood (1967) and Ito and Kennedy (1971) and are shown on Fig. 9b. Neither of these extrapolations have a sound theoretical basis and the large difference in pressure between the two may be entirely caused by differing bulk compositions. Green and Ringwood studied mineral assemblages in basalts at pressures from 1 to 30 kb and at temperatures above 1000°C. The linear extrapolation of their experimental data on the disappearance of plagioclase intersects the 500°C isotherm at pressures of 5 to 8 kb and the temperature axis at around 200°C at atmospheric pressure. This implies the stability of eclogite in a wide range of geological conditions. The recrystallization of a tholeiitic basalt to garnet granulite and to eclogite was experimentally investigated by Ito and Kennedy (1971) at temperatures between 800° and 1200°C. The extrapolation of their eclogite/plagioclase eclogite transition curve to lower temperatures lies 400 bars below the albite/jadeite + quartz boundary as determined by Newton and Smith

(1966). At 500°C, this yields a pressure of 14 kb for the disappearance of plagioclase, 6 to 9 kb higher than the equivalent reaction in Green and Ringwood's experiments.

There is some evidence that the extrapolation of Green and Ringwood lies at too low a pressure. An analysed omphacitic pyroxene from a Pinchi eclogite has $X_{jd}^{Px} = 0.26$. On Fig. 8b, this gives a minimum pressure of formation of 9.1 kb at 500°C which is 1.1 kb above the extrapolation of Green and Ringwood. Because of this fact and compatibility with the commonly accepted high pressure origin of eclogites the data of Ito and Kennedy are preferred.

Oxygen isotopes

Taylor and Coleman (1968) obtained temperatures of formation of glaucophanitic rocks from Cazadero using O^{18}/O^{16} fractionation between coexisting minerals. They conclude that *in situ* Type II and III blueschists (Coleman and Lee, 1963) form at temperatures of 200° to 325°C, whereas higher grade blueschists from New Caledonia and Type IV tectonic blocks from California form at 400° to 550°C. Mineral assemblages at Pinchi are similar to those of Cazadero Type II and III blueschists and therefore possibly formed at similar temperatures. The glaucophane bearing eclogite boulders at Pinchi contain a similar mineralogy to Type IV blueschists and possibly formed between 400° and 500°C.



Pressure-temperature Conditions of Metamorphism

Constraints on the P-T conditions of metamorphism are given by phase equilibrium studies and oxygen isotope geothermometry. These are consistent with a minimum geothermal gradient of 6°C/km. Inferred metamorphic conditions for the various fault-bounded blocks are illustrated in Figs. 9a and 9b. For the Pinchi Greenstones (Fig. 9a), the high temperature limit is somewhat arbitrary and is based on the stability of Fe-free pumpellyite given by Hinrichsen and Schürmann (1972). Fe-pumpellyite would limit the field even more but the shift in the equilibrium boundary towards lower temperatures is not known.

Estimated P-T conditions are as follows:

Murray Ridge greenstones	3-6 kb	100-225°C
Pinchi Mountain Greenstones	4.5-9 kb	100-250°C
Blueschists	8-12 kb	225-325°C
Eclogite	> 12-15 kb (Ito & Kennedy, 1971)	400-550°C
	> 9 kb (from X_{jd}^{Px} at 500°C)	"
	> 3-6 kb (Green & Ringwood, 1967)	"

Fluid Phase Composition

The presence of lawsonite, quartz and sphene in an assemblage severely limits the CO₂ content of the coexisting fluid. Experimental studies by Nitsch (1972) demonstrate

Fig. 10a P-T diagram illustrating pressure of CO_2 (i.e. $P_{\text{E}_{\text{CO}_2}}$) in equilibrium with the reaction: calcite + quartz + rütile + sphene + CO_2 (after Ernst, 1971). Estimated P-T conditions for formation of Pinchi blueschists are also shown.

Fig. 10b T- X_{CO_2} diagram illustrating phase equilibria at 4 kb and 7 kb in the system $\text{CaO-Al}_2\text{O}_3\text{-SiO}_2\text{-H}_2\text{O-CO}_2$ (after Nitsch, 1972).

py = pyrophyllite; zo = zoisite; lws = lawsonite; cc = calcite; qtz = quartz.

Fig. 10c diagram illustrating variation in partial pressure of gaseous species at 327°C and $P_{\text{gas}} = 10$ kb with change in f_{O_2} . The estimated oxygen fugacity within lawsonite-quartz-magnetite-carbonaceous cherts is indicated by the shaded area. Selected values of $n_{\text{CO}_2}/(n_{\text{CO}_2} + n_{\text{H}_2\text{O}})$ are also shown. Assuming ideal behaviour of gaseous phases, lawsonite + quartz is stable at values of $n_{\text{CO}_2}/(n_{\text{CO}_2} + n_{\text{H}_2\text{O}})$ less than .05 (Fig. 10b) in the stability field of fayalite. Displacement of stability field of lawsonite + quartz to values of f_{O_2} above the quartz-fayalite-magnetite buffer is attributed to non-ideal behaviour of gaseous species. Fig. 10d T-log f_{O_2} diagram illustrating experimental and calculated phase equilibria involving riebeckite and ferroglaucophane (after Ernst, 1962; Hoffman, 1972).

hem = hematite; qtz = quartz; mt = magnetite; acm = acmite; fay = fayalite; fegl = ferroglaucophane; alb = albite; arfved = arfvedsonite solid solution.

FIG. 10

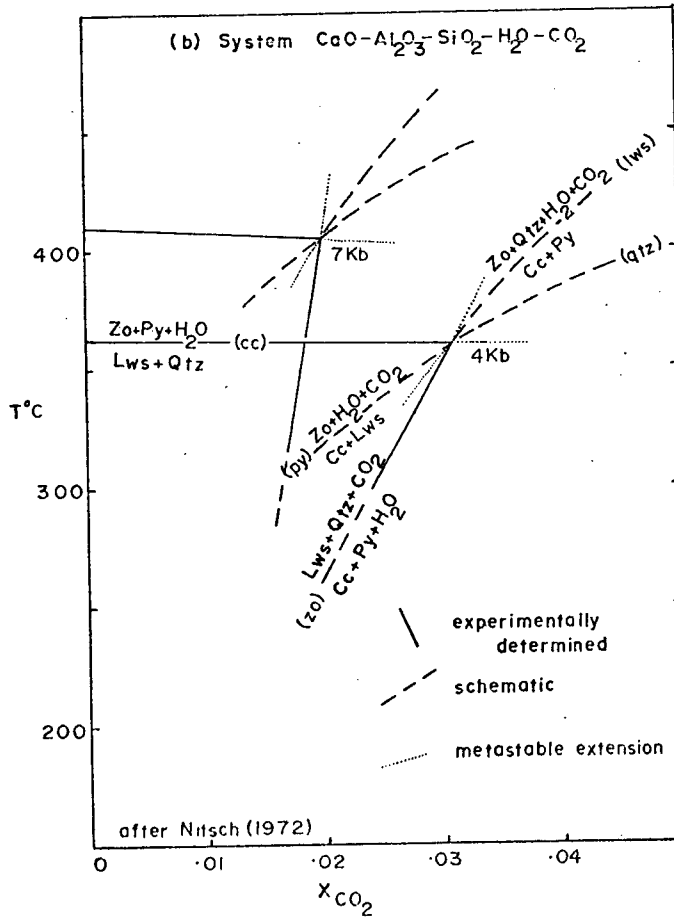
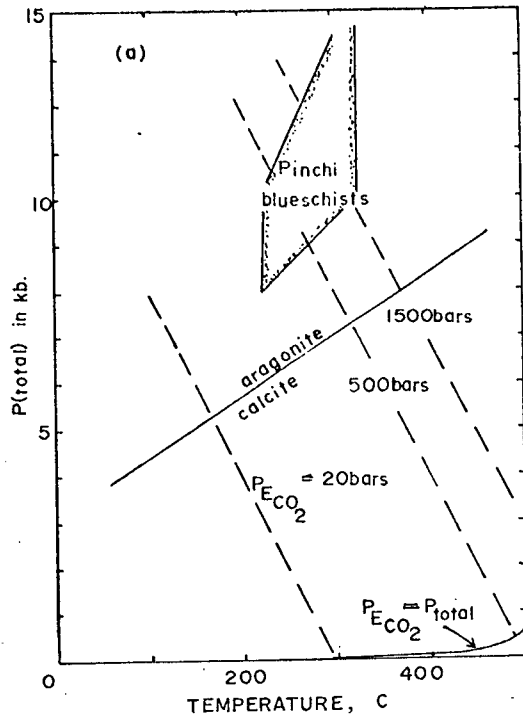
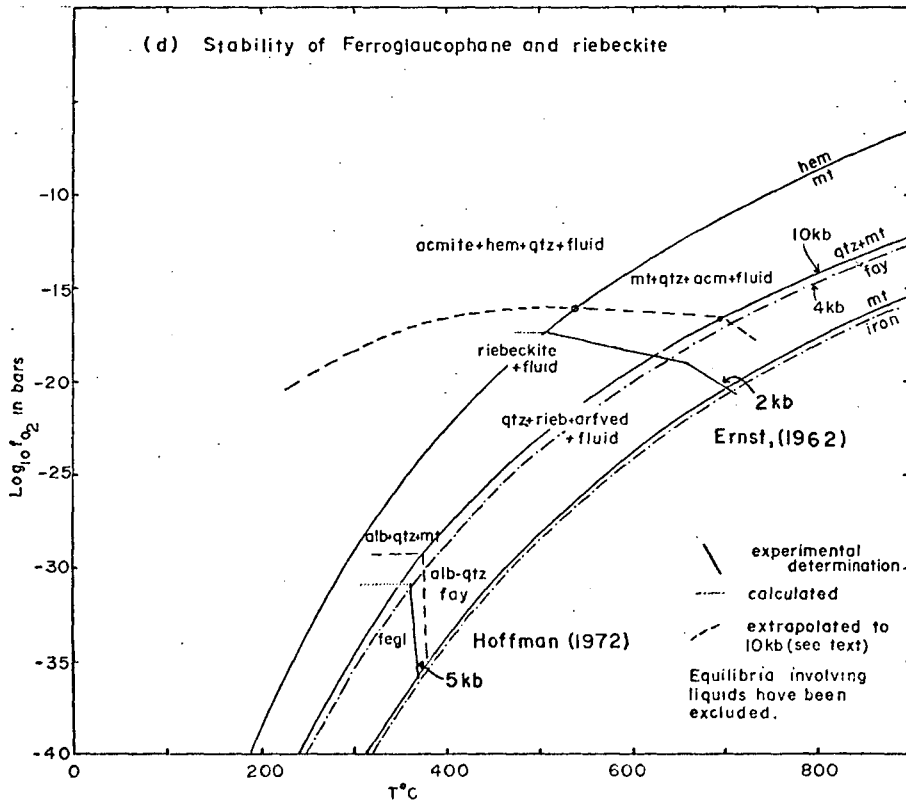
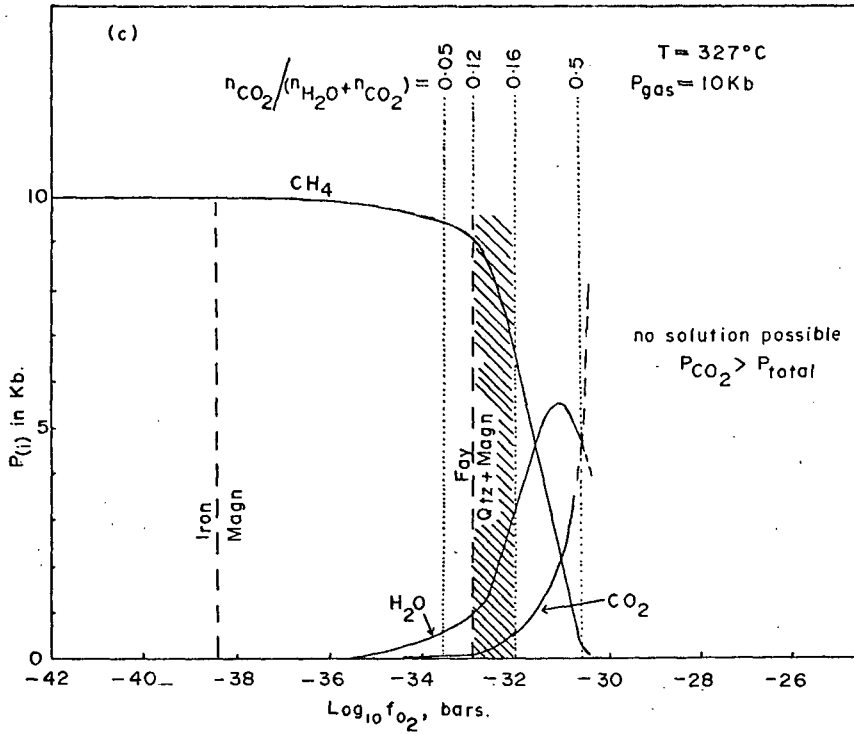


FIG. 10 (cont.)



that lawsonite and quartz can coexist with a fluid only if $n_{\text{CO}_2}/(n_{\text{CO}_2} + n_{\text{H}_2\text{O}})$ does not exceed 0.03 ± 0.02 at 4 kb (Fig. 10b). Calculations by Thompson (1971) support this conclusion. Schuiling and Vink (1967) determined the equilibrium for the reaction: calcite + quartz + rutile = sphene + CO_2 . The univariant curve demonstrated that sphene formation can only take place at extremely low P_{CO_2} (e.g. less than 35 bars at 300°C with $P_{\text{total}} = P_{\text{CO}_2}$) otherwise, the assemblage calcite + quartz + rutile would occur. Using this curve and additional thermochemical data, Ernst (1972) made a semiquantitative estimate of the maximum partial pressure of CO_2 in equilibrium with sphene in conditions where $P_{\text{CO}_2} < P_{\text{fluid}}$ (Fig. 10a). Values for X_{CO_2} were calculated independently and suggested that high grade Franciscan rocks equilibrated with a fluid phase in which X_{CO_2} was less than 0.01. This compares favourably with Nitsch's experimental results for the stability of lawsonite + quartz. From these data, it is concluded that for the Pinchi rocks at 7 kb, the assemblage lawsonite + quartz formed at $n_{\text{CO}_2}/(n_{\text{CO}_2} + n_{\text{H}_2\text{O}}) \leq 0.02 \pm 0.02$. Sphene bearing assemblages crystallized with $n_{\text{CO}_2}/(n_{\text{CO}_2} + n_{\text{H}_2\text{O}}) \leq 0.01$ or with P_{CO_2} at a maximum value of 1500 bars.

Phengitic mica coexists with lawsonite in the Pinchi metacherts. Velde (1965) and Ernst (1963) suggest that the presence of phengite is indicative of metamorphism under significant water pressures although $P_{\text{H}_2\text{O}}$ need not equal P_{load} .

Carbonaceous material is abundant in schists, meta-cherts and massive limestones. X-ray diffraction (Appendix II) indicated the presence of nearly amorphous graphitic material in one sample (graphite-d₃, according to Landis' classification, 1971) and amorphous material in 4 others. Calculations by French (1966) in the system C-H-O are strictly applicable only to crystalline graphite and not to amorphous carbonaceous material. They also depend on the assumption of ideal behavior of the gaseous species involved. It is considered, however, that partial equilibration has taken place between the carbonaceous material and the fluid phase and that the calculations have some applicability. Fig. 10c is adapted from French (1966, Fig. 1) and gives the fluid phase composition in the system C-H-O at 327°C and 10 kb, conditions approximating those of blueschist facies metamorphism. In rocks containing carbonaceous material, lawsonite and quartz, the experimental work of Nitsch requires that $n_{\text{CO}_2} / (n_{\text{H}_2\text{O}} + n_{\text{CO}_2})$ could not have exceeded 0.04 at 7 kb and possibly even less at 10 kb. From this and the ratios of the partial pressures of CO₂ and H₂O illustrated in Fig. 10c it can be inferred that the f_{O_2} must have been less than 10^{-33} bars. However, the presence of magnetite + quartz in graphitic metacherts implies an f_{O_2} greater than 10^{-33} bars. It is suggested that the excessively low values of f_{O_2} inferred from the

stability of lawsonite and graphite is brought about by the assumption of ideality and that a reasonable estimate for the f_{O_2} is between 10^{-33} and 10^{-32} bars. If this is the case, methane must have been a dominant constituent in the fluid phase in carbonaceous rocks.

Ernst (1962) constructed a $\log f_{O_2}$ -T diagram showing the stability fields of riebeckite and acmite at 2 kb (Fig. 10d). The curve which defines the reaction acmite + hematite + quartz + fluid = riebeckite + oxygen approximately parallels the abscissa at temperatures of 500°C. The position of this reaction curve at 10 kb can be approximately determined by recalculating the position of the buffer curves and by graphical extrapolation of the experimental data on acmite/riebeckite stability to high pressures. At 500°C, the increase in pressure from 2 to 10 kb raises the equilibrium f_{O_2} from 10^{-17} to 10^{-15} bars. The extrapolation of the reaction curve to lower temperatures, applicable to blueschist facies metamorphism, is critical but neither experimental nor thermochemical data are available. It is suggested that the curve takes on a positive slope with decrease in temperature. This is compatible with the steepening of the solid phase oxygen buffer curves with decrease in temperature.

At 300°C and 3 kb, ferroglaucophane is stable at an f_{O_2} of less than 10^{-32} bars (Hoffman, 1972). An extra-

polation similar to that carried out in the case of riebeckite enables an approximation of the stability field at 10 kb (Fig. 10d). Presumably, sodic amphiboles of intermediate composition have breakdown curves on a $\log f_{O_2}$ -T diagram between those of ferroglaucophane and riebeckite.

Oxidation ratios (Chinner, 1960), obtained from bulk analyses (Table 16a) should give a crude measure of the oxygen pressure at the prevailing pressure and temperature (Miyashiro, 1964). Within the unfoliated metavolcanics, oxidation ratios are commonly in the range 40 to 55. Rocks with a high modal per cent of acmite-jadeite yield the highest ratios and presumably equilibrated with an oxidising fluid phase. Foliated glaucophanitic metavolcanics with similar bulk composition have lower oxidation ratios (e.g. no. 55, Table 16a) and probably formed at lower oxygen pressures.

Opaque oxides can give clues as to fluid phase composition. Within carbonaceous cherts, magnetite coexists with glaucophane, This limits the f_{O_2} to values less than 10^{-27} bars at 10 kb and 325°C. If the coexisting carbonaceous material behaved as graphite, the f_{O_2} would be reduced to less than 10^{-31} bars at 10 kb and 325°C. Hematite is also found in cherts but is believed to have formed during retrograde metamorphism as it commonly rims magnetite. Opaque oxides are rare in metabasic rocks and where observed are composite, consisting of pyrite

rimmed by magnetite and hematite in turn (Fig. 30). It is uncertain whether pyrite, magnetite or hematite was stable during blueschist metamorphism.

Two phase fluid inclusions are present in metachert samples and provide evidence for the presence of a fluid phase during metamorphism. In general, they can be divided into two groups; 20 μ inclusions containing 3 μ gas bubbles (Plate 6) and aggregates of small 1 μ inclusions along partly healed fractures. Roedder (1968) considers that large inclusions showing no relationship to relict fracture zones are more likely to be primary. Therefore it is possible that the first type represent primary syn-metamorphic inclusions and the second type represent secondary inclusions.

Fluid Phase Composition at 10 kb and 327°C

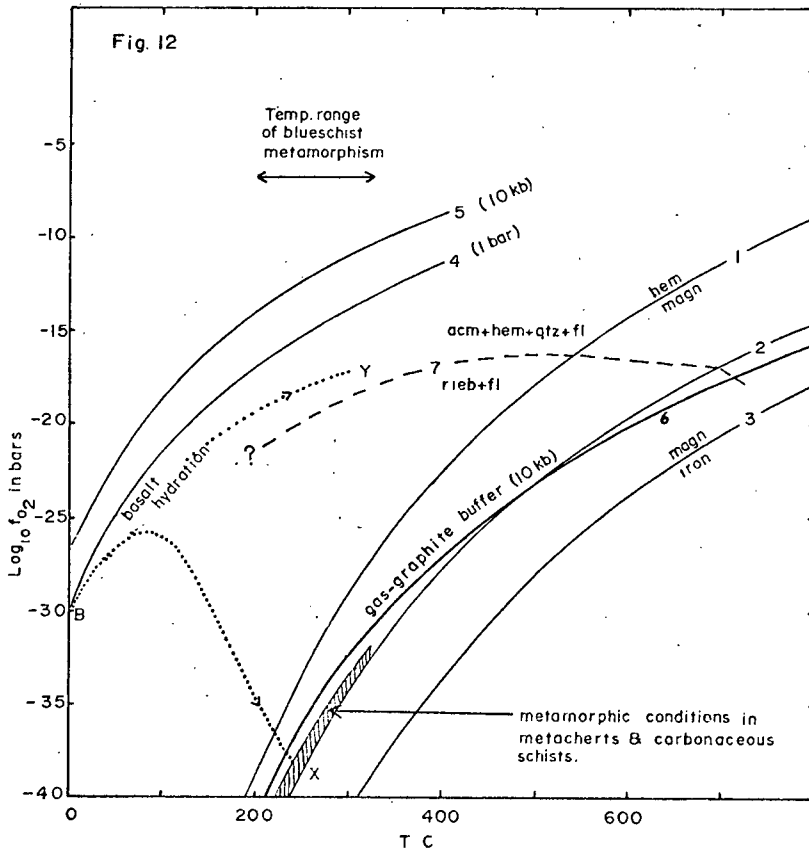
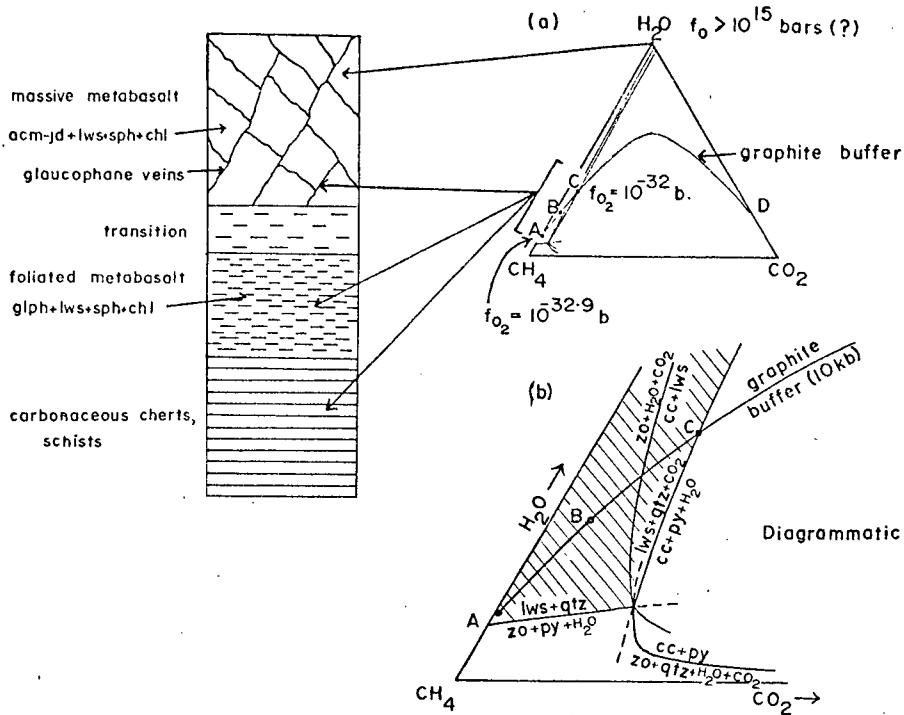
The fluid composition at 327°C and 10 kb, within contrasting rock types, is illustrated in Fig. 11. Water, methane and carbon dioxide are considered to be the major components with $P_{\text{H}_2\text{O}} + P_{\text{CH}_4} + P_{\text{CO}_2} = P_{\text{fluid}} = P_{\text{load}}$. The calculations of French (1966) suggest that CO and H₂ are of minor importance at the temperature and pressure of blueschist formation.

Within acmite-jadeite metavolcanics, the presence of lawsonite, quartz and sphene requires that the $n_{\text{CO}_2} / (n_{\text{H}_2\text{O}} + n_{\text{CO}_2})$ be less than 0.04 at 10 kb. The stability of acmite-jadeite suggests that the coexisting fluid was

Fig. 11 diagram illustrating fluid phase composition in Pinchi blueschists at 10 kb and 327°C. (a) The line AC (on the graphite buffer) represents possible fluid compositions in equilibrium with carbonaceous material, lawsonite, quartz and magnetite between $f_{O_2} = 10^{-32.9}$ (A) and 10^{-33} bars (C) as obtained from Fig. 10c. (b) Diagrammatic phase equilibrium boundaries in the system Ca-Al-Si-C-O-H. The inferred stability of lawsonite + quartz is indicated by shading.

Fig. 12 T-log f_{O_2} diagram illustrating fluid compositions in Pinchi rocks. Explanation is given in text.

FIG. II FLUID PHASE COMPOSITION AT 10KB & 327°C



relatively oxidizing, possibly with f_{O_2} greater than 10^{-25} bars. Methane is incompatible with f_{O_2} greater than 10^{-30} bars and therefore it appears that H_2O was the main component in the fluid phase.

In the ternary system $H_2O - CO_2 - CH_4$ the fluid composition in equilibrium with graphite at varying f_{O_2} lies on the graphite buffer curve AD. It was inferred earlier, that rocks containing coexisting lawsonite, quartz, carbonaceous material and magnetite may have crystallized in the f_{O_2} range 10^{-33} to 10^{-32} bars (i.e. just above the quartz-fayalite-magnetite buffer curve). If this is the case, fluid compositions lie on the curve AC. For $f_{O_2} = 10^{-32}$ bars (i.e. point C), $P_{CO_2} = 500$ bars, $P_{H_2O} = 3200$ bars and $P_{CH_4} = 6300$ bars. Decrease in value of $n_{CO_2}/(n_{H_2O} + n_{CO_2})$ (and f_{O_2}) results in increase of methane water ratio (Fig. 10c) and the fluid composition migrates towards A. On the extension of this curve (CD), lawsonite is considered to be unstable in the presence of graphite and quartz. Diagrammatic phase equilibrium boundaries in the system Ca-Al-Si-C-O-H and the inferred stability limit of the assemblage lawsonite + quartz are also shown in Fig. 11.

The carbonaceous metasediments are far more abundant than the metavolcanics and it is to be expected that with progressive metamorphism and deformation a methane-water mixture with arbitrary composition B permeated active

shear zones in the metavolcanics. The oxidized acmite-jadeite assemblage reacted with the fluid to give a reduced glaucophanitic assemblage which coexists with methane-water. A reaction involving the acmite end-member (Table 5, No. 16a) consumes methane, liberates water and precipitates graphite. As graphite was not identified in glaucophane veins or foliated metavolcanics, it appears that methane and water fugacities were externally controlled and the fluid phase composition in the metasediments migrated from B towards C.

Evolution of Fluid Phase

The changing composition of the fluid phase with progressive metamorphism can also be illustrated with reference to a $T-f_{O_2}$ diagram (Fig. 12). Curves 1, 2 and 3 are respectively the hematite-magnetite, the quartz-fayalite-magnetite and the magnetite-iron oxygen buffer curves calculated at 10 kb. The f_{O_2} in equilibrium with pure water at 1 bar and 10 kb (curves 4 and 5) were calculated after Miyashiro (1964). Curve 6 represents the gas-graphite buffer in the system C-O calculated at 10 kb employing an equation given by French and Eugster (1965). This curve is very close to the graphite buffer as calculated in the system C-H-O employing an H/O ratio of 2/1 (French, 1966). Curve 7 represents the hypothetical extrapolation

at 10 kb of the reaction acmite + quartz + hematite + fluid = riebeckite + oxygen described in the previous section.

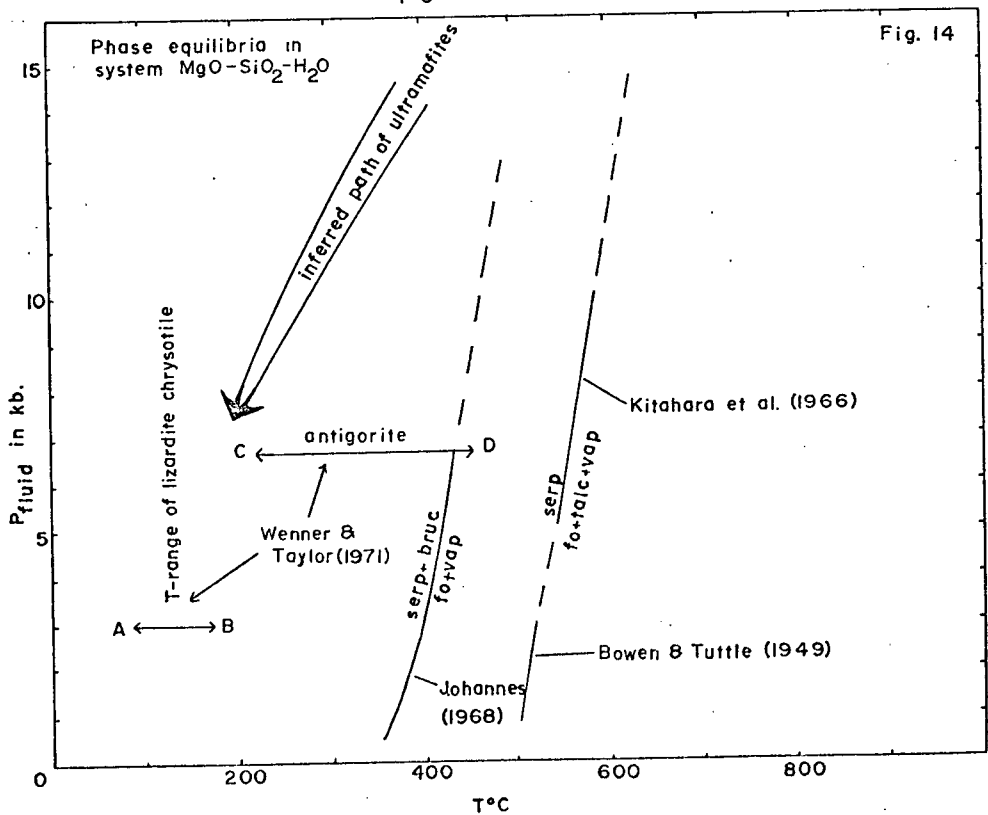
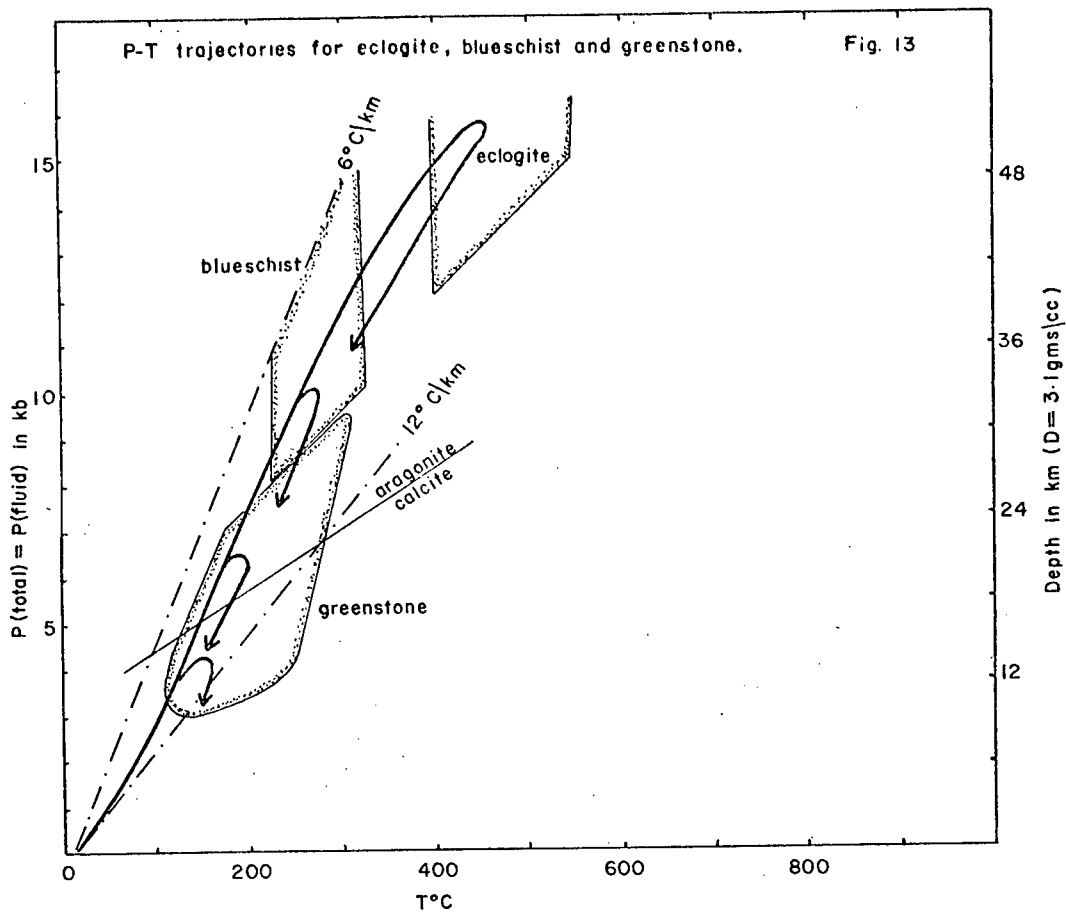
During diagenesis of the carbonaceous sediments, the interstitial liquid was probably a saline brine. It is supposed that the f_{O_2} in the liquid was initially similar to that of pure water, it can be inferred from curves 4 and 5 that f_{O_2} was approximately 10^{-30} bars (i.e. point B). With diagenesis and metamorphism, oxygen reacted with carbonaceous material to give CO_2 and the f_{O_2} changed along the arbitrary trajectory BX. Presumably, at temperatures in the 200° to 300°C range (shaded area) the carbonaceous material behaved as graphite with the result that the fugacities of the various components can be specified uniquely in terms of f_{O_2} at fixed temperature and total pressure (French, 1966).

Basalts within the sedimentary rocks may have undergone hydration in the zeolite or prehnite-pumpellyite facies during progressive burial and/or deformation. Presumably, the water originated in the adjacent metasediments prior to lowering of f_{O_2} and equilibration with graphite. After hydration, it appears that massive basalt units behaved essentially as closed systems and the f_{O_2} changed along the curve BY. The position of this curve is directly dependent on the extrapolation of the acmite/riebeckite reaction (Fig. 12, No. 7). Oxidation of iron to form acmite must have lowered the f_{O_2} in the hydrous pore fluid to

values below that of pure water (curves 4 and 5) but the presence of acmite-jadeite bearing rocks which do not contain glaucophane or crossite suggests that the f_{O_2} in the fluid remained within the acmite stability field and did not equilibrate with graphite as temperature increased. At Y, acmitic rocks were in disequilibrium with the reservoir of methane rich fluid and glaucophane forming reactions probably took place along shears and fractures.

Pressure-Temperature Trajectories of Pinchi Rocks

Three assumptions have been made in drawing the pressure-temperature trajectories shown in Fig. 13. They are: (a) an average crustal density of 3.1 grams/cc, (b) a minimum geothermal gradient of 6°C/km and (c) a maximum geothermal gradient of 12°C/km. The first assumption is based on a tectonic model (Chapter V) involving a major proportion of basic or ultramafic rocks. The second is hypothetical, but geothermal gradients as low as 8.56°C/km have been measured (Clark, 1957). The last assumption is based on a study of aragonite/calcite kinetics by Brown *et al.*, (1962), who inferred from this that for survival of metamorphic aragonite the geothermal gradient could not have greatly exceeded 10°C/km. This estimate was dependent on the calcite/aragonite transition as determined by Clark (1957) and Jamieson (1953). Later work by



Boettcher and Wyllie (1967) lowered the transition pressure, and geothermal gradients of 12°C/km can be accommodated. It is therefore concluded that the aragonite bearing rocks at Pinchi crossed the aragonite/calcite transition at temperatures less than 300°C on their return to the surface.

Uplift was accompanied by retrograde metamorphism. Eclogites were veined and partly replaced by glaucophane, lawsonite and stilpnomelane in their passage through the blueschist facies. Late albite veins in the blueschists must have formed below the albite/jadeite + quartz transition at pressure-temperature conditions similar to the metamorphism of the greenstones.

II METAMORPHISM IN THE REMAINING FAULT BLOCKS

Metabasic Rocks South of Pinchi Lake (Map I, Unit 4)

The following metamorphic mineral assemblages were noted during examination of six thin sections. Minerals are thought to be in equilibrium with one another except for white mica which only occurs within plagioclase.

- (a) metabasalts: albite + sphene + celadonite
± white mica (calcite + chlorite
veins)
- (b) metagabbro: albite + actinolite + sphene
± white mica ± serpentine
± epidote (?)

Relict minerals, namely orthopyroxene, clinopyroxene, ilmenomagnetite and calcic plagioclase are abundant in the gabbros and may constitute up to 90% of the rock. Metadiabase and metabasalt tend to be more highly reconstituted with few relicts. Significantly, actinolite is absent from the metavolcanic unit which also is apparently the highest in the sequence (*see* p. 24).

The presence of a pale green amphibole and possible epidote suggests that the lower gabbro unit was metamorphosed in the greenschist facies. No meaningful pressure estimates can be made, but the temperature may have been in the 200° to 400°C range based on the facies diagrams of Turner (1968, p. 366) and Liou (1971).

The albite/celadonite-calcite association in the overlying basalts suggests that they were metamorphosed in conditions equivalent to the prehnite-pumpellyite facies.

It was suggested (p. 27) that the basic rocks may represent part of an ophiolite sequence. It is therefore significant that the metamorphic mineral assemblages in these rocks are similar to those recently investigated from oceanic environments (Aumento *et al.*, 1970). Such rocks, characterized by a greenschist facies mineralogy, and general absence of a tectonite fabric are typical of ocean floor metamorphism (Miyashiro, 1972).

Mount Pope Belt (Map I, Units 7, 8 and 9)

Sensitive indicators of metamorphic grade are rare within the Mount Pope belt, as limestone and chert are the dominant lithologies. A schist interlayered with cherts on the northern margin of the limestone contains the assemblage: albite + chlorite + calcite + quartz + white mica + unidentified opaques and amorphous material. Outside of the map area on the northwest arm of Stuart Lake, the author noted a regionally metamorphosed basic assemblage containing actinolite + chlorite + clinozoisite + albite + sphene. Similar assemblages within the Cache Creek Group have been reported by Armstrong (1949). It is concluded that the Mount Pope belt was metamorphosed under lower greenschist facies conditions.

Takla Group (Map. I, Units 10, 11 and 12)

The greywackes and siltstones of the Takla Group are only incipiently metamorphosed. Detrital plagioclase, the main constituent of the sediments, commonly displays a turbid alteration and may be locally albitised. Relict mafic clasts (e.g. hornblende) are generally altered to chlorite + sphene + calcite. Matrix minerals include microgranular chlorite, sericite and the occasional grain of celadonite. At one locality, a dark grey, hard siltstone contains analcite dodecahedra coexisting with chlorite, quartz and partly albitised plagioclase. However, this locality is near the

Pinchi Fault and the analcite may have been formed as a result of hydrothermal activity.

Only one small outcrop of basalt was encountered within the area and contained the following domain assemblages:

matrix: albite + chlorite + sphene + calcite

amygdules: Prehnite + quartz

veins: Epidote + calcite

A puzzling feature is the occurrence of minor aragonite (Table 12, No. 230) in a bioclastic limestone thought to be of Upper Triassic age south of Pinchi Lake. Aragonite was not found in adjacent limestone beds or in Upper Triassic limestones to the northeast of the fault. Aragonite at this locality replaces rectangular clasts, which were possibly originally crinoid columnals.

The presence of prehnite and epidote in basaltic rocks suggests that the Takla Group was metamorphosed in transitional conditions between the prehnite-pumpellyite and greenschist facies. Lord (1949) estimated a thickness of 23,000 ft (7 km) for Takla Group sediments and volcanics in the McConnell Creek area so that lithostatic pressures in the Pinchi area may well have approached 3 kb. The occurrence of aragonite in Takla Group (?) rocks southwest of the fault may indicate that higher pressures were attained locally (i.e. 5.5 kb at 200°C).

Ultramafites (Map I, Units 14a and 14b)

Harzburgites and dunites at Pinchi have been thoroughly serpentinized. D.B. Wenner (Written communication) examined three harzburgites from the Pinchi area and identified the serpentine mineralogy by X-ray diffraction. The results were:

Spec. 85 (from Pinchi Mt.) : lizardite + chrysotile

Spec. 88 (from Pinchi Mt.) : chrysotile

Spec. 236 (from Murray Ridge) : lizardite + chrysotile

Brucite was identified by X-ray diffraction in three dunite samples (Nos. 87, 88, 240) and one harzburgite (No. 239).

Stability of serpentine-bearing mineral assemblages is illustrated on Fig. 14. At 10 kb and 585°C serpentine breaks down to forsterite, talc and water (Kitahara *et al.*, 1966). Brucite coexisting with serpentine lowers the stability limit to 460°C at 10 kb (Johannes, 1968). The occurrence of serpentine and brucite at Pinchi therefore indicates that serpentinization took place below 460°C at 10 kb and 390°C at 3 kb.

Oxygen isotope work (Wenner and Taylor, 1969) carried out on serpentinites from British Columbia and western North America indicates that serpentine minerals equilibrated with meteoric water at low temperature. Fractionation of oxygen isotopes between coexisting serpentine and magnetite suggest that continental lizardite-chrysotile serpentinites

equilibrated at 85° to 115°C and oceanic lizardite-chrysotile serpentinites at 130° to 185°C (Wenner and Taylor, 1971). Antigorite equilibrates at temperatures above 200°C. From this it may be inferred that a major episode of serpentinization occurred in the Pinchi ultramafites at temperatures less than 185°C to give the chrysotile-lizardite association.

For the survival of metamorphic aragonite, the fault blocks containing greenstones and blueschists must have been rapidly uplifted (p.110) along the P-T trajectory in Fig. 13. The possibility exists that ultramafic bodies, which are closely associated with these rocks, underwent a similar rapid uplift and a possible P-T trajectory in the system MgO-SiO₂-H₂O is illustrated in Fig. 14. From the oxygen isotope geothermometry it appears that antigorite is the stable serpentine mineral at blueschist facies temperatures. The absence of antigorite suggests that either antigorite never formed or that it was completely replaced by the lower temperature lizardite-chrysotile mineralogy during uplift and cooling. In the writer's opinion much of this serpentinization occurred during a period of strike-slip faulting associated with uplift and the F_2 deformation (Chapters V and VI).

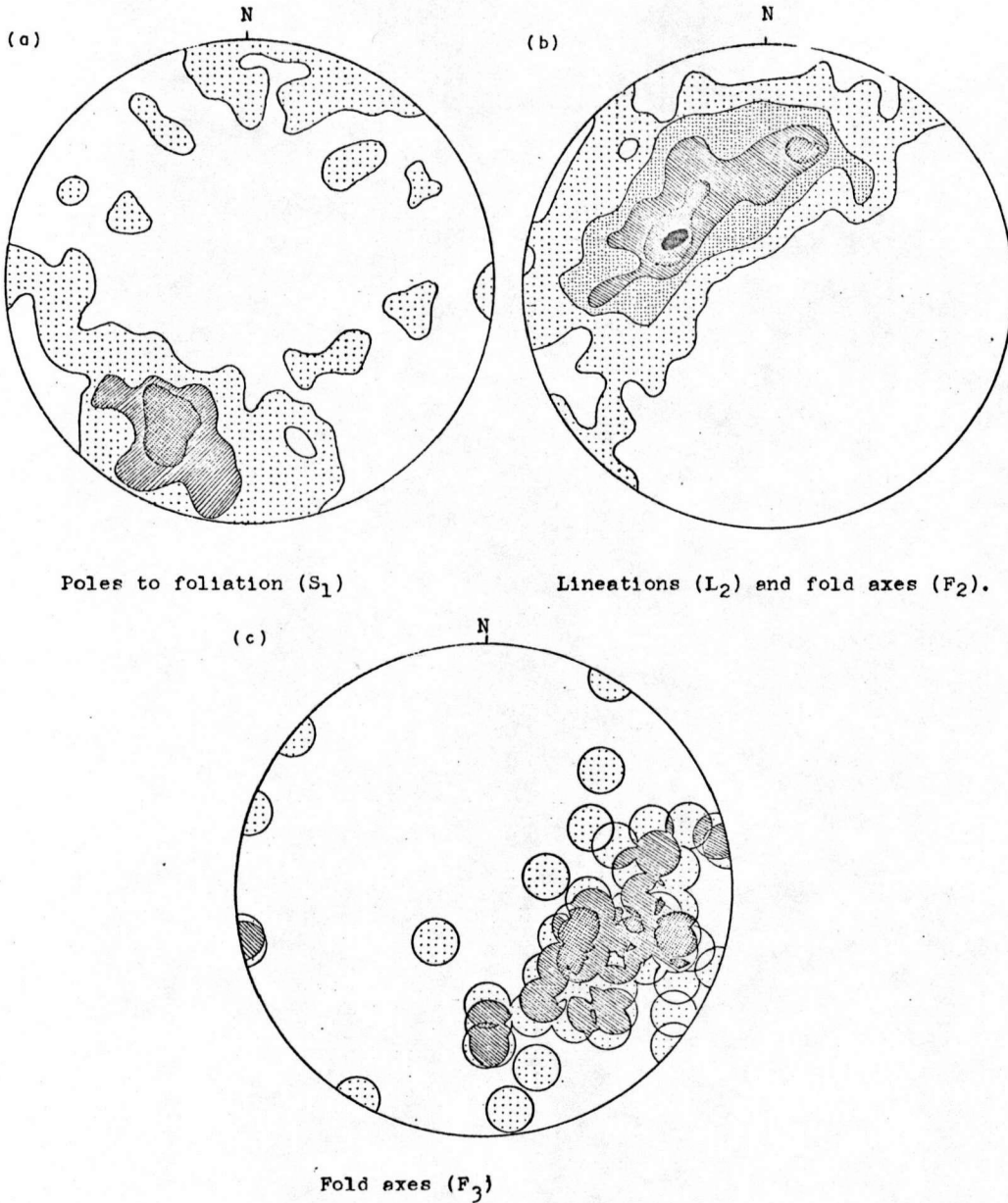
STRUCTURAL GEOLOGY

Introduction

The emphasis in this chapter is placed on the internal structure of the fault block containing the lawsonite-glaucophane bearing rocks (Fig. 3, Unit 2). It was hoped that a structural study of these rocks, which lie adjacent to the Pinchi Fault, would help to elucidate the history of movements on the fault. To this purpose, structural mapping was carried out in the vicinity of the mine (Map IV) and along the northwest shore of Pinchi Lake (Map V). Structural data collected in the vicinity of the mine were plotted on stereographic projections (Fig. 15). It should be emphasized that structural interpretation is seriously constrained by (a) the poor exposure, (b) the undoubtedly complex deformational history and (c) the lack of a stratigraphic sequence.

Structural geology of the remaining fault blocks has been adequately dealt with in Chapters II and III and will only be summarized in this section.

FIG. 15 EQUAL AREA STEREOGRAPHIC PROJECTIONS OF STRUCTURAL DATA OBTAINED
IN THE VICINITY OF PINCHI MINE (MAP IV)



- a : 116 points contoured using Kalsbeck counting net (Kalsbeck, 1963). Contour intervals at 1, 4, and 6% of points per 1% area of net.
- b : 153 points contoured using Kalsbeck counting net (Kalsbeck, 1963). Contour intervals at 2, 4, 6 and 8% of points per 1% area of net.
- c : 59 points contoured using the Mellis method (Turner & Weiss, 1963, p. 62) contour intervals at 1, 2 and 4% of points per 1% area of net.

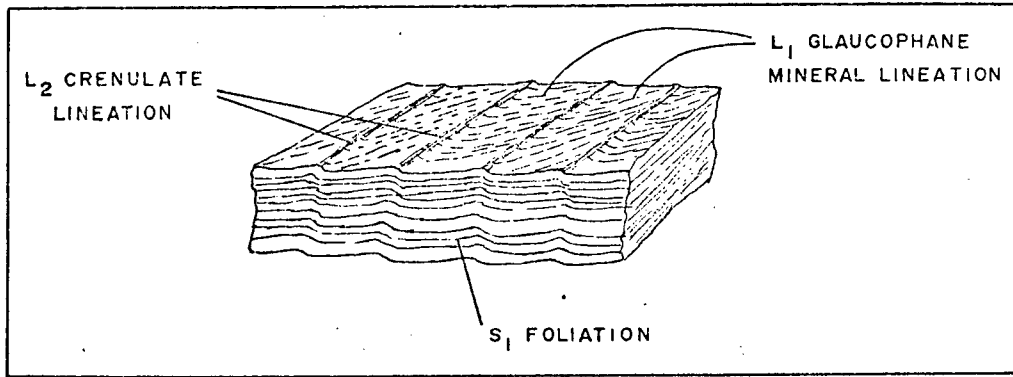


Fig. 16a Structural elements in foliated glaucophane rich metavolcanic (drawn from hand specimen).

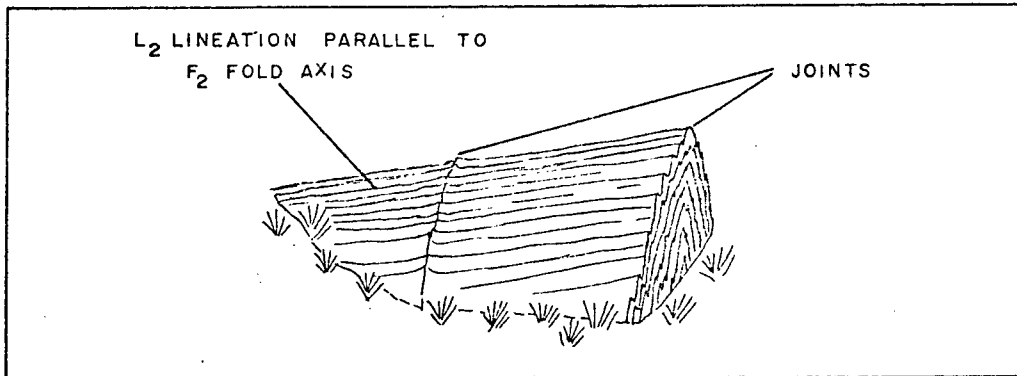


Fig. 16b F_2 fold in metachert.

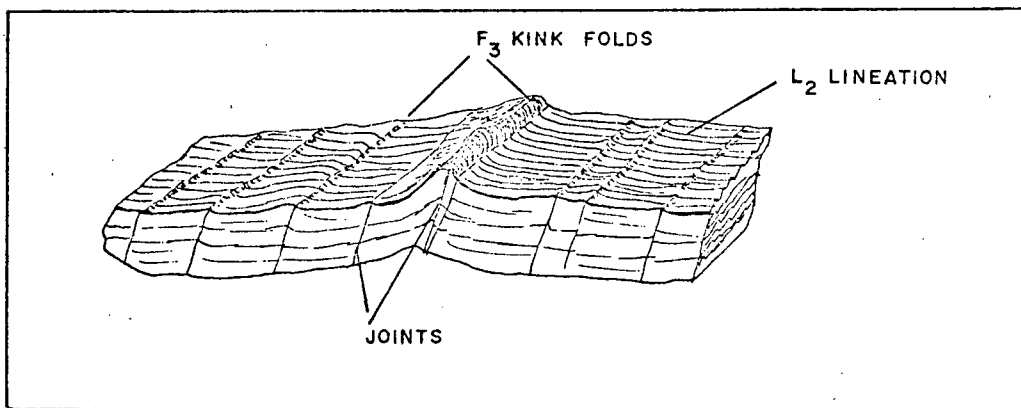


Fig. 16c F_3 kink folds in metachert.

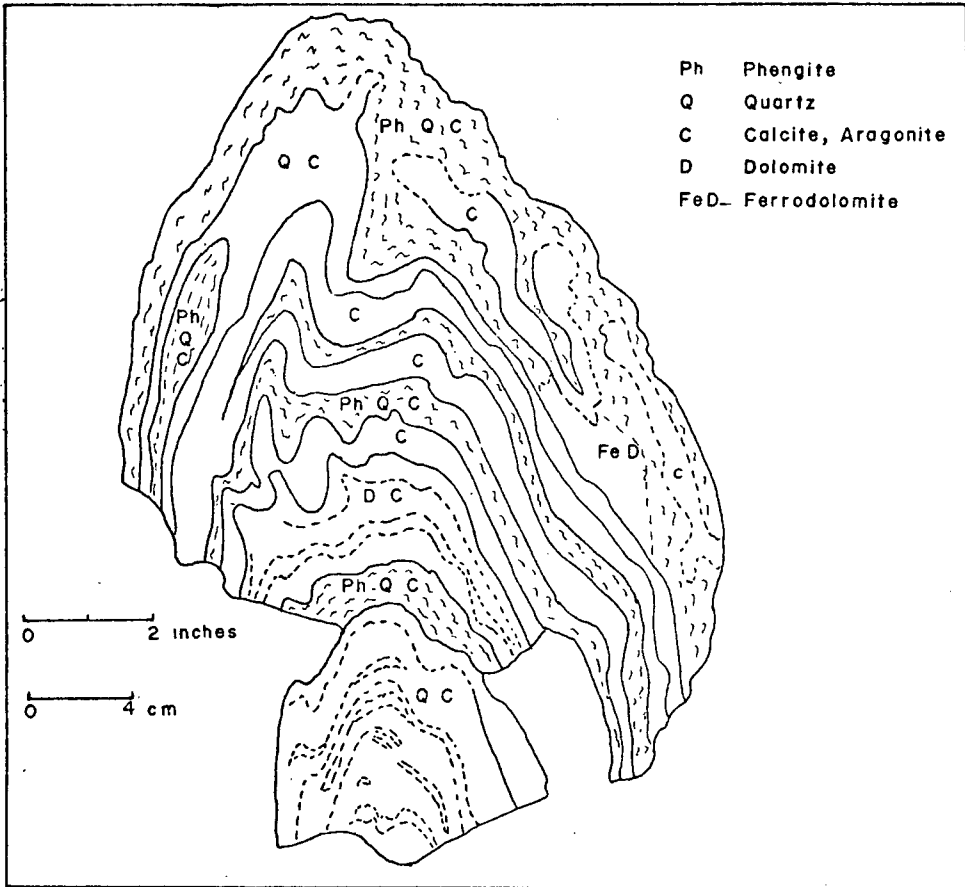


Fig. 17a F_2 fold in quartz-carbonate-mica schist. Note lensing out of micaceous layers.

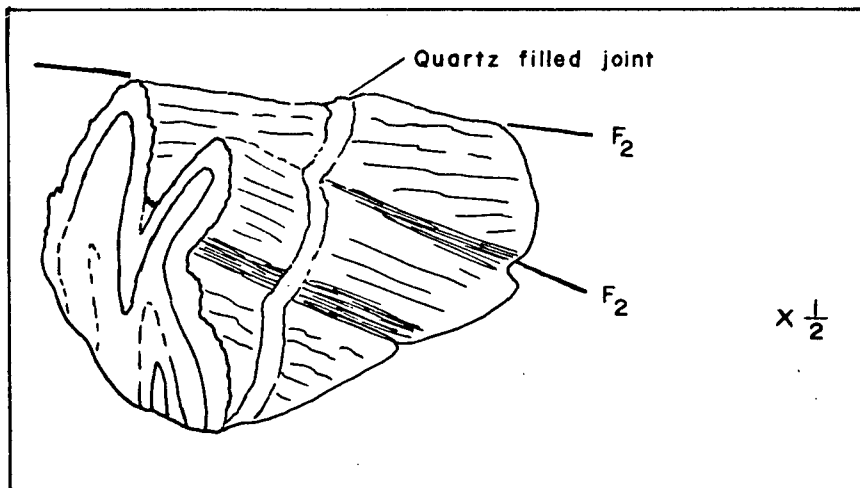
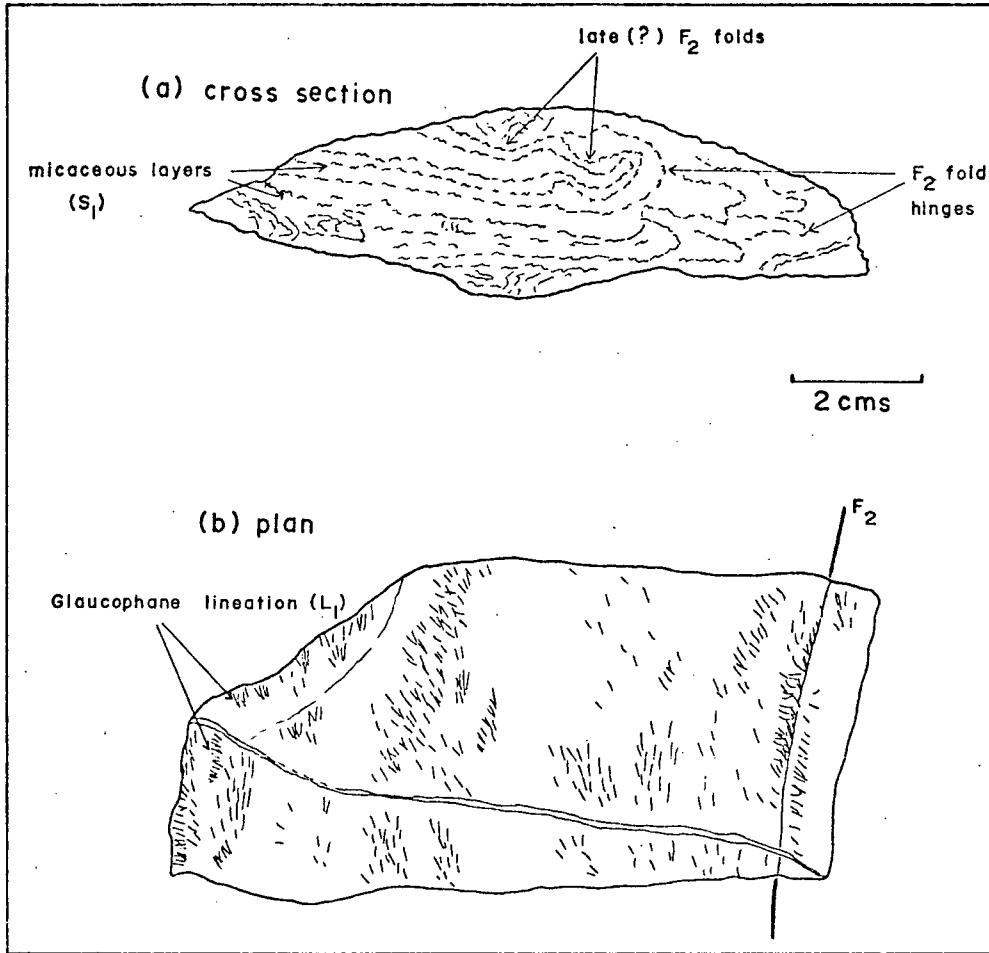


Fig. 17b F_2 folds in metachert. Note variation in plunge and curving axial plane of F_2 folds. Folds are cross-cut by quartz-filled joint.



Figs. 18a and b: Recumbent isoclinal F_2 folds in metachert. These F_2 folds appear to have been refolded by late (?) F_2 folds.

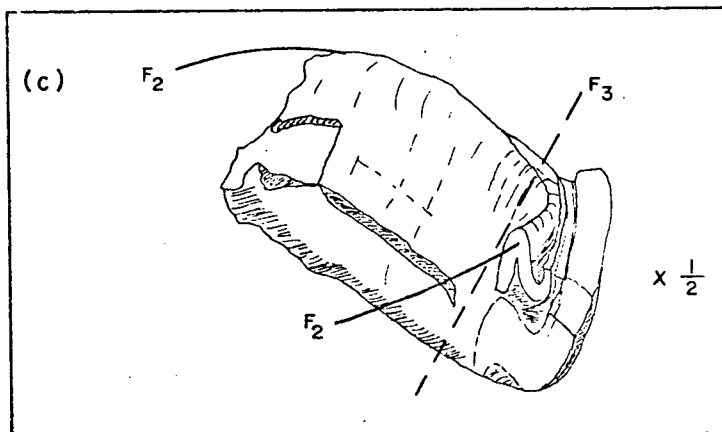


Fig. 18c F_2 fold in metachert folded by F_3 .

Structural Elements in the Lawsonite-Glaucophane Bearing Rocks

(a) Foliations (S -surfaces) : The most obvious structural feature of the metasediments and the foliated metavolcanics is the foliation (S_1) which appears to be concordant with the lithologic layering or bedding (S_0). In lithologies rich in white mica and glaucophane, this foliation might be termed a schistosity. Within limestones, S_1 is characterized by alternating layers of dolomite and streaky carbonaceous aragonite (Fig. 35). No trace of S_1 is seen in greywackes, massive metavolcanics and much of the limestone.

The S_1 foliation is cross-cut by an S_2 strain-slip cleavage best developed in foliated metavolcanics and glaucophane-mica schists. S_2 generally cannot be recognized in metacherts, metagreywackes and massive metavolcanics. Growth of mimetic minerals is not associated with S_2 .

Metacherts possess a fracture cleavage (S_3) with similar orientation to the joints described below. Where well developed, the cleavage is widely spaced (1 cm) and is axial planar to kink folds. On account of difficulty of recognition and confusion with complex fractures related to faults, only a few measurements of S_3 were made in the field.

(b) Lineations : The earliest structure (L_1) is a mineral lineation, best defined in foliated metavolcanics and metacherts by nematoblastic glaucophane (Figs. 16a, 16b). Very few measurements were made of L_1 in the field because of the scarcity of rocks in which the glaucophane was sufficiently coarse grained to discern the lineation.

Within the foliated metavolcanics, L_1 is deformed by an L_2 crenulate lineation (Fig. 16b). In the metacherts, L_2 occurs as a prominent crenulation on S_1 surfaces, defined by spindle-shaped aggregates of quartz and crenulated white micas. The L_2 lineation commonly parallels the L_1 mineral lineation within the metacherts but in samples possessing tight recumbent F_2 folds the orientation is variable (Fig. 18b). Coaxial L_1 and L_2 may result from rotation of glaucophane grains during the F_2 deformation.

At some localities, metacherts and quartz-carbonate schists form irregular mullions (Wilson, 1953) or elongate boudins with attitudes similar to L_2 (Plate 3).

(c) Joints: Most exposures of metachert and metavolcanic rock exhibit a prominent series of joints oriented approximately perpendicular to L_2 (Fig. 16b). Frequently, they are filled by vuggy, undeformed quartz veins.

(d) Folds : Three distinct periods of folding have been recognized and are termed F_1 , F_2 and F_3 , from oldest to youngest respectively.

Convincing fold closures associated with F_1 are seldom seen. The presence of mesoscopic tight isoclines with axial planes parallel to S_1 is inferred from the lensing out of compositional layering (Fig. 17) and apparent repetition of lithologic layering (on mesoscopic and macroscopic scales).

Within metacherts, mesoscopic F_2 folds (Figs. 17 and 18) are very conspicuous and, inasmuch as they do not show appreciable thickening of the hinge zones, are of concentric type. Slight thickening of fold hinges does occur in incompetent lithologies such as interbedded limestones and schists. F_2 fold axes are parallel to L_2 and in areas where F_3 is of mild intensity they trend at 300° and plunge at 55° (Fig. 15b). F_2 folds generally have a complex geometry with curving axial planes and may grade into fold mullions.

Kink folds (Fig. 16c) are characteristic of F_3 and deform F_2 folds and associated linear structures.

F_1 Deformation

Both mesoscopic and macroscopic fold closures associated with F_1 are very difficult to demonstrate. The only possible example of a mesoscopic closure is located on a

small island 4 km south of Pinchi Mine. Southerly dipping, bedded cherts form a tight southwesterly plunging isoclinal synform containing a schistose greywacke with S_1 axial plane cleavage deformed by L_2 crenulations.

The possible existence of F_1 isoclinal folds suggests that transposition of bedding may have caused the apparent parallelism of the primary lithologic layering with S_1 . Bedding transposition can be inferred in incompetent units such as graphitic cherts, where quartzitic layers are highly sheared and wedge out after a few inches. However, certain lithologies such as massive metavolcanics and metagreywackes generally show no signs of the pervasive shearing which must accompany transposition, and S_1 parallels the lithologic layering (S_0). It is considered likely that transposition has occurred only in the hinge zones of competent units thus explaining the rarity of convincing F_1 fold closures.

In summary, it appears that the F_1 deformation involved isoclinal folding, transposition of the bedding parallel to S_1 and synkinematic recrystallization of a blueschist facies mineralogy on attaining the necessary depth of burial (Fig. 19). The L_1 lineation possibly parallels F_1 fold axes.

F_2 Deformation

Mesoscopic F_2 structures are widespread within the area. L_2 and mullions parallel the axes of minor folds which deform S_1 and have an average trend and plunge of 300° and 55° (Fig. 15b). Minor folds are generally of the symmetric concentric type; both tight and open folds are common. Axial planes of minor folds are difficult to measure because of the prevalence of disharmonic folding and mullioning.

Because of widespread disruption by faulting and flexures associated with F_3 , macroscopic F_2 folds are difficult to recognize. In the mine area within domains of low F_3 intensity, the average strike and dip of the S_1 enveloping surface is 120° and 57° northeast (Fig. 15a and Map IV). Variation in strike is common in the vicinity of large limestone lenses which impose a local control on attitudes. However, on the northwest shore of Pinchi Lake, S_1 dip to the southwest along the lakeshore but dip to the northeast farther inland (Map V). Southerly dipping S_1 occur on the small island 4 km south of Pinchi Mine. These attitudes suggest the existence of a macroscopic antiformal structure with axial trace approximately centred on the long dimension of the glaucophanitic fault block and trending at 100° . There is no obvious girdle in the plot of poles to S_1 (Fig. 15a) which would demonstrate

the existence of this structure. This is because the structural data were obtained from the northern limb of the postulated antiform. A second possible antiform was identified 130 m north of the limestone lens 1.5 km west of Pinchi Mine.

There is a marked difference in plunge of L_2 between the northwest Pinchi area (Map V) and the mine area (Map IV); in the former the average plunge is 10°W and in the latter it is 55°W . It is considered that the steeper plunges are found immediately adjacent to the main Pinchi Fault where the intensity of the F_2 deformation was stronger.

In summary, the F_2 deformation is characterized by a prominent lineation and concentric, tight to open folds. Mullions are common and there is some suggestion that the intensity of deformation is related to the proximity of the Pinchi Fault. Major structures are interpretative but a probable east-west trending antiform is centered on Pinchi Lake. Blueschist facies minerals have been deformed by F_2 and metamorphic recrystallization is limited to albite, quartz and hematite (*see* p. 133).

F_3 Deformation

Structures related to F_3 are closely associated with faults and are best demonstrated in the Pinchi Mine area (Map IV) where a series of macroscopic F_3 cross folds deform earlier structures. Mesoscopic kink folds appear to be

associated with these cross-folds and trend 100° to 125° and plunge 10° to 60° southeast. The axial plane (S_3) is generally coplanar with the joints perpendicular to F_2 striking from 60° to 90° and dipping southeast at 45° . The variation in trend of F_3 fold axes depends on the initial orientation of S_1 with respect to F_3 . Therefore, varying orientations of S_1 theoretically should dispose F_3 fold axes in a great circle which defines S_3 . The spread of F_3 fold axes in Fig. 15c bears this out.

F_3 folds deform F_2 folds and lineations as illustrated in Fig. 18c. Theoretically, for concentric folding of L_2 situated on a plane of known orientation (e.g. S_1), the locus of L_2 should lie on a partial small circle on the local "b" kinematic axis (Turner and Weiss, p. 498). Little can be said as to whether the spread in L_2 in Fig. 15b defines a great circle or a small circle.

On the northern slopes of Pinchi Mine hill, S_1 strikes east-west and, rather unexpectedly, dips are southerly. This gives the impression that on the mine hill, the controlling structure is an easterly trending F_3 synform which plunges at 30° (Map IV). The occurrence of similar lithologic sequences on both north and south limbs reinforces this interpretation. However, the axial zone of this synform is highly faulted and carbonatized and relations between the limbs are obscure. Similar easterly trending

folds were mapped at various locations south of the fault separating the glaucophanitic rocks from the greenstones. It appears that the only way to make sense out of the structure in the mine area is to divide the area into domains which display some degree of homogeneity and draw faults along the domain boundaries. This is subjective to some degree but it presents a complex pattern of warping, faulting, block rotation and carbonatization along fault zones which is possibly close to the truth. Consideration of the trend and plunge of F_3 folds and of the sense of warping in the limestone beds suggest that right-lateral movement with a dip-slip component may have taken place along fault number 2 (Map VI) during F_3 .

Microscopic Analyses

The relationship between growth of metamorphic minerals and deformation is illustrated in Fig. 19.

Within the metacherts, thin layers of lepidoblastic white mica, acicular glaucophane and tabular lawsonite define S_1 and L_1 . In foliated metavolcanics the preferred orientation of glaucophane defines S_1 and L_1 . Some lithologies such as metagreywackes and massive metavolcanics do not have a preferred orientation of their metamorphic mineralogy and are unfoliated. Both lithologies do, however, grade into schistose types. It is assumed that

Fig. 19 Relationship of metamorphic recrystallization to deformation

Mineral	TYPE OF RECRYSTALLIZATION		
	Synkinematic (F_1)	Transitional stage	Synkinematic (F_2)
acmitic pyroxene	—————	-----	
jadeitic pyroxene	—————	-----	
lawsonite	—————	-----	
phengite	—————	-----	
sphene	—————	-----	
chlorite	—————	-----	
glaucophane	-----	—————	
aragonite	—————	-----	
calcite	-----		—————
stilpnomelane		—————	
brown amphibole		-----	
albite			—————
magnetite		?-----	
hematite			-----

unfoliated rocks possessed sufficient strength to withstand the F_1 penetrative deformation which gave rise to the foliated zones.

Some features offer fairly distinctive evidence that at least some minerals characteristic of the blueschist facies continued to recrystallize after the F_1 deformation. For instance, aragonite veins cross-cut S_1 in limestones (Fig. 35) and the mineral commonly is found closely associated with undeformed radiating clusters of a brown amphibole growing along fractures. A network of glaucophane or glaucophane + quartz veins typifies massive volcanics. Glaucophane is aligned either parallel or perpendicular to the walls. The problem arises as to whether these veins formed during or after the F_1 deformation. In hand specimen, some of them appear to be shears filled with glaucophane growing along small thrust faults which offset earlier glaucophane veins. Other veins are sigmoidal, resembling tension gashes, and in one specimen a glaucophane vein was seen cross-cutting a weak foliation (S_1). It was previously suggested in Chapter IV (p. 110) that minute fractures acted as channels for fluids which reacted with jadeite-acmite in the metavolcanics to form glaucophane. A reasonable explanation for the origin of the fractures is that some are shears related to F_1 and that others may be post- F_1 tension fractures which formed during uplift and/or the early stages of the F_2 deformation. Presumably,

this recrystallization came to a halt with decrease in pressure and temperature.

Blueschist facies minerals are deformed by F_2 crenulations. Glaucophane and lawsonite are commonly fractured, and white mica forms contorted swaths in metacherts (Fig. 36d). Quartz shows sutured boundaries and undulose extinction in some samples, but in others, strain-free polygonal aggregates suggest that recrystallization accompanied F_2 .

Restricted recrystallization of retrograde minerals occurred during F_2 . Albite veins form in metacherts and metavolcanics and also heal fractures in glaucophane crystals (Fig. 36c). Magnetite grains, believed to have formed during the glaucophanitic metamorphism, are commonly rimmed by retrograde hematite. Brecciation of the limestones resulted in partial inversion of aragonite to calcite and veining by sparry calcite.

F_3 deformation was accompanied by carbonatization along active fault zones. Vuggy quartz veins which commonly fill joints in metacherts may be associated with the latter stages of F_3 .

In summary, three stages of metamorphic recrystallization are proposed (Fig. 19). The first is a synkinematic stage associated with blueschist facies metamorphism and the formation of S_1 and the mineral lineation L_1 . The second is an ill-defined transitional stage between F_1 and

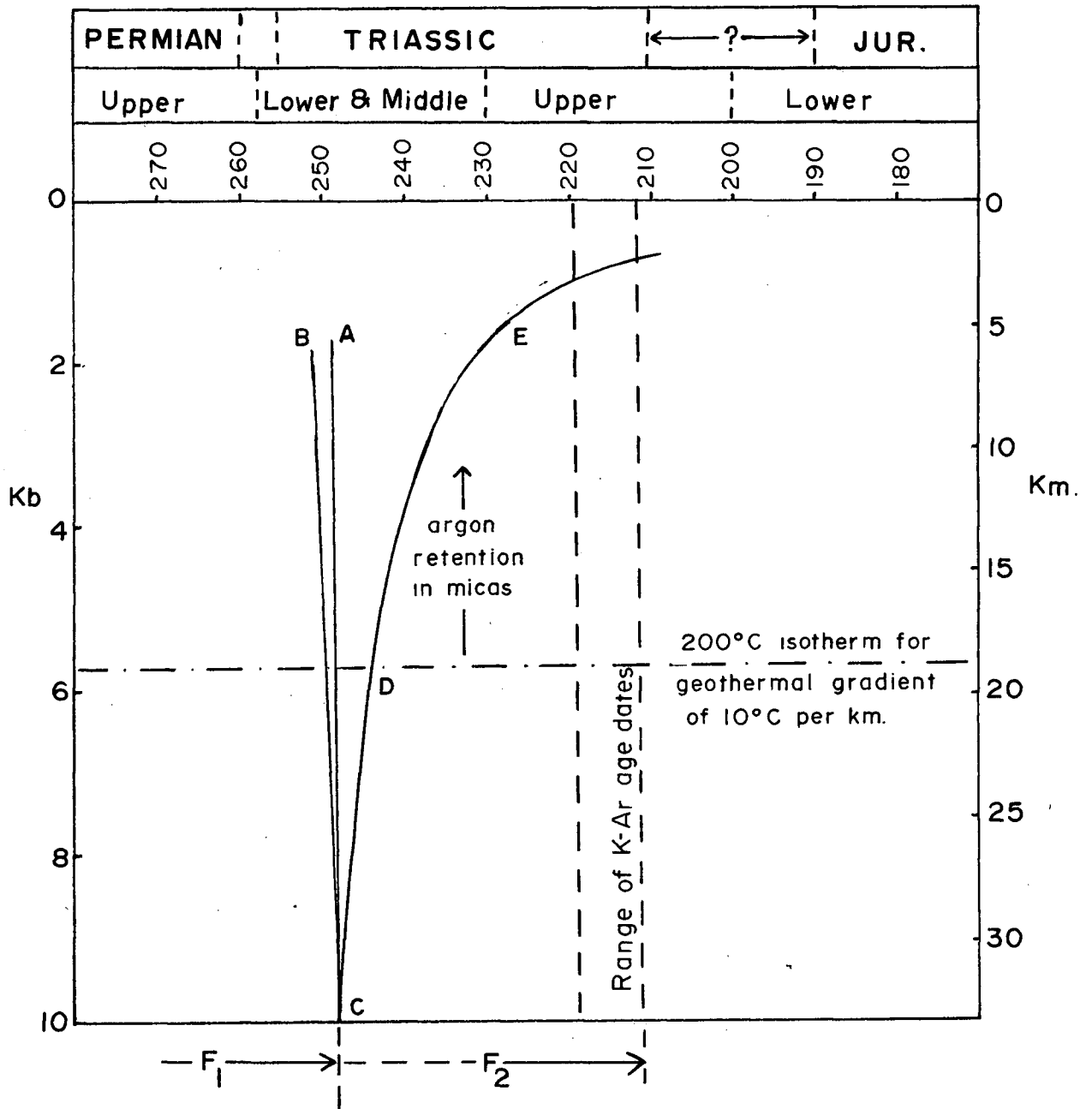
F_2 accompanied by recrystallization of minor glaucophane, aragonite, stilpnomelane and brown amphibole. A third stage involved deformation of blueschist facies minerals and recrystallization of quartz, and minor albite, white mica and hematite. This stage must have occurred at much lower pressure-temperature conditions than the first stage.

Timing of Metamorphism and Deformation

Because of the absence of fossils, the age of deposition of sediments in the blueschist bearing fault block is not known with certainty, but the lithologies present are similar to those in the Cache Creek or Slide Mountain Groups, suggesting a Mississippian to Permian age. Armstrong (1949) gave evidence for a Permo-Triassic deformation of the Cache Creek Group. It is inferred that this deformation was contemporaneous with the F_1 deformation in the blueschists, but the former occurred at a higher structural level.

A number of authors (e.g. Ernst, 1965) have argued that blueschist facies metamorphism takes place during rapid burial of sediments, creating conditions of low temperature and high pressure within the crust. For preservation of the characteristic mineralogy, it is essential that the metasediments have undergone a rapid uplift (Brown *et al.*, 1962). Metamorphic ages in a rapidly uplifted terrain should closely approximate the

FIG. 20 DEPTH-TIME TRAJECTORY FOR GLAUCOPHANITIC ROCKS



- Note :
- The Triassic-Jurassic boundary is arbitrarily placed at 200 m.yrs. with the uncertainty indicated. Data are from Tozer, 1964 (190-200 m.yrs.); Bochkarev & Pogorelov, 1967 (204 m.yrs.); Armstrong, 1970 (210 m.yrs.).
 - The Middle-Upper Triassic (230 m. yrs.) is taken from Borsi and Ferrara (1967)..
 - The Permo-Triassic boundary (255-260 m.yrs.) is obtained from Bochkarev & Pogorelov (1967).

actual age of metamorphism (Suppe, 1972). In the case of the Pinchi rocks, it has been argued that recrystallization of blueschist facies minerals was largely synkinematic but there is also evidence for a phase of post F_1 recrystallization which could only have occurred during the uplift.

Three K-Ar dates were obtained from phengitic micas present in schistose layers in cherts. Details of specimen location and analytical techniques are given in Appendix V. The dates obtained were 211, 214 and 216 \pm 7 m yrs. A fourth date of 218 m yrs was obtained from a micaceous eclogite.

These absolute ages correspond to Middle or Upper Triassic geologic ages depending on which time scale is used. If the Triassic-Jurassic boundary is taken at 190-200 m yrs (Tozer, 1964) it is conceivable that the dates could be Middle Triassic. Armstrong (1971) proposed a boundary between the periods at 210 m yrs and Borsi and Ferrara (1967) established a date of 230 m yrs for the Middle-Upper Triassic boundary. This being the case, the ages obtained at Pinchi are Upper Triassic.

If it is assumed that the micas did not absorb excess argon, two factors would have been responsible for these Triassic dates. They could reflect (a) the age of uplift and cooling to a temperature below the critical isotherm for argon retention and (b) the age of the

crenulation (L_2) which deforms the micas and is associated with the F_2 deformation. Typical F_2 structures such as minor folds, crenulations and mullions are not present in the Upper Triassic Takla Group even adjacent to the fault zone. This fact, together with the age dates, suggests that the F_2 deformation was in progress during deposition of the Upper Triassic but affecting rocks at a lower structural level. Uplift and cooling of the fault block to below 200°C must have occurred either before or during the F_2 deformation.

The foregoing facts and inferences suggest that F_1 deformation, metamorphism, uplift and F_2 deformation all took place between the beginning of the late Permian and the end of the Triassic (i.e. between 245 and 200 m yrs ago).

Possible depth time trajectories for the blueschists are illustrated in Fig. 20. If a subduction model is invoked (see Chapter VI), the rate of burial of sediments is approximately dependent on the rate of underthrusting and the dip of the subduction zone. For a subduction zone dipping at 45° , the times taken to descend 30 km at underthrusting rates of 10 cm per year (AC) and 1 cm per year (BC) are 0.35 m yrs and 3.5 m yrs respectively. The present day underthrusting rates of 10 cm per year in the Japan Trench (Oxburgh, 1971) suggest that the former appears

the more realistic time. At C, during blueschist facies metamorphism, it is assumed that there was a relaxation or change in orientation of the stress which caused the extreme depth of burial, and the block was allowed to isostatically re-equilibrate. Maximum uplift rates of the order of 1 cm per year have been used to reconstruct the CD part of the trajectory. Presumably, this uplift stage was accompanied by minor blueschist facies recrystallization until cooling resulted in a "freezing" of the metamorphic mineralogy. At D, assuming a geothermal gradient of 12°C/km, the glaucophanitic rocks passed through the 200°C isotherm which represents the approximate temperature for argon retention in muscovites (Suppe, 1972). Theoretically this should represent the maximum age date obtainable from the blueschists. From D to E the block continued to rise at a decreasing rate because of approach to isostatic equilibrium. The F_2 deformation must have occurred during this part of the trajectory, possibly causing argon loss in the micas and resetting the age dates. Point E is somewhat arbitrarily chosen at 4.6 km from the surface. This depth represents the amount of rock eroded in 230 million years, assuming an erosion rate of 1 m per 50,000 years.

F_3 deformation was accompanied by carbonatization along fault zones. It was previously inferred (p. 67) that the carbonatization occurred during the Eocene.

Structural Geology of Remaining Fault Blocks

The internal structure of the remaining fault blocks has been adequately dealt with in the appropriate sections in Chapter II. The following summary facilitates comparison of structures in different fault blocks.

Greenstones of Pinchi Mountain (Map I, Units 5 and 6)

These rocks are well foliated and interbedded graphite schists possess an S_1 . Drill hole intersections of an intercalated limestone unit indicate that these rocks dip north or northeast at 45° . This dip is conformable with the layering in the silica-carbonate rocks which form the northeastern boundary of the greenstone unit.

Mount Pope belt (Map I, Units 7, 8 and 9)

The Mount Pope belt is of Pennsylvanian to Middle Permian age and was deformed during the Permo-Triassic. The basic rocks belong to the lower greenschist facies. Argillites possess a slaty cleavage which commonly cross-cuts the bedding in the hinge zones of early folds. To the west of the map-area, a partial cross section of the Cache Creek Group is revealed in the north arm of Stuart Lake. The northwesterly striking cleavage is fanned and dips grade from vertical in the west to 25° southwest towards the east. Deformation is of Permo-Triassic age

(Armstrong, 1949) and is considered to be the low pressure, high level expression of the F_1 deformation in the blueschists.

Paleontological evidence (Appendix I) demonstrates the presence of a syncline which appears to run the length of the map area. Judging from the southwest dip of chert beds on either side of the limestone belt, it would appear that the syncline is asymmetric with a southwesterly dipping axial plane. At intervals along the strike of the belt, the limestone appears to cut out; this is thought to be due to local culminations in the plunge of the syncline.

Ultramafites (Map I, Units 14a and 14b)

Structural relationships outlined in Chapter III suggest that the following sequence of events has taken place within the ultramafites. Correlation of deformational phases with those recognized in the blueschists is tentative.

- (a) Magmatic crystallization of harzburgite and intrusion of dunite pods,
- (b) Formation of early pyroxenite and dunite layers,
- (c) Folding and high temperature metamorphic recrystallization within the mantle (?),
- (d) Formation of late pyroxenite layers,
- (e) Emplacement, pervasive fracturing, introduction of connate (?) water and serpentinization (This

event was possibly contemporaneous with F_1 and/or F_2 deformations).

- (f) Formation of late fracture cleavage, foliation of the serpentinite along fault zones and minor serpentinitization (contemporaneous with F_2 or F_3 deformations).

Basic rocks south of Pinchi Lake (Map I, Unit 4)

This belt of rocks is bounded to the north by Takla Group sediments of Upper Triassic (?) age and to the south by an elongate serpentinite body thought to be associated with a major fault (Map VI, No. 3). It is uncertain whether the northern contact of unit 4 is a fault or an unconformity. An unconformity is more probable because of the presence of a conglomerate containing pebbles of a metabasic rock near the base of a Takla Group (?) sedimentary sequence (unit 10). If this is an unconformity, the following sequence of events must have taken place:

- (a) fracturing, introduction of water and amphibolization of metabasic rocks prior to or during Permo-Triassic deformation,
- (b) deposition of Upper Triassic (?) sediments of the Takla Group, and
- (c) overturning of the sequence during Mesozoic or Tertiary deformation.

Takla Group (Map I, Units 10, 11 and 12)

Rocks belonging to this group are unfoliated and have been subject to low grade burial metamorphism rather than the dynamic metamorphism which characterizes the Cache Creek Group. Structural elements include a fracture cleavage in siltstones and sparse kink bands. Folds are rare and appear to be gentle warps in the vicinity of faults. The intensive faulting is the result of Mesozoic or Tertiary deformation.

Important Faults in the Pinchi Area

The fault pattern at Pinchi is highly complex and has divided the area into a series of elongate tectonic slices of contrasting metamorphic grade. All faults have been numbered for reference purposes (Map VI) with splay faults indicated by an alphabetical subscript (e.g. 2a, 2b).

In areas of poor exposure, fault recognition is extremely difficult. Some of the criteria used at Pinchi are as follows:

- (a) abrupt change in metamorphic grade, structural complexity or lithology,
- (b) presence of carbonatized zones in ultramafites or metasediments,
- (c) presence of serpentinites and associated linear magnetic highs,

- (d) occurrence of linear topographic lows containing sporadic sag ponds, and
- (e) fault breccias encountered in drill core or, rarely, in outcrop.

Once a fault has been established on these criteria, it is even more difficult to demonstrate the age of faulting and type of movement. This difficulty is largely because of the scarcity of rocks younger than Lower Jurassic. However, information on the age and type of fault activity can be obtained from

- (a) proven relationships in adjacent map-areas,
- (b) minor structures such as drag folds, lineations and slickensides, and
- (c) metamorphic grade of rocks which have been juxtaposed.

An additional factor which must be considered, especially in areas of major faults, is the possibility of reactivation of an old fault under a different stress system.

Pinchi Fault (No. 1)

Within the map area, the Pinchi Fault juxtaposes rocks of the Takla and Cache Creek Groups. To the southwest of the fault zone, the Cache Creek Group is closely associated with ultramafic bodies and has been metamorphosed under lower greenschist or blueschist facies conditions.

Evidence has been given for two periods of deformation, F_1 and F_2 , prior to the deposition of the Upper Triassic.

Most information on the fault zone was obtained just east of Pinchi Mine where it appears to be about 2000 ft wide. Percussion drill cores across the fault indicated the presence of slivers of serpentinite, brecciated volcanics, carbonatized ultramafites and contorted carbonaceous schists. Ground magnetics indicate an excellent correlation between serpentinite slivers and linear magnetic highs. The slight offset of the magnetic highs with respect to the drill hole information suggests that the serpentinites dip steeply to the northeast.

The only other evidence on the attitude of the fault zone is the occurrence of a northeasterly dipping fracture cleavage within the ultramafites along the northeast margin of Murray Ridge. These planar structures (S_2 ?) probably parallel the fault zone in the Pinchi area. However, 30 miles farther north, symmetric aeromagnetic profiles across the fault zone suggest that it is vertical, and indicate that the dip of the fault zone may be variable along its length.

The Pinchi Fault is one of the major tectonic lineaments in central British Columbia. It has been traced from near Quesnel 500 km north-northwest to the McConnell Creek map-area where it appears to dissipate in a number of splay faults. Lord (1949) and Eisbacher (1969) demonstrated

that in the McConnell Creek area Sustut Group rocks of late Cretaceous to Eocene age have been involved in north-easterly directed thrust faulting. Eisbacher (oral communication) believes that the presence of the extension of the Pinchi Fault at depth in a Paleozoic-early Mesozoic basement may have controlled the positioning of thrust faults in the cover rocks. This line of reasoning suggests active movement of the fault during the Eocene prior to the mercury mineralization (p. 67).

Along the northern part of the fault zone, rocks of the Cache Creek Group are faulted against the Hogem batholith which, according to Armstrong (1949), is of Jurassic age. A K-Ar radiometric date of 170 million years was obtained for the Hogem (Koo, 1968). Significantly, metasediments of the Cache Creek Group adjacent to the fault zone are highly sheared and show no sign of contact thermal metamorphism. These data also indicate that active faulting must have taken place after the emplacement of the Hogem batholith (i.e. post Middle Jurassic). The history of movement on the Pinchi Fault is complex and closely linked to the deformations as discussed in Chapter VI.

Fault system no. 2

The trace of this fault system is sub-parallel to the Pinchi Fault and numerous splays intersect it. The most persistent fault separates the Pinchi Mountain green-

stones to the north from the lawsonite-glaucophane bearing rocks. Drill intersections of fault 2d indicate that it dips to the northeast at 60° on the Darbar claim group and immediately east of Pinchi Mine. However, 3 km west of Pinchi Mine, the fault is apparently vertical. Splay faults juxtapose ultramafites, greenstones and blueschists. Carbonatization along these fault zones is locally extensive and ultramafic slivers have been partly converted to the silica-carbonate rocks (p. 63 ; Plate 5). The foliation in the silica-carbonate outcrop generally dips to the north or northeast at 60° to 70° and is parallel to the fault plane as verified by drill hole intersections and ground magnetic profiles.

A sliver of chert pebble conglomerate is located in the footwall of fault no.2d on the Darbar claim group. The only conglomerate with which it could possibly be correlated is found at the west end of Murray Ridge and is believed to be of Cretaceous or Paleocene age (p. 44). At the Darbar locality, fault 2d dips to the northeast at 60° and separates greenstones from a chaotic mixture of glaucophanitic metabasic rocks, carbonatized serpentinites, sandstones and conglomerates constituting the footwall. The involvement of a Cretaceous or Paleocene conglomerate in the faulting suggests that this fault was active during Eocene tectonic activity. Presumably, southwesterly directed thrusting of the greenstones caused the formation of a melange zone in the footwall.

A similar situation exists just to the east of Pinchi Mine where the so called "breccia" zone is found along the northeasterly dipping greenstone contact. This "breccia" mainly consists of angular chert fragments in a magnesitic matrix, but the presence of rare, rounded chert pebbles suggests that the "breccia" may originally have been a conglomerate. It is possible, however, that the rounded chert pebbles originated as angular fragments but were resorbed during the carbonatization.

Fault system no. 3

This fault system lies between the Mount Pope limestone belt and the southwest shore of Pinchi Lake. Along its length, lawsonite-glaucophane bearing rocks to the northeast are faulted against ultramafites, cherts and Upper Triassic (?) limestones and siltstones. The relationship among the last mentioned sediments, gabbros and ultramafites is not clearly understood and the contacts may or may not be the sites of faults associated with this system.

Judging from the aeromagnetic profiles across the serpentinite sliver which parallels the fault zone, it would appear that the dip of the fault varies along the strike. North of Mount Pope, the profile GH (Map II) suggests that the serpentinite has a moderate southwest dip, similar to the attitude of the bedding in cherts adjacent to the fault

zone. Towards the north-northwest however, cherts near the fault zone dip to the southwest at 80° and the aeromagnetic anomaly decreases in intensity, suggesting that the serpentinite sliver is no longer present.

Fault system no. 4

The lineaments 4a and 4c trend east-northeast and may well be major fracture zones rather than faults as there is no sign of offset of lithologic units. They form low lying swampy areas, and folds within the limestone belt tend to plunge away from the fracture zones. Faults 4b and 4d are inferred, firstly because they occupy topographic lows and secondly because of the apparent right-lateral offset of the linear magnetic high which follows the serpentinite belt (Map III) southwest of Pinchi Lake. Whether this "offset" is the result of normal or strike-slip movement is uncertain. It is interesting to note that the Pinchi Fault appears to have undergone left-lateral offset by fault 1a.

Fault system no. 5

The only evidence for this fault is an abrupt change in strike of the Takla sediments on either side of it. The fault is parallel to the Pinchi Fault and appears to intersect it north of Murray Ridge.

Faults in the vicinity of Pinchi Mine (Nos. 2c and 6)

The fault pattern around the mine is exceedingly complex and only the well documented faults will be listed here. Fault 2c trends southeast and dips to the northeast at 80°. It may well be an early fault as it is associated with ultramafic slivers. Faults 6b (the "south fault") and 6a dip to the southwest at 50° to 60° and are post-mineralization. According to Armstrong (1949) and the mine geologists, fault 6a is a thrust fault with left lateral oblique-slip displacement. These faults are crosscut by late northerly trending normal faults with near vertical dip.

TECTONIC IMPLICATIONS

Introduction

The general conclusion arrived at in recent studies is that the formation of orogenic belts containing blueschists is related to the interaction of lithospheric plates. Ernst (1970) suggested that blueschist facies metamorphism results from the down-warping of the earth's crust in a subduction zone and deep burial of sediments. Coleman (1971) agrees that this may be a valid mechanism but also suggests that blueschist formation takes place as the result of tectonic overpressures developed in shallow dipping zones underneath obducted oceanic crust. In contrast to subduction zones, obduction zones are characterized by a complete lack of associated volcanic activity.

An important feature of orogenic belts containing blueschists is their association with ophiolites, and their presence is commonly taken as evidence for involvement of oceanic crust during plate interaction (Dewey and Bird, 1970; Coleman, 1971). Commonly cited examples occur in New Caledonia (Lillie and Brothers, 1970) and western

California (Bailey *et al.*, 1970; Page, 1972) where ophiolitic sequences are believed to have been thrust over sediments undergoing blueschist facies metamorphism presumably during active subduction or obduction.

According to Ernst (1971), former subduction zones can be recognized by a characteristic metamorphic zonation with respect to a major fault. He gives examples from Japan, western California and the Alps where the commonly developed metamorphic sequence towards the fault is:

(a) zeolitized rocks, (b) pumpellyite bearing rocks, (c) greenschists and/or blueschists and (d) albite amphibolites. The preservation of this zonation is attributed to a change in orientation of the stress field which caused the formation of the subduction, and isostatic uplift of the buried sediments. An interesting feature of the areas referred to is the occurrence of post-uplift strike-slip movement on the major fault zones.

These fault zones separate regions with contrasting sedimentary records, structural style and grade of metamorphism, and are believed to be zones of plate interaction. The term "suture zone" is used to describe the contact between two such juxtaposed regions. Examples commonly given are the Median Tectonic Line in Japan, the Coast Range Thrust in California and the Insubric Line in the Swiss and Italian Alps. These suture zones are thought to represent fundamental zones of weakness in the earth's

crust which may have been the locus of underthrusting during subduction giving rise to Benioff zones. Thereafter, the suture zone may have been the site of post-subduction uplift or strike-slip movement.

Constraints to Tectonic Model (Factual and Inferred)

Conclusions of this study

- (a) The inferred pressure-temperature conditions for metamorphism within the various fault-bounded blocks are as follows:

Murray Ridge greenstones	3-6 kb	100-225°C
Pinchi Mountain greenstones	4.5-9 kb	100-250°C
Blueschists	8-12 kb	225-325°C
Eclogite	12-15 kb	400-550°C

- (b) The blueschist facies metamorphism was contemporaneous with the F_1 deformation. This was closely followed by the F_2 deformation which seems to have been associated with uplift and cooling. The K-Ar dates of 211, 214, 216 and 218 ± 7 m yrs are considered to record cooling below 200°C and/or the close of the F_2 deformation (p. 136).
- (c) Greywackes and conglomerates within the Upper Triassic Takla Group contain detritus which originated in a landmass consisting of basalt, amphibolitized gabbro, ultramafite and chert (p. 42).

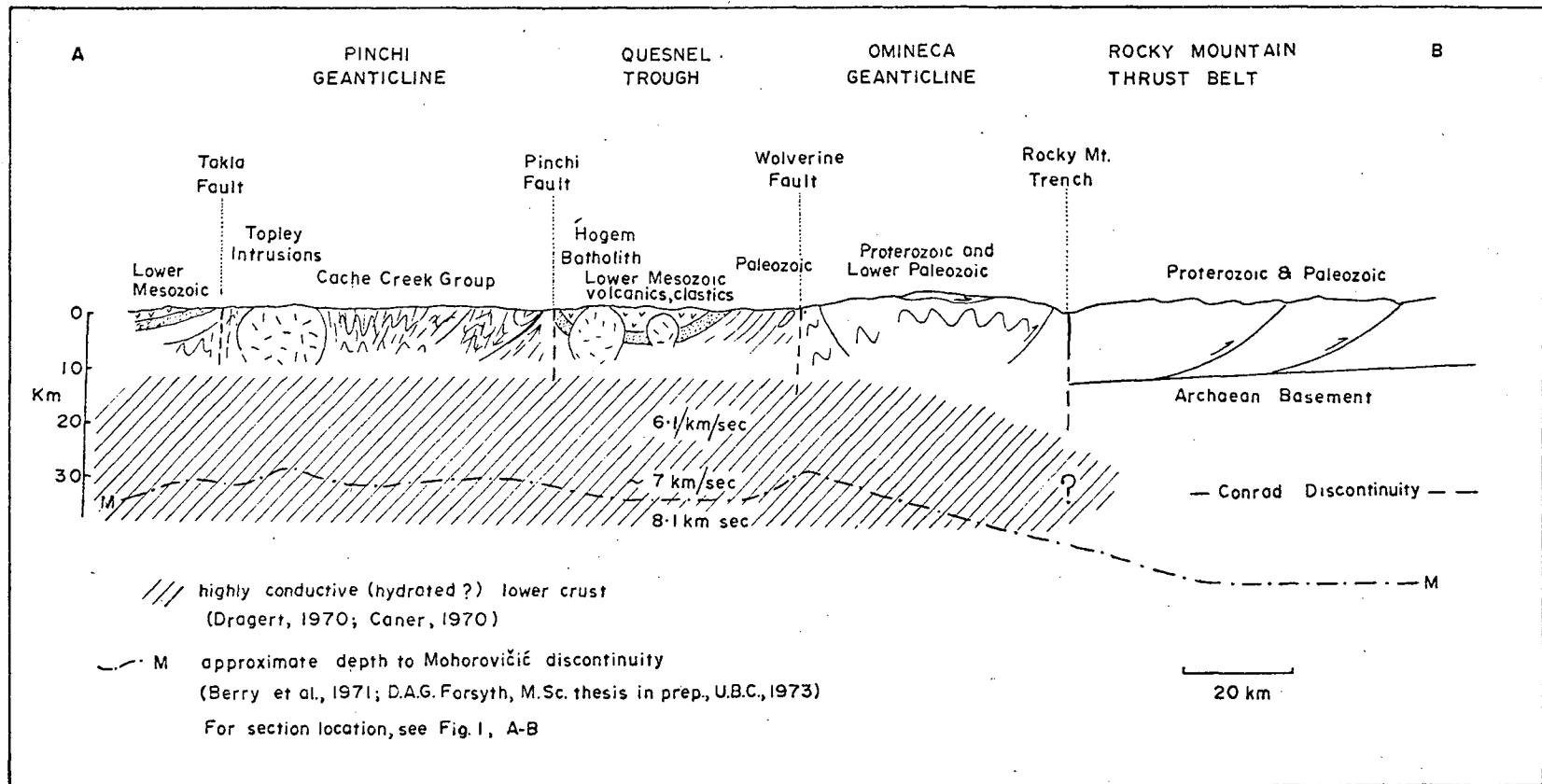
- (d) South of Pinchi Lake, serpentinite is overlain by amphibolitized gabbro, diabase, basalt and Upper Triassic (?) conglomerate. These basic and metabasic rocks may represent an ophiolitic sequence (p. 26).
- (e) The F_3 deformation was contemporaneous with the carbonatization of fault zones and possibly occurred during the Eocene (p. 67).

Inferred crustal structure in central British Columbia

Largely because there are no inliers of older rocks in the Cache Creek Group and because it contains ophiolitic sequences, Monger *et al.*, (1972) and Dercourt (1972) have implied that the Group is underlain by oceanic crust. By analogy with other regions (Bailey *et al.*, 1970; Page, 1972), such an oceanic crust would be expected to consist of basalts grading downwards into diabase, gabbro, harzburgite and dunite.

In central British Columbia seismic and gravity data suggest that the M-discontinuity lies between 30 and 35 km below the surface (Berry *et al.*, 1971). Evidence suggests that the oceanic M-discontinuity represents a gabbro/harzburgite transition (Coleman, 1971; Aumento *et al.*, 1970). Therefore it would appear that the Cache Creek Group within the Pinchi Geanticline must be at least 25 km thick, allowing for 5 km of basalt and gabbro. However, Armstrong

FIG. 21 CRUSTAL MODEL FOR CENTRAL BRITISH COLUMBIA



(1949) estimates the maximum thickness of the Cache Creek Group as being 6 km. This is considered an overestimate, as wherever detailed work has been done, repetitions of strata have been recognized (Douglas *et al.*, 1970, p. 416). It follows that if the interpretations of seismic and gravity data are valid, a surprising amount of tectonic thickening of the Cache Creek Group must have taken place to give a depth of over 25 km to oceanic crust.

Geomagnetic depth sounding and magnetotelluric studies in central British Columbia (Dragert, 1970) suggest the presence of an important discontinuity in the conductivity of the earth's crust at a depth of 10 to 15 km. The transition from a poorly conductive surface layer to a highly conductive lower layer is interpreted as being due to partial melting or hydration of the lower crust (Caner, 1970). Partial melting at depths of 10 to 15 km commences at approximately 700°C in a "wet" granite and would imply steep, unrealistic, geothermal gradients of the order of 40° to 70°C per km. Moreover, if partial melting did exist, it would be expected to give rise to Quaternary volcanicity at the surface. Study of nodules within Quaternary basalts from British Columbia (Littlejohn, 1972), suggests that they had a fairly deep-seated source, possibly around 35 to 70 km, and could not therefore be related to partial melting between 10 and 30 km. Therefore, hydration seems

to be the best mechanism for explaining the increase in conductivity of the lower crust.

The presence of a 10 to 15 km discontinuity beneath the Cache Creek Group therefore suggests that the somewhat unrealistic thickness of over 25 km inferred from seismic and gravity results may be in error. To compromise the geological and geophysical evidence, a crustal model is proposed (Fig. 21) in which the Pinchi Geanticline, consisting of tectonically thickened Cache Creek Group with associated ophiolites, is 10 to 15 km thick and the lower crust is a mixture of serpentinized peridotite, amphibolite, slivers of Cache Creek Group and possibly minor eclogite. Increasing temperatures may result in dehydration reactions which give rise to interstitial water vapour, thus creating the conductivity anomaly. The discontinuity at 30 to 35 km proposed by gravity and seismic models may represent the transition to anhydrous peridotite.

A possible alternative model would show the Cache Creek Group and associated ophiolites as being underlain by lower Paleozoic rocks and/or basement gneisses down to the M-discontinuity. Such a basement could have been thrust under the Cache Creek Group during Mesozoic tectonism. This model is thought unlikely as lower Paleozoic or gneissic rocks which could be interpreted as basement have not been recognized in the intermontane region. Also, serpentinite and peridotite have a much lower resistivity than granitoid

rocks (Caner, 1970) and would therefore be more likely to yield the conductivity anomaly below 15 km.

The Pinchi Fault as a "Suture Zone"

The possibility exists that the Pinchi Fault lies within a Permo-Triassic "suture zone" which welded together two tectonic belts of contrasting age and/or primary depositional environment. For much of the length of the fault, Cache Creek Group rocks are in contact with lower Mesozoic greywackes, volcanics and intrusives (Fig. 22). To the east of the Mesozoic is a belt of rocks formerly mapped as late Paleozoic by Armstrong (1949) and Roots (1954). These rocks were re-examined by Monger (1973) and his preliminary stratigraphic data are shown in Fig. 22. A number of important observations emerge from these studies. Firstly, the belt contains rocks ranging in age from Proterozoic to Middle Pennsylvanian. Younger rocks may be present but diagnostic fossils have not been found. Secondly, in the Lay Range, Pennsylvanian rocks are intruded by the Polaris ultramafite. Thirdly, the Pennsylvanian rocks, of similar age to the lower part of the Cache Creek Group west of the Pinchi Fault, consist of volcanic sandstone, agglomerate, carbonate pods, red radiolarian chert and argillite. It therefore appears that rocks of similar age, association and metamorphic grade are found on both sides of the Pinchi Fault and there is no obvious justification for calling

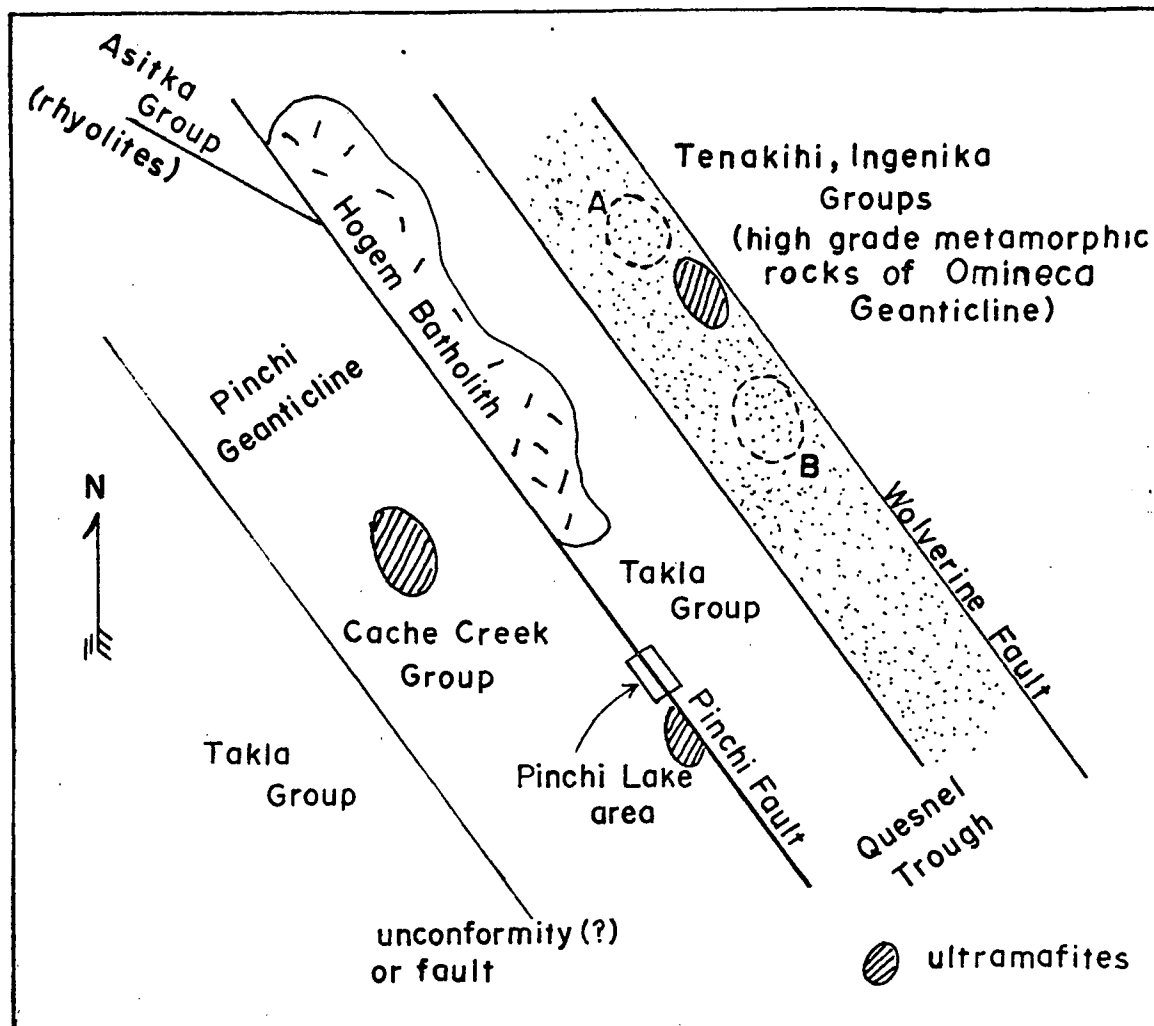


Fig. 22 Generalized diagram illustrating location of major geologic units in central British Columbia in relation to the problematical belt of Paleozoic rocks between the Takla Group and the Omineca Geanticline (stippled area). The stratigraphy in this belt was reported on by Monger (1973). Area "A" in the Lay Range contains a highly faulted section consisting of (a) Early Pennsylvanian (?) volcanic sandstone and agglomerates, and (b) Middle Pennsylvanian carbonate, breccia and sandstone. Area "B", near Germansen Landing, contains a section extending from latest Proterozoic to possible Mississippian.

the fault a "suture zone." However, in the eastern belt a much longer depositional history is recorded extending from the Proterozoic to the Upper Paleozoic. There are also differences in lithologies between the two belts, the most important of which are the paucity of bedded chert and the occurrence of an appreciable thickness of volcanic sandstone and agglomerate within the belt to the east of the fault. Whether these two factors present sufficient justification to call the Pinchi Fault a suture zone is open to speculation. Perhaps the term may equally well be applied to the major fault which separates the Omineca Geanticline from the Paleozoic rocks to the east (i.e. the Wolverine Fault).

Paleontological evidence suggests that the Pinchi Fault separates two late Paleozoic faunal belts (Monger and Ross, 1970) but there is uncertainty as to whether the different faunas are the result of local variation in depositional environment or the "juxtaposition of originally isolated biogeographic provinces by major crustal movements." On account of Asiatic faunal affinities, Wilson (1968) suggested that the western part of the Canadian Cordillera had drifted across from Asia. The collision zone as represented by Wilson lies to the west of the Omineca Geanticline and presumably follows the Pinchi or Wolverine fault zones.

Evidence for strike-slip movement on the Pinchi Fault

The length (450 km) and straightness of the Pinchi Fault suggest that at some time in its history, it may have been a strike-slip fault. In the McConnell Creek map-area, Upper Triassic Takla Group rocks are found astride the continuation of the fault, suggesting that if there was significant strike-slip displacement it must have taken place prior to the Late Triassic. As the fault cuts across folded Cache Creek Group limestones, strike-slip movement probably post-dates Permo-Triassic (F_1) deformation and may have been contemporaneous with the Triassic F_2 deformation in the blueschists.

It is interesting to speculate whether oblique-slip movement on the fault could have given rise to the F_2 structures at Pinchi. These structures are characterized by moderately plunging folds (55°) which trend sub-parallel to the Pinchi Fault and are associated with mullion structures in incompetent rocks and a crenulate lineation (L_2) parallel to the fold axes. If dip-slip movement on the fault resulted in elevation of the Pinchi Geanticline during the Middle and/or Upper Triassic, it is conceivable that the F_2 structures in the blueschists may well have formed as the result of right-lateral oblique-slip movement on the Pinchi Fault. Steeply plunging folds adjacent to major fault zones have also been described in the South

Island of New Zealand. Lillie (1964) has suggested that they formed during an episode of strike-slip faulting.

Possibility that the Pinchi Geanticline was overlain by oceanic crust

There is some evidence which suggests that the Cache Creek Group in central British Columbia may have been overlain by oceanic crust. The Upper Triassic rocks at Pinchi contain abundant detritus which indicates erosion of a landmass consisting of amphibolitized gabbro, basic volcanics and cherts. The presence of conglomerate and carbonaceous wood fragments in the Upper Triassic suggests that the landmass was close-by, most likely on the site of what is now the Pinchi Geanticline. South of Pinchi Lake, a serpentine-amphibolitized gabbro-diabase-basalt sequence is overlain by Upper Triassic (?) pebble conglomerates, siltstones and limestones. It is suggested that these basic rocks might represent a downfaulted remnant of the cover of the Pinchi Geanticline during the Upper Triassic and that the basalt/pebble conglomerate contact is a disconformity.

Absence of metamorphic zonation within the Cache Creek Group

Ernst (1971) has related progressive metamorphic zonations in Japan, California and the Alps to descent of lithospheric plates down subduction zones. Reconnaissance

work by Armstrong (1949) and the writer indicates that the bulk of the Cache Creek Group west of the fault zone has been metamorphosed in the lower greenschist facies, and apart from the elongate fault-bounded wedge of blueschist adjacent to the fault there is apparently no change in metamorphic grade. There is therefore no evidence within the Cache Creek Group of a metamorphic zonation which could be attributed to plate descent.

Tectonic Models

Subduction model

If hypotheses involving tectonic overpressures are discarded (p. 69), the most plausible mechanism for the generation of blueschists is by subduction. This model involves descent of an oceanic plate under the continental crust and formation of an eastward dipping Benioff zone. Downwarping of the earth's crust is accompanied by deep burial, deformation and metamorphism of the sediments which accumulated in an offshore oceanic trench. Consumption of oceanic crust is believed to be related to calc-alkaline plutonism and volcanism above a descending plate (Dickenson, 1968). Therefore the absence of Permo-Triassic volcanics or plutonics to the east of the Pinchi Fault could be looked upon as a major drawback to the subduction model. However,

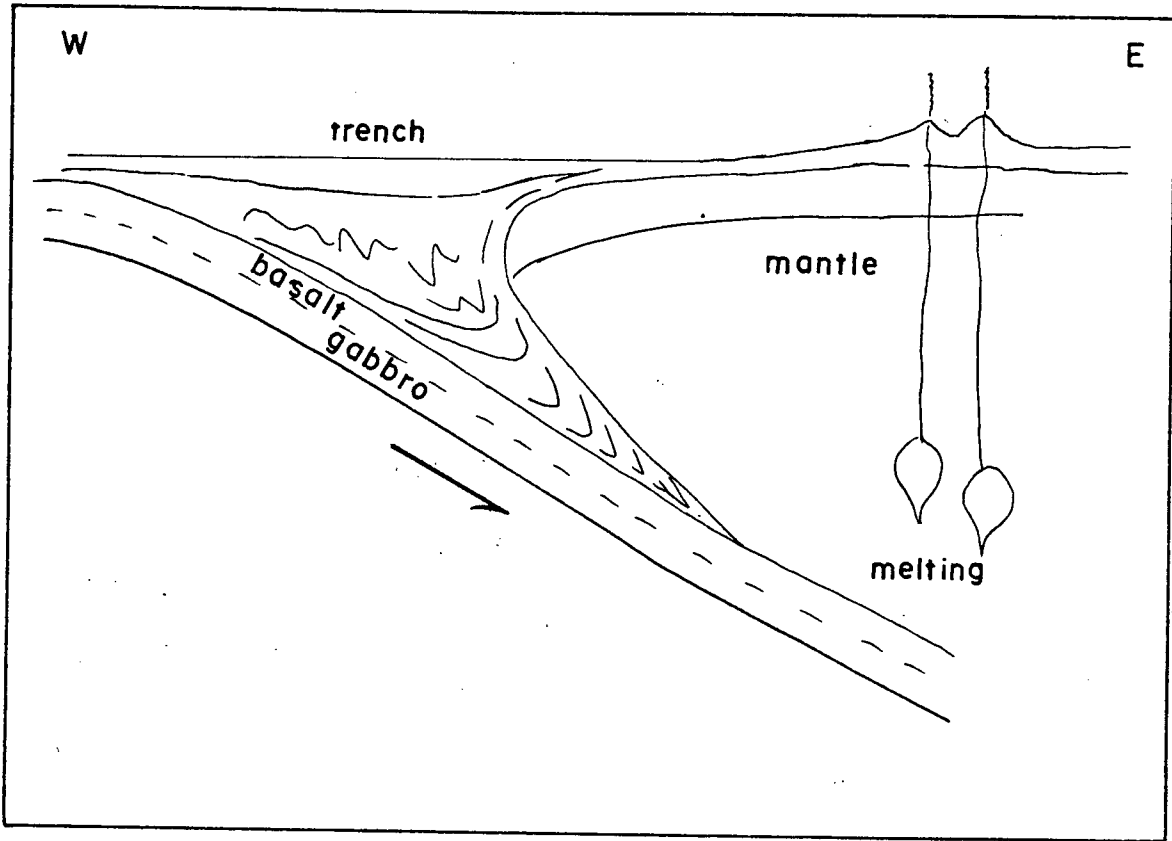


Fig. 23 Subduction model

major strike-slip movements on the fault may have taken place and the igneous rocks associated with the subduction have to be sought elsewhere. One possibility is the Asitka Group which is situated in the McConnell Creek map-area 240 km north of Fort St. James. It is considered to be of Permo-Triassic age (Monger, 1973) and consists of 2000 m of rhyolite and minor andesite.

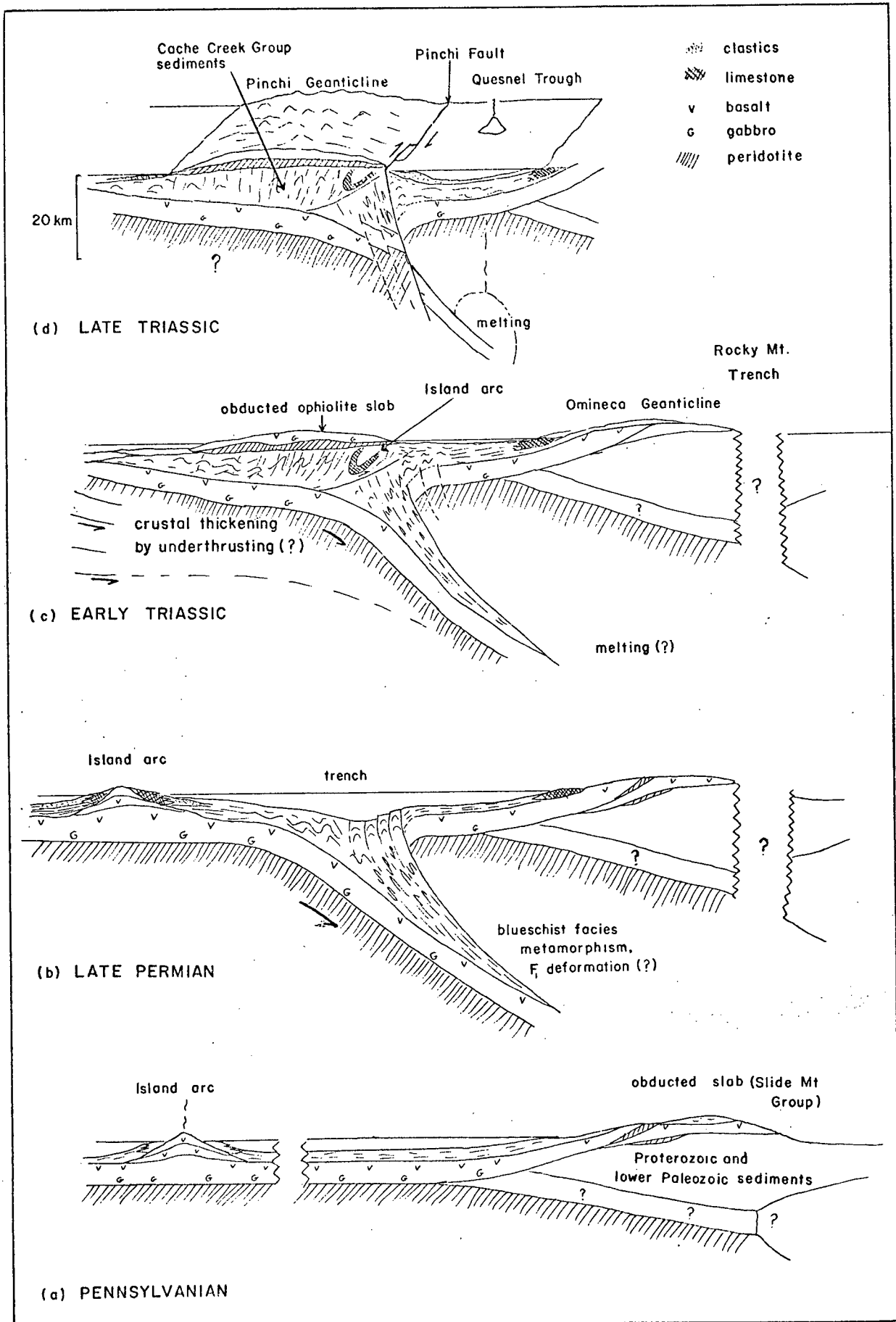
Intrusives are present in the Omineca Geanticline and could represent the source for overlying volcanics which have since been eroded, in which case the Tertiary K-Ar dates (Douglas *et al.*, 1970) would reflect a regional uplift or a reheating event. The Omineca Geanticline may therefore represent the high temperature-high pressure zone in a Permo-Triassic paired metamorphic belt which formed above an active east-dipping subduction zone.

On relaxation of the stresses which caused subduction, isostatic readjustment of the deeply buried sediment pile gave rise to a regional uplift resulting in the formation of the Pinchi Geanticline. The formation of the Quesnel Trough to the east of the Pinchi Geanticline may well have been caused by downwarping of the crust above the exhumed subduction zone. Such a mechanism is believed to be responsible for the formation of the Po Basin and the Great Valley of California (Ernst, 1971). The Pinchi Fault may originally have been one of the major faults in the

subduction zone. During the uplift, the sense of movement may well have been reversed and deeply buried sediments such as the blueschist-bearing fault-block exploited the fault zone as an easy upward path in establishing isostatic equilibrium.

There are three main drawbacks to this model. Firstly, it is difficult to explain the occurrence of ophiolites exposed at the surface of the uplifted Pinchi Geanticline. Presumably, the ophiolites were thrust over the Cache Creek Group either from the west or the east. Secondly, it is to be expected that a regional uplift of the metasedimentary pile should give rise to a progressive metamorphic zonation with respect to the Pinchi Fault as seems to have happened in Japan, the Alps and California (Ernst, 1971). However, the bulk of the Cache Creek Group is in the lower greenschist facies and the blueschists form an isolated fault-bounded wedge adjacent to the fault. The third drawback is the apparent absence of calc-alkaline plutonism and volcanism contemporaneous with subduction. A possible explanation could be that the subduction zone had a very shallow dip and was similar to an obduction zone. Coleman (1971) states that obduction zones are characterized by a complete lack of volcanic activity. However, a shallow dipping obduction zone would make it difficult to explain the high lithostatic pressures necessary to create the Pinchi blueschists without resorting to tectonic overpressures.

Fig. 24 Subduction-obduction model illustrating evolution of main tectonic features in central British Columbia (a) During the Pennsylvanian, rocks of the Slide Mountain Group were obducted over the Proterozoic and Lower Cambrian rocks constituting the Omineca Geanticline (after Monger, *et al.*, 1972). (b) The formation of an eastwards dipping subduction zone gave rise to blueschist facies metamorphism and deformation of Cache Creek Group sediments. (c) An island arc impinged on the subduction zone and because it contained a large thickness of buoyant low density material, was not subducted. Obduction of an ophiolite slab, either from the east or west appears to have accompanied this event. The crust below the Pinchi Geanticline may well have been thickened by underthrusting during or after this period to give the observed depth of 30 km to the M-discontinuity. (d) A change in orientation of the stress regime, resulted in right-lateral oblique-slip movement along the Pinchi Fault zone and uplift of the Pinchi Geanticline. Blueschist and serpentinitized ultramafite diapirs were emplaced along the fault. Detritus from ophiolitic rocks exposed on the Pinchi Geanticline was shed into the Quesnel Trough.



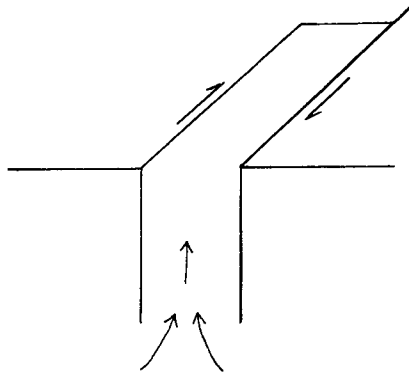
Subduction/obduction model

Because of the drawbacks of the subduction model, a second model is suggested which involves a combination of subduction and obduction (Fig. 24). At a number of localities in the Cordillera, late Paleozoic volcanics, cherts and minor volcanics overlie older miogeoclinal rocks and it has been suggested (Monger *et al.*, 1972; Dercourt, 1972) that the late Paleozoic rocks are allochthonous, having been thrust easterly over the miogeoclinal clastics constituting the Omineca Geanticline during the Caribooan Orogeny. This situation is illustrated in the eastern half of Fig. 24a. During the Pennsylvanian, an island arc with associated limestones was situated at an unknown distance from the North American craton (Fig. 24a). The limestones continued to grow in thickness during the Pennsylvanian and Permian and may have formed an extensive barrier reef type deposit adjacent to the island arc. At the close of the Permian an east-west principal stress, possibly the result of ocean floor spreading, caused the formation of a subduction zone, and the sea floor between the arc and the continent was consumed. There is no certain evidence that volcanicity accompanied the subduction. Eventually the island arc approached the subduction zone and because it contained a large thickness of buoyant low density rocks, did not descend the subduction zone. The scarcity of arc



(a) development of *en echelon* fractures

(b) strike-slip movement results in "rhombocasm" formation (Carey, 1958)



(c) diapiric intrusion of blueschist and serpentized ultramafite along zones of low lithostatic pressure

Fig. 25 Possible mechanism for intrusion of blueschists and serpentized ultramafites along strike-slip faults.

type volcanic rocks associated with the limestones in the Pinchi Geanticline is a major problem. It is possible that the volcanic basement (?) of the island arc was subducted. The collision of the island arc with the subduction zone was possibly followed by overthrusting or obduction of oceanic crust over the accumulation of Cache Creek Group sediments above the subduction zone.

A change in orientation of the principal stresses brought about oblique-slip movement along the main fault in the subduction zone (i.e. the Pinchi Fault ?). It is suggested that a strike-slip component of movement on the fault created zones of low pressure sporadically along the fault zone, which were at once filled from below by intrusion of low density fault bounded diapirs attempting to regain isostatic equilibrium and originating in the depths of the former subduction zone. These low pressure zones can possibly be compared with Carey's (1956) rhombochasms (Fig. 25). Using this mechanism, composite blocks of low average density containing blueschist, serpentized ultramafite and eclogite could have worked their way up to a higher structural level and are therefore representative of the lower crust or mantle at that time. As the blueschists rose in the crust, they cooled to temperatures below those necessary for argon retention (c. 200°C) and were deformed by F_2 . The Upper (?) Triassic K-Ar dates are considered to mark the close of the F_2 deformation.

During the Upper Triassic, uplift and erosion of the Pinchi Geanticline brought about deposition of conglomerates and flysch in the adjacent Quesnel Trough. The composition of the sediments is compatible with a land-mass which consisted of basic rocks, cherts and ultramafites.

This model is preferred for a number of reasons. Firstly, the presence of an obducted ophiolite cover to the Cache Creek Group is compatible with the presence of basic detritus in the Upper Triassic sediments. It is considered possible that the ophiolite sequence south of Pinchi Lake, which appears to be overlain conformably by Upper Triassic with no intervening Cache Creek Group sediments, is a remnant of this cover. Secondly, the presence of a major zone of crustal weakness associated with a subduction zone accounts for the development and subsequent reactivation of the Pinchi Fault.

The absence of a metamorphic zonation in the Cache Creek Group with respect to the Pinchi Fault is problematical. Perhaps such zonations are characteristic of regions where large amounts of material have been subducted and exhumed. It may be that a relatively small volume of rock was subducted and metamorphosed in the blueschist facies along the Pinchi Fault and a significant isostatic anomaly which could produce a regional uplift and exhumation of a metamorphic zonation was not formed.

Mesozoic and Tertiary events

Mesozoic movement on the Pinchi Fault is poorly recorded. Movement may well have occurred during the late Mesozoic, as the fault forms the western margin of the 170 million year old Hogem batholith. However, this feature may also have formed as the result of Tertiary activity.

The occurrence of Cretaceous or Paleocene conglomerate involved in faulting in the Pinchi area is convincing evidence for a period of Tertiary Fault activity. It was inferred (p. 67) that silica-carbonate rocks formed during a reactivation of the Pinchi Fault during the Eocene. Because of the association of carbonatization and intense F_3 deformation in the mine area, it is believed that formation of silica-carbonate rocks was contemporaneous with faulting and F_3 deformation. Consideration of the trend and plunge of F_3 folds and of the sense of warping in the limestone units suggests that right-lateral movement with a dip-slip component may have taken place along fault No. 2 (Map VI) during F_3 . Northeasterly directed thrusting was widespread 240 km to the north during the Eocene (Eisbacher, 1970). The common occurrence of northeasterly dipping fault planes suggests that similarly oriented stresses may have given rise to underthrusting in the Pinchi area, but this is speculative.

Mercury mineralization occurred after the carbonatization, possibly associated with hot spring activity.

Faulting continued after mineralization as demonstrated by the occurrence of post-mineralization thrust faults in the mine area.

REFERENCES CITED

- Agrell, S.D., Brown, M.G., and McKie, D., 1965, Deerite, howieite, and zussmanite, three new minerals from the Franciscan of the Laytonville District, Mendocino County, California (abs.): *Am. Mineral*, vol. 50, p. 278.
- Aitken, J.D., 1959, Atlin Map-area, British Columbia: *Geol. Surv. Canada, Mem.* 307.
- Armstrong, J.E., 1942, The Pinchi Lake Mercury Belt: *Geol. Surv. Canada, Paper* 42-11.
- _____, 1944, Northern Part of the Pinchi Lake Mercury Belt: *Geol. Surv. Canada, Paper* 44-5.
- _____, 1949, Fort St. James Map-area, Cassiar and Coast Districts, British Columbia: *Geol. Surv. Canada, Mem.* 252.
- _____, 1966, Tectonics and mercury deposits in British Columbia: in *Tectonic History and Mineral Deposits of the Western Cordillera*, *Can. Inst. Mining Metal, Spec. vol.* 8, p. 341.
- Armstrong, R.L., and Besancon, J., 1970, A Triassic time scale dilemma: K-Ar dating of Upper Triassic mafic igneous rocks, eastern U.S.A. and Canada and post-Upper Triassic plutons, western Idaho, U.S.A.: *Eclogae geol. Helv.*, vol. 63/1, p. 15.
- Aumento, F., Loncarevic, B.D., and Ross, D.I., 1970, Hudson Geotraverse: geology of the Mid-Atlantic Ridge at 45°N: *Phil. Trans, Roy. Soc. Lond., A.*, vol. 268, p. 623.
- Ave L'Allemand, H.G., 1967, Structural and petrofabric analysis of an "Alpine type" peridotite. The lherzolite of the French Pyrenees: *Leid. geol. Meded.*, vol. 42.
- Ave L'Allemand, H.G. and Carter, N.L., 1969, Syntectonic recrystallization of olivine (abs.): *Trans. Am. Geophys. Un.*, vol. 50, p. 324.

- Ave L'Allemand, H.G., Schiffmann, P.M., and Carter, N.L., 1968, Ductile Flow of peridotite and quartzite: Trans. Am. Geophys. Un., vol. 49, p. 313.
- Bailey, E.H., Blake, M.C., and Jones, D.L., 1970, On-land Mesozoic crust in California Coast Ranges: U.S. Geol. Surv. Prof. Paper 700-C, p. C70.
- Bailey, E.H., Irwin, W.P., and Jones, D.L., 1964, Franciscan and related rocks and their significance in the geology of western California: California Div. Mines and Geol. Bull., no. 183, 171 p.
- Banno, S., 1959, Aegerine-augites from crystalline schists in Shikoku: Geol. Soc. Japan Jour., vol. 65, p. 652.
- _____, 1964, Petrologic studies on Sanbagawa crystalline schists in the Bessi-Ino district, central Sikoku, Japan: Tokyo Univ. Fac. Sci. Jour., Sec. 11, vol. 15, p. 203.
- Berry, M.J., Jacoby, W.R., Niblett, E.R., and Stacey, R.A., 1971, A review of geophysical studies in the Canadian Cordillera: Can. Jour. Earth Sci., vol. 8, p. 788.
- Birch, F., and LeComte, P., 1960, Temperature-pressure plane for albite composition: Am. Jour. Sci., vol. 258, p. 209.
- Bischoff, J.L., and Fyfe, W.S., 1968, Catalysis, inhibition, and the calcite-aragonite problem. (I): Am Jour. Sci., vol. 266, p. 65.
- Blake, M.C., Irwin, W.P., and Coleman, R.G., 1967, Upside down metamorphic zonation, blueschist facies, along a regional thrust in California and Oregon: U.S. Geol. Survey Prof. Paper 575-C, p. C1.
- _____, 1969, Blueschist-facies metamorphism related to regional thrust faulting: Tectonophys., vol. 8, p. 237.
- Bloxam, T.W., 1956, Jadeite bearing metagreywackes in California: Am. Min., vol. 41, p. 488.
- Bochkarev, V.S., and Pogorelov, B.S., 1967, New data on the chronologic boundary of the Permian and Triassic systems: Akad. Nauk. S.S.R. Doklady, vol. 173, p. 153.

- Boettcher, A.L., and Wyllie, P.J., 1968, The calcite-aragonite transition measured in the system $\text{CaO-H}_2\text{O-CO}_2$: Jour. Geol., vol. 76, p. 314.
- Bonatti, E., Honnorez, J., and Ferrara, G., 1971, Peridotite-gabbro-basalt complex from the equatorial Mid-Atlantic Ridge: Phil. Trans. Roy. Soc. Lond., A., vol. 268, p. 385.
- Borsi, S., and Ferrara, G., 1967, Determinazione del teta delle rocce intrusive di Predazzo con i metodi del Rb/Sr e K/Ar: Miner. Petrogr. Acta, vol. 13, p. 45.
- Bowen, N.L., and Tuttle, F., 1949, The system $\text{MgO-SiO}_2\text{-H}_2\text{O}$: Geol. Soc. Am. Bull., vol. 60, p. 439.
- Brace, W.F., Ernst, W.G., and Kallberg, R.W., 1970, An experimental study of tectonic overpressure in Franciscan rocks: Geol. Soc. Am. Bull., vol. 81, p. 1325.
- Bramlette, M.N., 1946, The Monterey formation of California and the origin of its siliceous rocks: U.S. Geol. Surv. Prof. Paper 212.
- Brothers, R.N., 1970, Lawsonite-albite schists from northernmost New Caledonia: Contr. Mineral and Petrol., vol. 25, p. 185.
- Brown, W.H., Fyfe, W.S., and Turner, F.J., 1962, Aragonite in California glaucophane schists and the kinetics of the aragonite-calcite transformation: Jour. Petrol., vol. 3, p. 566.
- Burch, S.H., 1968, Tectonic emplacement of the Burro Mountain ultramafic body, Santa Lucia Range, California: Geol. Soc. Am. Bull., vol. 79, p. 527.
- Caner, B., 1970, Electrical conductivity structure of the lower crust and upper mantle in western Canada: Unpubl. Ph.D. thesis, Univ. of British Columbia.
- Carey, S.W., 1958, A tectonic approach to continental drift: in Continental Drift: A Symposium, University of Tasmania, p. 117.
- Chinner, G.A., 1960, Pelitic gneisses with varying ferrous/ferric ratio from Glen Clova, Angus, Scotland: Jour. Petrol., vol. 1, p. 178.

- Clark, S.P., 1957a, A note on calcite-aragonite equilibrium: Am. Min., vol. 42, p. 564.
- _____, 1957b, Heat flow at Grass Valley, California: Am. Geophys. Union Trans., vol. 38, p. 239.
- Coleman, R.G., 1971, Plate tectonic emplacement of upper mantle peridotites along continental edges: Jour. Geophys. Res., vol. 76, p. 1212.
- Coleman, R.G., and Clark, J.R., 1968, Pyroxenes in the Blueschist facies of California: Am. Jour. Sci., vol. 266, p. 43.
- Coleman, R.G., and Keith, T.E., 1971, A chemical study of serpentinization--Burro Mountain, California: Jour. Petrol., vol. 12, p. 311.
- Coleman, R.G., and Lee, D.E., 1963, Glaucofane-bearing metamorphic rock of the Cazadero area, California: Jour. Petrol., vol. 4, p. 260.
- Coleman, R.G., Lee, D.E., Beatty, L.B., and Brannock, W.W., 1965, Eclogites and eclogites: their differences and similarities: Geol. Soc. Am. Bull., vol. 76, p. 483.
- Coleman, R.G., and Papike, J.J., 1968, Alkali amphiboles from the blueschists of Cazadero, California: Jour. Petrol., vol. 9, p. 105.
- Coombs, D.S., 1961, Some recent work on the lower grades of metamorphism: Aust. Jour. Sci., vol. 24, p. 203.
- Crawford, W.A., and Fyfe, W.S., 1964, Calcite-aragonite equilibrium at 100°C: Science, vol. 144, p. 1569.
- Danner, W.R., 1964, in Geological History of Western Canada: Alberta Soc. Petrol. Geol., Calgary, p. 109.
- _____, 1967, Organic, shallow-water origin of bedded chert in the eugeosynclinal environment: Geol. Soc. Am. Abs., New Orleans, p. 42.
- Dawson, G.M., 1878, Report on explorations in British Columbia, chiefly in the basins of the Blackwater, Salmon, and Nechacco Rivers, and on Francois Lake: Geol. Surv. Canada, Rept. of Progr. 1876-1877, pt. III, p. 17.

- Deer, W.A., Howie, R.A., and Zussman, J., 1963, Rock Forming Minerals, vols. 1-5: Longmans, Green and Co. Ltd., London.
- Dercourt, J., 1972, The Canadian Cordillera, the Hellenides, and the sea-floor spreading theory: Can. Jour. Earth Sci., vol. 9, p. 709.
- Dewey, J.F., and Bird, J.M., 1970, Mountain belts and the new global tectonics: Jour. Geophys. Res., vol. 75, p. 2625.
- Dickenson, W.R., 1968, Evolution of calc-alkaline rocks in the geosynclinal system of California and Oregon: Proc. of the Andesite Conference, Oregon, Dept. Geol. Mineral. Ind. Bull., vol. 65, p. 143.
- Dietz, R.S., and Holden, J.C., 1966, Deep-sea deposits in but not on the continents: Am. Assoc. Petroleum Geologists Bull., vol. 50, p. 351.
- Douglas, R.J.W., Gabrielse, H., Wheeler, J.O., Stott, D.F., and Belyea, H.R., 1970, Geology of Western Canada: in Geology and Economic Mineral Deposits of Canada, Canada Geol. Surv. Econ. Geol. Rept. I, p. 366.
- Dragert, H., 1970, A geomagnetic depth-sounding profile across central British Columbia: Unpubl. M. Sc. thesis, Univ. of British Columbia.
- Eisbacher, G.H., 1970, Tectonic framework of Sustut and Sifton Basins, British Columbia: in Report of Activities, April to October, 1969, Geol. Surv. Canada, Paper 70-1, pt. A, p. 36.
- _____, 1971, Tectonic framework of Sustut and Sifton Basins, British Columbia: in Report of Activities, April to October, 1970, Geol. Surv. Canada, Paper 71-1, pt. A, p. 20.
- Engel, A.E.J., Engel, C.G., and Havens, R.G., 1965, Chemical characteristics of oceanic basalts and the upper mantle: Geol. Soc. Am. Bull., vol. 76, p. 719.
- Ernst, W.G., 1961, Stability relations of glaucophane: Am. Jour. Sci., vol. 259, p. 735.
- _____, 1962, Synthesis, stability relations, and occurrence of riebeckite and riebeckite-arfvedsonite solid solutions: Jour. Geol., vol. 70, p. 689.

- Ernst, W.G., 1963a, Polymorphism in alkali amphiboles: *Am. Mineral.*, vol. 48, p. 241.
- _____, 1963b, Significance of phengitic micas from low-grade schists: *Am. Mineral.*, vol. 48, p. 1357.
- _____, 1965, Mineral parageneses in Franciscan metamorphic rocks, Panoche Pass, California: *Geol. Soc. Am. Bull.*, vol. 76, p. 879.
- _____, 1970, Tectonic contact between the Franciscan melange and the Great Valley sequence--crustal expression of a Late Mesozoic Benioff Zone: *Jour. Geophys. Res.*, vol. 75, p. 886.
- _____, 1971a, Metamorphic zonations on presumably subducted lithospheric plates from Japan, California and the Alps: *Contr. Mineral. and Petrol.*, vol. 34, p. 43.
- _____, 1971b, Do mineral parageneses reflect unusually high-pressure conditions of Franciscan metamorphism?: *Am. Jour. Sci.*, vol. 270, p. 81.
- Ernst, W.G., Seki, Y., Onuki, H., and Gilbert, M.C., 1970, Comparative study of low-grade metamorphism in the California Coast Ranges and the outer metamorphic belt of Japan: *Geol. Soc. Am., Mem.* 124.
- Essene, E.J., and Fyfe, W.S., 1967, Omphacite in Californian rocks: *Contr. Mineral. and Petrol.*, vol. 15, p. 1.
- Evans, H.T. Jr., Appleman, D.E., and Handwerker, D.S., 1963, The least squares refinement of crystal unit cells with powder diffraction data by an automatic computer indexing method (abs.): *Amer. Crystallogr. Assoc. Ann. Meet.*, March 28, 1963, Cambridge, Mass., *Progr. Abstr.*, 42.
- Folk, R.L., 1968, *Petrology of Sedimentary Rocks*, University of Texas: Hemphill's, Austin.
- Freeze, A.C., 1942, *Geology of Pinchi Lake, British Columbia*: unpubl. Ph.D. thesis., Princeton University.
- French, B.M., 1964, Graphitization of organic material in a progressively metamorphosed Precambrian iron formation: *Science*, vol. 146, p. 917.

- French, B.M., 1964, Graphitization of organic material in a progressively metamorphosed Precambrian iron formation: *Science*, vol. 146, p. 917.
- _____, 1966, Some geological implications of equilibrium between graphite and a C-H-O gas phase at high temperatures and pressures: *Rev. Geophys*, vol. 4, p. 223.
- French, B.M., and Eugster, H.P., 1965, Experimental control of oxygen fugacities by graphite-gas equilibriums: *Jour. Geophys. Res.*, vol. 70, p. 1529.
- Friedman, G.M., 1959, Identification of carbonate minerals by staining methods: *Jour. Sed. Petrol.*, vol. 29, p. 87.
- Gray, J.G., 1938, Fort Fraser map-area, British Columbia: *Geol. Surv. Canada*, Paper 38-14.
- Green, D.H., and Ringwood, A.E., 1967, An experimental investigation of the gabbro to eclogite transformation and its petrological applications: *Geochim. et Cosmochim. Acta*, vol. 31, p. 767.
- Greenwood, H.J., 1961, The system $\text{NaAlSi}_2\text{O}_6\text{-H}_2\text{O-argon}$: total pressure and water pressure in metamorphism: *Jour. Geophys. Res.*, vol. 66, 3923.
- _____, 1967, Mineral equilibria in the system $\text{MgO-SiO}_2\text{-H}_2\text{O-CO}_2$: in *Researches in Geochemistry*, Abelson, P.H., ed.: John Wiley and Sons, New York, London, Sydney, p. 542.
- Gresens, R.L., 1969, Blueschist alteration during seppentinization: *Contr. Mineral and Petrol.*, vol. 24, p. 93.
- Henderson, F.B. III, 1969, Hydrothermal alteration and ore deposits in serpentinite-type mercury deposits: *Econ. Geol.*, vol. 64, p. 489.
- Hey, M.H., 1954, A new review of the chlorites: *Mineralog. Mag.*, vol. 30, p. 277.
- Hinrichsen, T., and Schürmann, K., 1972, Mineral reactions in burial metamorphism: *Neues Jahrb. Mineral., Monatch.*, no. 1, p. 35.
- Hoffman, C., 1972, Natural and synthetic ferroglaucophane: *Contr. Mineral. and Petrol.*, vol. 34, p. 135.
- Hollister, L.S., 1966, Garnet zoning: an interpretation based on Rayleigh fractionation model: *Science*, vol. 154, p. 1647.

- Irvine, T.N. and Baragar, W.R.A., 1971, A guide to the chemical classification of the common volcanic rocks: *Canad. Jour. Earth Sci.*, vol. 8, p. 523.
- Ito, K, and Kennedy, G.C., 1971, An experimental study of the basalt-garnet granulite-eclogite transition: in *The Structure and Physical Properties of the Earth's Crust: Geophys. Monograph 14*, John G. Heacock, editor, Amer. Geophys. Union Publication, Washington, D.C., p. 303.
- Iwasaki, M., 1963, Metamorphic rocks of the Kotu-Bizan area, eastern Shikoku: *Univ. Tokyo Jour. Fac. Sci.*, Sec. II, vol. 15, p. 1.
- Jamieson, J.C., 1953, Phase equilibria in the system calcite-aragonite: *Jour. Chem. Phys.*, vol. 21, p. 1385.
- Johannes, W., 1968, Experimental investigation of the reaction: forsterite + H₂O = serpentine + brucite: *Contr. Mineral. and Petrol.*, vol. 19, p. 309.
- _____, 1969, An experimental investigation of the system MgO-SiO₂-H₂O-CO₂: *Am. Jour. Sci.*, vol. 267, p. 1083.
- Jolly, W.T., and Smith, R.E., 1972, Degradation and metamorphic differentiation in the Keweenawan tholeiitic lavas of northern Michigan, U.S.A.: *Jour. Petrol.*, vol. 13, p. 273.
- Kerrick, D.M. and Cotton, W.R., 1971, Stability relations of jadeite pyroxene in Franciscan metagreywackes near San Jose, California: *Am. Jour. Sci.*, vol. 271, p. 350.
- Kitahara, S., Takenouchi, S., and Kennedy, G.C., 1966, Phase relations in the system MgO-SiO₂-H₂O at high temperatures and pressures: *Am. Jour. Sci.*, vol. 264, p. 223.
- Koo, J.H., 1968, Geology and mineralization in the Lorraine Property Area, Omineca Mining Division, British Columbia: Unpubl. M.Sc. thesis, Univ. of British Columbia.
- Krauskopf, K.B., 1967, *Introduction to Geochemistry*: McGraw-Hill, New York.
- Landis, C.A., 1971, Graphitization of dispersed carbonaceous material in metamorphic rocks: *Contr. Mineral. and Petrol.*, vol. 30, p. 34.

- Lillie, A.R., and Brothers, R.N., 1970, The geology of New Caledonia: *New Zealand Jour. Geol. Geophys.*, vol. 13, p. 145.
- Lillie, A.R., and Gunn, B.M., 1964, Steeply plunging folds in the Sealy Range, Southern Alps: *New Zealand Journ. Geol. Geophys.*, vol. 7, p. 403.
- Liou, J.G., 1971, P-T stabilities of laumontite, wairakite lawsonite, and related minerals in the system $\text{CaAl}_2\text{Si}_2\text{O}_8\text{-SiO}_2\text{-H}_2\text{O}$: *Jour. Petrol.*, vol. 12, p. 379.
- Littlejohn, A.L., 1972, A comparative study of lherzolite nodules in basaltic rocks from British Columbia: Unpubl. M. Sc. thesis, University of British Columbia.
- Logan, B.W., Rezak, R., and Ginsburg, R.N., 1964, Classification and environmental significance of algal stromatolites: *Jour. Geol.*, vol. 72, p. 68.
- Loney, R.A., Himmelberg, G.R., and Coleman, R.G., 1971, Structure and petrology of the alpine-type peridotite at Burro Mountain, California, U.S.A.: *Jour. Petrol.*, vol. 12, p. 245.
- Lord, C.S., 1949, McConnellCreek map-area, Cassiar District, British Columbia: *Geol. Surv. Canada, Mem.* 251.
- MacDonald, G.A., 1968, Composition and origin of Hawaiian lavas: *Geol. Soc. Am., Mem.* 116, p. 477.
- McConnell, J.D.C., and McKie, D., 1960, The kinetics of the ordering process in triclinic $\text{NaAlSi}_3\text{O}_8$: *Mineralog. Mag.*, vol. 32, p. 436.
- McTaggart, K.C., 1971, On the origin of ultramafic rocks: *Geol. Soc. Am. Bull.*, vol. 82, p. 23.
- Miyashiro, A., 1964, Oxidation and reduction in the earth's crust with special reference to the role of graphite: *Geochim. et Cosmochim. Acta*, vol. 28, p. 717.
- _____, 1972, Metamorphism and related magmatism in plate tectonics: *Am. Jour. Sci.*, vol. 272, p. 629.
- Miyashiro, A., and Seki, Y., 1958, Mineral assemblages and subfacies of the glaucophane-schist facies: *Jap. Jour. Geol. and Geogr.*, vol. 29, p. 199.

- Monger, J.W.H., 1969, Stratigraphy and structure of Upper Paleozoic rocks, northeast Dease Lake map-area, British Columbia: Geol. Surv. Canada, Paper 68-48.
- _____, 1973, Upper Paleozoic rocks of the western Canadian Cordillera: in Report of Activities, April to October, 1972, Geol. Surv. Canada, Paper 73-1, pt. A, p. 27.
- Monger, J.W.H. and Ross, C.A., 1971, Distribution of Fusulinaceans in the western Canadian Cordillera: Can. Jour. Earth Sci., vol. 8, p. 259.
- Monger, J.W.H., Souther, J.G., and Gabrielse, H., 1972, Evolution of the Canadian Cordillera: a plate tectonic model: Am. Jour. Sci., vol. 272, p. 577.
- Moore, E.M., and Vine, F.J., 1971, The Troodos Massif, Cyprus and other ophiolites as oceanic crust: evaluation and implications: Phil. Trans. Roy. Soc. Lond., A, vol. 268, p. 443.
- Morgan, B.A., 1970, Petrology and mineralogy of eclogite and garnet amphibolite from Puerto Cabello, Venezuela: Jour. Petrol., vol. 11, p. 101.
- Newton, R.C., Goldsmith, J.R., and Smith, J.V., 1969, Aragonite crystallization from strained calcite at reduced pressures and its bearing on aragonite in low-grade metamorphism: Contr. Mineral. and Petrol., vol. 22, p. 335.
- Newton, R.C. and Kennedy, G.C., 1963, Some equilibrium reactions in the join $\text{CaAl}_2\text{Si}_2\text{O}_8\text{-H}_2\text{O}$: Jour. Geophys. Res., vol. 68, p. 2967.
- Newton, R.C., and Smith, J.V., 1967, Investigations concerning the breakdown of albite at depth in the earth: Jour. Geol., vol. 75, p. 268.
- Nitsch, K.-H., 1968, Die Stabilität von Lawsonit: Naturwiss., vol. 55, p. 388.
- _____, 1972, Das P-T-X_{CO₂} Stabilitätsfeld von Lawsonit: Contr. Mineral. and Petrol., vol. 34, p. 116.
- Oxburgh, E.R., and Turcotte, D.L., 1971, Origin of paired metamorphic belts and crustal dilation in island arc regions: Jour. Geophys. Res., vol. 76, p. 1315.

- Page, B., 1972, Oceanic crust and mantle fragment in subduction complex near San Luis Obispo, California: Geol. Soc. Am. Bull., vol. 83, p. 957.
- Page, N.J., 1967, Serpentinization at Burro Mt., California: Contr. mineral Petrol., vol. 14, p. 321.
- Pettijohn, F.J., 1957, Sedimentary Rocks: Harper and Row, New York.
- Plas, L. van der, 1959, Petrology of the northern Adula region, Switzerland (with particular reference to glaucophane bearing rocks): Leidse Geol. Meded., vol. 24, p. 415.
- Raleigh, C.B., 1963, Fabrics of naturally and experimentally deformed olivine: Ph.D. thesis, Univ. of California, Los Angeles, California.
- _____, 1965, Structure and petrology of an alpine peridotite Cypress Island, Washington, U.S.A.: Beitr. Miner. Petrog., vol. 11, p. 719.
- Rich, J.L., 1951, Three critical environments of deposition, and criteria for recognition of rocks in each of them: Bull. Geol. Soc. Am., vol. 62, p. 1.
- Ringwood, A.E., 1962, A model for the upper mantle: Jour. Geophys. Res., vol. 67, p. 857.
- Robie, R.A., and Waldbaum, D.R., 1968, Thermodynamic properties of minerals and related substances at 298.15°K and one atmosphere (1.013b) pressure and at higher temperatures. U.S. Geol. Surv. Bull. 1259.
- Roedder, E., 1967, Fluid inclusions as samples of ore fluids: in Geochemistry of Hydrothermal Ore Deposits, H.L. Barnes, ed., Holt, Rinehart and Winston, Inc., New York.
- Roots, E.F., 1954, Geology and mineral deposits of the Aiken Lake map-area: Geol. Surv. Canada, Mem. 274.
- Rucklidge, J.C., Gasparrini, E., Smith, J.V., and Knowles, C.R., 1971, X-ray emission microanalysis of rock forming minerals: Can. Jour. Earth Sci., vol. 8, p. 1171.

- Scarfe, C.M., and Wyllie, P.J., 1967, Serpentine dehydration curves and their bearing on serpentinite deformation in orogenesis: *Nature*, vol. 215, p. 945.
- Schuiling, R.D., and Vink, B.W., 1967, Stability relations of some titanium minerals (sphenes, perovskite, rutile, anatase): *Geochim. Cosmochim. Acta*, vol. 31, p. 2399.
- Selwyn, A.R.C., 1872, Journal and report of preliminary explorations in British Columbia: *Geol. Surv. Canada, Rept. of Progr. 1871-72*, p. 16.
- _____, 1877, Report on exploration in British Columbia in 1875: *Geol. Surv. Canada, Rept. of Progr. 1875-76*, p. 29.
- Shido, F., 1959, Notes on rock-forming minerals (9). Hornblende bearing eclogite from Gongenyama of Higasi-Akaishi in the Bessi District, Sikoku: *Geol. Soc. Japan Jour.*, vol. 65, p. 701.
- Souther, J.G., 1970, Volcanism and its relationship to recent crustal movements in the Canadian Cordillera: *Can. Jour. Earth Sci.*, vol. 7, p. 553.
- Souther, J.G., and Armstrong, J.E., 1966, North central belt of the cordillera of British Columbia: *in* Tectonic history and mineral deposits of the western Cordillera, *Can. Inst. Min. Metal., Spec.*, vol. 8, p. 171.
- Stevenson, J.S., 1940, Mercury deposits of British Columbia: *Dept. of Mines, B.C., Bull, No. 5*, p. 18.
- Stueber, A.M. and Murthy, V.R., 1966, Strontium isotope and alkali element abundances in ultramafic rocks: *Geochim. Cosmochim. Acta*, vol. 30, p. 1243.
- Suppe, J., and Armstrong, R.L., 1972, Potassium-argon dating of Franciscan metamorphic rocks: *Am. Jour. Sci.*, vol. 272, p. 217.
- Sutherland-Brown, A., 1963, Geology of the Cariboo River area, British Columbia: *B.C. Dept. of Mines, Bull.* 47.
- Taylor, H.P., Jr., and Coleman, R.G., 1968, O^{18}/O^{16} ratios of coexisting minerals in glaucophane bearing metamorphic rocks: *Geol. Soc. Am. Bull.*, vol. 79, p. 1727.

- Thompson, A.B., 1970, Laumontite equilibria and the zeolite facies: *Am. Jour. Sci.*, vol. 269, p. 267.
- _____, 1971, PCO_2 in low-grade metamorphism; zeolite, carbonate, clay mineral, prehnite relations in the system $CaO-Al_2O_3-SiO_2-CO_2-H_2O$: *Contr. Mineral. Petrol.*, vol. 33, p. 145.
- Thompson, M.L., 1965, Pennsylvanian and Early Permian fusulinids from Fort St. James area, British Columbia, Canada: *Jour. Paleontol.* vol. 39, p. 224.
- Tipper, H.W., 1971, Glacial geomorphology and Pleistocene history of central British Columbia: *Geol. Surv. Canada, Bull.* 196.
- Tozer, E.T., 1964, The Triassic Period in The Phanerozoic Time Scale: *Geol. Soc. Lond. Quart. Jour.*, vol. 1205, p. 207.
- Trumpy, R., 1960, Paleotectonic evolution of the central and western Alps: *Geol. Soc. Am. Bull.*, vol. 71, p. 843.
- Turner, F.J., 1968, *Metamorphic Petrology*: McGraw-Hill Co., New York.
- Turner, F.J., and Verhoogan, J., 1960, *Igneous and Metamorphic Petrology*: McGraw-Hill, New York.
- Turner, F.J., and Weiss, L.E., 1963, *Structural Analyses of Metamorphic Tectonites*: McGraw-Hill, New York.
- Vance, J.A., 1968, Metamorphic aragonites in the prehnite-pumpellyite facies, Northwest Washington: *Am. Jour. Sci.*, vol. 266, p. 299.
- Velde, B., 1965, Phengitic micas: synthesis, stability and natural occurrence: *Am. Jour. Sci.*, vol. 263, p. 886.
- Wenner, D.B., and Taylor, H.P. Jr., 1969, δD and δO^{18} studies of serpentinization of ultramafic rocks (abs.): *Geol. Soc. Am. Annual Meeting, Atlantic City, N.J.*
- _____, 1971, Temperatures of serpentinization of ultramafic rocks based on O^{18}/O^{16} fractionation between coexisting serpentine and magnetite: *Contr. Mineral. Petrol.*, vol. 32, p. 165.

- White, D.E., 1967, Mercury and base-metal deposits with associated thermal and mineral waters: in Geochemistry of Hydrothermal Ore Deposits, H.L. Barnes, ed., Holt, Rinehart and Winston, Inc., New York, p. 575.
- White, W.H., Erickson, G.P., Northcote, K.E., Dirom, G.E., and Harakal, J.E., 1967, Isotopic dating of the Guichon Batholith: Canad. Jour. Earth Sci., vol. 4, p. 677.
- Wilson, G., 1953, Mullion and rodding structures in the Moine series of Scotland: Geol. Assoc. Proc., vol. 64, p. 118.
- Wilson, J.T., 1968, Static or mobile earth: the current scientific revolution: Proc. Am. Phil. Soc., vol. 112, p. 309.
- Winchell, A.N., 1936, A third study of chlorite: Am. Mineral., vol. 21, p. 642.
- Yoder, H.S. and Tilley, C.E., 1962, Origin of basalt magmas: an experimental study of natural and synthetic rock systems: Jour. Petrol., vol. 3, p. 342.
- Zwart, H., 1969, Metamorphic facies series in the European orogenic belts and their bearing on the causes of orogeny: in Age Relations in High Grade Metamorphic Terrains, Geol. Assoc. Canada, Spec. Paper no. 5, p. 7.

APPENDIX I

FOSSIL LOCALITIES IN THE PINCHI AREA

The positions of the following fossil localities are shown in Map I. In the list which follows, localities assigned by other authors are given in brackets immediately after the locality number used in this study.

- A. Collected by I. Paterson; identified by W.R. Danner
Fauna from fossil localities F-1 to F-6 are given on
p. 40.
- B. Collected by J.E. Armstrong and identified by various
workers F-7 (5): southeast end of a ridge lying between
Pinchi village, Stuart Lake and Pinchi
Lake; *Triticites*; age; probably Upper
Pennsylvanian.
F-8 (8): south side of Mount Pope; *Lonsdaleia*-
like coral and crinoid discs and stems.
Age; Carboniferous (?).
- C. Collected and identified by M.L. Thompson.
F-9 (BC-12); *Eoschubertella*; *Millerella*; *Paramillerella*.
F-10 (BC-14); *Fusulinella jamesensis*; *Fusulinella*;
Pseudostaffella sandersoni; *Millerella*;
Paramillerella.

- F-11 (BC-17): *Pseudostaffella sandersoni*; *Fusulinella jamesensis* (?); *Paramillerella*; *Millerella*
- F-12 (BC-11): *Eoschubertella*; *Fusulinella*.
- F-13 (BC-13): *Fusulina* ? *occasa* ?
- F-14 (BC-15): *Quasifusulina popensis* n. sp.; *Schubertella popensis* n. sp.
- F-15 (BC-18): *Quasifusulina* ?; *Schubertella*.
- F-16 (BC-52): *Schubertella* ?; *Fusulinella*.
- F-17 (BC-24): *Profusulinella* ?; *Pseudostaffella*;
- F-18 (BC-23): *Fusulina* ? *occasa* n. sp.; *Pseudostaffella*; *Schubertella*.
- F-19 (BC-49): *Fusulina pitrati* n. sp.; *Fusulina*; *Fusulinella*; *Schubertella*.
- F-20 (BC-48): *Fusulina pitrati* n. sp.; *Fusulina*; *Fusulinella*; *Schubertella*.
- F-21 (BC-21): *Quasifusulina americana* n. sp.; *Triticites pinchiensis* n. sp.; *Schubertella kingi*? *Oketaella*; *Triticites stuartensis* n. sp.?
- F-22 (BC-53): *Pseudoschwagerina arta*; *Triticites stuartensis* n. sp.
- F-23 (BC-19): *Fusulina pitrati*?; *Fusulinella*; *Eoschubertella*; *Pseudostaffella*.

D. Collected by I.A. Paterson, identified by W.R. Danner.

F-24: *Fusulinella jamesensis*; *Akiyoshiella* sp.?

Middle Pennsylvanian.

F-25: *Schwagerina* sp.

Early Permian.

F-26: *Tetrataxis* sp.

Pennsylvanian and Permian range.

Algal structures, bryozoa and echinoderm clasts
are also present.

APPENDIX II

MINERALOGY

Analytical Methods

Approximately 200 thin sections and 10 polished sections of greenstones, glaucophanitic rocks and carbonates were examined. Whole rock or single mineral diffraction traces were used to confirm optical identification of minerals. X-ray standards were prepared by repeatedly centrifuging the 200-250 mesh fraction in diodomethane or bromoform. Measurements of refractive indices were not made because of uncertainty of correlation of refractive index with chemical composition.

Cell parameters of three glaucophanes and one jadeitic pyroxene are given along with the diffraction method in Table 7.

To illustrate textures in carbonate rocks, slabs from 7 dolomitic limestones were etched with HCl and stained using alizarine red solution and Fiegl's solution (Friedman, 1959).

Because of fine grain size, fabric heterogeneity and difficulty of recognition of phases, accurate modal analyses are difficult to obtain. However, modal analyses using a Zeiss micrometer eyepiece were obtained for four rocks and

estimates made for many more (Tables 20, 22, 24 and 25).

Mineral compositions were determined using an A.R.L. electron microprobe at the University of Washington. Operating conditions were as follows: 15 KV accelerating potential, 1-2 μ spot size, specimen current of 0.09 μ -amps for major elements and 0.18 μ -amps for minor elements. The time taken for a constant amount of current to pass was monitored for all points. A check was also made on the specimen current prior to analyses of each mineral in order to monitor sample conductivity. Within each polished thin section, three to five grains of each mineral were analysed. Approximately 5 spots were probed on each grain. Compositional heterogeneity gave rise to a spread of 1-2 wt.% for major elements within individual grains and from grain to grain. Any grain or spot with an analysis differing significantly from the norm was omitted in the final averaging. In order to obtain a crude estimate of the analytical precision, a normal distribution of grain composition within one slide was assumed and the standard deviations for each element in a pyroxene (Px-74) and a glaucophane (Gl-103) were calculated (Table 14).

Chlorite compositions were obtained from a working curve prepared for each element using chlorite standards. Glaucophanes and pyroxenes were analyzed using natural and synthetic pyroxene standards for Mg, Fe, Al, Ti, Si, Na and Ca, a garnet standard for Mn and a muscovite standard

for K. All standards were obtained from the University of Washington collection. Absorption, fluorescence and atomic number corrections were carried out in addition to those for deadtime, drift and background using computer programmes (UWPROBE, EMX2A) in the possession of the University of Washington. A considerable increase in totals was noted after correction on account of high absorption by Fe of radiation from elements of low atomic number.

As no distinction can be made between Fe^{3+} and Fe^{2+} using the microprobe, results are reported as FeO or Fe_2O_3 depending on which oxide predominates in published wet chemical analyses of similar minerals. Therefore, iron is given as FeO in chlorite and glaucophane. In the case of the pyroxenes FeO and Fe_2O_3 values have been calculated.

Minerals

Sodic amphiboles

Sodic amphiboles are widely distributed within the lawsonite-glaucophane bearing rocks, where they occur in metabasic rocks, metacherts and interlayered schists. A few small grains of glaucophane were also observed in the greenstones of Pinchi Mountain approximately 50 feet north of a faulted contact with the glaucophanitic block.

TABLE 6 OPTICAL PROPERTIES OF PYROXENES AND AMPHIBOLES

Spec. no.	Mineral	Pleochroism		Optic plane	2V	γ°	α°
		α	β				
26	glaucophane	colourless	lavender	blue	010	-	10°
31	"	"	"	"	"	-	9°
33	"	"	"	"	"	-	17°
49*	"	"	"	"	"	-	4°
205*	"	"	"	"	"	-	20°
103*	"	"	"	"	"	-20°	9°
210	"	"	"	"	"	-38°±4°#	5°
134	"	"	"	"	"	-15°	8°
155	green amphibole	pale green	green	blue-green	"	-50°	20°
36] 201]	brown amphibole	fawn	pale brown	dark brown	"	0°-8°	31°
27	relict augite	-	-	-	-	+55°#	46°
211	relict augite	-	-	-	-	+60°#	45°
36] 48*] 205*]	acmitic pyroxene	-	-	-	-	-	10° 0°-2° 0°-2°
49*	acmitic pyroxene	pale green	fawn	fawn	-	-	0°
103*	omphacitic pyroxene	pale green	pale green	green	-	+75°	39°
74*	jadeitic pyroxene	-	-	-	-	-	40°

* analysed mineral

2V determined using universal stage

All other 2V measurements were estimated from curvature and separation of isogyres.

TABLE 7
CELL DIMENSIONS FOR GLAUCOPHANE AND JADEITIC PYROXENE

Cell Dimensions	G1-206	G1-208	G1-207	Px-209
a	9.636±6 Å	9.571±9 Å	9.602±3 Å	9.484±3 Å
b	17.909±6 Å	17.79±3 Å	17.860±9 Å	8.633±3 Å
c	5.30 ±1 Å	5.314±5 Å	5.316±4 Å	5.244±2 Å
β	103°20'±8'	103°33'±6'	103°24'±3'	107°27'±2'
V	890±2 Å ³	880±1 Å ³	887±1 Å ³	409.6±0.2 Å ³

- (a) Diffractometer patterns were obtained from a Phillip's X-ray diffractometer. For the jadeitic pyroxene (Px-209), a K-Br internal standard was employed and the 8 or 9 best peaks in 3 oscillations were measured to within 0.01° 2θ and averaged. The chart speed was 5 x 240 mm/hr and the scan rate $\frac{1^\circ}{2}$ /min. A similar method was used for the glaucophanes except that a silicon internal standard was employed to measure the 6 best peaks. Peaks were indexed by comparison with published data for similar minerals: jadeitic pyroxene-Coleman and Clark, 1968; glaucophane-Coleman and Papike, 1968.
- (b) Cell parameters were calculated to three decimal places using a programme which gave a least squares refinement of the unit cell (author: Evans *et al.*, 1963; supplier: E.P. Meagher, U.B.C.).
- (c) Given errors are standard errors and refer to the final decimal place in the cell dimensions.
- (d) Specimens have not been analyzed. Locations are given in Map VII.

TABLE 8

ELECTRON MICROPROBE ANALYSES OF GLAUCOPHANES

	G1-103	G1-49	G1-205
SiO ₂	56.5	56.2	56.7
Al ₂ O ₃	8.9	7.4	6.3
TiO ₂	0.00	0.13	0.09
FeO [†]	15.1	17.2	21.5
MnO	0.03	0.19	0.03
MgO	9.2	8.4	5.9
CaO	0.9	1.0	0.3
Na ₂ O	6.9	6.8	7.3
K ₂ O	0.02	0.07	0.04
H ₂ O*	2.1	2.1	2.1
Total	99.7	99.5	100.3

* assumed H₂O content on basis of average analyses of two glaucophanes reported by Rucklidge *et al.*, (1971).

† total Fe calculated as FeO.

103: assemblage is glaucophane + lawsonite + sphene + stilpnomelane; occurs as alteration of garnet + pyroxene in eclogite.

49: assemblage is glaucophane + lawsonite + sphene + white mica + acmitic pyroxene.

205: the assemblage glaucophane + white mica + aragonite + chlorite occurs as fracture fillings in an acmite + sphene + lawsonite + quartz rock.

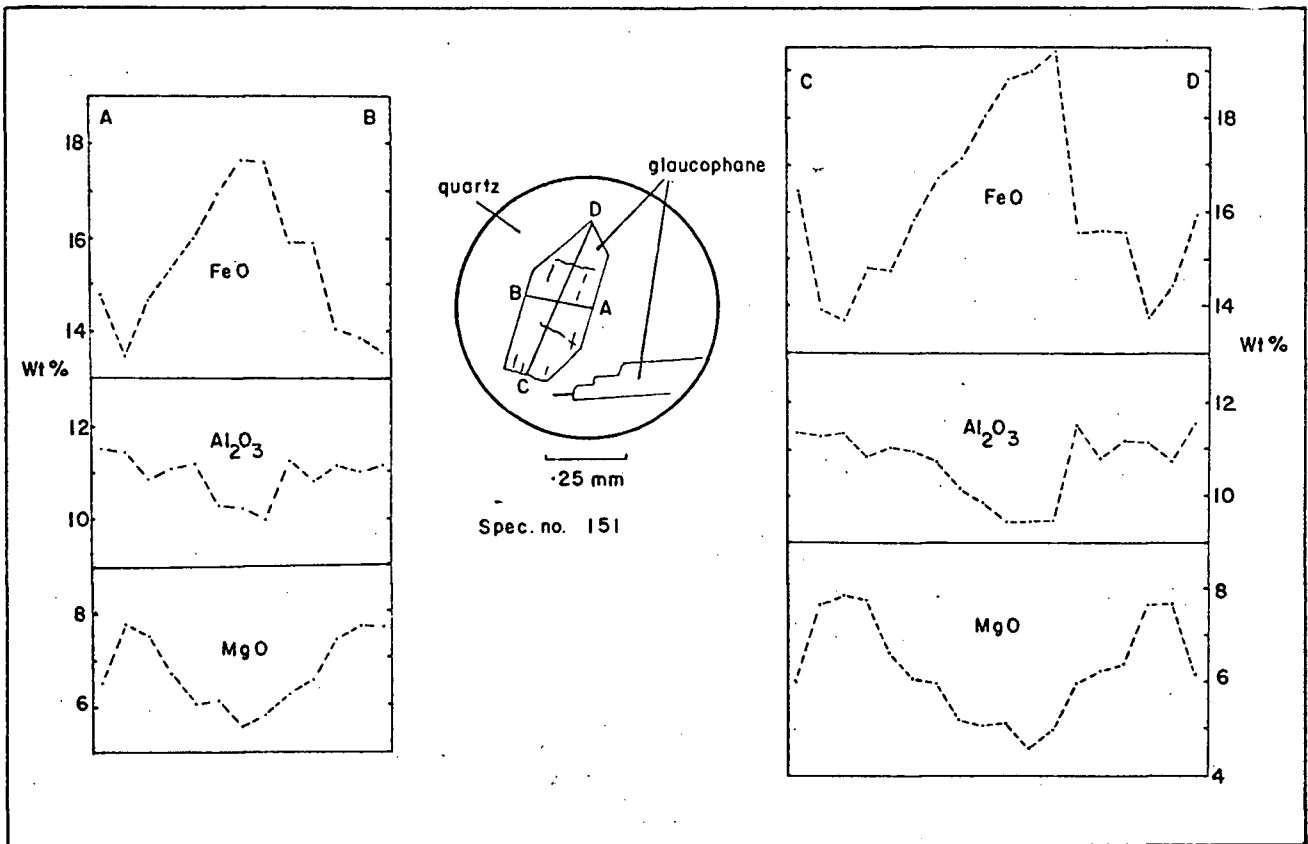


Fig. 26 Element variation in zoned glaucophane. Note iron enrichment at cores and margins of glaucophane crystals with Al_2O_3 and MgO showing an antipathetic variation. Oxide percentages are considered semiquantitative.

Optical properties are given in Table 6.

Cell dimensions for three glaucophanes are given in Table 7. Cell volumes are characteristic of the "high pressure" polymorph, glaucophane II (Ernst, 1963) rather than the lower pressure higher temperature glaucophane I which has not been recognized in nature.

Microprobe analyses for three sodic amphiboles are given in Table 8 together with host rock lithology and mineral assemblage. Atomic proportions of elements were not calculated on account of the absence of volatile analyses and the inability of the probe to distinguish Fe^{3+} and Fe^{2+} .

A glaucophane from a metachert was traversed with the electron-probe giving the zonation illustrated in Fig. 26. Of particular interest is the antipathetic variation of MgO and Al_2O_3 with FeO , the latter oxide being concentrated in the cores and the margins. The weight per cent oxide values are to be considered semiquantitative as absorption corrections were not made, and an unsatisfactory standard was used for silicon. The significance of this zonal distribution is discussed on p. 83.

Brown and green amphiboles

At two localities, just west of Pinchi Mine (Map VII, No. 36) and on the Darbar claim group (Map VII, No. 201), dark radiating sprays of amphibole (1 cm max length) were

TABLE 9

ELECTRON MICROPROBE ANALYSES OF RELICT PYROXENES

	Px-163	Px-165
SiO ₂	51.0	50.0
Al ₂ O ₃	2.7	2.3
TiO ₂	0.96	0.81
Fe ₂ O ₃	-	-
FeO	9.7	8.1
MnO	0.14	0.13
MgO	15.2	17.5
CaO	19.6	19.4
Na ₂ O	0.7	0.3
Total	100.0	98.5

Numbers of ions on the basis of 6 oxygens

Si	1.90	1.89
Al ^{IV}	0.10	0.10
Ti	0.03	0.02
Al ^{VI}	0.03	-
Fe ²⁺	0.30	0.25
Mg	0.85	0.98
Mn	-	0.01
Na	0.05	0.02
Ca	0.78	0.78
Total	4.04	4.05

noted occurring along fractures. The amphibole coexists with coarse grained aragonite and in places forms rims on glaucophane. Optical properties (Table 6) suggest that it is either kataphorite ($\text{Na}_2\text{CaFe}_4^{2+}(\text{Fe}^{3+}\text{Al})\text{Si}_2\text{AlO}_{22}(\text{OH},\text{F})_2$) or an arfvedsonitic amphibole.

Green amphibole was observed at only one locality, as a minor constituent in a large boulder one mile northeast of Pinchi Mine (Map VII, No. 155). It coexists with lawsonite and is locally rimmed with glaucophane. Optical properties are given in Table 6.

Pyroxenes

Five types of pyroxene are present in the area: relict augites, sodic-augites, acmite-jadeites, jadeitic pyroxenes and omphacitic pyroxenes. Pyroxene nomenclature is illustrated on an acmite-jadeite- $\text{Ca}(\text{Mg},\text{Fe})\text{Si}_2\text{O}_6$ triangular diagram in Fig. 27 (after Essene *et al.*, 1967). Relict igneous augites are found in most metabasic rocks. Metamorphic sodic-augites are found only in the Pinchi Mountain greenstones and acmite-jadeites are found in lawsonite bearing metabasic rocks. Jadeitic pyroxene is present in lawsonite bearing metagreywackes, and omphacitic pyroxene is observed only in eclogite boulders.

Optical properties of pyroxenes are given in Table 6 and cell parameters of a jadeitic pyroxene in Table 7.

TABLE 10

ELECTRON MICROPROBE ANALYSES OF METAMORPHIC PYROXENES

	Px-49	Px-205	Px-48	Px-74	Px-103
SiO ₂	53.9	57.3	56.1	58.1	53.2
Al ₂ O ₃	8.4	13.3	7.5	18.5	6.7
TiO ₂	0.10	0.34	0.41	0.20	0.08
Fe ₂ O ₃	16.2*	14.0*	19.6*	4.2*	4.8*
FeO	2.2	0.4	0.9	0.8	6.6
MnO	0.20	0.03	0.04	0.03	0.07
MgO	2.0	0.5	1.5	1.7	8.0
CaO	4.5	1.1	2.7	3.0	16.3
Na ₂ O	12.1	14.3	12.8	13.4	6.2
K ₂ O	0.01	0.00	0.00	0.00	0.01
Total	99.6	101.3	101.5	99.9	102.0

Numbers of ions on the basis of 6 oxygens

Si	1.99	2.01	2.02	2.01	1.94
Al ^{IV}	0.01	-	-	-	0.06
Ti	-	0.01	0.01	0.01	-
Al ^{VI}	0.35	0.55	0.32	0.75	0.23
Fe ³⁺	0.45	0.37	0.53	0.11	0.13
Fe ²⁺	0.07	0.01	0.03	0.02	0.20
Mg	0.11	0.03	0.08	0.09	0.43
Mn	0.01	-	-	-	-
Na	0.87	0.97	0.89	0.90	0.44
Ca	0.18	0.04	0.11	0.11	0.64
Total	4.04	3.99	3.99	4.00	4.07

TABLE 10 (continued)

* (a) Approximate values of Fe_2O_3 and FeO were obtained from total Fe after assuming charge balance, negligible Mn and no Al^{IV} . In this case $\text{Ca}^{2+} = \text{Mg}^{2+} + \text{Fe}^{2+}$.

(b) Standard deviations for Px-74 are given in Table 14.

Specimen Data

- Px-49: assemblage: glaucophane + lawsonite + acmitic pyroxene + sphene + white mica
- Px-205: assemblage: acmitic pyroxene + sphene + lawsonite + quartz
- Px-48: assemblage: lawsonite + acmitic pyroxene + sphene + chlorite; glaucophane is present but may not be in equilibrium with the assemblage.
- Px-74: metagreywacke; assemblage: jadeitic pyroxene + quartz + white mica + lawsonite + sphene + glaucophane + pyrite + carbonaceous material.
- Px-103: glaucophane-lawsonite eclogite; assemblage: omphacitic pyroxene + garnet.

Specimen locations are given in Map VII.

Fig. 27a: diagram illustrating nomenclature (Essene and Fyfe, 1967) and compositions of Franciscan and Sanbagawa clinopyroxenes (Ernst *et al.*, 1970).

Franciscan terrain

- : jadeitic pyroxene from metagreywackes (Bloxam, 1956, 1959; Coleman, 1965; Ernst *et al.*, 1970).
- ▲ : omphacitic pyroxene from "greenstones" and eclogites (Switzer, 1945; Bloxam, 1959; Coleman *et al.*, 1965; Essene and Fyfe, 1967).

Mt.B. : compositional range of jadeite-acmite from Mount Boardman (Essene and Fyfe, 1967)

Sanbagawa

- : clinopyroxenes from eclogite schlieren in ultramafic rocks (Miyashiro and Seki, 1958; Shido, 1959; Ernst *et al.*, 1970).
- : clinopyroxenes from siliceous metasedimentary schists (Banno, 1959, 1964; Iwasaki, 1963).

Fig. 27b: diagram illustrating compositional range of clinopyroxenes from Pinchi Lake.

- 74 : jadeitic pyroxene from metagreywacke
- 103 : omphacitic pyroxene from eclogite
- 48
- 49 { : jadeite-acmites from lawsonite bearing metabasic rocks
- 205
- P.M.G. : compositional range of sodic augites from Pinchi Mountain greenstones

Note (a) End member proportions were calculated employing procedure outlined by Banno (1959).

$$Jd = \frac{(Na+K)}{(Na+K+Ca)} \cdot \frac{100Al^{VI}}{(Al^{VI}+Fe^{+3})} ; \quad Ac = \frac{(Na+K)}{(Na+K+Ca)} \cdot \frac{100Fe^{+3}}{(Al^{VI}+Fe^{+3})}$$

$$Ca(Mg,Fe)Si_2O_6 = 100 - (Jd + Ac)$$

PLOT OF PYROXENE COMPOSITIONS

Fig. 27a

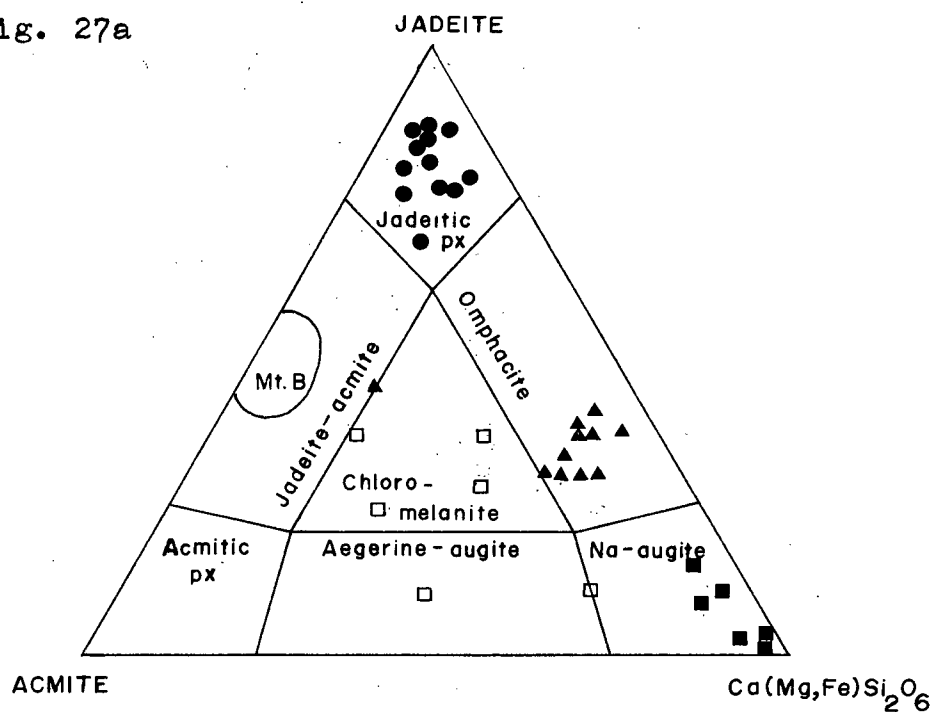


Fig. 27b

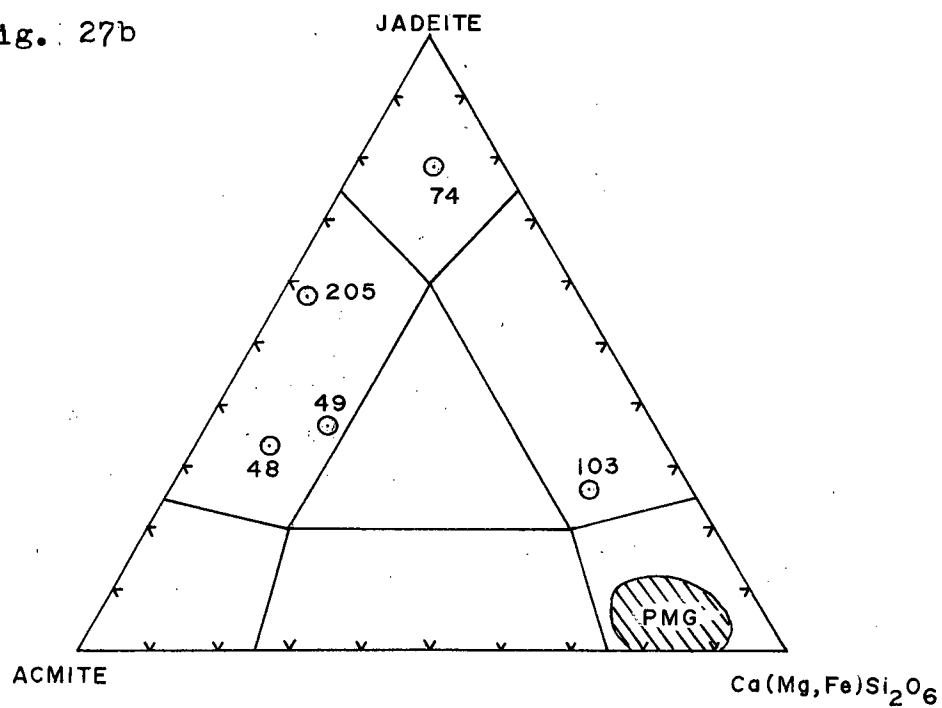


Fig. 27b (continued):

Spec. No.	Jadeite (Jd)	Acmite (Ac)	Ca (Mg,Fe) Si ₂ O ₆ ("Augite")
Px-74	77.9	11.3	10.8
Px-103	26.0	14.8	59.2
Px-49	36.7	46.4	16.9
Px-48	33.5	55.9	10.6
Px-205	57.5	38.5	4.0

Note (b) 98% of cations are represented on the diagram.
The remaining 2% is comprised of Al^{IV}, Mn
and Ti.

Relict igneous augites within the Pinchi Mountain greenstones have been metamorphosed to blotchy sodic-augites which coexist with albite and have small α^c . Microprobe analyses of two relict augites are given in Table 9 together with atomic proportions. Reproduceable analyses of sodic-augites were not obtained but they show an increase in Na, Fe (Fe³⁺?) and Al and an antipathetic decrease in Ca and Mg with respect to the relict pyroxenes which they commonly replace. The approximate values for Na₂O (2-3 wt.%), CaO (13-17 wt.%) and Al₂O₃ (2.5-4 wt.%) obtained from partial probe analyses indicate that Px-163 and Px-165 plot in the sodic-augite field in the system acmite-jadeite-Ca(Mg,Fe)Si₂O₆ (Fig. 27b).

Analyses of three acmite-jadeites, a jadeitic and an omphacitic pyroxene are given in Table 10. The totals range between 99.6 and 102 wt.% and cation totals between 3.99 and 4.07. Approximate values of Fe₂O₃ and FeO were obtained from total Fe after making the reasonable assumptions of charge balance, negligible Mn and Al^{IV}. In this case, Ca²⁺ = Mg²⁺ + Fe²⁺. This enabled calculation of atomic proportions of elements and of end-member proportions after Banno (1959). Compositions are illustrated in Fig. 27b. The compositional range of clinopyroxenes from the Franciscan (Ernst *et al.*, 1970) is indicated for comparison with the Pinchi analyses. The jadeitic pyroxene (Px-74)

and the omphacitic pyroxene (Px-103), obtained respectively from a metagreywacke and an eclogite at Pinchi, are similar to jadeitic and omphacitic pyroxenes from the Franciscan. The acmite-jadeites (Px-48,49,205) are compositionally similar to Franciscan pyroxenes from the Mount Boardman area analyzed by Essene *et al.*, (1967). They may be similar to the "omphacitic" pyroxenes from metavolcanic rocks in the Pacheco Pass area (Ernst *et al.*, 1970) but chemical analyses were not performed because of fine grain size. At Pacheco Pass these metavolcanics are considered to have formed under P-T conditions similar to the jadeitic pyroxene bearing metagreywackes with which they are closely associated. This is also the case at Pinchi. The contrast in compositions is accounted for by Fe-Mg enrichment in metavolcanics.

Chlorite

Chlorite is widespread in the greenstones of Pinchi Mountain and the glaucophanitic rocks. It is generally pleochroic in greens, but may be colourless, in which case it is pseudoisotropic. Almost all samples studied are length slow (i.e. optically negative) but a few specimens were found containing both length slow and length fast chlorite. Interference colours are low first order and produce anomalous blue or brown tints in some samples.

TABLE 11

ELECTRON MICROPROBE ANALYSES OF CHLORITES

Specimen Number	Chl-38	Chl-48	Chl-165
SiO ₂	31.6	30.0	29.3
Al ₂ O ₃	15.9	15.3	15.9
FeO*	19.1	26.5	27.4
MnO	0.27	0.33	0.25
MgO	22.4	17.4	15.8
H ₂ O**	11.0	11.0	11.0
Total	100.3	100.5	99.7

* Total Fe calculated as FeO

** based on approximate water content of chlorites according to Deer, Howie and Zussman (1963), H₂O content for most chlorites ranges between 10.3 and 12²

Numbers of ions on basis of 28 oxygens

Specimen Number	38	48	165
Si	6.30	6.11	6.11
Al ^{IV}	1.70	1.89	1.89
Al ^{VI}	2.04	1.78	2.00
Fe ²⁺	3.20	4.56	4.78
Mg	6.62	5.33	4.89
Total	19.86	19.67	19.67

Specimen Data

Chl-38: chlorite blebs in lws + acm + sph + chl ± wh m
+ glph ± stilp matrix

Chl-48: assemblage: lws + acm + chl + sph ± late(?) glph

Chl-165: assemblage: chl + acm + ab + sph; Pinchi Mt.
Greenstones

Chemical analyses are given in Table 11. Chlorite formulae were calculated on the basis of 28 oxygen equivalents and all iron was assumed to be ferrous, as Ernst, (1970, p. 163) states that three Franciscan chlorites, analyzed by wet chemical methods, contain an average of 1.57 wt.% Fe_2O_3 . The analyses plot within the pycnochlorite or diabantite fields (Hay, 1954). According to Winchell (1936) and Hey (1954), Al poor chlorites are optically negative (length slow) and Al rich are optically positive (length fast). It follows that the predominance of optically negative chlorites at Pinchi suggests that they are compositionally similar to those of the Californian Coast Ranges. In a comparison of Californian and Japanese blueschists, Ernst (1970) notes a tendency for the Al content of chlorites to increase with rise in metamorphic temperatures.

Aragonite

Aragonite, the high pressure polymorph of calcite, is commonly found in the metasediments and metabasic rocks of the Pinchi Mountain greenstones and the glaucophanitic rocks. Localities are shown in Fig. 28. It occurs as veins or blebs in mafic rocks and is an important constituent of the limestones north of Pinchi Lake. Almost invariably, partial inversion to calcite may be noted on grain margins or along cleavages.

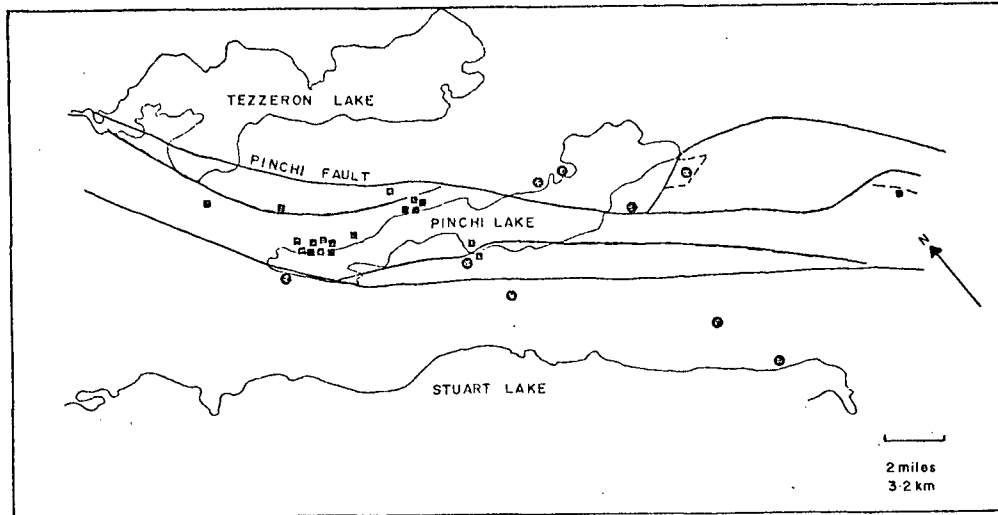


Fig. 28 Aragonite occurrences

- aragonite ± inverted calcite
- calcite only
- fault

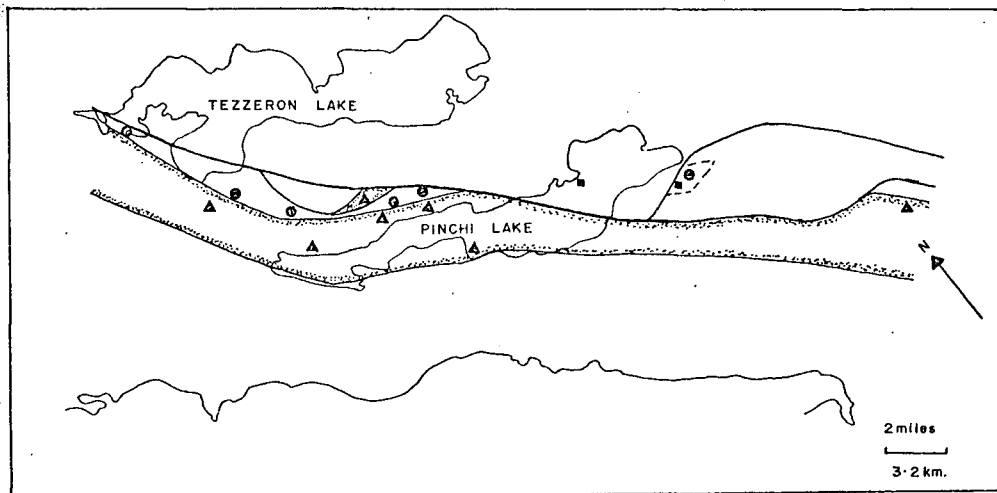


Fig. 29 Prehnite, pumpellyite and selected glaucophane-lawsonite occurrences

- pumpellyite
- prehnite
- ▲ lawsonite + glaucophane
- boundary of lawsonite + glaucophane
- bearing fault black

TABLE 12

CARBONATE MINERALOGY AND SAMPLE DISTRIBUTION

Mineralogy

- (a) arag + dol + cc ± qtz(tr): spec. nos. 77, 78, 79, 82,
215, 217, 221, 224, 227.
- (b) arag + dol: spec. no. 213.
- (c) arag + cc ± qtz(tr): spec. nos. 80, 222, 223, 225, 230.
- (d) dol + cc ± qtz: spec. nos. 216, 226, 234.
- (e) cc + qtz + barite: spec. no. 81.
- (f) cc ± qtz ± plag: spec. nos. 219, 220, 228, 229, 231,
232, 233, 235.

Sample distribution

- (i) samples from carbonates associated with lawsonite-glaucophane rocks: 77, 78, 79, 80, 81, 82, 215, 216, 217, 218, 221, 222, 223, 224, 225, 226, 227, 234.
- (ii) samples from carbonates interbedded with Pinchi Mt Greenstones: 82, 218.
- (iii) samples from Mt. Pope belt: 228, 235, 229, 232.
- (iv) samples from Takla Group limestones: 219, 220, 230, 231, 233.

Note: (a) Specimen locations are given on Fig. 28.

(b) cc = calcite; dol = dolomite; arag = aragonite;
qtz = quartz; plag = plagioclase; tr = trace.

Argonite can be easily identified in thin section by its characteristic negative 2V of 18° , straight extinction on its prismatic cleavage, low relief with α parallel to the polariser and {110} twinning on basal sections. Thirty X-ray diffractometer traces of limestones from the area were also made. Carbonate mineralogy and sample distribution are given in Table 12.

White mica

White mica is most abundant within glaucophanitic metacherts and schists. Greenstones and glaucophanitic metabasic rocks commonly contain disseminated sericite ($<5\mu$) with coarser grained varieties near fractures or as clusters in amygdules.

The white mica appears greenish to the unaided eye and shows faint pleochroism in thin section with α -colourless and $\beta = \gamma$ -very pale green. Micas examined in two specimens (151, 212) are uniaxial negative but some show a negative 2V of up to 10° . Deer, Howie & Zussman (Vol. 3, p. 22) state that small 2Vs are occasionally seen in white micas. The reason is uncertain, but it may be caused by anomalous optical effects resulting from superimposition of mica flakes. X-ray examination of three micas indicated that they were the normal $2M_1$ polytype.

Partial microprobe analyses of micas from a glauco-

TABLE 13

PARTIAL ELECTRON MICROPROBE ANALYSES OF PHENGITES AND CELADONITE

	Ph-151	Ph-205	Cel-196	A	B
SiO ₂	-	-	-	50.50	46.50
Al ₂ O ₃	26	21	6.1	20.57	29.82
TiO ₂	0.1	0.1	tr	0.76	0.18
Fe ₂ O ₃	-	-	-	6.95	1.50
FeO	3.3*	5.3*	16.4*	0.00	1.86
MnO	tr	tr	0.05	0.82	0.02
MgO	4.4	4.7	6.1	5.68	3.97
CaO	0.00	0.04	0.09	0.26	0.23
Na ₂ O	tr	tr	0.00	tr	0.37
K ₂ O	-	-	-	10.95	9.15
H ₂ O	-	-	-	2.74	4.77

* Total Fe calculated as FeO

- = not determined

tr = trace

Specimen data

Ph-151: metachert, Pinchi Lake; assemblage: glaucophane + lawsonite + quartz + phengite.

Ph-205: metabasic rock; assemblage: glaucophane + phengite + aragonite + chlorite (occurs as fracture fillings in acmite + sphene + lawsonite + quartz rock).

Cel-196: assemblage: albite + chlorite + pumpellyite + sphene + celadonite. Prehnite, calcite and white mica are also present sporadically in blebs (Pinchi Mt. Greenstone).

A: ferriphengite from quartz + alkali feldspar + green biotite + calcite + epidote gneiss (Plas, 1959).

B: phengite from glaucophane + chlorite + aragonite + jadeitic pyroxene schist (Ernst, 1963, Table 1, No. 10).

TABLE 14

STANDARD DEVIATIONS FOR SELECTED MINERAL ANALYSES

	Px-74	σ	Gl-49	σ
SiO ₂	58.1	± 1.0	56.2	± 0.4
Al ₂ O ₃	18.5	± 0.6	7.4	± 0.8
TiO ₂	0.20	± 0.20	0.13	± 0.06
Fe ₂ O ₃	5.1*	± 0.81	-	-
FeO	-	-	17.2**	± 0.2
MnO	0.03	-	0.19	± 0.07
MgO	1.7	± 0.2	8.4	± 0.4
CaO	3.0	± 0.4	1.0	± 0.4
Na ₂ O	13.4	± 0.3	6.8	± 0.1
K ₂ O	0.00	-	0.07	+ -

* total Fe calculated as Fe₂O₃

** total Fe calculated as FeO

phanitic metachert (Ph-151) and from veins in a metabasic rock (Ph-205) are given in Table 13. These results are uncorrected for absorption and fluorescence and should be considered semiquantitative. The MgO values (4.4, 4.7 wt.%) and the FeO values (3.3, 5.3 wt.%) show that the micas are phengites or ferriphengites.

Celadonite

Celadonite is sporadically present within the Pinchi Mountain greenstones, typically occurring in radiating aggregates. It is easily recognized by its bright green pleochroism (α -fawn, $\beta = \gamma$ -blue-green) and its length slow character. Optical identification was confirmed by X-ray diffraction. A partial semiquantitative analysis is given in Table 13.

Albitic plagioclase

Albite occurs within the Pinchi Mountain greenstones as replacements of primary plagioclase microlites and phenocrysts, and as veins. In the glaucophanitic rocks it is exceedingly rare, occurring only as late veins in metabasic rocks (No. 49, 58) and graphitic cherts (No. 118).

Blastoporphyritic albites are generally charged with inclusions (sericite, pumpellyite, chlorite and unknowns) and relief determinations are difficult. Where determined

the relief is low with the Michel-Levy method giving compositions of An_{0-5} . Vein albite in the glaucophanitic rocks has positive sign, and β' or $\gamma' = 1.536$.

Pumpellyite

Pumpellyite is found only within the greenstones of Pinchi Mountain (for localities see Fig. 29). It occurs as matted acicular aggregates in veins, ferromagnesian pseudomorphs and blastoporphyrific albites. Optical properties are obtained only with difficulty because of fine grain size. These are: $\alpha = \gamma$ -fawn, β -green; $\beta^c = 5^\circ$; anomalous bluish or brownish interference tints. Optical identification was confirmed by X-ray diffraction.

Stilpnomelane

Stilpnomelane typically occurs as late veins in glaucophanitic rocks and also as an alteration product of garnet in an eclogite boulder. The green pleochroic variety, ferrostilpnomelane, (α -colourless, $\beta = \gamma$ -pale green) occurs with the more common brown stilpnomelane.

Lawsonite

Metabasic rocks, metasediments and eclogite boulders all contain lawsonite. The mineral was also tentatively identified in one thin section from the greenstones of

Pinchi Mountain. Within the eclogite boulder and some schists it commonly occurs as polysynthetically twinned porphyroblasts, but otherwise it is recognized by its tabular habit, straight extinction and negative elongation.

Prehnite

Colourless sheaf-like aggregates of prehnite were noted in the Pinchi Mountain greenstones at the west end of Murray Ridge in association with pumpellyite, celadonite, chlorite, albite and calcite (Fig. 29). The mineral also occurs with quartz in amygdules in basic volcanics of presumed Upper Triassic age.

Garnet

An eclogite boulder contains subhedral garnets (1 mm max diameter) partly replaced by stilpnomelane. Reconnaissance probe work indicates that they are chemically similar to those found elsewhere in eclogites associated with blueschists (Coleman *et al.*, 1965). They are slightly zoned with the cores having the composition almandine (60%), grossular (30%) and spessartine + pyrope (10%).

Deerite

A specimen of drill core taken from the Pinchi Mine area contains dark brown radiating sprays up to 1 cm in

diameter of deerite (Agrell *et al.*, 1965). The mineral appears late in the paragenetic sequence and cross-cuts glaucophane, lawsonite and sodic pyroxene. It is slightly pleochroic on thin edges (dark brown to black), has straight extinction and an amphibole-like cross section (Fig. 34).

X-ray examination of a deerite concentrate using a KBr internal standard and Phillip's diffractometer revealed a fairly good correspondence with the calculated d_{hkl} obtained from the cell parameters published by Agrell. The well defined (020) and (110) reflections yielded d-spacings of $9.42 \pm 0.02 \text{ \AA}$ and $9.04 \pm 0.02 \text{ \AA}$. The difference from the calculated values (9.42 and 9.18 \AA respectively) can be attributed to shift of peak positions due to solid solution. Deerite peaks at higher 2θ values were difficult to index because of contamination by riebeckite, sodic pyroxene and lawsonite.

Opagues

Within metabasic rocks, opaque minerals other than relict ilmenomagnetites are very fine grained (0.3 mm max). Grains studied with the reflecting microscope are composite, with creamy yellow pyrite forming the nucleus, surrounded by magnetite (or maghemite). This in turn is rimmed by hematite (Fig. 30). Pyrite is widespread within graphite schists.

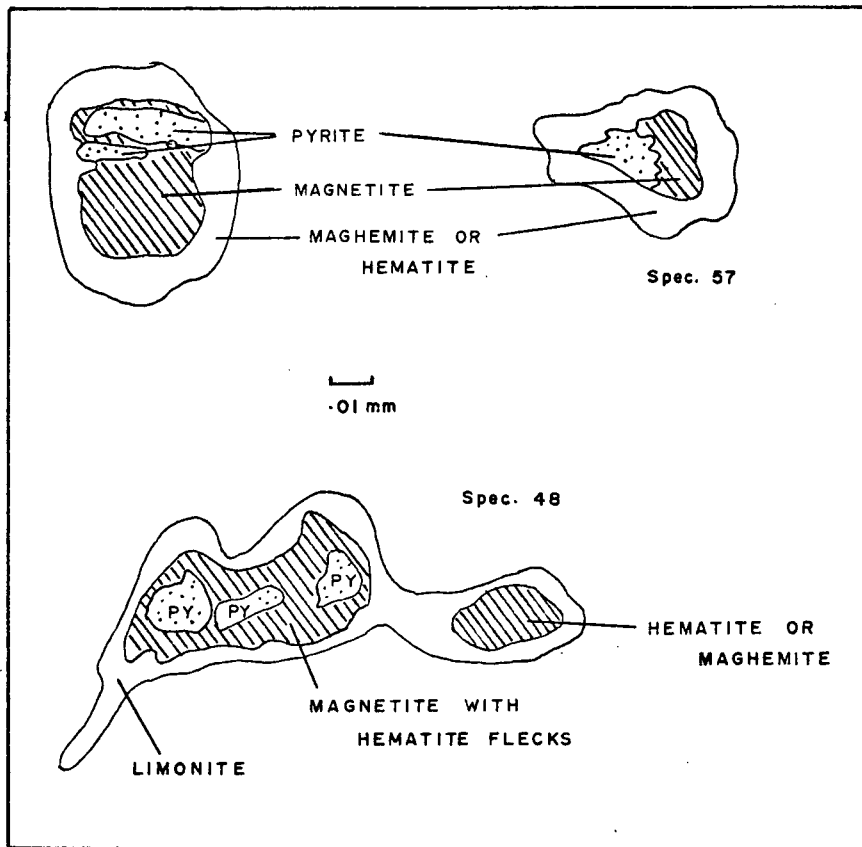


Fig. 30 Textures in opaque minerals

Carbonaceous material

Carbonaceous material from schists and cherts was separated employing the method of French (1964) by digestion with HF and HCl and X-rayed using a Phillip's diffractometer (CuK_α radiation; scan-rate - $2^\circ/\text{min}$; chart speed - $5 \times 240 \text{ mm/hr}$). After digestion, pyrite and ralstonite were the only phases present in addition to carbonaceous material. One sample out of the five studied gave a broad diffuse peak at 26° , suggesting the presence of nearly amorphous graphitic material (graphite- d_3 according to the classification of Landis, 1971). Four samples yielded featureless diffractometer charts indicative of amorphous material.

APPENDIX III

BULK CHEMICAL ANALYSES

Representative homogeneous samples of thirteen metabasic rocks and two metagreywackes were analysed by the Geological Survey of Canada laboratory in Ottawa. Analyses for MnO, TiO₂, CaO, K₂O, SiO₂ and Al₂O₃ were obtained by X-ray fluorescence methods; Fe (total), FeO, Na₂O, P₂O₅, CO₂ and H₂O (total), by "rapid chemical analytical techniques" and MgO by atomic absorption. Estimated errors quoted by the Geological Survey are given in Table 15. The analyst also noted that some of the high values for TiO₂ were outside the normal range of the method used. Precision may be estimated by inspection of the duplicate specimens (36a and 36b). Totals range from 97.8% to 101.2% by weight.

Metabasic rocks

Prior to norm calculation for metabasic rocks, two adjustments were made to the analytical data as suggested by Irvine and Baragar (1971). This involved recalculation of the ferric-ferrous ratio to correct for oxidation during metamorphism, and recalculation of the analyses to 100% omitting H₂O and CO₂. Original analyses and oxidation

TABLE 15
ACCURACY OF BULK CHEMICAL ANALYSES

Oxide	Range in Value	one σ
SiO ₂	30-75%	± 1.2
Al ₂ O ₃	0-20%	± 0.7
Fe _{tot} (Fe ₂ O ₃)	0-15%	± 0.5
CaO	0-40%	± 0.3
MgO	0-40%	± 1.0
K ₂ O	0-5%	± 0.1
TiO ₂	0-2%	± 0.05
MnO	0-1%	± 0.02
FeO	0-15%	± 0.2
Na ₂ O	0-10%	± 0.15
P ₂ O ₅	0-1%	± 0.04
CO ₂		± 0.1
H ₂ O		± 0.1

Note: errors are those reported by the analyst of the Geological Survey of Canada.

TABLE 16a CHEMICAL ANALYSES OF METABASALTS FROM THE PINCHI LAKE AREA

	GREENSTONES OF			LAWSONITE-GLAUCOPHANE BEARING METABASALTS													
	PINCHI MT.			MASSIVE ROCKS									FOLIATED				
	170	163	162	45	36a	36b	48	61	202	23	37	31	55	A	B	C	D
SiO ₂	43.8	44.6	44.2	45.6	33.1	32.3	42.9	47.9	40.2	42.7	44.8	46.7	47.5	49.20	44.10	45.40	49.16
TiO ₂	4.35	2.72	3.36	3.22	1.75	1.63	5.51	1.49	2.45	1.20	4.00	1.49	3.64	3.40	2.70	3.60	2.29
Al ₂ O ₃	14.7	13.1	18.1	13.7	9.1	9.2	10.5	14.4	12.2	13.8	16.4	14.1	14.6	12.87	12.10	14.70	13.33
Fe ₂ O ₃	3.9	5.0	3.1	5.6	5.2	5.0	4.2	4.1	7.5	4.4	5.2	5.1	3.6	4.94	3.20	4.10	1.31
FeO	9.6	6.7	6.8	6.3	4.3	4.3	8.1	7.8	5.7	5.5	5.2	7.0	7.6	12.04	9.60	9.20	9.71
MnO	0.13	0.16	0.18	0.17	0.20	0.21	0.11	0.14	0.14	0.10	0.06	0.14	0.13	0.27	0.20	0.20	0.16
MgO	4.5	7.2	3.0	5.4	6.2	6.0	7.3	5.6	11.1	7.0	4.4	7.5	4.9	4.94	13.00	7.80	10.41
CaO	6.5	9.5	8.6	9.8	20.0	21.0	11.1	7.9	8.8	13.8	8.8	9.2	8.9	8.54	11.50	10.50	10.93
Na ₂ O	4.8	2.0	5.1	2.6	3.2	3.1	2.9	2.9	2.7	1.1	2.7	1.9	3.3	3.09	1.90	3.00	2.15
K ₂ O	0.1	2.6	0.3	0.8	1.3	1.4	0.1	0.2	0.1	0.2	1.7	0.1	0.8	0.31	0.70	1.00	0.51
P ₂ O ₅	0.56	0.28	0.36	0.37	1.29	2.14	0.08	0.13	0.27	0.11	0.17	0.11	0.46	0.36	0.30	0.40	0.16
CO ₂	0.8	0.6	0.7	0.3	9.2	10.4	0.8	1.2	0.2	4.0	0.1	1.3	0.1				
H ₂ O _t	4.7	4.3	4.6	4.5	3.9	3.8	4.8	5.1	6.4	6.0	5.7	6.6	5.0				
Total	98.4	98.8	98.4	98.4	98.7	100.5	98.2	98.9	97.8	99.9	99.1	101.2	100.5				
Oxidn. ratio	26	40	29	44	51	52	32	32	54	41	47	39	30	27	23	29	11

A : Franciscan greenstone; Coleman & Lee, (1963, Table 2, no. 60-804).
 B : Average Hawaiian ankaramite; Macdonald (1968, Table 8).
 C : Average Hawaiian alkali-olivine basalt; Macdonald (1968, Table 8)
 D : Olivine tholeiite, Kilauea volcano, Hawaii; Yoder & Tilley, (1962, Table 2, no.14).
 Note : for mineral assemblages, see Table 22.

TABLE 17 C. I. P. W. NORMS FOR ANALYSED METABASALTIC ROCKS

	GREENSTONES OF			LAWSONITE-GLAUCOPHANE BEARING METABASALTS									
	PINCHI MT.			MASSIVE ROCKS								FOLIATED	
	170	163	162	45	36	48	61	202	23	37	31	55	
quartz	-	-	-	2.43	-	-	3.11	-	-	0.94	2.85	1.85	
orthoclase	0.65	16.37	1.77	5.32	-	0.59	1.18	0.59	1.18	10.75	0.65	4.96	
albite	41.85	17.08	33.07	23.69	-	26.49	26.57	20.08	10.15	24.45	17.26	29.28	
anorthite	19.68	20.38	27.56	24.77	-	16.60	27.83	22.88	35.93	29.54	31.83	23.74	
nepheline	0.98	0.51	7.20	-	-	-	-	2.88	-	-	-	-	
diopside	9.05	22.37	12.82	19.68	-	32.94	11.24	18.66	31.99	12.47	13.37	15.65	
hypersthene	-	-	-	9.38	-	1.97	21.99	-	12.34	5.95	26.07	10.70	
olivine	11.43	10.57	4.96	-	-	3.39	-	22.83	1.11	-	-	-	
magnetite	6.09	6.52	4.83	7.32	-	6.73	4.68	6.23	4.35	5.74	4.65	5.47	
ilmenite	8.89	5.51	6.86	6.53	-	11.30	3.06	5.13	2.54	8.13	3.04	7.24	
apatite	1.39	0.70	0.90	0.93	-	0.21	0.32	0.70	0.28	0.42	0.28	1.11	

Note : a) norms in wt.%

TABLE 16b "ADJUSTED" CHEMICAL ANALYSES OF METABASALTS

	GREENSTONES OF			LAWSONITE-GLAUCOPHANE BEARING METABASALTS									
	PINCHI MT.			MASSIVE ROCKS								FOLIATED	
	170	163	162	45	36a	36b	48	61	202	23	37	31	55
SiO ₂	47.1	47.6	47.5	48.8	38.7	37.5	46.3	51.8	44.3	47.5	48.0	50.1	49.8
TiO ₂	4.68	2.90	3.61	3.44	2.04	1.89	5.95	1.61	2.70	1.34	4.28	1.60	3.81
Al ₂ O ₃	15.8	14.0	19.4	14.7	10.7	10.7	11.3	15.6	13.4	15.4	17.6	15.1	15.3
Fe ₂ O ₃	4.2	4.5	3.3	5.1	3.8	3.6	4.6	3.2	4.3	3.0	5.6	3.2	3.8
FeO	10.3	7.9	7.3	7.6	7.1	7.0	8.8	9.5	9.8	7.9	5.6	9.6	8.0
MnO	0.14	0.17	0.19	0.18	0.23	0.24	0.12	0.15	0.15	0.11	0.06	0.15	0.14
MgO	4.8	7.7	3.2	5.8	7.3	7.0	7.9	6.1	12.2	7.8	4.7	8.1	5.1
CaO	7.0	10.1	9.2	10.5	23.4	24.4	11.9	8.6	9.7	15.4	9.4	9.9	9.3
Na ₂ O	5.2	2.1	5.5	2.8	3.8	3.6	3.1	3.1	3.0	1.2	2.9	2.0	3.5
K ₂ O	0.1	2.8	0.3	0.9	1.5	1.6	0.1	0.2	0.1	0.2	1.8	0.1	0.8
P ₂ O ₅	0.60	0.30	0.39	0.40	1.51	2.49	0.09	0.14	0.30	0.12	0.18	0.12	0.48

The analyses were a) recalculated to 100% omitting H₂O and CO₂ and b) corrected for oxidation during metamorphism by adjusting the ferric-ferrous ratio (assuming % Fe₂O₃ = % TiO₂ + 1.5) - after Irvine and Baragar (1971).

FIG. 31 A-F-M DIAGRAM ILLUSTRATING BASALT COMPOSITIONS

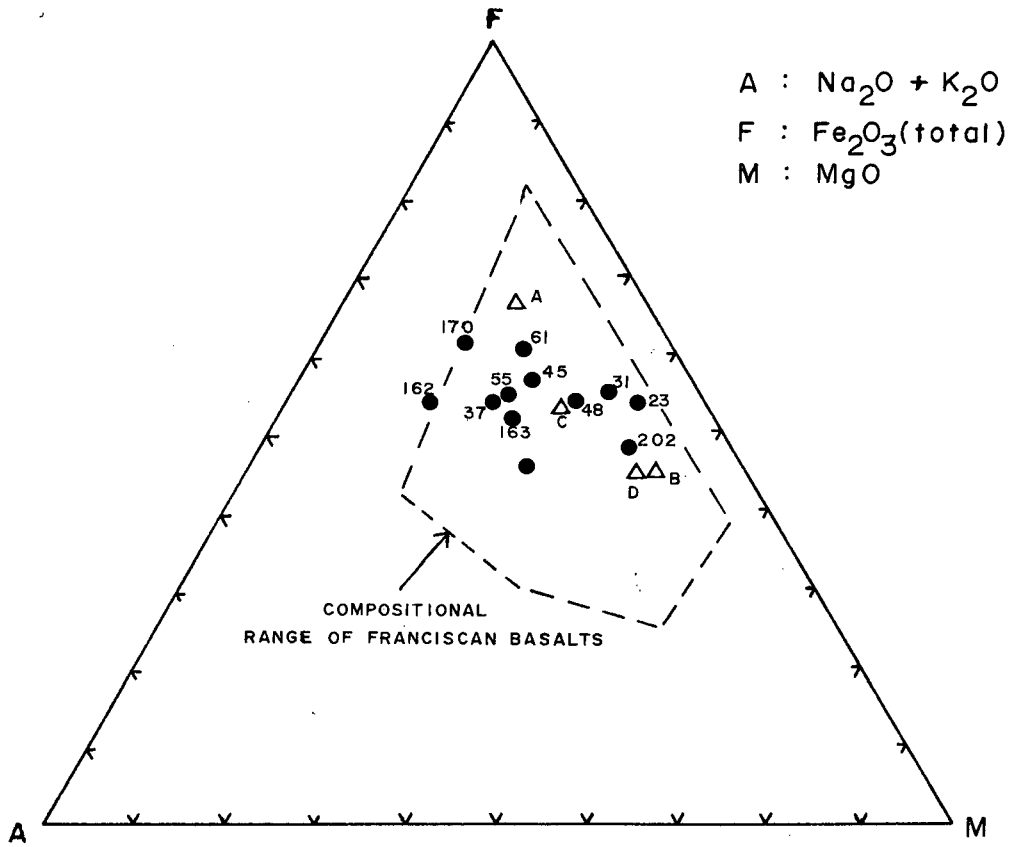
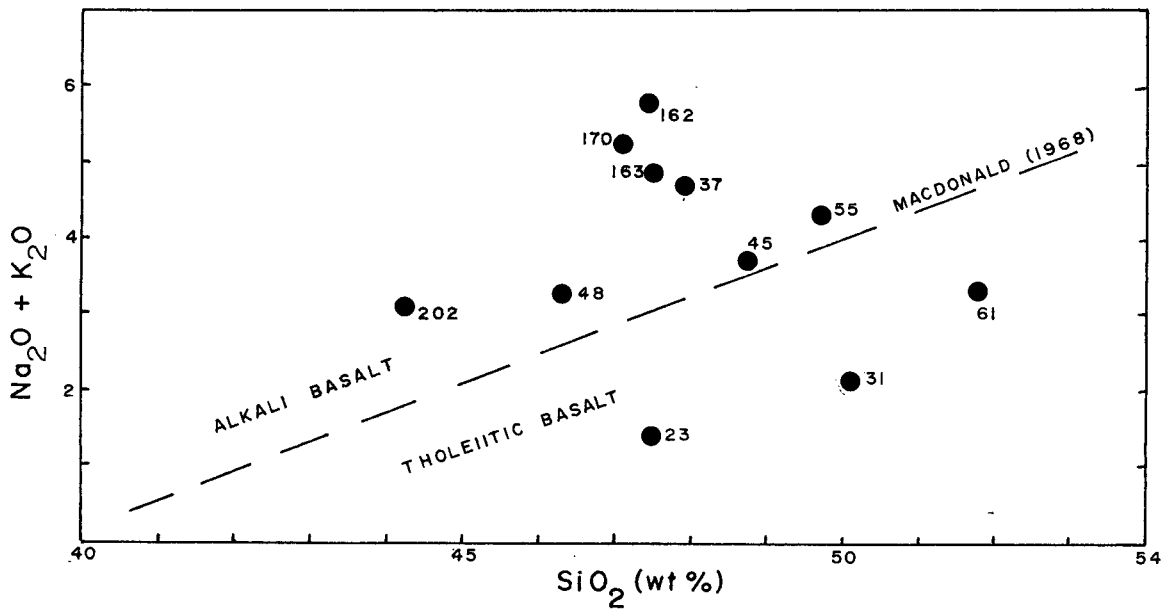


FIG. 32 ALKALI-SILICA VARIATION DIAGRAM FOR BASALTS



ratios are given in Table 16a and adjusted analyses in Table 16b. C.I.P.W. norms are presented in Table 17.

Relict mineralogy and textures show that the majority of the basic rocks were originally volcanics prior to the formation of the metamorphic minerals (Appendix IV). Two rocks (Nos. 23 and 48) are considered to have been basic intrusives. The basaltic composition of the analysed rocks is illustrated in an A.F.M. diagram (Fig. 31) with the area encompassing Franciscan basalts shown for comparison (Ernst *et al.*, 1970).

Relevant information relating to the classification of the primary basalt type is presented in Table 18 and in the alkali-silica variation diagram (Fig. 32). The Pinchi Mountain greenstones (Specs. 162, 163 and 170) possess the chemical characteristics of alkali basalts. Normative hypersthene is absent and on the alkali-silica variation diagram, the basalts plot in the alkali field as given by MacDonald (1968). The high TiO_2 values (>2.9) are thought to be representative of the primary basalt, as titanium is generally considered immobile during metamorphism. Engels *et al.*, (1965) present the following average TiO_2 values for basalts: (a) oceanic tholeiites (1.49 wt.% TiO_2); (b) alkali basalts (2.87 wt.% TiO_2). The range of TiO_2 values in the Pinchi Mountain greenstones (4.7, 2.9, 3.6 wt.%) suggests an affinity with the alkali basalt type.

Within the glaucophane-lawsonite bearing metabasic rocks, both types of basalt appear to be represented. Three

TABLE 18 SUMMARY OF SIGNIFICANT CHEMICAL CHARACTERISTICS OF METABASALTS

Spec. no.	Normative hyp.	qtz.	Na ₂ O + K ₂ O	TiO ₂	Basalt type
170*	-	-	5.2 + 0.1	4.7	alkali basalt
163*	-	-	2.1 + 2.8	2.9	alkali basalt
162*	-	-	5.5 + 0.3	3.6	alkali basalt
45	9.4	2.4	2.8 + 0.9	3.4	?
36	highly carbonated sample				
48	2.0	-	3.1 + 0.1	6.0	alkali basalt
61	22.0	3.1	3.1 + 0.2	1.6	tholeiitic basalt
202	-	-	3.0 + 0.1	2.7	alkali basalt
23	12.3	-	1.2 + 0.2	1.3	tholeiitic basalt
37	6.0	0.9	2.9 + 1.8	4.3	?
31	26.1	2.9	2.0 + 0.1	1.6	tholeiitic basalt
55	10.7	1.9	3.5 + 0.8	3.8	?
* Pinchi Mountain greenstones					
Oxide values obtained from Table 16b					

out of eight analyzed rocks have normative hypersthene and quartz, have low TiO_2 values (1.3 - 1.6 wt.%) and plot in the tholeiitic field on an alkali-silica variation diagram. One basalt (No. 202) has an analysis similar to a Hawaiian ankaramite (Table 16a) and possesses the characteristics of an alkali basalt. The four remaining basalts are alkaline in that the TiO_2 content is high and they plot in the alkali basalt field in the variation diagram. However, they also contain normative hypersthene and quartz which, according to Yoder and Tilley is characteristic of tholeiitic basalts. The conflicting evidence as to the basalt type suggests either titanium and alkali enrichment of a tholeiitic basalt or silica enrichment of an alkali basalt during metamorphism. Considering the probable immobility of titanium during metamorphism, the latter suggestion is preferred. It is therefore concluded that both tholeiitic and alkali basalts were present in the rock sequence prior to metamorphism.

Metagreywackes

Analyses for two metagreywackes are shown in Table 19. Also included for purposes of comparison are the average of 21 Franciscan greywackes (Bailey *et al.*, 1964, Table 2, No. 1). The Pinchi metagreywackes have lower

TABLE 19
 CHEMICAL ANALYSES OF METAGREYWACKES

Specimen Number	71	70	A	B
SiO ₂	50.5	57.0	67.5	65.0
TiO ₂	0.82	0.68	0.5	0.69
Al ₂ O ₃	19.8	17.6	13.5	14.14
Fe ₂ O ₃	3.4	2.7	1.2	0.58
FeO	4.4	4.0	3.0	5.44
MnO	0.16	0.12	0.1	0.08
MgO	3.2	3.1	2.2	3.44
CaO	5.7	3.3	2.4	2.28
Na ₂ O	3.7	5.4	3.6	2.29
K ₂ O	1.9	1.4	1.7	2.24
P ₂ O ₅	0.28	0.23	0.1	0.14
CO ₂	0.1	0.1	0.8	0.01
H ₂ O _t	5.4	2.1	2.9	4.02
Total	99.4	97.7	99.5	100.35

71: metagreywacke, Pinchi Lake (analysed by G.S.C.)

70: metagreywacke, Pinchi Lake (analysed by G.S.C.)

A: average of 21 Franciscan metagreywackes (Bailey *et al.*, 1964, Table 2, No. 1).

B: jadeitic pyroxene bearing metagreywacke (Ernst, 1965, Table 12, No. 190).

SiO₂ and higher Al₂O₃ and CaO values. Presumably this reflects either less quartz or a higher anorthite content in the initial sediment.

APPENDIX IV

PETROLOGY

Greenstones of Pinchi Mountain

Metamorphic and relict minerals present in the greenstones of Pinchi Mountain are given in Table 20. Chlorite, albite, sodic pyroxene and sphene are the main minerals with celadonite, quartz, pumpellyite, prehnite, ferrostilpnomelane, aragonite and white mica sporadically distributed. A few small grains of lawsonite and glaucophane were also observed. Optical properties and mineral compositions are covered in Appendix II.

The relict mineralogy and bulk chemistry (Appendix III) suggest that the primary rocks were alkali basalts consisting of augite, plagioclase, ilmenite and olivine (?) exhibiting porphyritic, trachytic and amygdaloidal textures.

Domains within individual thin sections are of five textural types: matrix, relicts, blebs, pseudomorphs and veins. Metamorphic mineral assemblages characteristic of each domain are given in Table 21 and are illustrated in Fig. 33. The distinction between blebs and pseudomorphs is somewhat arbitrary and dependant on the latter possessing a euhedral or subhedral outline. Blebs may have originated

TABLE 20 MINERAL ASSEMBLAGES IN THE GREENSTONES OF PINCHI MOUNTAIN

Spec. No.	160	161	162	163*	164	165	166†	169	170	171	172	173	193	195	196	197	203	204
albite		x	60	20	x	55	-	-	40	x	x	x	x	x	x	x	x	x
chlorite	x	x	20	3	x	10	x	x	35	x	x	x	x	x	x	x	x	x
quartz	x	-	-	7	-	-	x	x	-	-	-	x	-	-	-	-	-	-
sodic pyx.	x	x	8	12	x	tr	x	x	11	x	x	-	x	x	-	-	x	x
pumpellyite	-	x	3	-	-	3	-	-	-	-	-	-	x	x	x	x	x	-
white mica	x	-	2	7	-	-	-	-	5	-	-	-	x	-	-	-	x	-
sphene	x	x	8	2	x	5	x	x	5	x	x	x	x	x	x	x	x	x
aragonite	x	-	-	-	x	-	x	-	4	x	x	x	-	-	-	-	-	-
celadonite	-	-	-	7	-	-	-	-	-	-	-	-	-	-	-	x	-	-
prehnite	-	-	-	-	-	-	-	-	-	-	-	-	-	-	x	x	-	-
calcite	-	-	-	-	-	-	-	-	-	-	-	-	-	-	x	x	-	-
augite (r)	x	x	-	35	-	27	-	x	x	x	-	-	-	x	x	x	x	-
ilmenite (r)	-	-	-	5	-	-	-	-	-	-	-	-	-	-	-	-	-	-

* = trace of lawsonite x = mineral present
† = trace of glaucophane
r = relict mineral
Modes are approximate.

TABLE 21

TEXTURAL DOMAINS WITHIN THE PINCHI MOUNTAIN GREENSTONES

<u>Size range:</u>	relicts	0.5 - 1.5 mm
	matrix	albite microlites (0.2 mm), chlorite, sphene (0.01 mm average), acmitic pyroxene (0.05 mm average)
	blebs	0.5 - 5 mm
	pseudomorphs	2 - 8 mm
	veins	0.1 - 3 mm

Relict minerals: augite, ilmenite

Matrix assemblages:

ab + Na px + chl + sph ± wh m ± celad ± arag ± lws

qtz + chl + Na px + sph ± wh m ± arag

ab + chl + pump + sph ± prehn ± cc ± celad ± wh m

Relict microgranular augite may also be present in the matrix

Blebs: chl (radiating aggregates)

pump ± chl ± celad ± prehn ± wh m

arag ± celad ± pump

celad

Pseudomorphs:

plagioclase -- ab ± ser ± chl ± pump

olivine (?) -- chl

-- cc

-- chl ± pump ± celad ± prehn

clinopyroxene -- blotchy sodic pyroxene

TABLE 21 (continued)

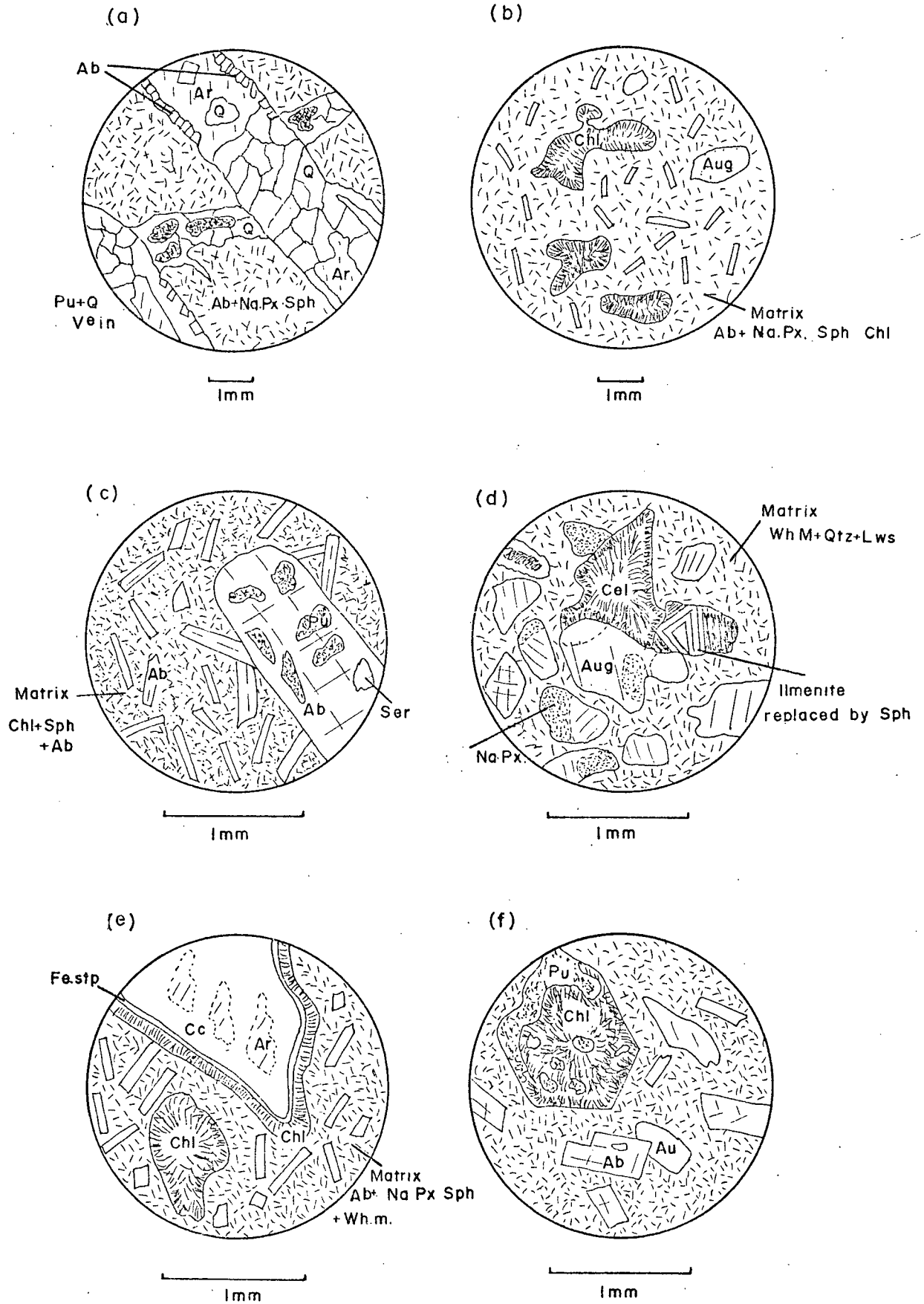
<u>Veins:</u>	pump + qtz ± wh m	early
	qtz + Na px + arag	
	arag + qtz ± ab	late
	ab	

Note: Abbreviations given on p. 74.

Figure 33 Textures in Pinchi Mountain Greenstones

- (a) Early quartz-pumpellyite vein is cross-cut by an aragonite-quartz vein rimmed with albite. Microgranular matrix consists of albite + sodic pyroxene + sphene (Spec. 204).
- (b) Chlorite blebs and relict augites occur in matrix consisting of albite microlites, sodic pyroxene, sphene and chlorite (Spec. 165).
- (c) Plagioclase phenocrysts are pseudomorphed by albite, pumpellyite and sericite. Matrix contains albite laths, chlorite and sphene (Spec. 162).
- (d) Relict augites are partly replaced by a brownish sodic pyroxene with straight extinction. Note celadonite blebs, ilmenite partly replaced by sphene and white mica + quartz + lawsonite matrix (Spec. 163).
- (e) Large bleb contains aragonite partly inverted to calcite and rimmed by ferrostilpnomelane and chlorite. Matrix consists of albite + sodic pyroxene + sphene + white mica (Spec. 170).
- (f) Chlorite and pumpellyite replace ferromagnesian phenocrysts (olivine?). Albite and augite crystals lie in a microgranular matrix (Spec. 196).

FIG. 33 TEXTURES IN PINCHI MT. GREENSTONES



either as phenocrysts or amygdules which were later subject to deformation and recrystallization. Chlorite blebs are by far the most common type. Hornblende or olivine are the most likely precursors of some blebs, but the latter is preferred on account of the basic composition of the rocks and absence of acicular pseudomorphs.

Prehnite occurs only in the greenstones at the west end of Murray Ridge, coexisting with albite, chlorite, pumpellyite, celadonite and calcite.

Lawsonite-Glaucophane Bearing Rocks

Metabasic rocks

Metamorphic mineral assemblages and relict minerals observed in 39 thin sections are given in Table 22. Modal analyses were performed for four representative rocks using a Zeiss micrometer eyepiece. Rough estimations were made for all other modes. Sample locations are given in Map VII. The metabasic rocks have been subdivided into two groups: foliated glaucophanitic rocks and massive rocks containing jadeite-acmite pyroxene. Gradations between each of these rock types are, however, common.

Foliated metabasic rocks are characterized by a high glaucophane content, a dearth of relict minerals and fairly uniform fabric. Typically they contain: glaucophane

TABLE 22 MINERAL ASSEMBLAGES IN LAWSONITE-GLAUCOPHANE BEARING METAVOLCANICS

	24	27	28	29	31	32	33	34	36	37	38	39	40	42	44	45	46	47	48	49
aragonite	10	-	-	-	-	-	-	-	8	-	5	10	-	-	-	-	-	-	-	2
chlorite	-	tr	-	x	6	x	x	10	1	x	15	10	20	x	5	-	tr	tr	10	10
glaucophane	5	30	15	x	27	x	x	11	1	x	5	5	20	x	16	15	-	65	5	45
lawsonite	52	35	41	x	48	x	x	22	10	x	35	20	32	x	50	46	50	22	39	27
sphene	-	12	12	x	6	x	x	11	3	x	10	8	13	x	17	23	-	10	1	5
quartz	-	tr	-	-	1	tr	-	-	-	-	-	-	-	-	-	-	-	tr	tr	-
acmitic px.	15	-	-	-	5	x	x	37	70	x	5	27	5	-	12	16	30	tr	25	7
white mica	8	-	2	x	tr	x	x	9	-	x	-	-	-	-	-	-	-	tr	tr	-
pyrite	-	-	-	x	-	-	-	-	-	-	-	-	-	-	-	-	-	-	-	-
stilpnomelane [#]	-	-	20	x	7	-	-	-	-	x	15	10	-	x	-	-	-	tr	-	-
brown hbl. #	-	-	-	-	-	-	-	-	-	-	-	-	-	-	-	-	-	-	-	-
magnetite #	-	-	-	-	tr	-	-	-	-	-	-	-	-	-	-	tr	-	-	-	-
hematite #	-	3	3	-	-	tr	-	tr	-	-	tr	-	-	-	-	-	-	-	-	-
deerite #	10	-	-	-	-	-	-	-	-	-	-	-	-	-	-	-	-	-	-	-
dolomite #	-	-	-	-	-	-	x	-	-	-	-	-	-	-	-	-	-	-	-	-
calcite #	-	-	tr	-	-	-	-	-	-	-	-	-	-	-	-	-	-	-	-	-
augite (r)	-	20	5	x	-	x	x	9	7	x	10	10	10	x	-	-	20	3	15	-
opagues (r)	-	-	-	-	-	-	-	-	-	-	-	-	-	-	-	-	-	-	-	-

	50	51	52	53	54	55	56	57	58	59	60	61	62	63	64	65	66	201	202	205
aragonite	-	x	-	-	-	-	-	-	-	-	-	-	-	-	x	-	-	-	x	-
chlorite	x	x	5	-	-	-	-	x	-	x	x	15	x	x	x	-	x	-	15	x
glaucophane	x	-	tr	x	8	54	x	x	-	-	x	2	-	-	x	x	-	x	-	x
lawsonite	x	x	68	x	65	31	x	x	57	-	x	40	x	x	x	x	x	x	30	x
sphene	x	x	10	-	11	15	x	x	15	x	x	8	x	x	x	x	x	x	10	x
quartz	-	x	-	x	-	-	-	x	-	-	x	10	x	x	-	-	x	-	-	x
acmitic px.	x	-	15	x	-	-	-	x	18	x	x	10	x	x	-	x	x	x	15	x
white mica	x	x	-	-	2	-	x	-	-	x	-	-	x	x	x	-	x	x	-	-
pyrite	-	-	-	-	-	-	-	-	-	-	-	-	-	-	-	-	-	-	-	-
stilpnomelane [#]	-	x	-	x	11	tr	-	-	-	-	-	-	-	-	-	-	-	-	-	-
brown hbl. #	-	-	-	-	-	-	-	-	-	-	-	-	-	-	-	-	-	-	-	-
magnetite #	-	-	tr	-	-	-	-	-	-	-	-	-	-	-	-	-	-	-	-	x
hematite #	-	-	-	-	-	-	-	-	-	-	-	-	-	-	-	-	-	-	-	-
deerite #	-	-	-	-	-	-	-	-	-	-	-	-	-	-	-	-	-	-	-	-
dolomite #	-	-	-	-	-	-	-	-	-	-	-	-	-	-	-	-	-	-	-	-
calcite #	-	-	-	-	-	-	x	-	-	-	x	-	-	-	-	-	-	-	-	-
augite (r)	x	x	2	x	5	-	-	-	8	x	-	15	-	-	-	-	-	-	30	-
opagues (r)	-	-	-	-	-	-	-	-	-	-	-	-	-	-	-	-	-	-	-	-

Note a) approximate modes given in some cases, b) * modal analysis obtained using a Zeiss micrometer eyepiece and counting over 500 points, c) "tr" means trace of mineral is present, d) (r) = relict mineral, e) # = retrogressive or alteration mineral and c) x = mineral present.

TABLE 23

TEXTURAL DOMAINS IN LAWSONITE-GLAUCOPHANE BEARING METABASIC ROCKS

Matrix: jd-acm + lws + sph + chl ± glph ± wh m ± stilp
± qtz ± py

Relict minerals: ilmenite, augite (often altered to jadeite-
acmite pyroxene or glaucophane)

Blebs and pseudomorphs:

lws + wh m + chl (plagioclase pseudomorphs)
lws + chl + arag + glph + stilp (plag. pseudomorphs)
arag + chl + wh m ± stilp (plag. pseudomorphs)
lws
chl ± stilp (olivine pseudomorphs ?)
jd-acm + lws ± wh m ± glph
arag ± sph (rims) (amygdules)

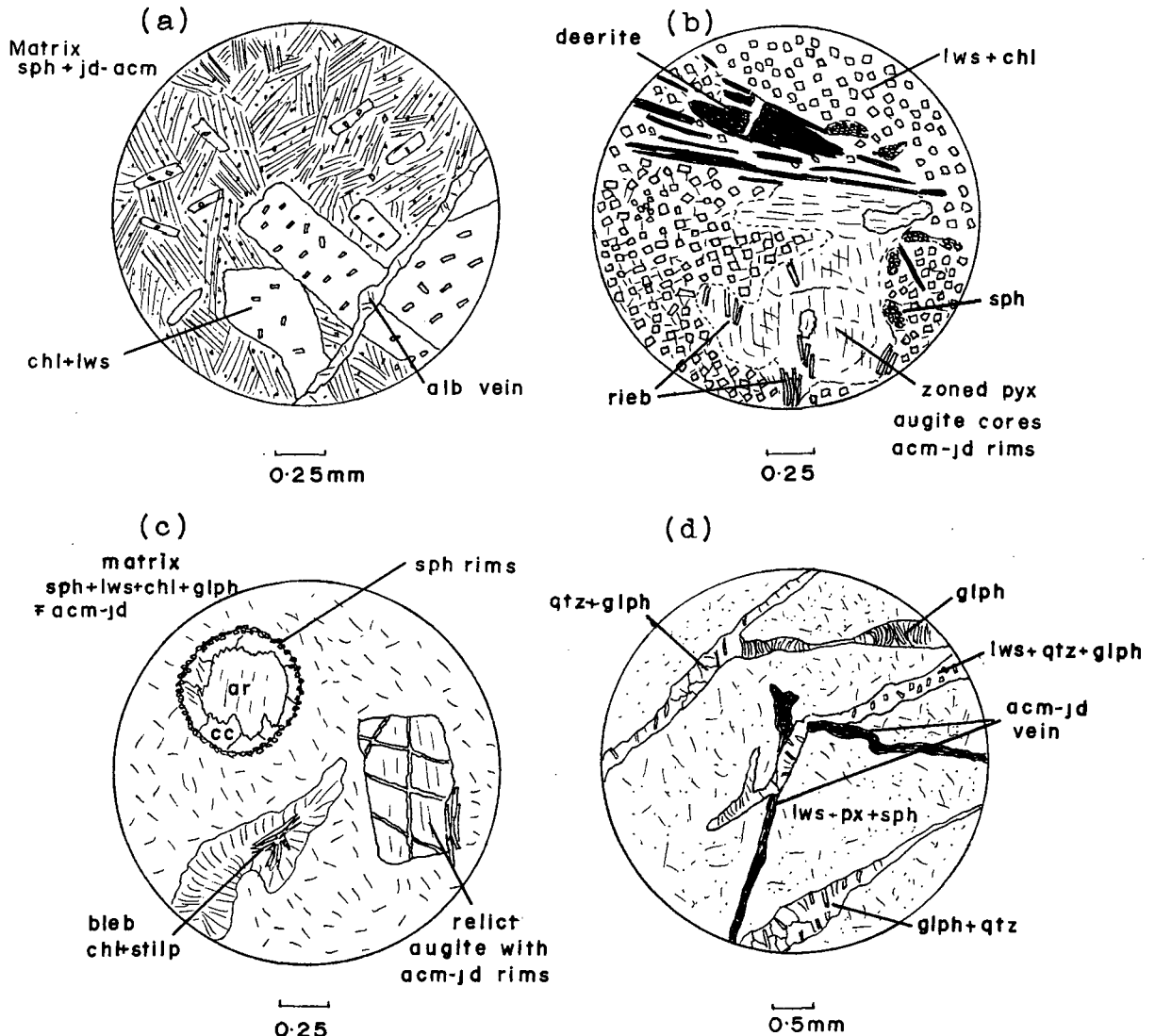
Vein assemblages and paragenesis:

	Time
jd-acm	_____
lws + chl ± wh m	_____
arag + chl ± wh m	_____
glph + qtz ± stilp	-?- _____
stilp	_____
ab + magn	-?- - _____
arag + brown hbl	-?- _____
calcite	_____

Relict textures: porphyritic, trachytic, amygdaloidal,
glomeroporphyritic.

Note: Abbreviations given on p. 74 .

FIG. 34 TEXTURES IN LAWSONITE-GLAUCOPHANE BEARING
METABASIC ROCKS



- a) Plagioclase phenocrysts pseudomorphed by tabular lawsonite and chlorite in sphene + jadeite-acmite matrix; cross-cutting albite vein (Spec. 61).
- b) Relict augite zoned to jadeite-acmite and sporadically rimmed by riebeckite in lawsonite + chlorite matrix; late deerite sprays (Spec. 23).
- c) Aragonite/calcite blebs rimmed with sphene in lawsonite + sphene + chlorite + glaucophane ± jadeite-acmite matrix; relict augite with acmite-jadeite on rims and along fractures; bleb contains chlorite + stilpnomelane (Spec. 38)
- d) glaucophane ± quartz ± lawsonite ± chlorite veins cross-cutting jadeite-acmite vein in lawsonite + jadeite-acmite + sphene matrix (Spec. 57).

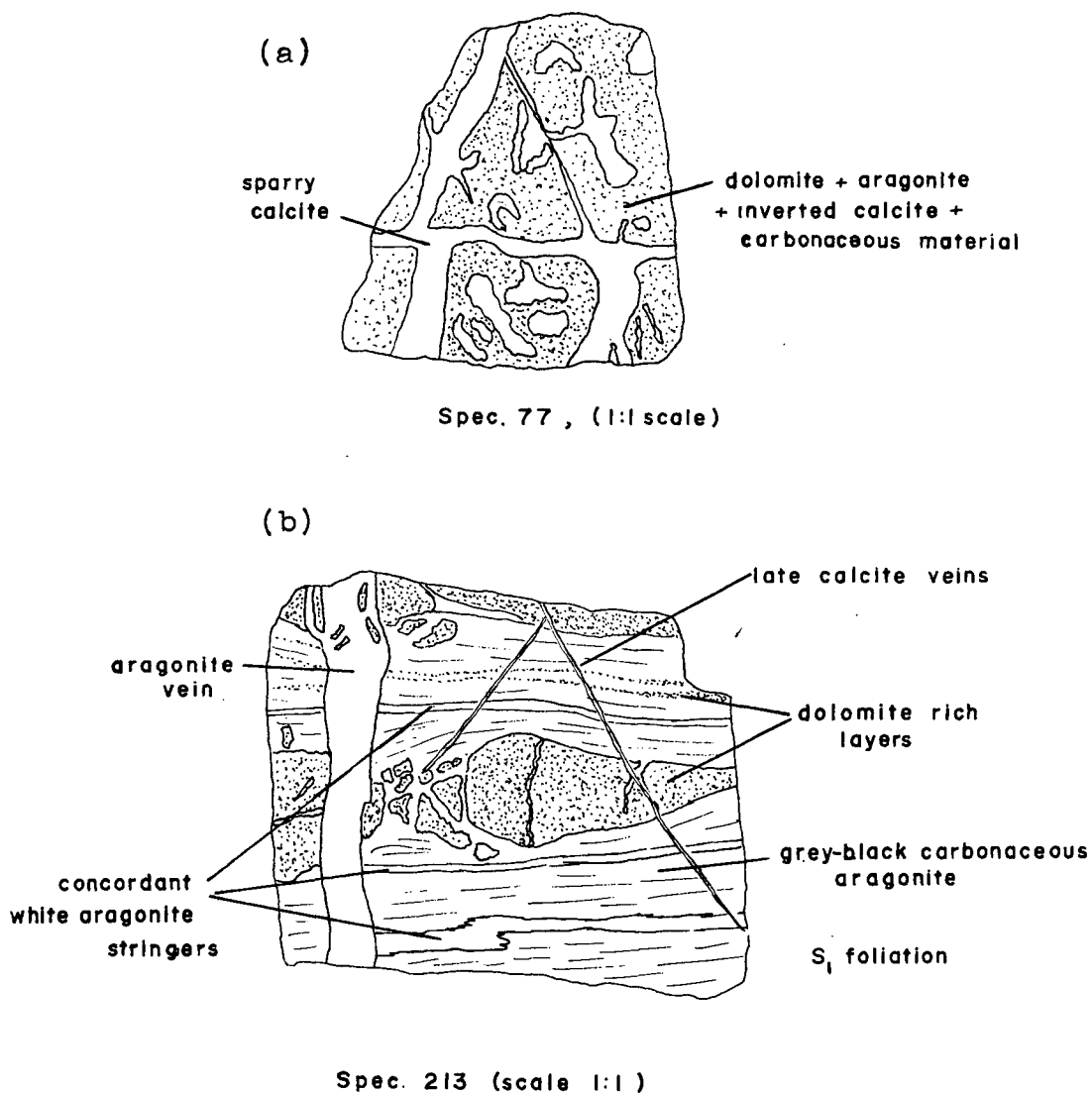
+ lawsonite + sphene ± chlorite ± stilpnomelane. Sporadic grains containing hematite rimming pyrite and/or magnetite may also be present. Idioblastic lawsonites are set in a finely woven matrix of lineated glaucophane with sphene occurring in stringers parallel to the foliation.

Massive rocks display an abundance of relict igneous textures similar to the greenstones of Pinchi Mountain. Mineral assemblages characteristic of thin section domains are given in Table 23: textures are illustrated in Fig. 34. The typical assemblage contains jadeite-acmite, lawsonite, sphene and chlorite with glaucophane, aragonite and white mica as possible additional phases. Glaucophane is commonly found filling fractures or immediately adjacent to fractures (Fig. 34). In rocks containing both acmite-jadeite and glaucophane, textures indicate that the pyroxene formed prior to the glaucophane. Pyrite, rimmed by magnetite and hematite (Fig. 30) constitutes about 0.1% of all thin sections.

Dolomitic carbonates

The main minerals present within the dolomitic limestones are aragonite, calcite and dolomite (Table 12). Disseminated carbonaceous material is a minor accessory in most limestones and barite and quartz are found locally. Limestones have been subdivided into two categories:

FIG. 35 TEXTURES IN CARBONATES



Note : samples were stained for CaCO_3 using alizarine red solution and for aragonite using Fiegl's solution (Friedman, 1959)

: identification of carbonate mineralogy was confirmed by optics and X-ray diffraction.

massive limestones which constitute most exposures and foliated limestones occurring either as thin layers in volcanics or as foliated zones in massive limestones.

A typical specimen of massive limestone (Fig. 35a) contains 50% euhedral dolomite rhombs (0.2 mm) closely associated with granular, opaque carbonaceous material in an aragonite-calcite matrix. In thin section, aragonite shows no signs of disequilibrium with dolomite and is preferentially replaced along cleavages and margins by fine grained (80 μ) calcite. Late irregular fracturing and veining by white sparry calcite (0.4 mm) tends to give the rock a brecciated appearance. A concentration of carbonaceous granules is commonly seen at the margins of these late calcite veins.

A foliated limestone is illustrated in Fig. 35b. It contains concordant stringers of carbonaceous aragonite, white aragonite and dolomite which are cross-cut by an aragonite vein. There is no inversion of aragonite to calcite, the latter mineral being found only in late fractures.

In summary, it appears that a carbonaceous limestone with variable dolomite content was metamorphosed in the blueschist facies to aragonite + dolomite. The dolomite-aragonite laminae within foliated carbonates may indicate that the metamorphism was synkinematic during the F_1 deformation. This was followed by aragonite veining which

TABLE 24 MINERAL ASSEMBLAGES IN METAGREYWACKES

spec. no.	69	70	76	75	74	71	72
jadeitic px.	x	x	x	x	x	-	x
glaucofane	x	x	x	x	x	3	x
lawsonite	x	x	x	x	x	38	x
quartz	x	x	x	x	x	7	x
white mica	x	x	x	x	x	10	x
chlorite	x	x	-	-	-	5	x
stilpnomelane	x	-	-	-	-	-	x
sphene	-	-	x	-	-	2	x
aragonite	x	-	-	x	-	-	x
pyrite	-	-	x	x	x	-	-
opaques	x	x	x	x	-	-	-
carbonaceous clasts	-	-	-	x	x	-	-

TABLE 25 MINERAL ASSEMBLAGES IN CHERTS AND CHERTY GRAPHITE SCHISTS

spec. no.	116	122	127	143	134	151	118	123	148	150
quartz	98	90	65	x	x	x	x	x	x	x
glaucofane	-	2	5	tr	x	x	-	-	-	-
lawsonite	tr	4	5	x	x	x	x	x	-	-
white mica	-	2	10	x	tr	x	x	x	x	x
carb. granules	1	-	3	-	x	-	-	x	x	x
pyrite	-	tr	-	-	-	-	-	-	x	x
acmitic px. #?	-	-	-	-	x	-	-	-	-	-
aragonite	1	-	-	-	-	-	-	-	-	-
sphene	-	tr	-	-	x	x	-	-	-	-
stilpnomelane	-	-	-	x	-	-	-	-	-	-
albite #	-	-	-	-	-	x	x	-	-	-
magn./hem. #	tr	1	-	-	tr	x	-	-	-	-

note : a) modes are approximate
b) "tr" means trace.
c) # : retrograde mineral
d) x : mineral present

cross-cuts the foliation and presumably took place in a different stress regime from that existing during the F_1 deformation. Sparry calcite veins and inversion of aragonite to calcite occurred during a later deformation ($F_2?$) presumably at a higher structural level.

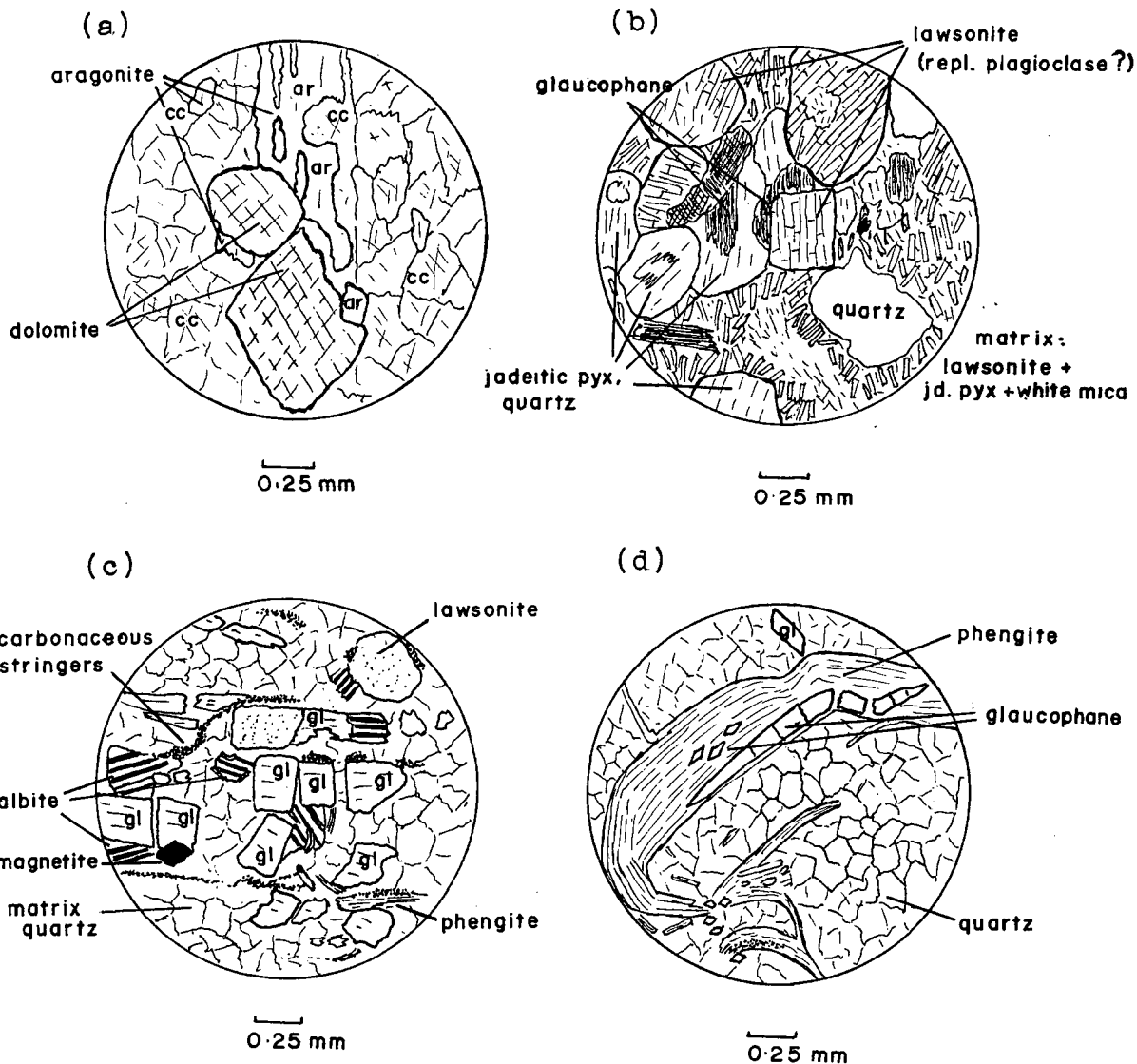
Metagreywackes

The metagreywackes retain many sedimentary features despite having a thoroughly recrystallized fabric. The original sediment appears to have been poorly sorted and consisted predominantly of plagioclase with minor quartz, ilmenite and carbonaceous clasts; clay minerals and carbonates probably constituted much of the matrix. Drill core shows fine-grained carbonaceous interbeds and a close association with graphitic cherts.

Metamorphic reconstitution of the greywacke produced the mineral assemblage: jadeitic pyroxene + lawsonite + white mica + quartz + glaucophane + chlorite + stilpnomelane + aragonite + sphene. Apparent equilibrium assemblages with modes are given in Table 24.

Fabric elements can be considered under four headings: matrix, pseudomorphs, relict minerals and veins. The matrix consists of microgranular quartz, white mica, chlorite, jadeitic pyroxene, sphene, and lawsonite. Aragonite may be present. Rectangular clasts, thought to have been plagio-

FIG. 36 TEXTURES IN METASEDIMENTS



- a) Dolomite rhombs in aragonite/inverted calcite matrix (dolomitic limestone-spec. 82).
- b) Pseudomorphed detrital grains in metagreywacke; plagioclase is replaced by lawsonite aggregates and jadeite + quartz grains appear to replace detrital pyroxene, amphibole or plagioclase. Note detrital quartz and unfoliated fabric (Spec. 71).
- c) Fractured glaucophane in metachert (assemblage : glaucophane + quartz + lawsonite + phengite + magnetite + carbonaceous granules); albite grains appear to have crystallized after the deformation which fractured the glaucophanes (i.e. F_2) (Spec. 153).
- d) Contorted phengite in metachert (Spec. 153).

class prior to metamorphism, contain lawsonite aggregates (Fig. 36b). These generally show a preferred orientation, presumably controlled by the atomic structure of the pre-existing albite (?). Jadeitic pyroxene and quartz also appear to replace relict detrital grains which by their morphology could have been pyroxene, amphibole or plagioclase. However, as lawsonite commonly replaces plagioclase, pyroxene or amphibole are considered the most likely precursors. Other relict clastic grains include quartz, pyritic carbonaceous material and skeletal ilmenite pseudomorphed by sphene. Aragonite veins were observed in a few thin sections. Glaucophane crystals are idioblastic and generally comprise only a small proportion of the rock.

Retrograde metamorphism or alteration gave rise to stringers of leucoxene, yellow or white in reflected light and veining all metamorphic minerals. The stringers are commonly associated with hematite granules.

Metacherts

Typical metacherts consist of 1 mm to 2 cm quartzitic beds separated by thin laminae of glaucophane + white mica + lawsonite ± carbonaceous material ± sphene ± pyrite. Metacherts grade into graphite schists. Individual mineral assemblages are given in Table 25. Quartz grain size varies between 20 and 200 μ . Grain boundaries are generally polygonal but may be sutured in specimens where undulose

extinction is observed. Idioblastic, fractured glaucophanes, averaging 1 mm in length (Fig. 36c) show a strong preferred orientation generally with the c axes sub-parallel to the (L_2) crenulate lineation. A microprobe traverse of a glaucophane in specimen 151 showed the crystals to be zoned with Fe rich cores and margins (Fig. 26). Phengitic mica is generally contorted (Fig. 36d) and wraps around lawsonite (0.5 mm) and glaucophane porphyroblasts. Carbonaceous granules commonly occur as inclusions in the mica.

Retrogressive minerals appear to have formed during a post-metamorphic period of deformation (F_2 ?). Glaucophanes are broken, with the fractures filled with quartz or occasionally albite (Fig. 36c). Within graphitic cherts post-tectonic pyritic quartz veins are common and contain albite at intersections with micaceous layers. Magnetite and hematite replace pyrite and form as inclusions in glaucophane. Lawsonite tablets contain microgranular aggregates and possess cross-fractures filled by quartz veins. Some samples (e.g. 134) contain aggregates of 50 to 70 μ acmitic (?) pyroxene. Whether this pyroxene is part of the initial equilibrium assemblage or is retrogressive is uncertain. It is concluded that the albite, hematite, magnetite, leucoxene, the quartz-pyrite veins and possibly the acmitic pyroxene formed during retrogressive metamorphism which was possibly associated with the F_2 deformation.

Quartz-carbonate rocks and schists

In the vicinity of the mine, where exposures are plentiful, the following assemblages were noted in lithologies interbedded with cherts or limestones:

- (i) quartz + aragonite + white mica
- (ii) quartz + white mica + glaucophane + lawsonite
+ chlorite.

The first assemblage consists of equigranular (30 μ) quartz and aragonite containing occasional aragonite porphyroblasts (0.7 mm). Within the second assemblage lawsonite forms euhedral porphyroblasts (1 mm max) exhibiting polysynthetic twinning and is commonly fractured and altered. In general, phengitic mica and glaucophane display textural relationships similar to those in metacherts.

Most thin sections from the mine vicinity show signs of a pervasive alteration which preceded the mercury mineralization and post-dated the formation of metamorphic minerals. Calcite, dolomite, ankerite, quartz and limonite are commonly found as replacements or veins in most rocks, locally obscuring the primary metamorphic mineralogy.

APPENDIX V

ECLOGITE BOULDERS

Glaucophane bearing eclogite boulders were found at two localities in the course of this study. The first (Fig. 37, spec. 103) is located 9 km east of Pinchi Lake Mercury Mine on the Tezzeron Lake logging road. It measures 12 x 4 x 3 m and is apparently embedded in glacial till overlying Takla Group rocks. The boulder contains foliated and lineated blocks up to 30 cm in diameter consisting of green pyroxene and garnet altering to stilpnomelane. Glaucophane and lawsonite occupy interstices between blocks and also permeate them. Late cross-cutting fractures are filled with chlorite and a brown amphibole. The second locality (Fig. 37, spec. 214) lies outside the thesis area 24 km east-southeast of Fort St. James beside the Beaver Lake logging road. Two boulders are present, measuring 4 x 2 x 2 m and 7 x 5 x 3 m; both are embedded in till and possess glacial striae on their surfaces. The main lithology is dark blue massive glaucophanitic rock containing zones rich in garnet, white mica, pyroxene, lawsonite and pyrite. Quartz veins are also present. In thin section the white mica appears undeformed. A K-Ar radiometric date on the white mica (Appendix VI) gave an age of 218 ± 7 m yrs.

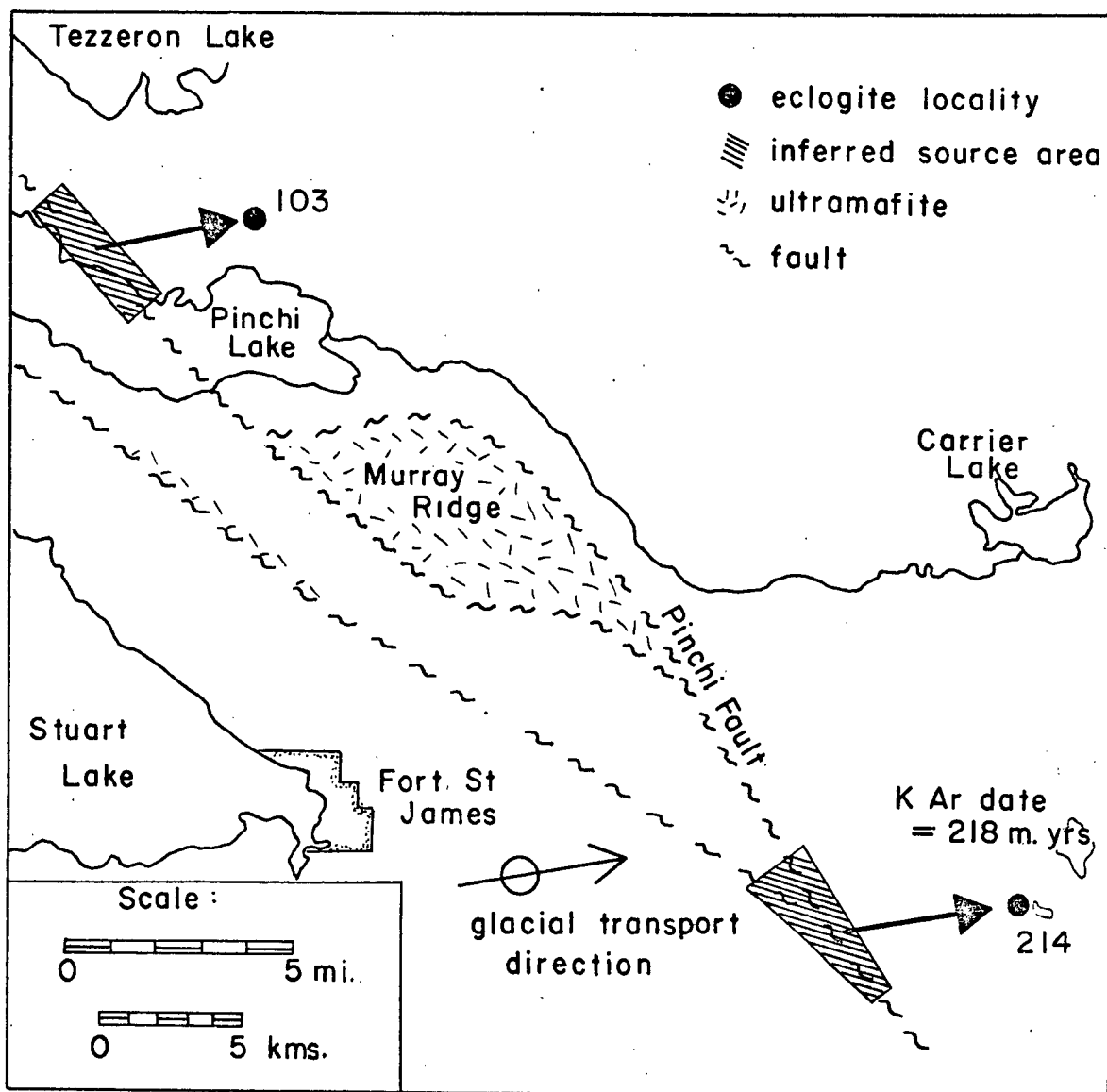


Fig. 37 Eclogite localities and source areas (as inferred from glacial transport direction)

The inferred source area for these boulders is illustrated in Fig. 37. Because the direction of ice movement during the latest glaciation was towards the east-northeast (Armstrong, 1949) it is assumed that the boulders were derived from the west. Eclogite has not been found within the glaucophane lawsonite bearing region but considering the high pressure origin of eclogites (Chapter IV) and their association with glaucophane, it is believed that they originated from within the Pinchi Fault zone. In California, eclogite specimens have been obtained from isolated tectonic blocks within glaucophane schist terrain. Coleman *et al.*, (1965) consider:

That these eclogites are not in place and have been transported to their present position as inclusions in diapiric serpentines or in shear zones of major faults.

A similar origin is proposed for the Pinchi eclogites.

APPENDIX VI

POTASSIUM-ARGON RADIOMETRIC DATES

Sample locations are given in Map VII (237, 124, 151) and Fig. 37 (214). Specimens 237 and 124 (quartz + white mica + lawsonite + glaucophane schist) were collected from the open pit at Pinchi Lake Mercury Mine. There is considerable carbonatization in the area but the micas appear to be fresh and unaltered in thin section apart from the presence of minute acicular rutile (?) needles. Glaucophane, lawsonite and white mica are deformed by F_2 . Sample 151 (quartz + glaucophane + phengite + magnetite metachert) was collected 3.5 km northwest of Pinchi Mine. Phengitic muscovites are deformed by F_2 and contain minor amounts of carbonaceous material. Approximately 10% of the micas are slightly iron stained. Sample 238 was obtained outside the thesis area 24 km east-southeast of Fort St. James, from an eclogite boulder containing glaucophane + lawsonite + pyroxene + garnet + pyrite and white mica occurring in *schlieren*. In thin section, the white mica is undeformed.

After crushing and sieving, essentially pure white mica separates were obtained using a water column and heavy liquids. Potassium-argon analyses were carried out by J.E. Harakal and V. Bobik in the laboratories of the

TABLE 26 ANALYTICAL DATA FOR POTASSIUM-ARGON ANALYSES

Sample no.	237	124	151	214
Location : lat.	54° 38' 5"	54° 38' 5"	54° 39' 9"	54° 24' 30"
long.	124° 26' 15"	124° 26' 15"	124° 28' 48"	123° 53' 00"
Rock type	mica-schist	mica-schist	metachert	eclogite
Mineral	muscovite	muscovite	muscovite	muscovite
Mesh size	28-48	48-65	48-65	60-80
K % ± σ **	8.63 ± 0.05	8.36 ± 0.04	7.60 ± 0.04	7.96 ± 0.02
$\frac{^{40}\text{Ar rad}^*}{^{40}\text{Ar total}}$	0.95	0.96	0.93	0.94
$\frac{^{40}\text{Ar rad}}{(10^{-5}\text{cc STP/gm})}$	7.810	7.375	6.823	7.285
$\frac{\text{Ar}^{40}}{\text{K}^{40}}$	1.337×10^{-2}	1.303×10^{-2}	1.326×10^{-2}	1.352×10^{-2}
Apparent age	216 ± 7 m.y.	211 ± 7 m.y.	214 ± 7 m.y.	218 ± 7 m.y.

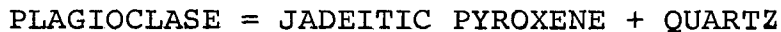
** Potassium analyses by J.E. Harkal, and V. Bobik using KY and KY-3 flame photometers; σ = standard deviation.
* Argon analyses by J.E. Harkal using MS-10 mass spectrometer.
Constants used in model age calculations : $\lambda_e = 0.585 \times 10^{-10}\text{y}^{-1}$,
 $\lambda_p = 4.72 \times 10^{-10}\text{y}^{-1}$, $^{40}\text{K}/\text{K} = 1.181 \times 10^{-4}$.

Specimen locations are given in Fig. 43(237, 124, 151) and Fig. 42 (214).

Geology and Geophysics Departments at the University of British Columbia using procedures and equipment previously described by White *et al.*, (1967). Analytical data and apparent ages are given in Table 26.

APPENDIX VII

CALCULATION OF EQUILIBRIUM CONSTANT FOR REACTION:



Since $\Delta G = -RT \ln K$

and $\frac{\partial \Delta G}{\partial P} = \Delta V$

then $\frac{\partial \ln K}{\partial P} = \frac{-\Delta V}{RT}$

whence $\ln K_2 - \ln K_1 = \frac{-\Delta V}{RT} (P_2 - P_1)$

Now, if standard state is taken at P_1 then $\ln K_1 = 0$

and $\ln K_{(P_2)} = \frac{-\Delta V}{RT} (P_2 - P_1) \dots \dots (A)$

According to McConnell and McKie (1960) most disordering in albite takes place between 575° and 625°C. Therefore, in the calculation of ΔV , data for low albite has been used. Employing theoretical and experimental data, Newton and Smith (1966) produced a breakdown curve for low albite = jadeite + quartz. Two points on this curve are:

- (a) $T_a = 773^\circ K, P_a = 14.3 \text{ kb}$
- (b) $T_c = 473^\circ K, P_c = 8.2 \text{ kb}$

Equation (A) can be solved for several different values of K at each temperature using $R = 83.14 \text{ bar cm}^3 \text{ deg}^{-1} \text{ mol}^{-1}$ and

$$\Delta V = 16.98 \text{ cm}^3 \text{ mol}^{-1}.$$

$$\text{At } T_a = 773^\circ\text{K}$$

$$\ln K = \frac{-\Delta V}{RT} (P_b - 14300)$$

$$\text{and at } T_c = 473^\circ\text{K},$$

$$\ln K = \frac{-\Delta V}{RT} (P_d - 8200)$$

Results are tabulated below, and illustrated on Fig. 8b.

K	P_b	P_d
.05	2.96	1.26
.1	5.58	2.87
.2	8.21	4.47
.3	9.74	5.41
.4	10.81	6.08
.5	11.68	6.59
.6	12.37	7.02
.7	12.95	7.37
.8	13.45	7.68
.9	13.90	7.95

Assuming unit activity for quartz and mole fraction (X) equal to activity, $K = x_{jd}^{px} / x_{alb}^{plag}$.

APPENDIX VIII
SPECIMEN NUMBERING SYSTEM

Note: locations of most specimens are given in Map VII using "thesis number".

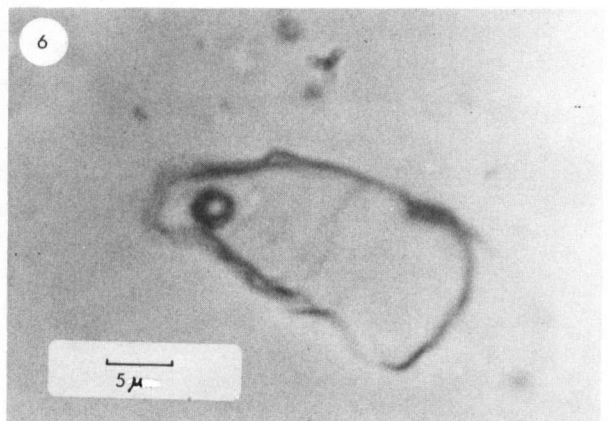
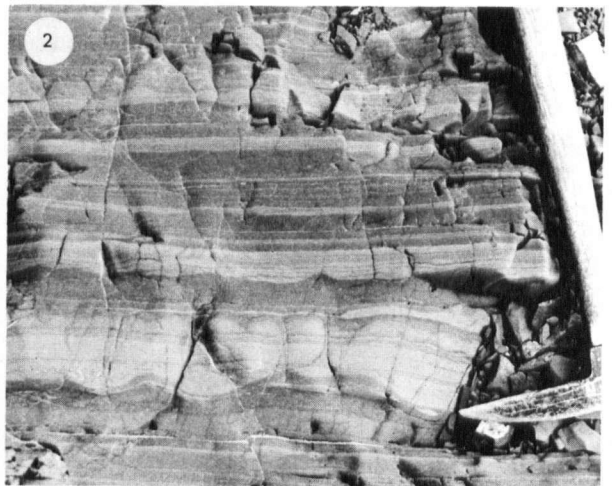
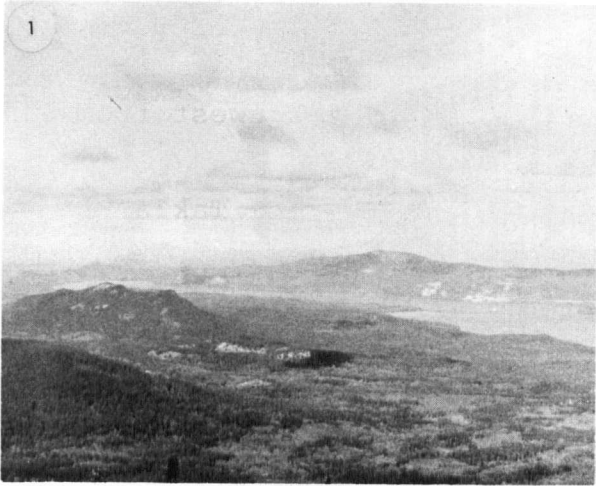
Thesis Number	Hand Specimen Number	Thesis Number	Hand Specimen Number
1	P-17-69	39	P-81-68
2	P-66-69	40	P-91-68
3	P-218-69	41	P-93-68
4	P-234-69	42	P-94-68
5	5-71P-5A	43	P-79-68
6	8-71P-4	44	P-27-69
7	P-70-69	45	P-30-69
8	P-19-69	46	P-31-69
9	P-60-69	47	P-33-69
10	P-68-69	48	P-92-69
12	P-116-69	49	P-93-69
13	P-117-69	50	P-96-69
14	P-200-69	51	P-101-69
15	P-210-69	52	P-105-69
16	P-214-69	53	P-106-69
17	P-225-69	54	P-119-69
18	P-232-69	55	P-121-69
19	P-242-69	56	P-131-69
20	P-243-69	57	P-138-69
21	S-6-69	58	P-140-69
22	P-122-68	59	P-142-69
23	420-1589	60	H-C-5
24	420-1579	61	P-188-69
25	420-1581	62	P-195-69
26	P-2(1)-67	63	P-196-69
27	P-8-67	64	P-249-69
28	P-9-67	65	HM-10-604
29	P-6-68	66	HM-8-149
30	P-18-68	67	HM-200-417
31	P-23-68	68	P-131-135
32	P-23-68	69	P-7-68
33	P-29-68	70	P-99-68
34	P-30-68	71	P-191-69
35	P-44-68	72	P-207-69
36	P-45-68	73	HM-20-651
37	P-78-68	74	HM-11-344
38	P-80-68	75	HM-11-185

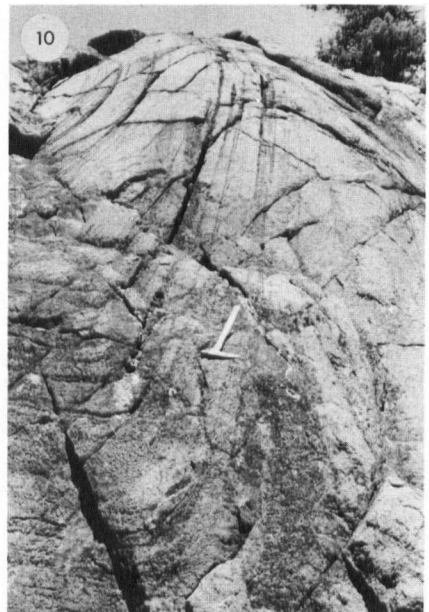
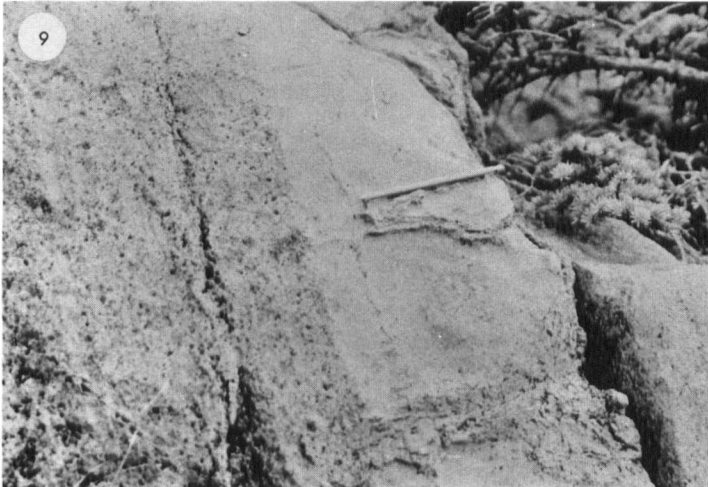
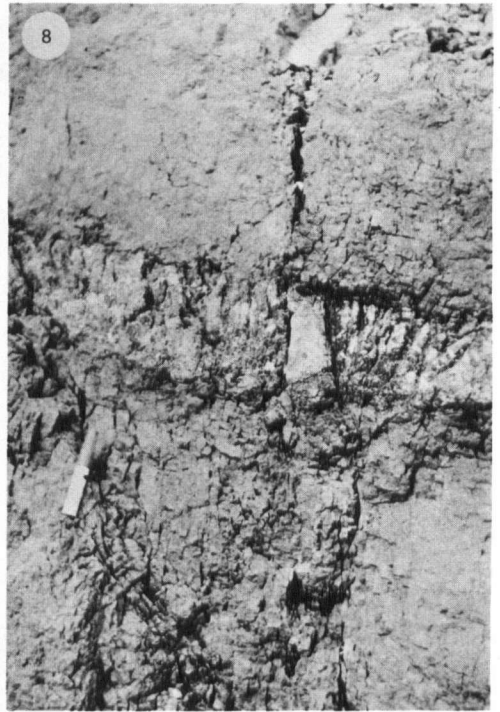
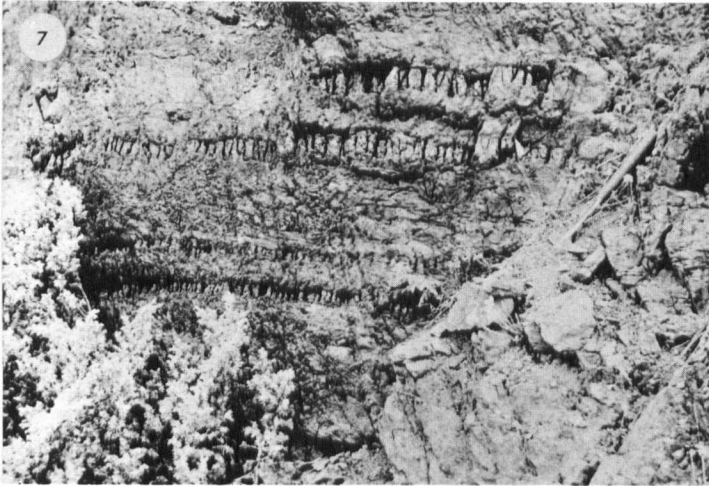
Thesis Number	Hand Specimen Number	Thesis Number	Hand Specimen Number
76	HM-8-610	126	P-76-68
77	P-1-67	127	P-82-68
78	P-19-68	128	P-88-68
79	P-58-68	129	P-89-68
80	P-75-68	130	P-135-68
81	P-98-68	131	P-10-69
82	P-148-68	132	P-12-69
83	P-90-68	133	P-13-69
84	P-65-68	134	P-25-69
85	P-70-68	135	P-48-69
86	P-72-68	136	P-53-69
87	P-73-68	137	P-73-69
88	P-152-68	138	P-77-69
89	P-153-68	139	P-83-69
90	P-154-68	140	P-88-69
91	P-165-69	141	P-90-69
92	P-2-70	142	P-143-69
94	P-28-68	143	P-146-69
95	P-38-68	144	P-157-69
96	P-40-68	145	P-170-69
97	P-56-68	146	421-155
98	P-62-68	147	HM-10-79
99	P-104-68	148	HM-10-458
100	P-105-68	149	HM-10-690
101	P-110-68	150	HM-11-613
102	5-71P-9E	151	P-220-69(1)
103	5-71P-9E	152	P-220-69(2)
104	5-71P-9E	153	P-220-69(3)
105	5-71P-9E	154	P-152-69
106	P-59-69	155	P-152-69
107	5-71P-3	156	P-154-69
108	11-71P-1	157	
109	16-71P-3	158	{ Stuart Lake
110	6-71P-5B	159	{ Antimony Mine
111	8-71P-3	160	P-112-68
112	8-71P-2A	161	P-145-68
113	8-71P-2B	162	P-146-68
115	P-3-67	163	P-39-69
116	P-5-68A	164	P-162-69
117	P-5-68B	165	P-189-69
118	P-8-68	166	HM-2-54
119	P-14-68	167	HM-4-102
120	P-15-68	168	HM-3-94
121	P-16-68	169	HM-5-308
122	P-21-68	170	P-37-69
123	P-48-68	171	P-100-68
124	P-50-68	172	P-101-68
125	P-49-68	173	P-161-69

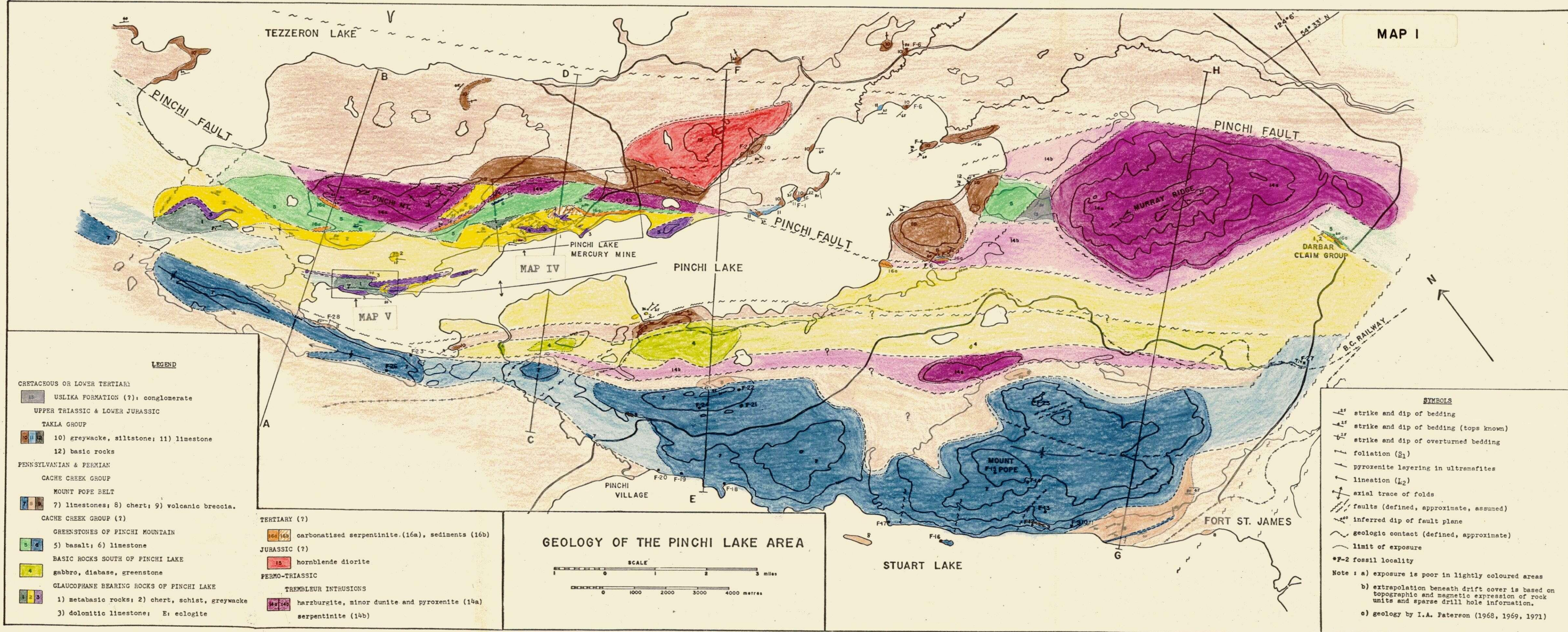
Thesis Number	Hand Specimen Number	Thesis Number	Hand Specimen Number
174	HC-1	210	P-87-68
175	HC-2	211	P-6-68
176	HC-3	212	P-224
177	HC-4	213	P-112-69
178	P-275-69	214	24-72P-1
179	P-110-69	215	P-2-68
180	P-282-70	216	P-12-68
181	2020-169	217	P-25-68
182	1-Nat Cu	218	P-102-68
183	2-Nat Cu	219	P-123-68
184	2022-362	220	P-65-69
185	HMP-11-120	221	P-94-69
186	HMP-12-140	222	P-97-69
187	P-68-68	223	P-116-69
188	P-216-69	224	P-118-69
191	S-71P-7	225	P-124-69
192	10-71P-6	226	P-131-69
193	P-147-68	227	P-247-69
194	HMP-8-100	228	S-7-69
195	3-71P-7A	229	1-71P-2
196	9-71P-2A	230	4-71P-1C
197	9-71P-2B	231	4-71P-2
198	6-71P-4A	232	6-71P-3
199	P-2(2)-67	233	7-71P-2
200	10-71P-4B	234	13-71P-1
201	10-71P-4C	235	P-201-69
202	P-282	236	P-4-67
203	10-71P-SC	237	15-71P-4
204	P-252-69	239	P-109-68
205	P-85-68	240	S-11-69
206	P-85-68	241	15-71P-2
207	P-283-69	242	15-71P-3
208	P-721	243	P-87-68
209	P-185-69	244	P-278-69

LIST OF PLATES

1. View of the Pinchi Lake area looking northwest from the summit of Mount Pope.
2. Laminated siltstones and sandstones in the Takla Group.
3. Northwesterly plunging mullions in quartz-mica-carbonate schist. Note prominent joint surfaces perpendicular to mullions.
4. Angular limestone cobble conglomerate in Takla Group. "M" points to *Monotis subcircularis* occurring within cobbles and in matrix.
5. Northerly dipping compositional layering in silica-carbonate rocks. Note layers of rough weathering ferroan magnesite veined by quartz, enclosing layer of pure white magnesite.
6. Primary (?) two phase fluid inclusion in metachert.
7. Late pyroxenite layers parallel to dunite rich layers in harzburgite.
8. Late discordant pyroxenite layer cross-cutting irregular dunite. To the left, off the photograph, this pyroxenite cross-cuts the dunite harzburgite contact and also an early pyroxenite layer. Note slight offset of pyroxenite by fracture cleavage.
9. Smooth weathering dunite layer parallel to foliation in harzburgite outlined by variation in olivine/pyroxene ratio. Note the chromite stringer in the dunite layer.
10. Folded early pyroxenite layer.
11. Folded dunite layer in harzburgite. Note the weak foliation which parallels joints on right side of outcrop.



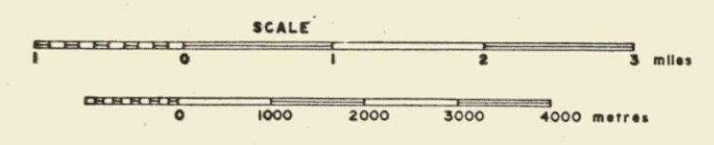




- LEGEND**
- CRETACEOUS OR LOWER TERTIARY
 USLIKA FORMATION (?); conglomerate
- UPPER TRIASSIC & LOWER JURASSIC
 TAKLA GROUP
 10) greywacke, siltstone; 11) limestone
 12) basic rocks
- PENNSYLVANIAN & PERMIAN
 CACHE CREEK GROUP
 MOUNT POPE BELT
 7) limestones; 8) chert; 9) volcanic breccia.
- CACHE CREEK GROUP (?)
 GREENSTONES OF PINCHI MOUNTAIN
 5) basalt; 6) limestone
- BASIC ROCKS SOUTH OF PINCHI LAKE
 4) gabbro, diabase, greenstone
- GLAUCOPHANE BEARING ROCKS OF PINCHI LAKE
 1) metabasic rocks; 2) chert, schist, greywacke
 3) dolomitic limestone; E: eclogite

- TERTIARY (?)
 16a, 16b carbonatised serpentinite (16a), sediments (16b)
- JURASSIC (?)
 15 hornblende diorite
- PERMO-TRIASSIC
 TREMBLEUR INTRUSIONS
 14a harzburgite, minor dunite and pyroxenite (14a)
 14b serpentinite (14b)

GEOLOGY OF THE PINCHI LAKE AREA



- SYMBOLS**
- ↘ strike and dip of bedding
 - ↗ strike and dip of bedding (tops known)
 - ↖ strike and dip of overturned bedding
 - ⊥ foliation (S₁)
 - ⊥ pyroxenite layering in ultramafites
 - ⊥ lineation (L₂)
 - ⊥ axial trace of folds
 - faults (defined, approximate, assumed)
 - inferred dip of fault plane
 - ~ geologic contact (defined, approximate)
 - limit of exposure
 - *F-2 fossil locality
- Note: a) exposure is poor in lightly coloured areas
 b) extrapolation beneath drift cover is based on topographic and magnetic expression of rock units and sparse drill hole information.
 c) geology by I.A. Paterson (1968, 1969, 1971)

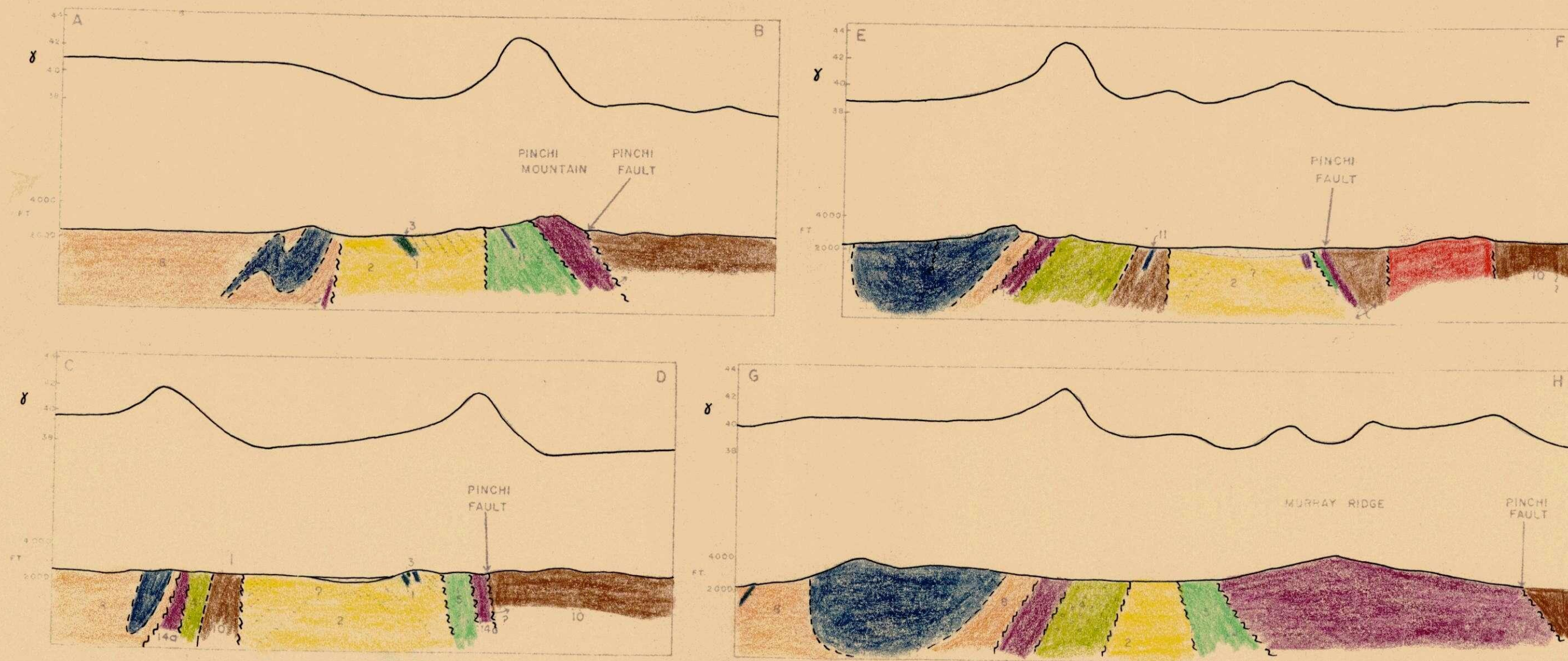
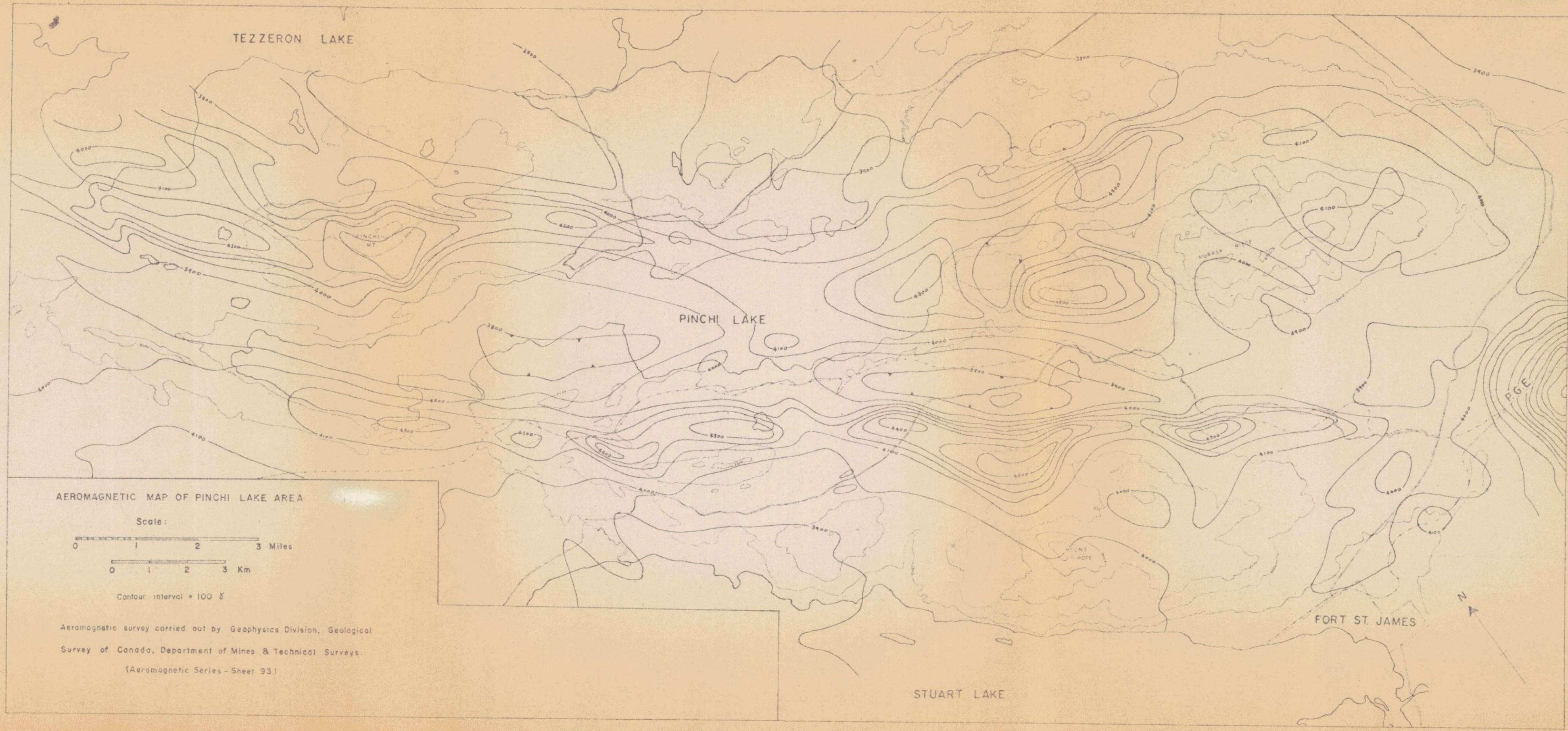


FIG. 25 CROSS SECTIONS OF THE PINCHI LAKE AREA FOR LOCATIONS AND LEGEND SEE MAP I
 AEROMAGNETIC PROFILES OBTAINED FROM MAP III



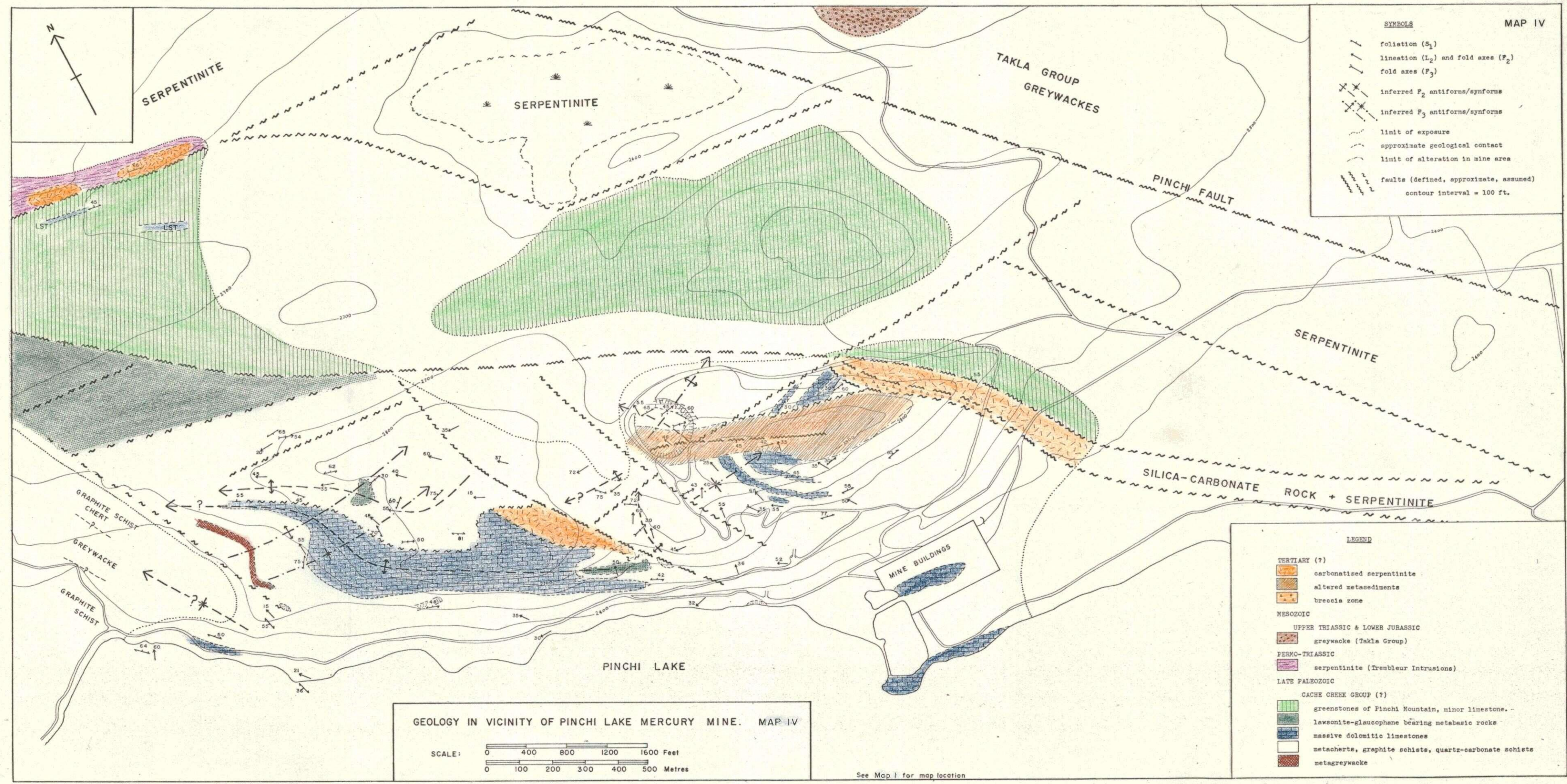
AEROMAGNETIC MAP OF PINCHI LAKE AREA

Scale:
0 1 2 3 Miles
0 1 2 3 Km

Contour interval = 100 δ

Aeromagnetic survey carried out by Geophysics Division, Geological Survey of Canada, Department of Mines & Technical Surveys.

(Aeromagnetic Series - Sheer 93)



SYMBOLS **MAP IV**

	foliation (S ₁)
	lineation (L ₂) and fold axes (F ₂)
	fold axes (F ₃)
	inferred F ₂ antiforms/synforms
	inferred F ₃ antiforms/synforms
	limit of exposure
	approximate geological contact
	limit of alteration in mine area
	faults (defined, approximate, assumed)
	contour interval = 100 ft.

LEGEND

TERTIARY (?)	
	carbonatised serpentinite
	altered metasediments
	breccia zone
MESOZOIC	
UPPER TRIASSIC & LOWER JURASSIC	
	greywacke (Takla Group)
PERMO-TRIASSIC	
	serpentinite (Trembleur Intrusions)
LATE PALEOZOIC	
CACHE CREEK GROUP (?)	
	greenstones of Pinchi Mountain, minor limestone
	lawsonite-glaucophane bearing metabasic rocks
	massive dolomitic limestones
	metacherts, graphite schists, quartz-carbonate schists
	metagreywacke

GEOLOGY IN VICINITY OF PINCHI LAKE MERCURY MINE. MAP IV

SCALE: 0 400 800 1200 1600 Feet
0 100 200 300 400 500 Metres

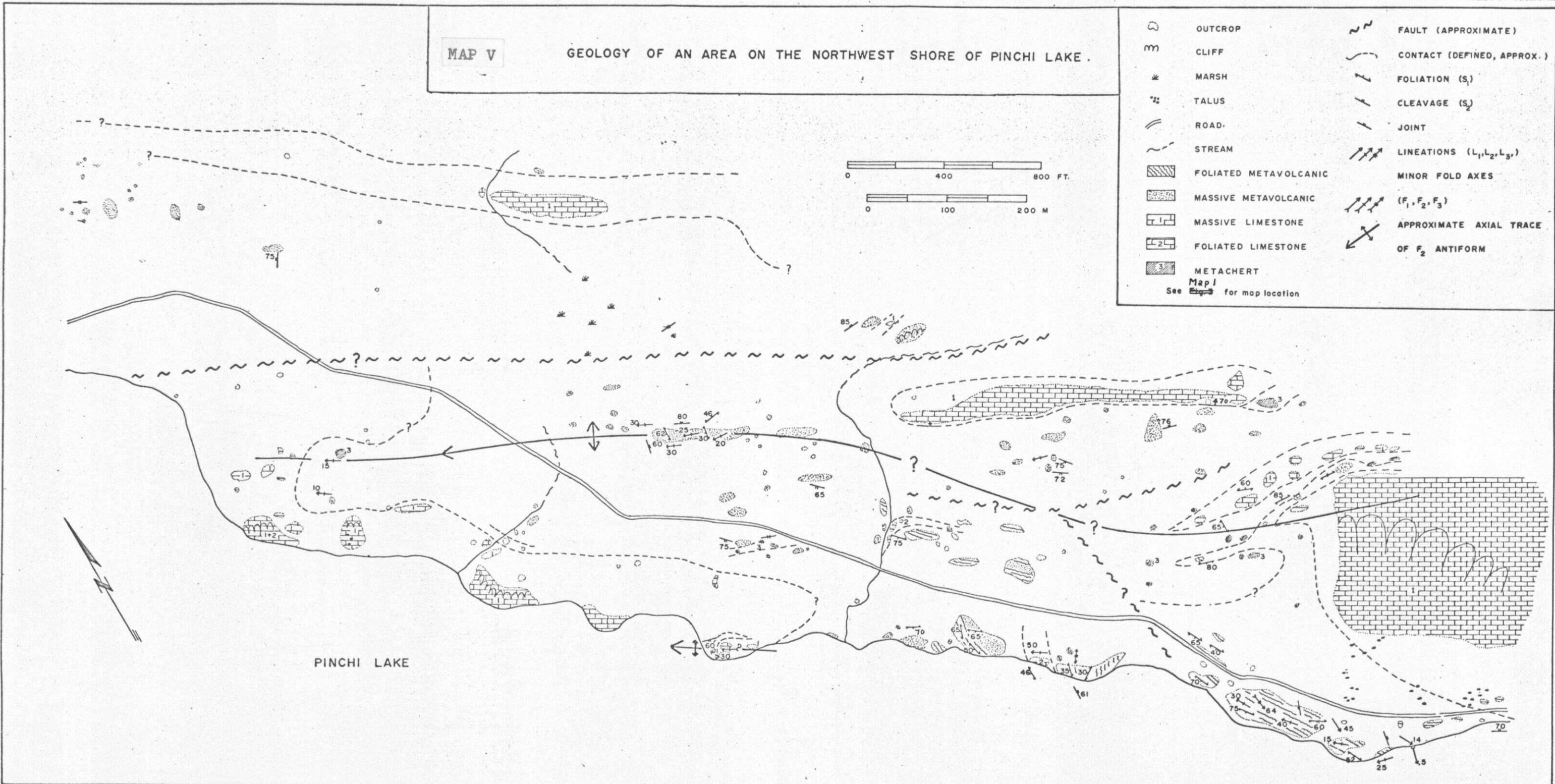
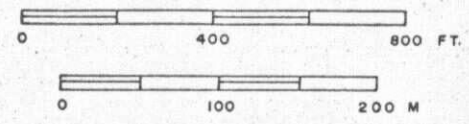
See Map I for map location

MAP V

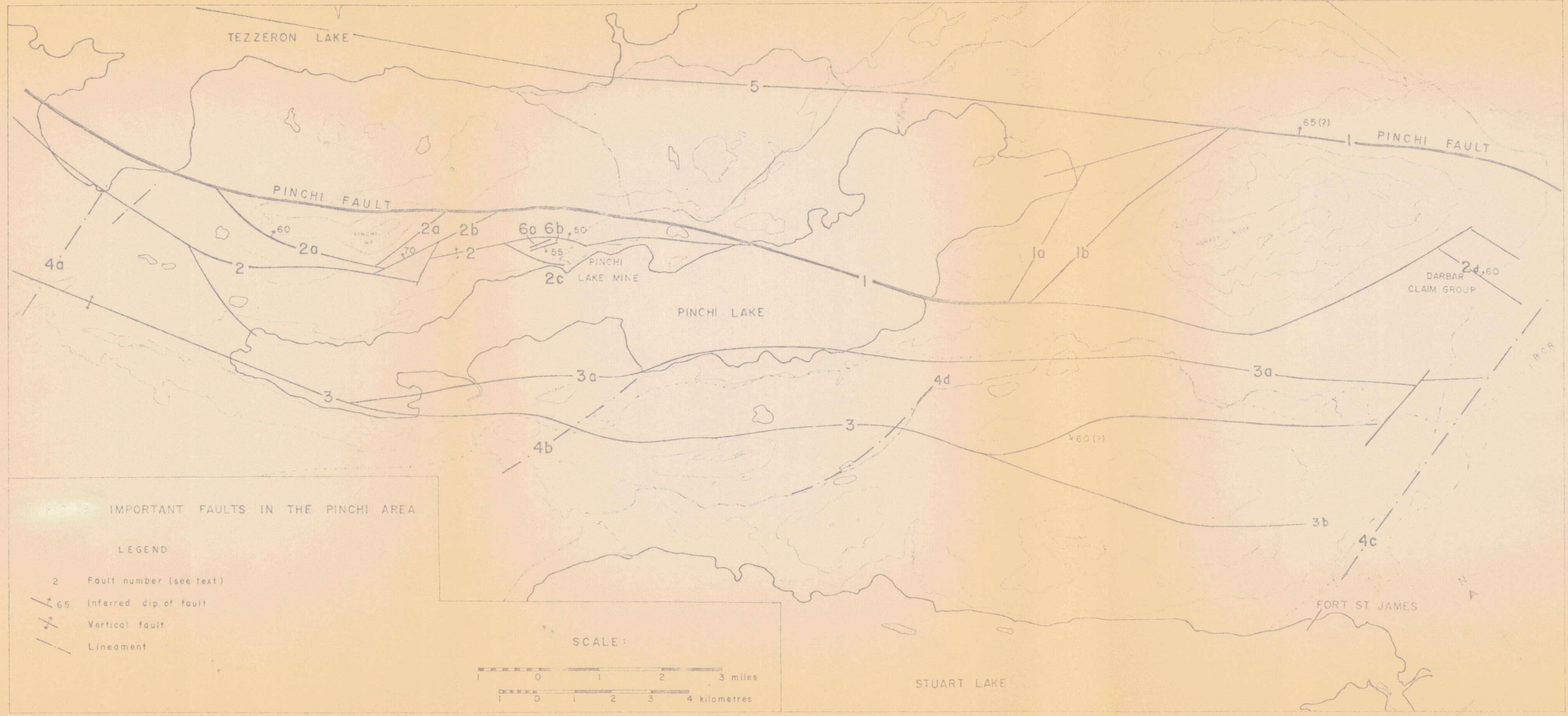
GEOLOGY OF AN AREA ON THE NORTHWEST SHORE OF PINCHI LAKE.

	OUTCROP		FAULT (APPROXIMATE)
	CLIFF		CONTACT (DEFINED, APPROX.)
	MARSH		FOLIATION (S ₁)
	TALUS		CLEAVAGE (S ₂)
	ROAD		JOINT
	STREAM		LINEATIONS (L ₁ , L ₂ , L ₃)
	FOLIATED METAVOLCANIC		MINOR FOLD AXES
	MASSIVE METAVOLCANIC		(F ₁ , F ₂ , F ₃)
	MASSIVE LIMESTONE		APPROXIMATE AXIAL TRACE
	FOLIATED LIMESTONE		OF F ₂ ANTIFORM
	METACHERT		

See *Map 1* for map location



PINCHI LAKE



IMPORTANT FAULTS IN THE PINCHI AREA

LEGEND

- 2 Fault number (see text)
- 65 Inferred dip of fault
- Vertical fault
- Lineament

SCALE:



TEZZERON LAKE

PINCHI FAULT

PINCHI FAULT

PINCHI LAKE

PINCHI LAKE MINE

DARBAR CLAIM GROUP

FORT ST JAMES

STUART LAKE

4a

2

60

2a

2a

2b

60

6b

50

2c

70

2

55

1a

1b

2d

60

3

3a

4d

3a

3

4b

60 (?)

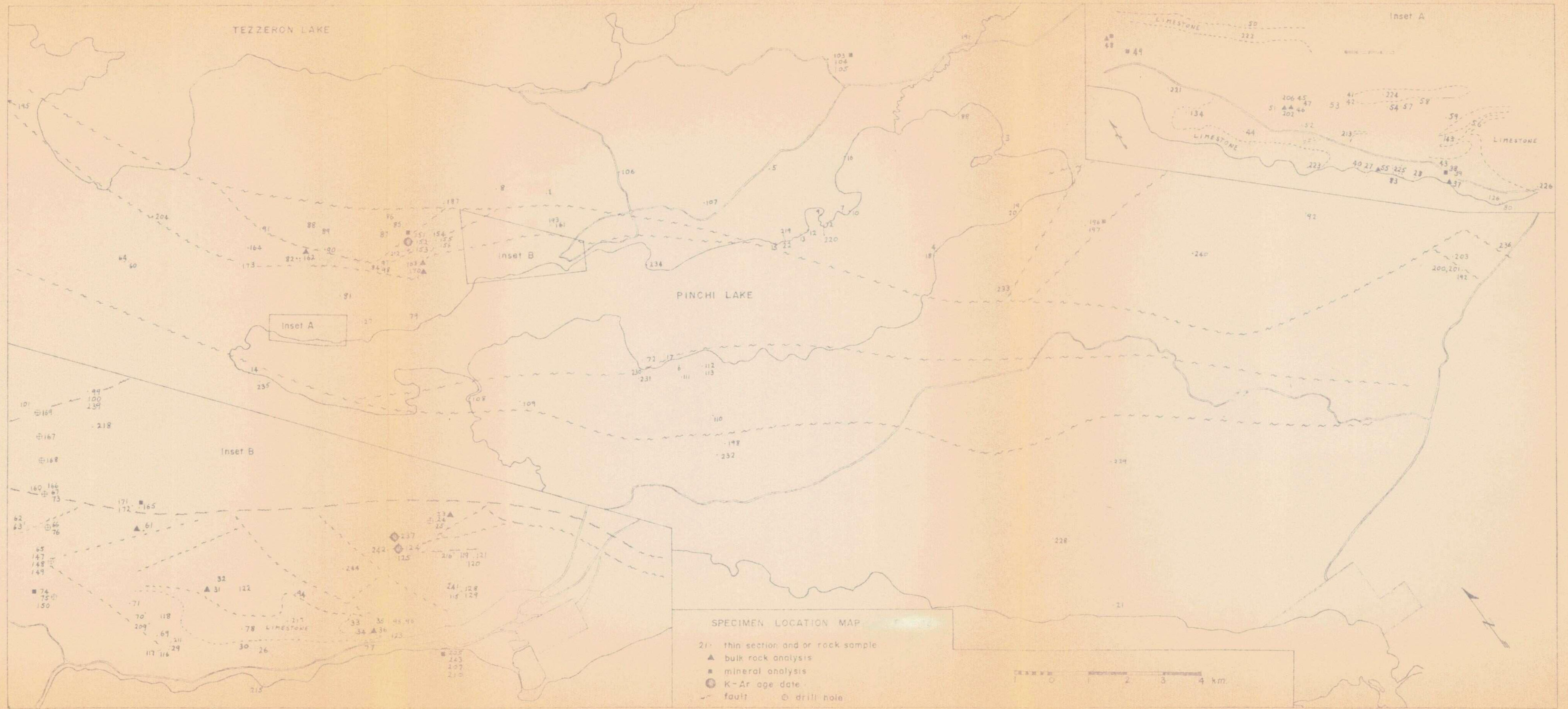
3b

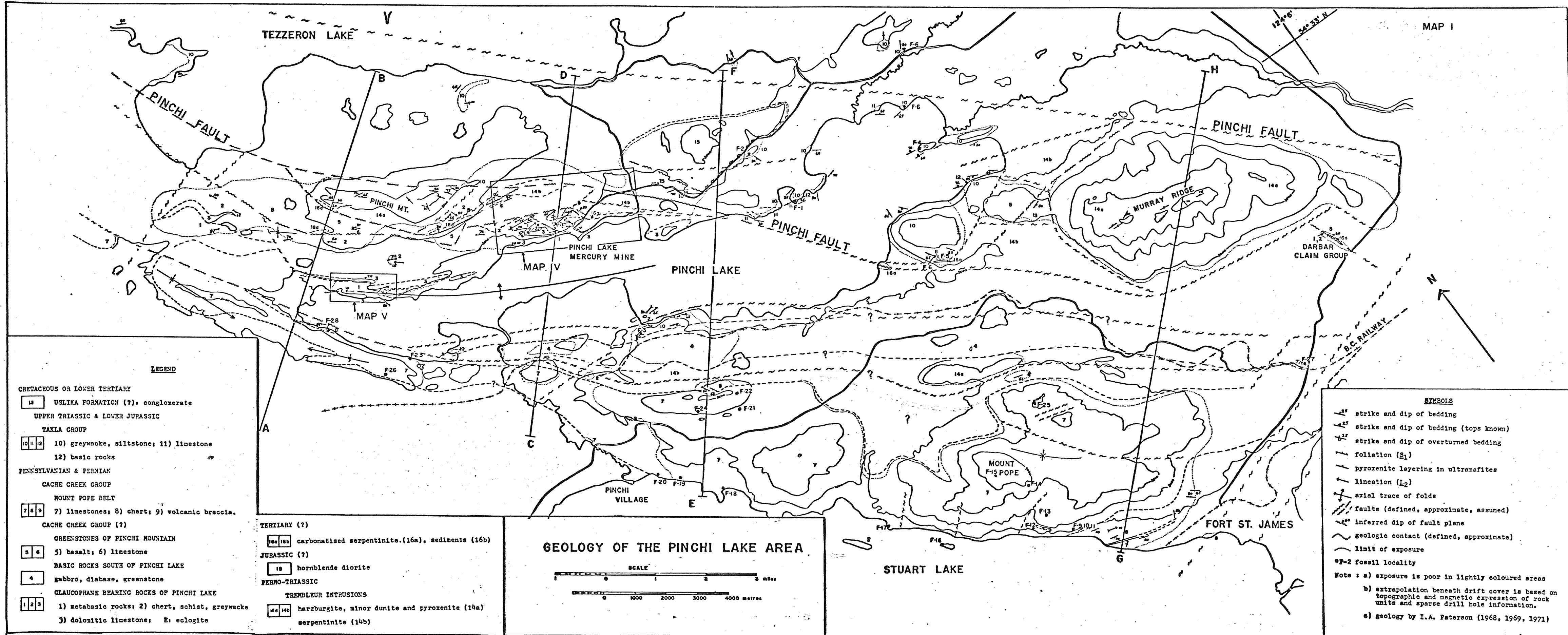
4c

5

65 (?)

N

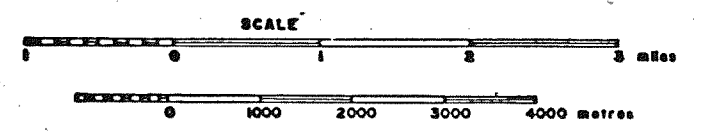




- LEGEND**
- CRETACEOUS OR LOWER TERTIARY
- 13 USLIKA FORMATION (?): conglomerate
- UPPER TRIASSIC & LOWER JURASSIC
- TAKLA GROUP
- 10 11 12 10) greywacke, siltstone; 11) limestone
 - 12) basic rocks
- PENNSYLVANIAN & PERMIAN
- CACHE CREEK GROUP
- MOUNT POPE BELT
- 7 8 9 7) limestones; 8) chert; 9) volcanic breccia.
- CACHE CREEK GROUP (?)
- GREENSTONES OF PINCHI MOUNTAIN
- 5 6 5) basalt; 6) limestone
- BASIC ROCKS SOUTH OF PINCHI LAKE
- 4 gabbro, diabase, greenstone
- GLAUCOPHANE BEARING ROCKS OF PINCHI LAKE
- 1 2 3 1) metabasic rocks; 2) chert, schist, greywacke
 - 3) dolomitic limestone; E: eclogite

- TERTIARY (?)
- 16a 16b carbonatised serpentinite (16a), sediments (16b)
- JURASSIC (?)
- 18 hornblende diorite
- PERMO-TRIASSIC
- TREMBLEUR INTRUSIONS
- 14a 14b harzburgite, minor dunite and pyroxenite (14a)
 - serpentinite (14b)

GEOLOGY OF THE PINCHI LAKE AREA



- SYMBOLS**
- strike and dip of bedding
 - strike and dip of bedding (tops known)
 - strike and dip of overturned bedding
 - foliation (S₁)
 - pyroxenite layering in ultramafites
 - lineation (L₂)
 - axial trace of folds
 - faults (defined, approximate, assumed)
 - inferred dip of fault plane
 - geologic contact (defined, approximate)
 - limit of exposure
 - *F-2 fossil locality
- Note: a) exposure is poor in lightly coloured areas
 b) extrapolation beneath drift cover is based on topographic and magnetic expression of rock units and sparse drill hole information.
 c) geology by I.A. Paterson (1968, 1969, 1971)

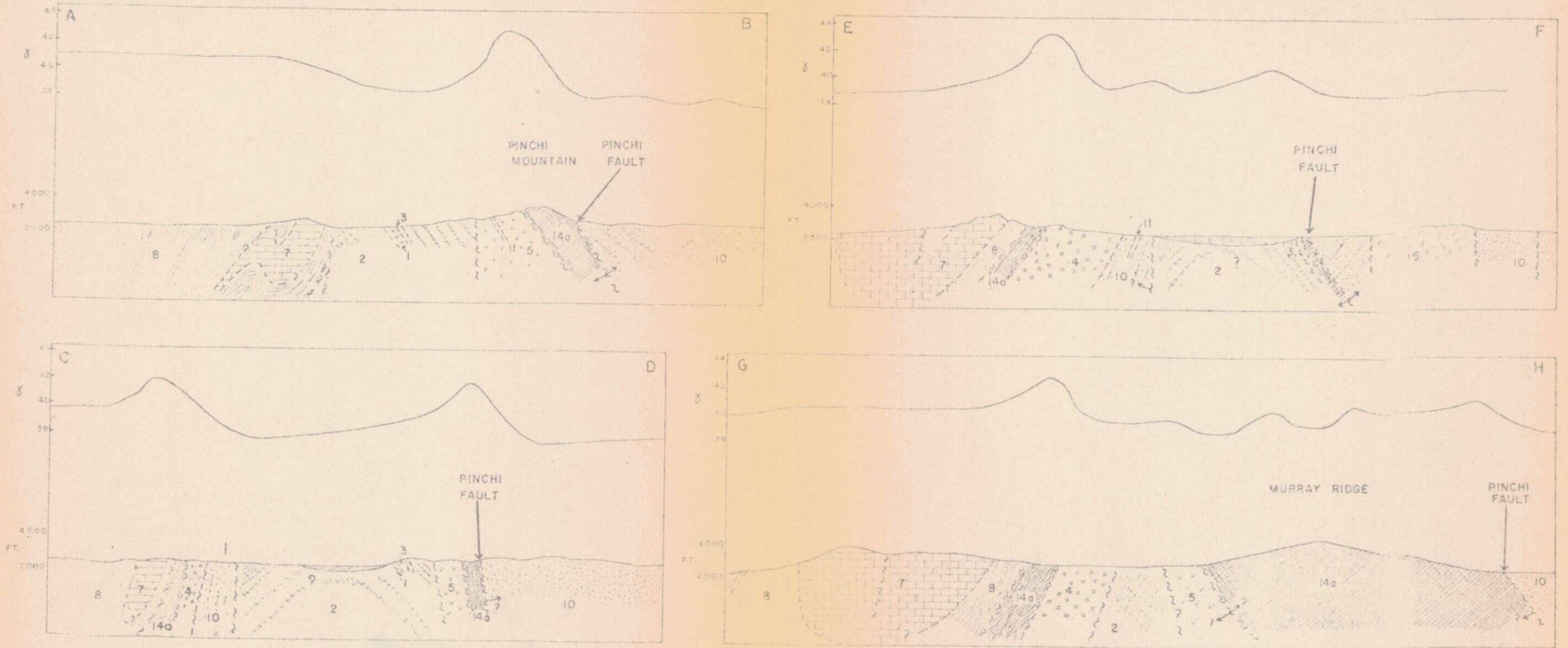
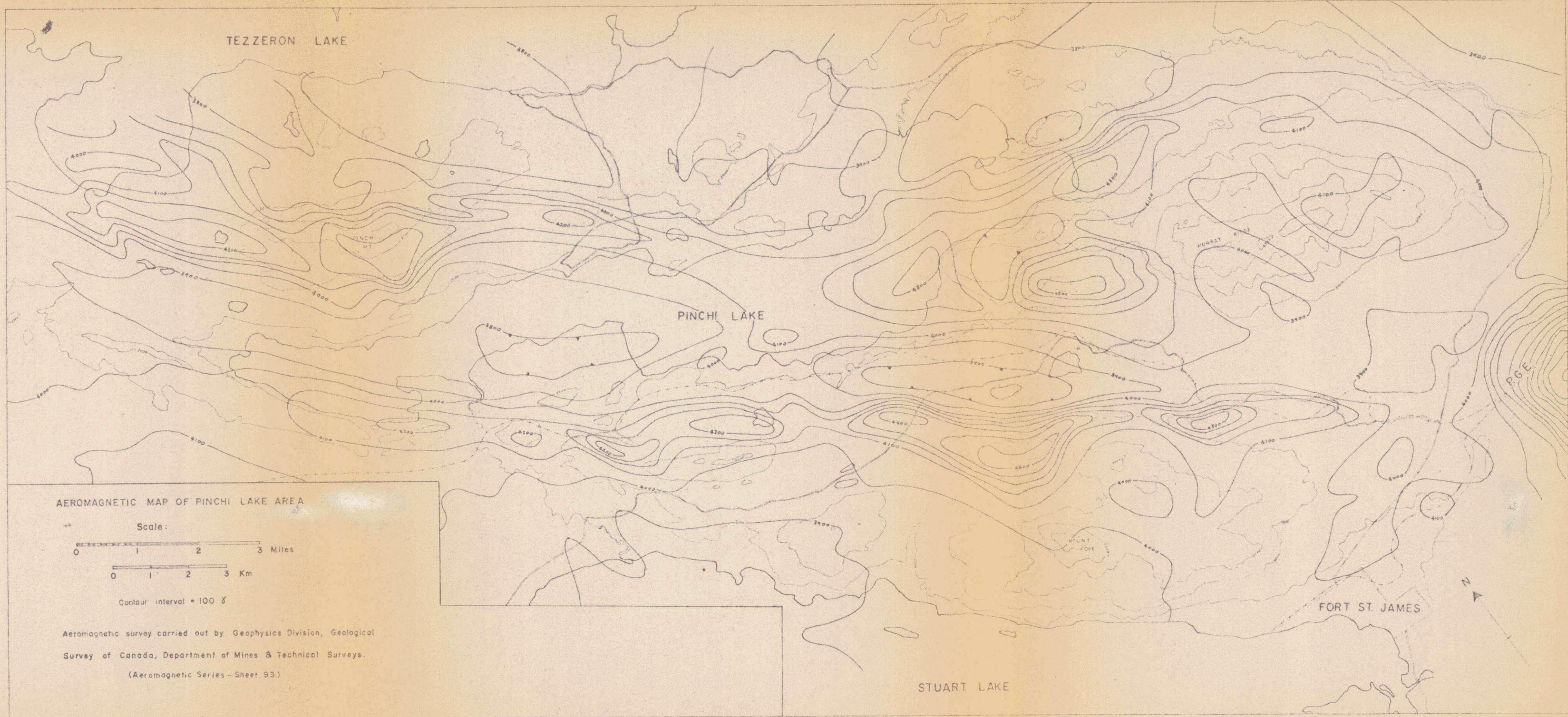


FIG. 24. CROSS SECTIONS OF THE PINCHI LAKE AREA FOR LOCATIONS AND LEGEND SEE MAP I. AEROMAGNETIC PROFILES OBTAINED FROM MAP III.



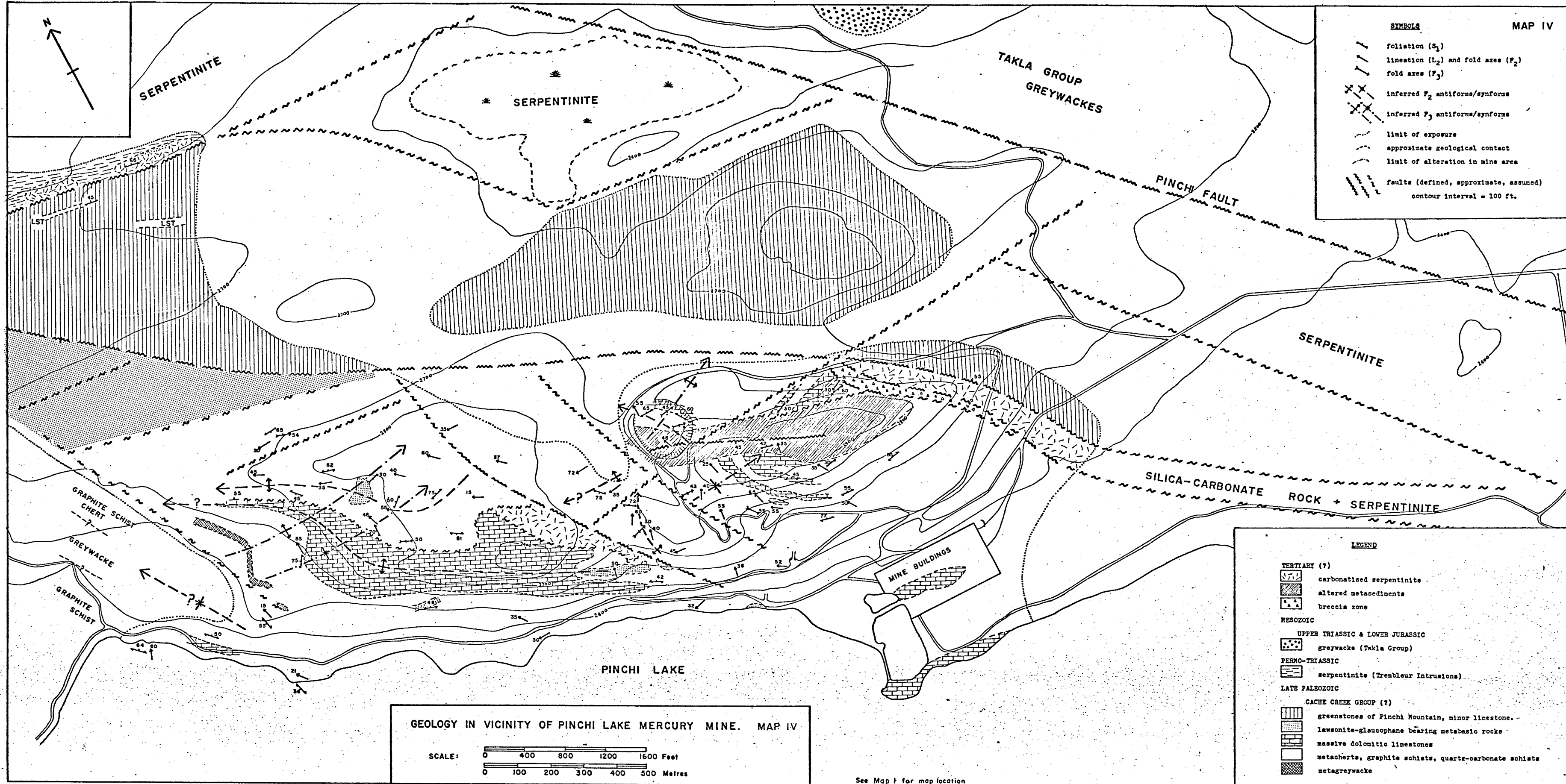
AEROMAGNETIC MAP OF PINCHI LAKE AREA

Scale:
0 1 2 3 Miles
0 1 2 3 Km

Contour interval = 100 γ

Aeromagnetic survey carried out by Geophysics Division, Geological Survey of Canada, Department of Mines & Technical Surveys.

(Aeromagnetic Series - Sheet 93)



MAP IV

SYMBOLS

- foliation (S_1)
- lineation (L_2) and fold axes (F_2)
- fold axes (F_3)
- inferred F_2 antiforms/synforms
- inferred F_3 antiforms/synforms
- limit of exposure
- approximate geological contact
- limit of alteration in mine area
- faults (defined, approximate, assumed)
- contour interval = 100 ft.

LEGEND

TERTIARY (?)

- carbonatised serpentinite
- altered metasediments
- breccia zone

MESOZOIC

UPPER TRIASSIC & LOWER JURASSIC

- greywacke (Takla Group)

PERMO-TRIASSIC

- serpentinite (Trembleur Intrusions)

LATE PALEOZOIC

CACHE CREEK GROUP (?)

- greenstones of Pinchi Mountain, minor limestone.
- lawsonite-glaucophane bearing metabasic rocks
- massive dolomitic limestones
- metacherts, graphite schists, quartz-carbonate schists
- metagreywacke

GEOLOGY IN VICINITY OF PINCHI LAKE MERCURY MINE. MAP IV

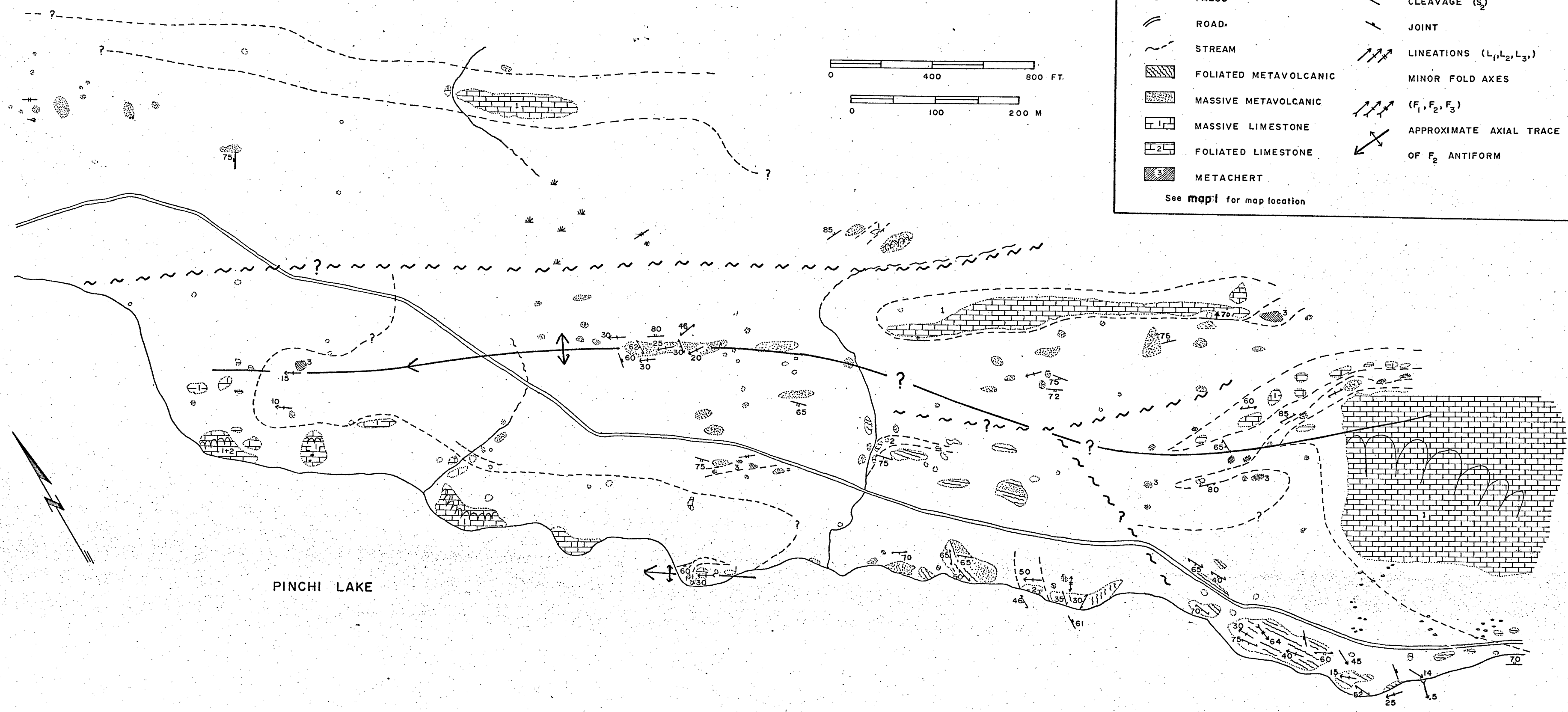
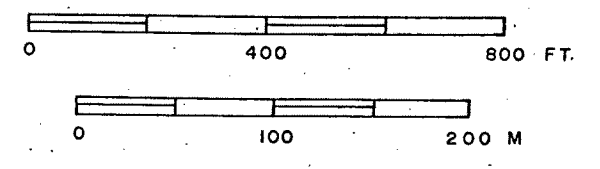
SCALE: 0 400 800 1200 1600 Feet
0 100 200 300 400 500 Metres

See Map I for map location

MAP V GEOLOGY OF AN AREA ON THE NORTHWEST SHORE OF PINCHI LAKE.

	OUTCROP		FAULT (APPROXIMATE)
	CLIFF		CONTACT (DEFINED, APPROX.)
	MARSH		FOLIATION (S ₁)
	TALUS		CLEAVAGE (S ₂)
	ROAD		JOINT
	STREAM		LINEATIONS (L ₁ , L ₂ , L ₃)
	FOLIATED METAVOLCANIC		MINOR FOLD AXES (F ₁ , F ₂ , F ₃)
	MASSIVE METAVOLCANIC		APPROXIMATE AXIAL TRACE OF F ₂ ANTIFORM
	MASSIVE LIMESTONE		
	FOLIATED LIMESTONE		
	METACHERT		

See map I for map location



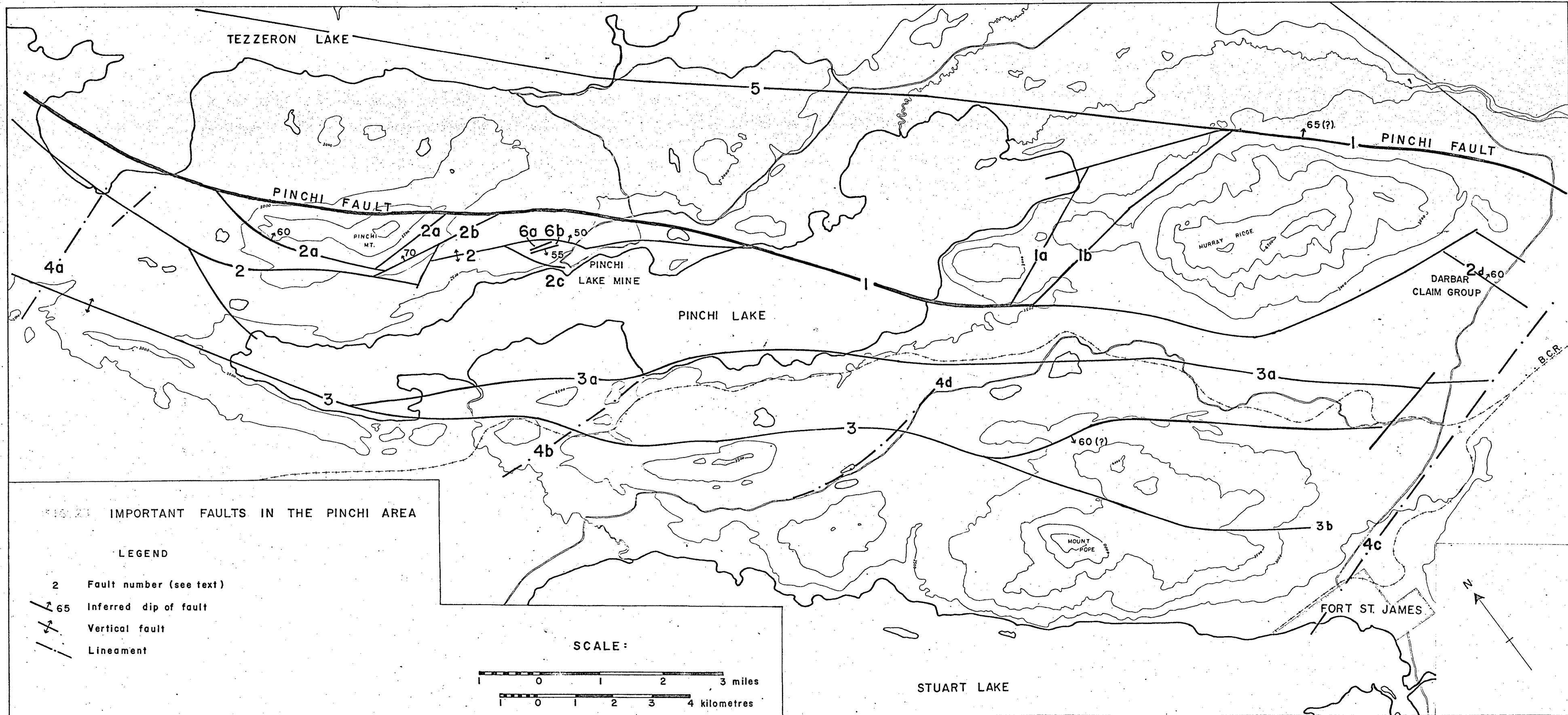


FIG. 21 IMPORTANT FAULTS IN THE PINCHI AREA

